ABSTRACT

HEINECKE, CHRISTINE LORAINE. Small Molecule Control over Biological Processes. (Under the direction of Dr. Christian Melander).

Myotonic Dystrophy Type 1 (DM1) is a multisystemic neuromuscular disorder characterized by a $(CTG)_n$ ($n > 50$) triplet repeat expansion in the 3'-UTR of the myotonic dystrophy protein kinase gene (*DMPK*). Transcription produces aberrant poly(CUG) expansions which sequester a family of alternative splicing regulators, the muscleblind proteins (MBNL1-3). In the absence of muscleblind, CUG-binding proteins mediate aberrant splicing leading to the disease pathology. We investigated cyclic peptides for their ability to disrupt a $(CUG)_{54}$:MBNL1 interaction as a unified approach towards treating DM1. To this end, we performed a phage display selection using a cysteine constrained cyclic heptapeptide library against immobilized $(CUG)_{54}$, which evolved four highly conserved cyclic peptides. In an effort to develop cellularly irreducible analogs of the cysteine constrained heptapeptides, we performed solid phase peptide synthesis substituting allyl glycine at the N- and C-terminal positions, which were subjected to ring closing metathesis. One of the selected peptides was shown to bind $(CUG)_{54}$ and disrupt the $(CUG)_{54}$:MBNL1 interaction characteristic of DM1 to a small extent.

Kinamycin D is a potent antitumor antibiotic; however, its biological mode of action is poorly understood. In order to further elucidate the mechanism by which kinamycin D mediates DNA damage, we employed DNA sequencing gel electrophoresis. We have demonstrated that under reducing conditions, acidic media promotes enhanced DNA cleavage. Additionally, our results indicate that kinamycin D is capable of generating reactive oxygen species under acidic pH in the presence of a reducing agent and that DNA cleavage is dependent on trace iron and hydroxyl radicals.

Bone biology and architecture are regulated by the interplay between osteoclasts and osteoblasts. Imbalances in this relationship, which favor osteoclastogenic activity are

implicated in a variety of skeletal diseases. In an effort to target osteoclasts and inhibit osteoclastogenesis, we have synthesized 1,4-substituted triazole libraries. Qualitative analysis of osteoclast maturation when treated with our compounds indicates some members of our triazole libraries to be the most potent known inhibitors of osteoclastogenesis ever disclosed.

Bacterial biofilm infections are implicated as the cause of many persistent and chronic infections due to antimicrobial resistance and virulence factors conferred by their protective extracellular matrices. *Bordetella bronchiseptica* is a gram-negative bacterial pathogen known to colonize the respiratory tracts of animals forming biofilms that are highly resistant to antimicrobial therapy. We synthesized and screened a library of 1,4-substituted triazoles for modulation of *B. bronchiseptica* biofilm formation. We identified one small molecule, which displayed agonistic activity towards *B. bronchiseptica* in multiple nutrient sources.

Small Molecule Control over Biological Processes

by
Christine Loraine Heinecke

A dissertation submitted to the Graduate Faculty of
North Carolina State University
in partial fulfillment of the
requirements for the Degree of
Doctor of Philosophy

Chemistry

Raleigh, North Carolina

2010

APPROVED BY:

_____	_____
David Shultz	Jonathan Lindsey
_____	_____
Reza Ghiladi	Christian Melander Chair of Advisory Committee

DEDICATION

For my grandfather, William Gestwick

"My grandfather used to say nobody gives a damn anymore and the thing I remember most about him is the way he never let that stop him from giving a damn all the days of his life."

For my mother, Deborah Heinecke

"I didn't listen to her because she was my mother and wouldn't know anything until I was much older."

For my father, David Heinecke

"When I was young, I used to wear my father's shoes and stomp around, making the world a better place for us all, and today I see I'm not the only one who did that and those shoes aren't anywhere big enough for who we are now."

For my grandmother, Margaret "Ellen" Heinecke

"I wish you could have been there for the sun and the rain and the long, hard hills. For the sound of a thousand conversations scattered along the road. For the people laughing and crying and remembering at the end. But, mainly, I wish you could have been there."

~Brian Andreas~

BIOGRAPHY

The author, Christine Loraine Heinecke, was born in Baltimore, MD on May 4, 1982 to Deborah and David Heinecke. She spent her childhood in Baltimore, MD and later in Glen Rock, PA. At the age of 14 she moved to Powhatan, Virginia where she graduated from high school. After high school graduation she attended James Madison University and received a B.S. in Chemistry with a concentration in Materials Science and was the proud recipient of the American Institute of Chemists Award. Her undergraduate research experience with Professor Barbara Reisner facilitated her appreciation of science and encouraged her to attend graduate school to further her scientific endeavors. In the fall of 2004, Christine began her graduate research studies at North Carolina State University under the advisement of Professor Christian Melander. After graduation, Christine began a postdoctoral research position at Colorado State University under the direction of Professor Christopher J. Ackerson.

TABLE OF CONTENTS

LIST OF TABLES vii
LIST OF FIGURES viii
LIST OF SCHEMES x
LIST OF ABBREVIATIONS AND TERMS xi
CHAPTER 1: A Unified Approach at Targeting Myotonic Dystrophy 1
1.1 Introduction 1
1.1.1 *DMPK* Haploinsufficiency Hypothesis 2
1.1.2 RNA Gain of Function Hypothesis 3
1.2 Previous Approaches to Targeting DM1 4
1.2.1 Dynamic Combinatorial Peptide Library Approach 4
1.2.2 Triaminotriazine-DNA Intercalator Approach 5
1.3 Our Approach at Targeting DM1 with Phage Display Libraries 6
1.3.1 Target Immobilization 8
1.3.2 Phage Display Selection 9
1.3.3 Synthesis of Cellularly Irreducible Analogs 12
1.3.4 Expression of MBNL Proteins 13
1.3.5 Electromobility Shift Assays for $(CUG)_{54}$:MBNL-N Interactions 14
1.4 Conclusion 17
1.5 Experimental 18
References 36
Appendix 39
CHAPTER 2: Kinamycin D Mediated DNA Cleavage 46
2.1 Introduction 46
2.2 Previous MOA Studies: Model Systems 48
2.2.1 Oxidative Activation Mechanism 48

2.2.2 Electrophilic Activation Mechanism 49
2.2.3 Reductive Activation Mechanism....49
2.3 Previous MOA Studies: Biomimetic Approaches 51
2.3.1 Biomimetic DNA Cleavage Mediated by Kinamycin D 51
2.3.2 Biomimetic DNA Cleavage Mediated by Kinamycin F 52
2.4 Current MOA Examination of Kinamycin D Mediated DNA Cleavage 53
2.5 Conclusion 58
2.6 Experimental 59
References 62
CHAPTER 3: Osteoclastogenesis Inhibition using Substituted 1,4-Triazoles 64
3.1 Introduction 64
3.2 Known Inhibitors of Osteoclastogenesis 65
3.2.1 Bisphosphonates 65
3.2.2 Selective Estrogen Receptor Modulators 66
3.3 Library Design 68
3.3.1 Synthesis of Second Generation Triazole Library 69
3.3.2 Osteoclastogenesis Inhibition Screen of Second Generation Library 71
3.3.3 Synthesis of Third Generation Library 73
3.3.3.1 2,4,6-Trichlorobenzamide Third Generation Library 73
3.3.3.2 Osteoclastogenesis Inhibition Results of Third Generation C-Series Library 74
3.3.3.3 Cyclohexylmethyl Third Generation Library 76
3.3.3.4 Osteoclastogenesis Inhibition Results of Third Generation Series Library 77
3.4 Conclusion 80
3.5 Experimental 80
References 104
Appendix 107

CHAPTER 4: Substituted 1,4-Triazole Modulation of *Bordetella bronchiseptica* Biofilms.....171
4.1 Bacterial Biofilms 171
4.1.1 Anti-Biofilm Modulating Small Molecules 172
4.2 *Bordetella* Genus.....173
4.3 Library Design 174
4.4 Biofilm Screening Results 175
4.4.1 Nutrient Broth Mediated RB50 Screens 176
4.4.2 Stainer Scholte Mediated RB50 Screens.....177
4.5 Conclusion 179
4.6 Experimental 179
References 185
Appendix 187

LIST OF TABLES

Table 1. Buffers assayed for EMSAs 14
Table 2. Cytotoxicity profile of lomaiviticin A.....47
Table 3. Evaluation of second-generation library by osteoclast formation stages.....72
Table 4. Evaluation of third-generation C-series library by osteoclast formation stages.....75
Table 5. Evaluation of third generation cyclohexylmethyl library by osteoclast formation Stages 77
Table 6. RB50 biofilm inhibition results in NB at 100 μM.....176
Table 7. RB50 biofilm inhibition results in SSB at 100 μM 178

LIST OF FIGURES

Figure 1. DNA slippage model for triplet repeat expansion disorders....2
Figure 2. RBDCL selected peptides....5
Figure 3. Ligand **L** and Janus-wedge hydrogen bonding....6
Figure 4. Phage display selection cycle....8
Figure 5. Cyclic peptides identified through phage display selection....12
Figure 6. $(CUG)_{54}$:MBNL-N EMSAs....14
Figure 7. Competitive EMSAs for $(CUG)_{54}$:MBNL-N with **IN23**....16
Figure 8. Representative kinamycins and lomaiviticins....47
Figure 9. Feldman's reductive activation mechanism....50
Figure 10. Potential routes to DNA cleavage....52
Figure 11. DNA sequencing gel electrophoretic radiograms....54
Figure 12. DNA sequencing gel electrophoretic radiograms....56
Figure 13. Revised mechanistic rationale for DNA cleavage....58
Figure 14. Osteoclast maturation pathway....64
Figure 15. Common bisphosphonates and nitrogen-containing bisphosphonates....66
Figure 16. Comparison of raloxifine, estradiol and estrogen receptor 1....67
Figure 17. First generation 2-aminoimidazole-triazole library for osteoclastogenesis Inhibition....68
Figure 18. Retrosynthetic analysis of triazole library....69
Figure 19. Complete second generation triazole library....71
Figure 20. Stages of osteoclast development for analysis of triazole library mediation of osteoclast formation....72
Figure 21. **C2** as a scaffold for third generation triazole libraries....73
Figure 22. Third generation triazole library based on 2,4,6-trichlororbenzamide....74

Figure 23. Comparison of cyclohexyl and cyclopentyl pendant groups on osteoclastogenesis Inhibition.....75
Figure 24. Third generation cyclohexylmethyl-triazole library.....77
Figure 25. Comparison of various benzamide EWG substitution patterns on osteoclastogenesis inhibition.....78
Figure 26. Comparison of benzamide aliphatic substituents on osteoclastogenesis Inhibition.....79
Figure 27. Most successful compounds from cyclohexylmethyl triazole library.....80
Figure 28. Stages of biofilm maturation.....172
Figure 29. Representative small molecules that inhibit biofilm formation.....173
Figure 30. Representative 2-aminoimidazole containing small molecules.....173
Figure 31. 1,4-Substitued triazole library for biofilm modulation screens.....175
Figure 32. Dose response curve of **B3** against RB50.....177
Figure 33. Dose response curves of **B2** and **D2** against RB50.....179

LIST OF SCHEMES

Scheme 1. Synthesis of biotinylated $(CUG)_{54}$ template for phage display.....9
Scheme 2. Synthetic route to linear and cyclic peptides 13
Scheme 3. Jebartanam's oxidative activation hypothesis.....48
Scheme 4. Dmietrienko's supporting data for an electrophilic activation.....49
Scheme 5. Feldman's reductive activation supporting data.....51
Scheme 6. Synthesis of azido precursors.....70
Scheme 7. Synthesis of 1,4-substituted triazoles for second-generation library.....70
Scheme 8. Synthesis of C-series third generation library.....73
Scheme 9. Synthesis of cyclohexylmethyl (2-series) third generation library 76

LIST OF ABBREVIATIONS AND TERMS

A	alanine
Ac	acetyl
2-AI	2-aminoimidazole
AIBN	azobisisobutyronitrile
amp	ampicillin
2-AIT	2-aminoimidazole-triazole
AHL	N-acylhomoserine lactone
aq	aqueous
Ala	alanine
Asn	asparagine
bd	broad doublet
BP	bisphosphonate
brine	saturated aqueous sodium chloride
bs	broad singlet
C	cysteine
CAT	catalase
CTG	cytosine-thymidine-guanosine
CUG	cytosine-uracil-guanosine
CUG-BP	CUG-binding protein
cTnT	cardiac troponin T
Cys	cysteine
d	doublet
DCM	dichloromethane

dt	doublet of triplets
dd	doublet of doublets
DMAP	4-(dimethylamino)pyridine
DM	myotonic dystrophy
DMF	N,N-dimethylformamide
DMPK	myotonic dystrophy protein kinase
DMSO	dimethyl sulfoxide
DNA	deoxyribonucleic acid
DTT	dithiothreitol
EDTA	ethylene diamine tetraacetic acid
EMSA	electrophoretic mobility shift assay
EtBr	ethidium bromide
EtOAc	ethyl acetate
EtOH	ethanol
FLAG	Fmoc-L-allylglycine
Fmoc	Fluorenylmethyloxycarbonyl
Gln	glutamine
GMPS	guanosine monophosphorothioate
GRL	genome research laboratory
GSH	glutathione
GST	glutathione S-transferase
h	hour(s)
H	histidine
His	histidine
HRMS	high-resolution mass spectrometry
HSC	hematopoeitic stem cells

Hz	hertz
IC_{50}	inhibitory concentration: 50%
IPTG	isopropyl-β-thiogalactoside
J	coupling constant
K	lysine
K_d	dissociation constant
LB	Luria-Bertani media
Lys	lysine
m	multiplet
MBNL	muscleblind protein
MBNL-FL	full length muscleblind (MBNL1)
MBNL-N	N-terminal muscleblind
M-CSF	macrophage colony stimulating factor
MeOH	methanol
MOA	mode-of-action
MHz	megahertz
min	minute(s)
NaAsc	sodium ascorbate
NBP	nitrogen-containing bisphosphonates
NMR	nuclear magnetic resonance spectrometry
Nu	nucleophile
OD_{600}	optical density at 600 nm
OPG	osteoprotegrin
P	proline
PFU	plaque forming unit
Pro	proline

Q	glutamine
q	quartet
QS	Quorum Sensing
RA	rheumatoid arthritis
RANK	receptor activator of nuclear factor κB
RANKL	receptor activator of nuclear factor κB ligand
RBDCL	resin bound dynamic combinatorial library
RB50	*Bordetella bronchiseptica* wild type strain
RCM	ring closing metathesis
RT	room temperature
RNA	ribonucleic acid
s	singlet
SDS-PAGE	sodium dodecylsulfate-polyacrylamide gel electrophoresis
SERM	selective estrogen receptor modulator
SOD	superoxide dismutase
TBE	Tris/boric acid/EDTA
TIS	triisopropylsilane
TFA	trifluoroacetic acid
TRAP	tartrate resistant acid phosphatase
Tris	tris(hydroxymethyl)aminomethane
UTR	untranslated region
V	volts
W	watts
XGal	bromo-chloro-indolyl-galactopyranoside

CHAPTER 1

A Unified Approach to Targeting Myotonic Dystrophy

1.1 Introduction

Myotonic dystrophy (DM) was first recognized as a multisystemic neuromuscular disorder in 1909.[1, 2] DM is the most common form of adult onset muscular dystrophy with an incidence of 1:8000. Muscular dystrophy and myotonia are classic symptoms of DM; however, various superficially unrelated clinical features are also symptomatic of the disease as well. Some of the seemingly unusual phenotypes consistent with DM include cataracts, heart conduction defects, insulin resistance and specific endocrine system irregularities including premature frontal baldness and testicular atrophy.[3-5] DM is inherited in an autosomal dominant fashion and as a progressively degenerative disease it exhibits anticipation through generations. Currently there are two well-established types of DM, myotonic dystrophy type 1 (DM1) and type 2 (DM2), each triggered by specific genetic modifications. The symptoms of DM2 are similar but typically mild in comparison to DM1, and there is no known congenital form of DM2. Additionally, the prevalence of DM1 far exceeds that of DM2.

The genetic basis for DM1 was first realized in 1992 as a triplet repeat expansion in the 3'-untranslated region (UTR) of the myotonic dystrophy protein kinase (*DMPK*) gene.[6-10] A $(CTG)_n$ expansion was found to be the determinant factor for the disease phenotypes exhibited in affected individuals; where the most severe symptoms and age of onset are correlated with a high index of repetition. Unaffected individuals have between 5 – 37 copies of the trinucleotide repeat, whereas affected individuals have upwards of 50 – 3,000 copies. As the number of genetic repeats increases, it becomes more likely that the cellular machinery involved in DNA replication will slip and extra copies of the repeat will be inserted into the gene during cell division (**Figure 1**). The propensity of slippage during DNA replication as the number of repeats increases provides DM1 with the feature of anticipation and the congenital disease form seen in infants.

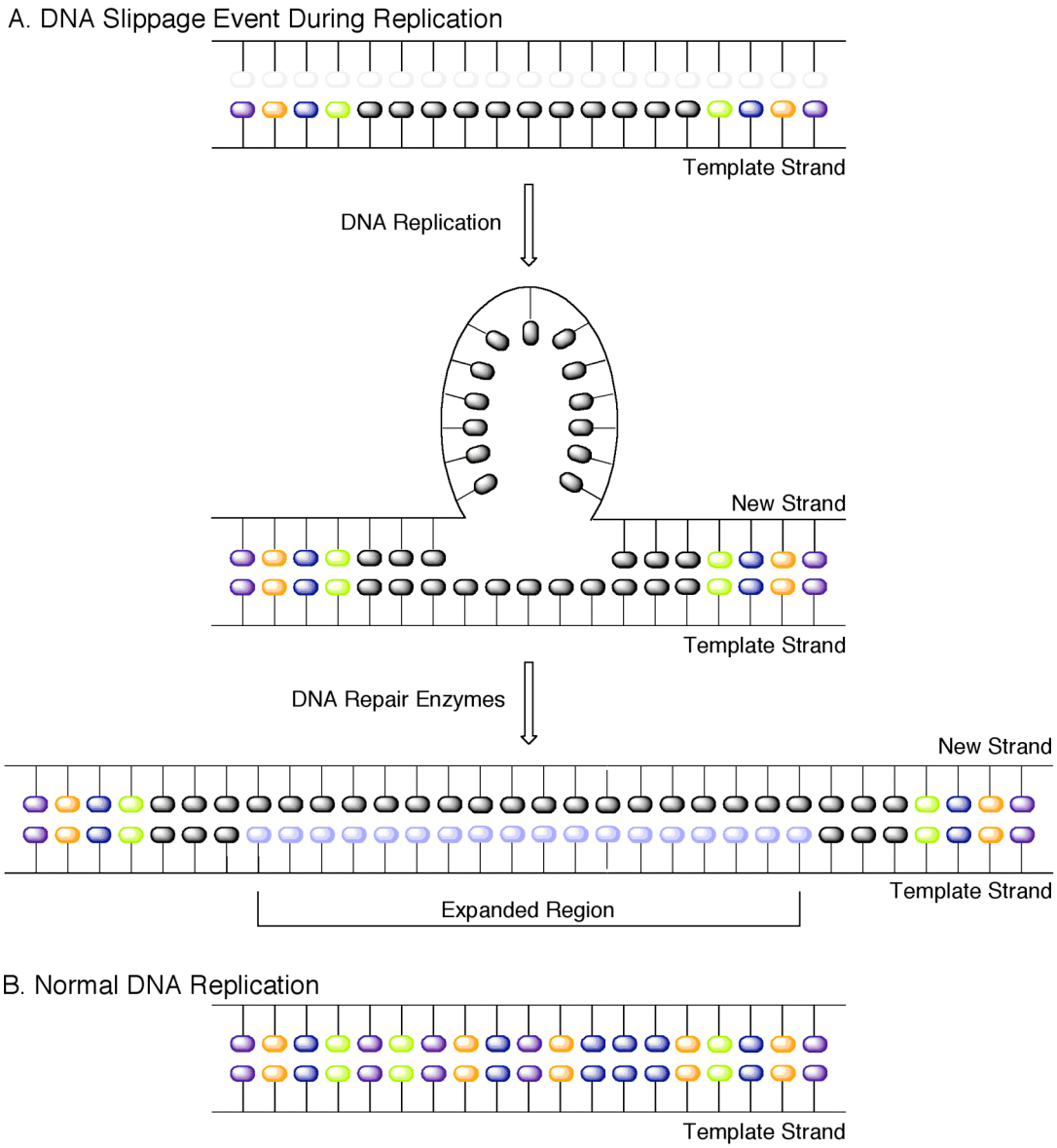

Figure 1. DNA slippage model for triplet repeat expansion disorders.

1.1.1 *DMPK* Haploinsufficiency Hypothesis

The dominance model exhibited in DM1 initially prompted Tapscott to propose that a haploinsufficiency of *DMPK* accounted for the disease pathology.[11] Although *DMPK* expression is generally downregulated in DM1,[12] this postulate could not explain the multisystemic phenotypes characteristic of DM1. In addition, no reported cases of DM1 have

been shown to be caused by a point mutation in the *DMPK* gene, suggesting that the multisystemic features of the disease are not caused by *DMPK* haploinsufficiency.[13]

1.1.2 RNA Gain of Function Hypothesis

Houseman and Singer later demonstrated that aberrant poly(CUG) transcripts of the mutant *DMPK* gene localized within nuclei, leading to general downregulation of *DMPK*. [14, 15] The nuclear accumulation of expanded CUG was proposed to account for the deleterious effects of the repeat expansion. This unprecedented RNA gain of function mechanism predicted that aberrant CUG transcripts exerted a *trans*-dominant effect capable of disrupting alternative splicing as well as other cellular events.[16-20] This mechanism was further substantiated by the observation that an expanded repeat in the 3'-UTR of *DMPK* RNA inhibited myogenic differentiation of C2C12 myoblasts.[21] In addition, transcription of an expanded CUG RNA was shown to generate a DM1 phenotype in transgenic mice when expressed in a gene entirely unrelated to *DMPK*.[22]

The toxic RNA gain of function hypothesis for DM1 pathology directed researchers to study the ability of proteins to bind expanded CUG transcripts. Initial explorations revealed that CUG-binding protein (CUG-BP) regulated the alternative splicing of cardiac troponin T (cTnT) by binding CUG. This splicing pattern was shown to be disrupted in DM1 cardiac and skeletal muscle tissues.[17] However, CUG-BP activity was shown to increase in DM1, which did not support a *trans*-dominant effect of RNA-mediated inactivation of binding proteins. Furthermore, studies failed to exhibit co-localization of CUG-BP with aberrant CUG in nuclear foci.[23] The inability of CUG to sequester CUG-BP suggested a secondary role for CUG-BP in the pathogenesis of DM1.

Although CUG-BP was eliminated as a sequestration target, emerging evidence indicated that the accumulation of expanded CUG within nuclei altered the localization of a family of alternative splicing regulators: the muscleblind-like proteins (MBNL1–3).[19, 24, 25] Each of

these three isoforms was recruited into mutant RNA nuclear foci in DM1 cells, which was presumed to disrupt their customary biological functions.[26] Consequently, MBNL proteins became attractive targets for the toxic RNA gain of function exhibited after transcription of aberrant *DMPK* RNA. Further substantiation for this mechanism was achieved when MBNL1 knock-out mice developed myotonia, cataracts and splicing irregularities consistent with the DM1 phenotype.[27] In addition, cell culture experiments involving siRNA depletion of MBNL1, MBNL2 and CUG-BP indicated that nuclear accumulation favored MBNL1.[17, 20, 27] Complementary evidence revealed that upon MBNL1 co-localization with expanded CUG in nuclei, aberrant alternative splicing events were mediated by CUG-BP, supporting the earlier suggestion of a secondary role for CUG-BP in DM1 disease pathology.

1.2 Previous Approaches to Targeting DM1

The emergent data supporting the poly(CUG) gain of function mechanism via sequestration of MBNL promoted other researchers to investigate small molecule disruption of this interaction as well.

1.2.1 Dynamic Combinatorial Peptide Library Approach

The first published account of small molecule mediated poly(CUG):MBNL disruption was achieved by Miller et al. in 2008.[28] This achievement was accomplished by employing a resin-bound dynamic combinatorial library (RBDCL)[29] with a theoretical diversity of 11,325 members. Resin bound tripeptides (150) containing a variable cysteine at each position were equilibrated with solution phase tripeptides (150) also containing cysteine at each variable position. After disulfide exchange, these bead bound peptides were incubated with a fluorescently labeled $(CUG)_{10}$ RNA. Subsequently, the library of resin-bound peptides was washed to remove unbound RNA and the beads were imaged for fluorescence. Fluorescent beads indicated RNA binding peptide sequences, which were then identified through mass spectrometry. Four monomers were identified containing sequence similarity: (Quin/Pip)-(Asn/Pro)-Cys-Lys (**Figure 2**). They synthesized all possible non-redundant mixtures

(assuming commutative property transfer) and then identified 4 disulfide-crosslinked peptides capable of high affinity binding (K_d ~2 μM) to $(CUG)_{109}$ via a filter binding assay (disulfides **3-3**, **4-4**, **2-4**, **3-4**). However, when the selected peptides were incubated with $(CUG)_{109}$ in the presence of MBNL1, the maximum displacement measured through an enzyme complementation assay was only 50% even at concentrations of 100 μM. This result showed the first promise of small molecules and their ability to mediate the interaction between poly(CUG) and MBNL. However, the therapeutic use of these crosslinked peptides would be irrelevant due to the reduction of the disulfide linkage mediated by intracellular thiols, given that the individual peptides alone were unable to bind poly(CUG).

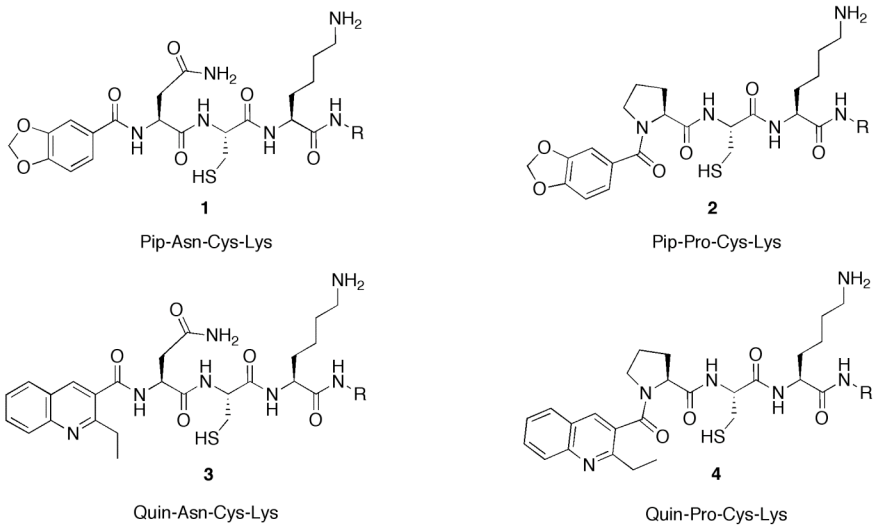

Figure 2. RBDCL selected peptides.

1.2.2 Triaminotriazine-DNA Intercalator Approach

Recently, an alternative strategy for targeting DM1 was published delineating the rational design and synthesis of a ligand capable of selectively disrupting the poly(CUG):MBNL interaction.[30] Zimmerman et al. chose to target the U-U mismatch in poly(CUG) with a triaminotriazine unit tethered to a known DNA intercalator. The use of triaminotriazine was posited to target U-U or T-T mismatches through Janus-wedge hydrogen bonding, potentially forming a full set of six simultaneous hydrogen bonds (**Figure 3**). They chose to tether triaminotriazine to a 9-aminoacridine derivative and argued that although 9-aminoacridine is

a minor groove DNA intercalator, the joined molecule could target CUG or CTG through the major or minor groove due to a "stacking intercalator" effect. The designed ligand **L** was assayed for affinity and selectivity for T-T, C-C, G-G and A-A mismatches in $[(CG)_m(CXG)_n(CG)_m]_2$ hairpins and found to only bind to DNA with T-T mismatches. Furthermore, when at least two T-T mismatches were present, **L** bound DNA with high nanomolar affinities. This affinity was also translated to an RNA counterpart, where $(CUG)_4$ was shown to bind **L** with a K_d of 0.43 μM using isothermal titration calorimetry. Furthermore, upon 1:1 binding of MBNL-N and $(CUG)_{12}$, the addition of compound **L** disrupted the RNA-protein complex with IC_{50} values of 40 – 50 μM. Electromobility shift assays also indicated almost complete inhibition when treated with 250 μM compound **L**. This salient result renders compound **L** as the most promising lead for therapeutic intervention of DM1 known to date.

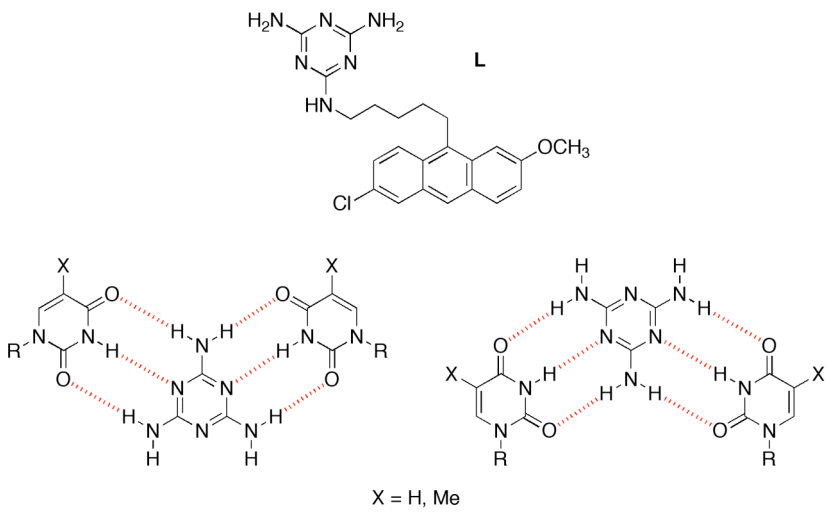

Figure 3. Ligand **L** and Janus-Wedge hydrogen bonding.

1.3 Our Approach at Targeting DM1 with Phage Display Libraries

Given that poly(CUG) sequestration of MBNL1 is the primary determinant driving DM1 pathology, we chose to target poly(CUG) in an attempt to disrupt the poly(CUG):MBNL1 interaction. We reasoned that the release of MBNL1 could reestablish the biologically

intended alternative splicing events, which are aberrantly regulated in DM1. Given that peptides and proteins are endogenous RNA binding molecules, we chose to identify peptides capable of binding poly(CUG) selectively. Additionally, given that cyclic peptides have enhanced bioavailability, do not suffer entropic losses on binding and are less susceptible to protease degradation than their linear counterparts,[31] we chose to investigate a library of cyclic peptides for their ability to bind poly(CUG).

The selection technique we employed in our search for selective poly(CUG) binders was cyclic peptide phage display. Phage display is a system that displays a peptide on the surface of a viral coat protein. DNA encoding the displayed peptide is located within the bacteriophage virion. By cloning DNA sequences into the phage, display libraries are produced with a repertoire that exceeds a billion of uniquely displayed proteins or peptides. This process (biopanning) allows an immobilized target to incubate with a phage library and employs simple washing steps to remove any unbound phage, thus eliminating peptides unable to bind the target of interest. A key advantage of this technique is the ability for phage to be infected into *E. coli* for rapid amplification of binding members of the library. In addition, the genotype/phenotype relationship of the encoded DNA and the displayed peptides facilitates rapid identification of the active peptides. The selection cycle, depicted in **Figure 4**, is repeated until the remaining peptides within the pool of phage possess high sequence homology.

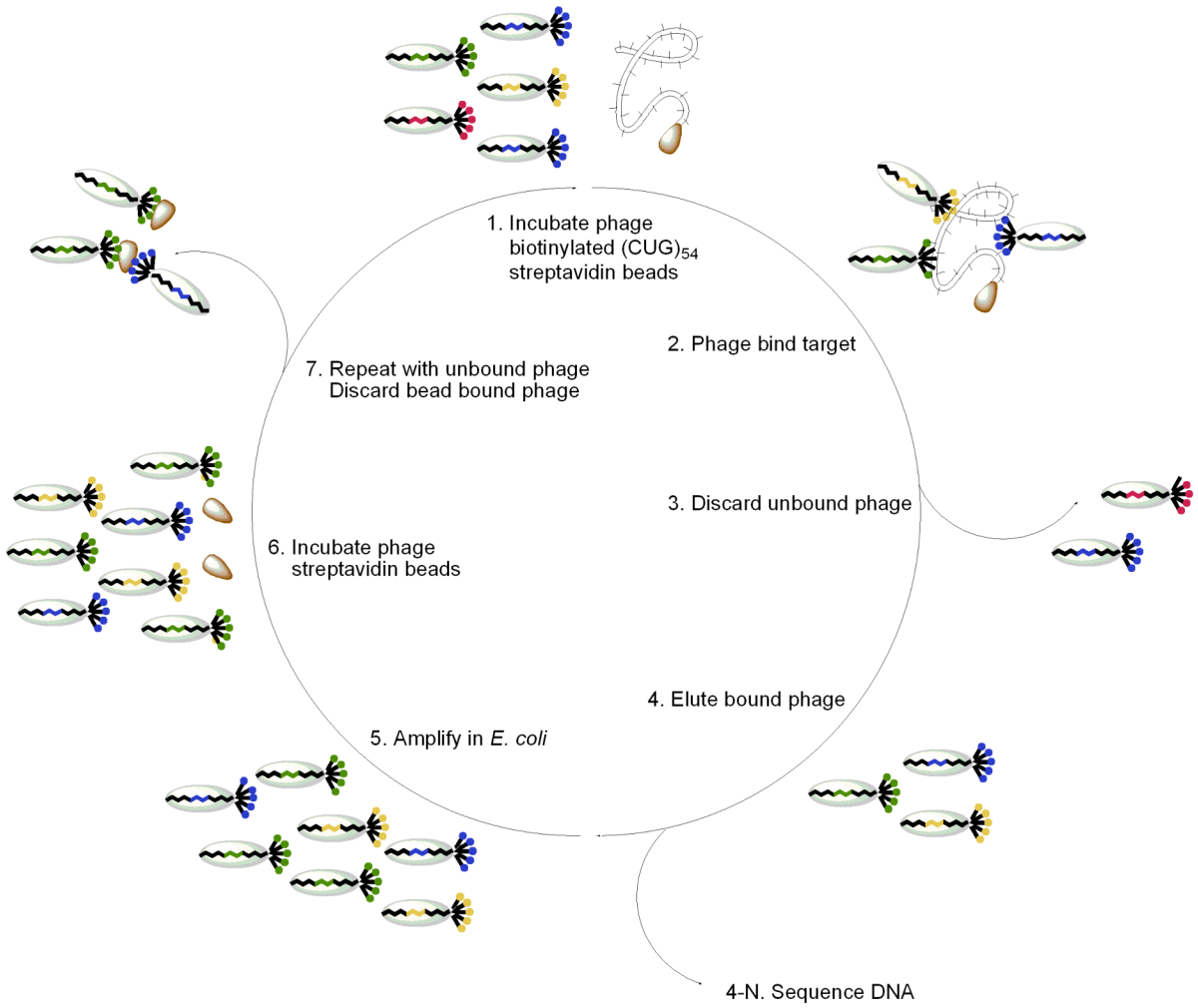

Figure 4. Phage display selection cycle.

1.3.1 Target Immobilization

Preceding the selection, we first prepared a target RNA capable of immobilization. Professor Swanson (UFL) kindly provided an ampicillin resistant plasmid encoding $(CTG)_{54}$ engineered into a DH5α *E. coli* cell line. The $p(CTG)_{54}$ encoded cell line was amplified in LB supplemented with 100 µg/mL ampicillin; after enough cells were harvested and lysed, $p(CTG)_{54}$ was isolated by midiprep purification. The plasmid was then linearized with the BamHI restriction endonuclease and utilized as a template for *in vitro* run off transcription with 5'-guanosine monophosphorothioate (GMPS). The 5'$GMPS(CUG)_{54}$ transcript was then

coupled with biotin-PEG_2-maleimide to provide our immobilizable target for phage display (**Scheme 1**). The RNA target was then immobilized by exploiting the extremely high affinity biotin-avidin interaction using magnetic streptavidin beads.

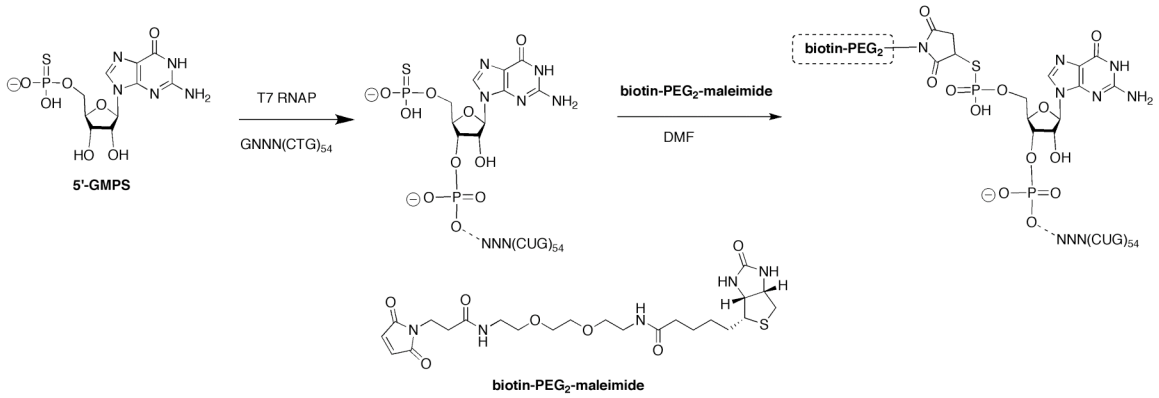

Scheme 1. Synthesis of biotinylated $(CUG)_{54}$ template for phage display selection.

1.3.2 Phage Display Selection

After target immobilization, we began performing selections using a commercially available cysteine constrained heptapeptide library with a complexity of 1.28 billion unique peptides (according to the literature provided with the library). During preliminary selection experiments, the library of phage was found to evolve the known HPQ (His-Pro-Gln) consensus motif specific for streptavidin within three rounds of positive selection. In order to prevent the selection and amplification of phage specific for binding streptavidin, we chose to perform alternating rounds of positive and negative selection. The addition of a negative selection round in each cycle confers a higher degree of stringency by removing any peptides or phage, which could bind the streptavidin beads and provide false positive results.

We defined a complete selection cycle as one round of positive selection followed by one round of negative selection. During a positive round of selection the phage library was incubated with the immobilized RNA target (**Figure 4**, Step 1). During this incubation period any phage displayed peptides capable of binding $(CUG)_{54}$ with high affinity were then

immobilized as well by association (**Figure 4**, Step 2). All nonbinding phage were then eliminated through numerous washing steps (**Figure 4**, Step 3). The RNA-bound phage were then eluted with an acidic solution of glycine (a general phage eluent, **Figure 4**, Step 4). The desired RNA-binding phage were then infected into *E. coli* and amplified (**Figure 4**, Step 5). After phage amplification, a negative selection round was employed to remove phage capable of binding streptavidin. During a negative round of selection the amplified phage library was incubated only with streptavidin beads (**Figure 4**, Step 6). Any phage that did not bind the streptavidin immobilization support were then removed and saved (**Figure 4**, Step 7), while the streptavidin beads and bead-binding phage were discarded. This was the final step for the selection cycle; at this point, these phage were then placed onto a subsequent selection cycle and this protocol was repeated until sequence homology was achieved.

The selection cycle we employed as described above begins with a round of positive selection. However, given our previous results of identifying streptavidin-binding phage in only three selection cycles we chose to also employ a parallel selection which began with a round of negative selection. The initial negative selection cycle was posited to immediately remove any streptavidin binding phage, which could complicate our selection results. This parallel selection was performed exactly as described above and in **Figure 4**, excepting only that this selection began with Step 6 (as illustrated) and then continued through the subsequent steps as delineated above.

The convergence of CUG-binding peptide sequences within the remaining pool of phage during each repetitive selection cycle was discerned by monitoring the number of remaining phage within the pool by counting plaque forming units (PFU) prior to phage amplification (always counted at Step 4). This process, called phage titering, is analogous to bacterial colony counting. Once CUG-bound phage were eluted, a small portion of the phage library was serially diluted and plated onto IPTG/XGal/LB/Agar. After overnight incubation at 37 ºC, the plaques were counted as an indication of the number of remaining phage within the

library. During the early selection cycles, the total number of phage within the remaining pool decreased via the removal of non-CUG-binding phage; therefore, the number of PFUs decreased as expected. However, after the majority of nonbinding phage were removed, only CUG-binding phage remained in the pool and continued to be amplified through multiple cycles of selection. This result was indicated by a sharp increase the number of PFUs during later selection cycles.

After six cycles of selection, we observed a dramatic increase in the unamplified phage titer for both the initial positive and initial negative selection cycles. Consequently, we plated the remaining phage from the pools onto IPTG/XGal/LB/Agar and picked 48 random phage plaques from each selection (initial positive and initial negative), amplified them in *E. coli*, and isolated the phage DNA. The DNA was then PCR amplified and submitted for automated DNA sequencing to the Genome Research Laboratory (GRL) at NCSU. The coding DNA sequences obtained from GRL were then translated into the peptide binders for $(CUG)_{54}$. The sequencing data yielded three sequences that were highly conserved: **IN23**, **IN8**, **IP17** and one sequence, which was evolved from both selections **IPN2** (**Figure 5**). Although there are not many conserved amino acids within these peptides, three of them contain Thr as the first variable amino acid, two contain Tyr at position 3 and two contain Ser at position 7. The sequencing results we obtained were promising, given the modest cross homology and the repetitive nature of the identified peptides. Additionally, none of the selected peptides were polycationic or contained the HPQ motif known for streptavidin, suggesting that these peptides bind $(CUG)_{54}$ in a specific fashion.

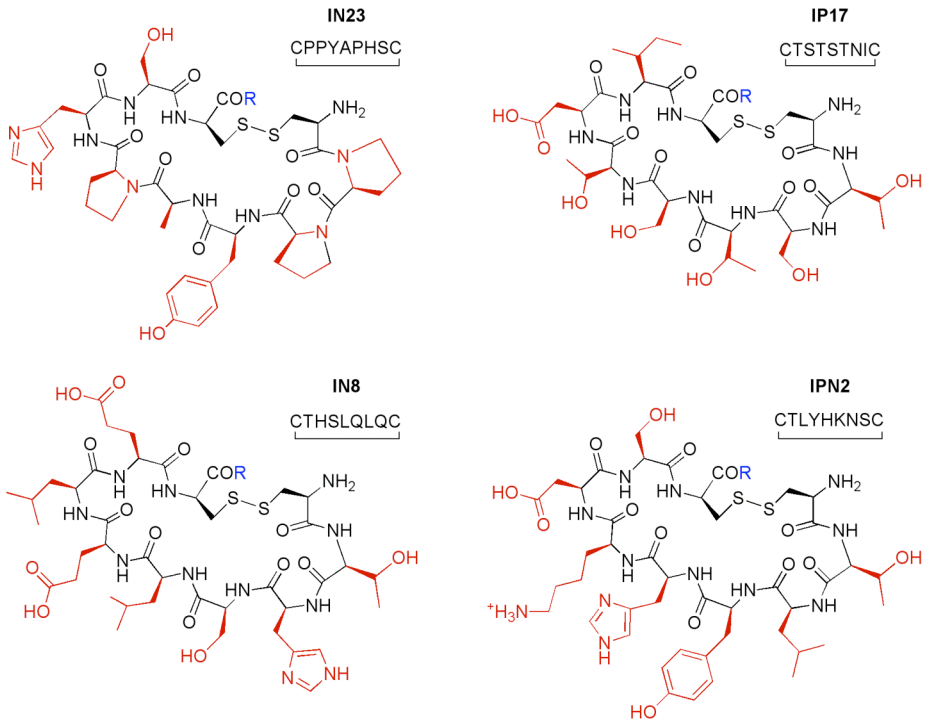

Figure 5. Cyclic peptides identified through phage display selection.

1.3.3 Synthesis of Cellularly Irreducible Analogs

After the identification of poly(CUG)-binding cyclic peptides, we sought to investigate their ability to disrupt the poly(CUG)-MBNL interaction characteristic of DM1. However, cysteine constrained cyclic peptides undergo reduction to their linear forms mediated by cellular thiols. Although linear peptides are capable of binding RNAs, most literature suggests enhanced binding favorability for their cyclic counterparts.[31] In addition, linear peptides are more susceptible to degradation by intracellular proteases. Therefore, we aimed to synthesize cellularly irreducible analogs of these cyclic peptides by employing ring-closing metathesis (RCM). This was achieved by replacing the first and last cysteine amino acids with an allyl glycine. Peptides were synthesized using the standard solid phase Fmoc protocol on a Rink amide MBHA resin (**Scheme 2**). Once the linear peptide chain had been synthesized, attempts were made to cyclize the peptide using RCM.

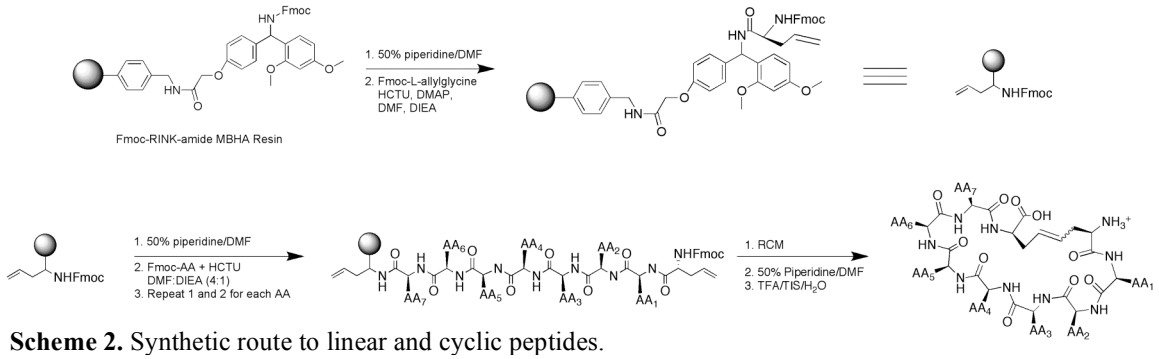

Scheme 2. Synthetic route to linear and cyclic peptides.

A former group member, Anne Basso was able to cyclize peptides of this length using Hoyveda-Grubbs 2nd Generation Catalyst; therefore, we chose to employ her optimized procedure for RCM. The long refluxing times and amount of catalyst necessary; however inhibited the amount of product isolated due to degradation and purification obstructions respectively. A typical loading of 500 mg resin generally yielded less than 5 mg crude solid after cleavage from the resin and subsequent precipitation. Furthermore, the only successful metathesis reaction was performed on **IN23**; which contains 3 proline residues. Given that purification of peptides after subjection to RCM procedures proved extremely difficult, we chose to test our methodology using linear analogs of the peptides identified during the selection. Although they would suffer an entropic loss upon folding into the active conformation for binding, we reasoned they should still be capable of binding the target RNA.

1.3.4 Expression of MBNL Proteins

Before we could assess the ability of these peptides to displace the poly(CUG):MBNL interaction we first needed to express the muscleblind protein and determine its binding capabilities toward $(CUG)_{54}$. Professor Swanson also provided us with fusion constructs of GST::MBNL1::His and GST::MBNL-N::His (N-terminus AAs: 1 – 253) as plasmids engineered into a BL21 strain of *E. coli*. Expression of full-length MBNL1 proved extremely difficult due to the inherent instability of muscleblind. SDS-PAGE analysis indicated when

the protein was successfully expressed it would frequently degrade during affinity column purification or during storage even in the presence of protease inhibitors.

The N-terminal domain of MBNL1 (MBNL-N) has been identified as the region that poly(CUG) binds *in vitro*.[32, 33] MBNL-N, in addition to full length MBNL1 (MBNL-FL), has been shown to cross-link with $(CUG)_{54}$,[19] form RNA-protein complexes with cTnT RNAs (Tnnt3/T5.1 and T5.45) and $(CUG)_{54}$;[32] however, the truncated protein was more likely than MBNL-FL to form unresolved complexes which remained in the wells of polyacrylamide gels during elecrophoresis.[32] Additionally, MBNL-N has been shown to possess higher binding affinities than MBNL-FL and is more stable than the full-length protein. Therefore we chose to employ MBNL-N for use in binding reactions and electrophoretic mobility shift assays (EMSA) with $(CUG)_{54}$.

The GST::MBNL-N::His encoded cell line was amplified in 2XYT supplemented with 500 μg/mL carbenicillin and protein expression was induced under IPTG control. After the cells were harvested and lysed, the N-terminal fusion construct was purified through GST-affinity chromatography and dialyzed into storage buffer supplemented with protease inhibitors. MBNL-N was then utilized in electromobility shift assays to determine the ability of our selected peptides to disrupt the poly(CUG):MBNL interaction.

1.3.5 Electromobility Shift Assays for $(CUG)_{54}$:MBNL-N Interactions

The first electromobility shift experiments we performed were to determine the appropriate concentrations of $(CUG)_{54}$ and MBNL-N to effect 100% complex formation. Several buffer systems were investigated for their ability to facilitate the $(CUG)_{54}$:MBNL-N interaction and are shown in **Table 1**. Buffer A is known in the literature to host MBNL interactions with pyrimidine-pyrimidine mismatches.[34] Some reports have shown that increased levels of NaCl disrupt RNA-protein interactions; therefore, Buffer B was also used to host this interaction. Buffer C is also modified from the literature[16] and is the buffer the selection was carried out

in. Initial explorations of MBNL-N interactions with $(CUG)_{54}$ indicated some binding in Buffer C (selection buffer); however, the alternative buffers were explored in an effort to enhance the binding constant, and consequently lower the necessary concentrations of MBNL-N needed to effect a binding event. These buffers showed little deviation in their ability to promote binding, thus Buffer C was used for the subsequent EMSAs for consistency given that the selection was performed in this buffer.

Table 1. Buffers assayed for EMSAs.

Buffer	Components
A	175 mM NaCl, 20 mM Tris-HCl, 5 mM $MgCl_2$, 1.25 mM BME, 12.5% glycerol, 2 mg/ml BSA, 0.1 mg/ml heparin
B	100 mM NaCl, 20 mM Tris-HCl, 5 mM $MgCl_2$, 1 mg/ml BSA, 0.1 mg/ml heparin
C	20 mM Tris-HCl, 100 mM KCl, 5 mM $MgCl_2$, 0.1% Triton-X

After some optimization we were able to observe 100% complex formation between MBNL-N and $(CUG)_{54}$, this is depicted in **Figure 6** (Gel A) where as the concentration of MBNL-N is increased, the free RNA (lower band) starts to disappear; while a higher molecular weight band is formed indicating a binding event between the RNA and protein. The EMSA indicated that with our conditions 100% of $(CUG)_{54}$ was bound with 4 μM MBNL-N, which was in agreement with literature results.

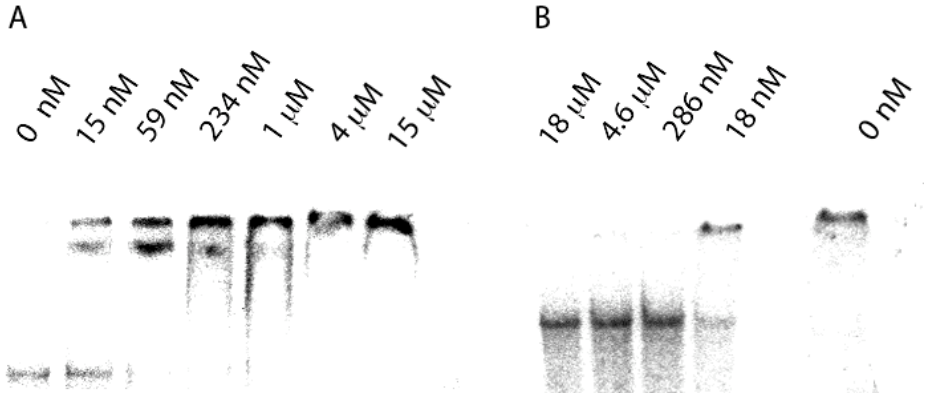

Figure 6. $(CUG)_{54}$:MBNL-N EMSAs **A.** $(CUG)_{54}$ + [MBNL-N]. **B.** $(CUG)_{54}$ + [**IN23L**]: 30 min, + 234 nM MBNL-N.

The next step in our investigation of the MBNL-poly(CUG) interaction was to assess the ability of our selected peptides to competitively disrupt the MBNL-N:$(CUG)_{54}$ interaction. The first preliminary competitive gel shift experiment was performed with linear **IN23** (**IN23L**). When increasing concentrations of **IN23L** were pre-incubated with $(CUG)_{54}$ for 30 min and were then treated with 234 nM MBNL-N, we discovered as little as 286 nM **IN23L** was able to completely disrupt this interaction and release free RNA (**Figure 6**, Gel B). Unfortunately, this result could never be duplicated even after preparing every reaction component (MBNL-N, $(CUG)_{54}$, buffer systems, etc.) again under strict sterile conditions.

While trying to repeat the result of this experiment we observed that upon increasing the peptide concentrations dramatically, **IN23L** inhibited the formation of the $(CUG)_{54}$:MBNL-N complex to a small extent at 723 µM. To measure the observed effect, we counted the pixels of free RNA and the RNA-protein complexes in the gel. The percent of the lower band (e.g. free RNA) was as follows: $(CUG)_{54}$ control = 92%, $(CUG)_{54}$:MBNL-N control = 68%, 723 µM **IN23L** + $(CUG)_{54}$:MBNL-N = 80%. Thus **IN23L** mediated a 12 percentage point increase in free RNA when compared to the RNA:protein control. Although this effect is not as dramatic as our initial competitive EMSA, the results of this assay nonetheless indicate that **IN23L** is capable of mildly disrupting this RNA-protein interaction (**Figure 7**, Gel A).

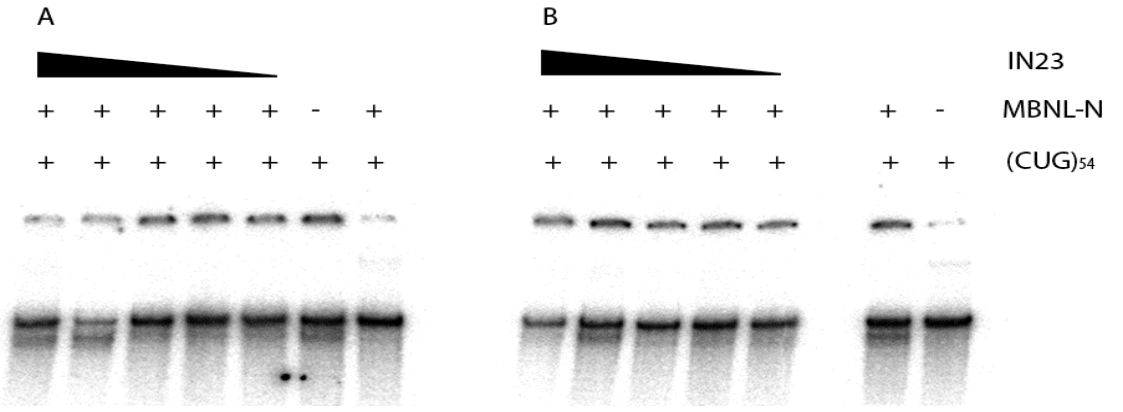

Figure 7. Competitive EMSAs for $(CUG)_{54}$:MBNL-N with **IN23**. **A. IN23L** (723 µM, 145 µM, 28.9 µM, 5.78 µM, 1.16 µM). **B. IN23C** (2.2 mM, 440 µM, 88 µM, 17.6 µM, 3.52 µM).

Although cyclic **IN23** (**IN23C**) posed purification difficulties, we chose to test the ability of crude **IN23C** to disrupt the $(CUG)_{54}$:MBNL-N interaction as well. Crude **IN23C**, however did not display any extent of $(CUG)_{54}$:MBNL-N inhibition, even at extremely high peptide concentrations (2.2 mM). The results of this assay are shown in **Figure 7**, Gel B. Pixel counts were also measured for the competitive **IN23C** EMSA: the percent of the lower band (free RNA) was as follows: $(CUG)_{54}$ control = 94%, $(CUG)_{54}$:MBNL-N control = 73%, 2.2 mM **IN23C** + $(CUG)_{54}$:MBNL-N = 63%. In fact, the competitive EMSA using higher concentrations of crude **IN23C** appeared to have a noticeable effect of *decreasing* free RNA. This effect is most likely due to RNA degradation from the remaining RCM impurities.

Although **IN23L** was demonstrated to be capable of disrupting the CUG_{54}:MBNL-N interaction to some extent, unfortunately the affinity of **IN23L** for $(CUG)_{54}$ was not strong enough to disrupt the RNA-protein interaction at therapeutically relevant concentrations. Perhaps the inclusion of MBNL-N during the selection could have increased the stringency enough to prompt the evolution of peptides capable of binding $(CUG)_{54}$ with enough affinity to competitively displace muscleblind at lower concentrations. The selected peptides currently represent leads for future analog development.

1.4 Conclusion

We investigated cyclic peptides for their ability to disrupt a $(CUG)_{54}$:MBNL1 interaction as a unified approach towards treating DM1. To this end, we performed a phage display selection using a cysteine constrained cyclic heptapeptide library against immobilized $(CUG)_{54}$. After six cycles of selection, we identified four highly conserved cyclic peptides that were not polycationic, suggesting RNA binding is probably specific. In an effort to develop cellularly irreducible analogs of the cysteine constrained heptapeptides, we performed solid phase peptide synthesis substituting allyl-glycine at the N- and C-terminal positions, which were subjected to ring closing metathesis. Linear peptide **IN23** was easily cyclized using Hoveyda Grubbs 2nd Generation catalyst, most likely due to the three proline residues providing the

peptide with a round initial conformation. We then assayed the peptides for their ability to disrupt the $(CUG)_{54}$:MBNL1 interaction characteristic of DM1. One selected peptide was capable of binding $(CUG)_{54}$ and was able to disrupt the $(CUG)_{54}$:MBNL1 complex to a small extent. These cyclic peptides currently represent leads for further analog development.

1.5 Experimental

All chemicals were used without further purification. Transformed cell lines were obtained from the Maurice Swanson laboratory at UFL. All Fmoc protected peptides and resins were obtained from Peptides International. All other chemicals were supplied by Aldrich, unless otherwise noted. All buffer and media recipes are included in the Appendix.

Isolation of $(CTG)_{54}$ plasmid from *E. coli*

The ampicillin resistant (amp^r) $p(CTG)_{54}$ was transformed into a DH5α strain of *E. coli* and kindly provided by the Maurice Swanson Laboratory at the University of Florida at Gainesville. 50 mL modified LB media (10 g tryptone, 5 g yeast, 10 g NaCl) was dispensed into a sterile 250 mL Erlenmeyer flask doped with 10 mg/ml carbenicillin. A single colony was selected and inoculated for 16 – 20 hours at 37 ºC and 220 rpm in a shaking incubator. After the cellular density was large enough, the cells were centrifuged for 10 min at 10,000 x *g*; the supernatant was discarded and the plasmid was extracted using a Promega Pure Yield™ Plasmid Midi Prep DNA Purification System. The isolated DNA was resuspended in 600 µL nuclease free water and quantified by ultraviolet absorption at 260 nm where [DNA] µg/ml = A_{260} * 50 µg/mL * dilution factor. Plasmid DNA was stored in aliquots at -20 ºC.

BamHI Restriction Enzyme Digest of $p(CTG)_{54}$

Seven µL DNA (1 µg/mL) was incubated with 0.5 µL BSA (10 mg/mL), 5 µL 10X Buffer E (Promega) 34.25 µL nuclease free water, and 3.25 µL BamHI (10 U/µL) for one hour at 37 ºC. The BamHI (G$^{\blacktriangledown}$GATC C) DNA cleavage was monitored by agarose gel electrophoresis (0.8%) in 1X TBE run at 100 V for 3 h. Once the plasmid was successfully linearized, the

DNA was separated from the restriction enzyme by phenol/chloroform extraction. An equal volume of well-suspended phenol/chloroform/isoamyl alcohol (25/24/1) was added to the sample of DNA and vortexed at a low setting for five min. The mixture was then centrifuged for 5 min at 13.2 rcf and most of the top aqueous layer was carefully removed with a micropipette. The aqueous layer containing the DNA was then precipitated with 2.5 volumes of ice-cold ethanol and 1/3 volume 5 M NH_4OAc for at least 30 min at -20 ºC. The samples were then centrifuged for 30 min at 4 ºC, 13.2 rcf, the supernatant was removed and the pellet was washed with 200 µL ice cold 70% ethanol. The sample was centrifuged briefly, the supernatant was removed and the pellet was allowed to air dry for at least 30 min at RT. The DNA was then resuspended in 50 µL nuclease free water.

Transcription of $(CUG)_{54}$

The linearized $(CTG)_{54}$ was used as a template for *in vitro* run off transcription for "cold" RNA, "hot" RNA and biotinylated RNA. All transcription components (specifics described below the general conditions presented here) were combined in a 200 µL PCR tube and heated to 37 ºC for no more than 6 h. The transcript was separated from the enzyme by a phenol/chloroform/isoamyl alcohol (25/24/1) extraction employing a volume equal to reaction volume. The suspension was vortexed for 5 min on a low setting and subsequently centrifuged for 5 min at 13.2 rcf. The majority of the aqueous layer was removed using a micropipet, carefully avoiding the chloroform layer. The transcript was then precipitated with 3 volumes of ice-cold isopropanol and 1/3 volume of 5 M NH_4OAc. The mixture was centrifuged at 4 ºC, 13.2 rcf for 30 min, the supernatant was removed and the pellet was washed with 200 µL ice-cold 70% ethanol. The sample was then centrifuged briefly, the supernatant was removed and the pellet was allowed to air dry for at least 30 min. Samples of RNA were resuspended in nuclease free water and were purified on 8 M Urea, 8% polyacrylamide (19:1) gel electrophoresis. Cold RNA was visualized with Ethidium Bromide (EtBr) staining for at least 20 min and 3-4 rounds of hour long destaining. The desired transcript as visualized by molecular weight markers and the pink color exhibited during

EtBr intercalation was excised with a nuclease free scalpel and placed into a microfuge tube. Hot RNA was visualized on X-Ray film (Fuji Film); the gel (wrapped in cellophane) was exposed to the film for approximately 20 min before developing. After the film was developed it was aligned with the gel and the desired band of RNA was excised using a nuclease free scalpel and placed into a microfuge tube. The gel slices were gently crushed with a pipet tip and the transcripts were eluted overnight in 400 µL Gel Elution Buffer (500 mM NH_4OAc, 1 mM EDTA pH 8.0, 0.1 % SDS). The following morning the samples were centrifuged for 10 min at 13.2 rcf and the liquid was carefully separated from the gel fragments. The transcripts were precipitated with 3 volumes of ice-cold isopropanol, placed at -20 ºC for at least 30 min and then centrifuged at 4 ºC, 13.2 rcf for 30 min. The supernatant was carefully removed and the pellet was washed with 200 µL of ice-cold 70% isopropanol and centrifuged briefly. The supernatant was removed and the pellet was allowed to air dry for at least 30 min at RT.

Cold RNA

Cold RNA was transcribed by combining 4 µL 5X transcription buffer (Promega), 2 µL 5 mM ATP, 2 µL 5 mM UTP, 2 µL 5 mM CTP, 2 µL 5 mM GTP, 0.5 µL RNAsin (40 U/µL), 3 µL nuclease free water, 1.5 µL T7 RNA polymerase (RNAP, 20 U/µL) and 3 µL DNA template.

Hot RNA

Hot RNA was uniformly body labeled with 50 µCi α-^{32}-P-UTP (MPBiomedicals) by combining 4 µL 5X transcription buffer, 2 µL 5 mM ATP, 2 µL 5 mM CTP, 2 µL 5 mM GTP, 0.5 µL UTP, 5 µL α-^{32}-P-ATP (3000 Ci/mmol) 0.5 µL RNAsin (40 U/µL), 3 µL DNA template, 1 µL T7 RNAP.

Biotinylated RNA

Biotinylated RNA was transcribed by including an excess of 5'-guanosinemonophosporothioate (GMPS, Axxora LLC, G-018-10) during standard "cold" transcription. GMPS-$(CUG)_{54}$ was transcribed with 17 µL nuclease free water, 20 µL 5X transcription buffer, 0.5 µL RNAsin, 8 µL 5 mM ATP, 8 µL 5 mM CTP, 8µL 5 mM UTP, 8 µL 5 mM GTP, 20 µL GMPS (2 mM final), 4.5 µL DNA (1 µg/mL), 2 µL T7 RNAP. 5'-GMPS$(CUG)_{54}$ was then reacted with 25 mM Maleimide-PEG_2-biotin (Pierce) in DMF for 2 hours and purified on a MWCO-10 microcon. Percent biotinylation was quantified by comparison of free RNA after a streptavidin-binding assay, where free (non-biotinylated) RNA was quantified by EtBr staining on an agarose gel and the concentration of biotinylated RNA determined by difference.

Expression and Isolation of GST::MBNL1::His

The full-length muscleblind protein was received as an amp^r (BL21) and as an amp^r and $camp^r$ (BL21 Codon Plus) fusion construct with both GST and His affinity tags from the Swanson Laboratory at UFL. The protein was expressed by a modified literature procedure.[32] A single colony of GST::MBNL::His was inoculated in 5 mL of LB dosed with 100 µg/mL carbenicillin (or 100 µg/mL carbenicillin and 34 µg/mL chloroamphenicol for the BL21 Codon Plus strain) and incubated overnight at 37 ºC, 220 rpm. The following morning the overnight culture was diluted 1:100 into 250 mL of pre-warmed 2XYT media dosed with 500 µg/mL carbenicillin and incubated at 37 ºC, 220 rpm until the OD_{600} = 0.6 (3 – 5 hours). When the desired OD was achieved the temperature was lowered to 30 ºC and GST::MBNL::His expression was induced by the addition of IPTG (1 mM final) for 3 h. The cells were then centrifuged at 10,000 rpm, 4 ºC for 15 min. The supernatant was removed and the cells were placed at -20 ºC for at least 2 h. The cells were then thawed on ice and purified using the PIERCE B-PER® GST Spin Purification Kit. The GST::MBNL1::His fusion construct was bound to immobilized glutathione-agarose beads, washed 4 times with Tris-Glycine and eluted with free glutathione (GSH). A small amount of eluate was denatured in

loading dye at 95 ºC for 5 min and run on 8% SDS-PAGE in 1X Tris-Glycine-SDS for 30 min at 200 V. The gel was then stained with Coomassie Brilliant Blue for 30 min and then destained by washing 4-5 times with Destain Buffer over the course of several hours. The visibility of a blue band at approximately 67 – 70 kDa was indicative of the full-length construct (~67 – 68 kDa). Western blotting analysis was also performed to ensure the fusion construct was isolated and intact. A nitrocellulose membrane was presoaked in Transfer Buffer, then a clean gel was placed on the surface of the nitrocellulose and transferred to the membrane at 100 V for 1 h. The gel was then removed, and the membrane was washed 3 times with TBST for 10 min. The membrane was then blocked with 5 mL of TBS + Casein for at least 1 h at 4 ºC. The blocking solution was then decanted and the membrane was washed 4 times with TBST for 15 min. A GST-HRP Conjugate Antibody was diluted 1:5000 in 10 mL of TBST and exposed to the membrane with gentle shaking for 1 h. The membrane was then washed 2 times for 2 min, 1 time for 15 min and 3 times for 5 min to removed any residual antibody. The membrane was then dried and developed using a 1:1 solution of luminol and peroxide developer (BioRad, Immunostar HRP) for 5 min. The membrane was wrapped in cellophane and imaged on a GE Storm™ 840 Chemiluminescent Detector. Pure protein samples were then dialyzed overnight at 4 ºC into Protein Storage Buffer using a 10,000 MWCO Dialysis Cassette (3 buffer changes of 1 L). Protein concentration was measured with the DC Protein Assay® (BioRad) using BSA as the standardization control.

Expression and Isolation of GST::MBNL-N::His

The N-terminal muscleblind protein (AA 1 – 253) was received as an amp^r fusion construct with both GST and His affinity tags from the Swanson Laboratory at UFL. A single colony of GST::MBNL-N::His was inoculated in 5 mL of LB dosed with 100 µg/mL carbenicillin and incubated overnight at 37 ºC, 200 rpm. The following morning the overnight culture was diluted 1:100 into 200 mL of prewarmed 2XYT media dosed with 500 µg/mL carbenicillin and incubated at 37 ºC, 220 rpm until the OD_{600} was approximately 0.6. At this point the temperature was lowered to 30 ºC and GST::MBNL-N::His expression was induced by the

addition of IPTG (1 mM final) for 3 h. The cells were then centrifuged at 10,000 rpm, 4 ºC for 15 min. The supernatant was removed and the cells were placed at -20 ºC for at least 2 h. The cells were then thawed on ice and purified using the PIERCE B-PER® GST Spin Purification Kit. The GST::MBNL1::His fusion construct was bound to immobilized glutathione-agarose beads, washed 4 times with Tris-Glycine Buffer and eluted with free GSH. A small amount of eluate was denatured in loading dye at 95 ºC for 5 min and run on 8 % SDS-PAGE in 1X Tris-Glycine-SDS for 30 min at 200 V. The gel was then stained with Coomassie Brilliant Blue for 30 min and then destained by washing 4-5 times with Destain Buffer over the course of several hours. The visibility of a blue band at approximately 50 – 55 kDa was indicative of the N-terminal construct (~53 – 54 kDa). The protein was dialyzed overnight at 4 ºC into Protein Storage Buffer using a 3,000 MWCO Dialysis Cassette (4 buffer changes of 1 L). Protein concentration was measured using the DC Protein Assay® (BioRad) with BSA as the standardization control.

Negative Selection Protocol

Magnetic streptavidin beads (50 µL) were introduced into a 1.5 mL eppendorf tube and first washed with 1 mL Binding Buffer by vortexing for approximately 30 sec. The suspension was then centrifuged for 1 min to pellet the beads, and the eppendorf was placed in a magnetic rack, which pooled the beads to the edge of the eppendorf. The solution was then removed from the beads. The beads were then blocked for nonspecific binding at 4 ºC for 1 h with the addition of 1 mL Blocking Buffer. The beads were then centrifuged for 1 min again, placed in the magnetic rack and the supernatant was removed. The beads were then washed 4 x 1 mL Binding Buffer. *ROUND 1.* A solution of phage was prepared by combining 10 µL of a cysteine constrained cyclic heptapeptide phage library (NEB Ph. D. C7C) with 190 µL Binding Buffer and allowed to equilibrate for 15 min at RT. *ROUND 2-6.* A solution of phage was prepared by combining 10 µL of the amplified pool of phage from the previous positive selection round and 190 µL Binding Buffer. *ALL ROUNDS.* The phage solution was then added to the streptavidin beads, vortexed gently and incubated for 15 min at RT. The

sample was then centrifuged for 1 min, the supernatant was removed and immediately placed onto a positive selection or stored at 4 ºC overnight until a positive selection could be performed.

Positive Selection Protocol

Magnetic streptavidin beads (50 µL) were transferred into a 1.5 mL eppendorf tube and washed with 1 mL Binding Buffer by gently vortexing. The suspension was then centrifuged for 1 min, placed on a magnetic rack and once the beads were pooled together, the supernatant was removed. The beads were then treated to disrupt any nonspecific binding events by incubating with 1 mL Blocking Buffer for 1 h at 4 ºC. At this time, the beads were centrifuged for 1 min, placed on the magnetic rack and the supernatant was removed. The beads were then washed 4 x 1 mL Binding Buffer. A solution of 30 pmol biotinylated-$(CUG)_{54}$ in 100 µL Binding Buffer was introduced to the streptavidin beads and allowed to incubate at RT for 15 min (Biotin-Avidin $K_d \sim 10^{-15}$ M). The sample was then centrifuged and the supernatant was removed. Any remaining unbound RNA was removed through 4 x 1 mL wash steps with Binding Buffer. *INITIAL POSITIVE.* A solution of phage was prepared by combining 10 µL of a cysteine constrained cyclic heptapeptide phage library (NEB Ph. D. C7C) with 190 µL Binding Buffer and allowed to equilibrate for 15 min at RT. The solution of phage was then allowed to incubate with the target RNA for 15 min at RT. *INITIAL NEGATIVE*. The unbound phage supernatant (200 µL) of the negative selection was added to the beads and allowed to incubate at RT for 15 min. *ALL CONTINUED.* The beads were centrifuged for 1 min, placed on the magnetic rack and the supernatant was removed. The beads were then washed 8 x 1 mL Binding Buffer to ensure the removal of all phage that are unable to bind $(CUG)_{54}$. After the final wash step, 1 mL Elution Buffer was added and incubated at RT for 10 min. The samples were then centrifuged, placed on the magnetic rack and the supernatant was transferred to another eppendorf. The solution was then neutralized by the addition of 150 µL Neutralization Buffer. At this step 10 µL saved for phage titer and the remaining phage are amplified in *E. coli.*

Phage Amplification and Isolation

A tet^r *E. coli* (ER2738) cell line was inoculated in 20 mL LB and incubated at 37 ºC, 200 rpm. While ER2738 was growing the selection procedure was performed. After approximately 4 h the neutralized phage solution from the positive selection (less 10 µL for titer) was infected into the ER2738 cell line. The cells were incubated for another 4 h at 37 ºC, 200 rpm. After amplification the cells were centrifuged for 10 min at 4 ºC, 10,000 rpm. The supernatant was then transferred to a new vessel and centrifuged again. The upper 80 % was transferred to a new vessel and 1/6 volume of PEG-NaCl Buffer was added. The phage were allowed to precipitate overnight at 4 ºC. The following morning the samples were centrifuged for 15 min at 4 ºC and 10,000 rpm. The supernatant was decanted and all residual liquid was removed with a micropipette. The pellet was suspended in 1 mL TBS and centrifuged at 10,000 rpm for 5 min at 4 ºC to remove any remaining debris. The supernatant was removed, transferred to a new tube and re-precipitated with 1/6 volume PEG-NaCl Buffer while at -20 ºC for 40 min. The sample was then centrifuged at 13.2 rcf for 10 min at 4 ºC, the supernatant was removed and the pellet suspended in TBSA. This solution comprised the amplified pool of phage, 10 µL of which were used for the amplified phage titer (to ensure amplification is successful) and the remaining pool was placed on the next round of negative selection.

Phage Titering

Both unamplified and amplified pools of phage were titered. The variance between the two allowed the determination of a successful amplification procedure. The variance between unamplified phage titers allowed a measure of sequence homology to be assessed. The procedures for both were exactly the same, and as follows. The saved 10 µL sample of phage was used to prepare a working range of four 10-fold serial dilutions in LB (100 µL total volume). The unamplified pools were diluted serially from $10^1 – 10^4$ and the amplified pools from $10^8 – 10^{11}$. First, a single colony of ER2738 was inoculated in 5 mL LB and incubated at 37 ºC, 200 rpm until the OD_{600} was approximately 0.5. LB Agar IPTG/XGal plates (lowest

dilutions were plated on one plate, as the dilution increased another plate was added for easier plaque counting) were pre-warmed to 37 ºC. While the cells were growing, a 50 mL stock of Agarose Top was melted in the microwave and 3 mL aliquots were dispensed into sterile 10 mL culture tubes (one for each plate), the tubes were then placed in a 45 ºC water bath until needed. When the OD_{600} finally reached mid log phase, 200 µL of the culture was added to empty eppendorf tubes (one for each dilution). Then 10 µL of each serially diluted solution of phage in LB was added to the ER2738, quickly vortexed and incubated at RT for 5 min. The infected cells were then transferred to a 3 mL aliquot of Agarose Top, vortexed and immediately poured onto a pre-warmed LB Agar IPTG/XGal plate. The plate was tilted so the entire surface area was covered with Agarose Top and it was allowed to solidify over the course of 5 min at RT. After each dilution was plated, the plates were inverted and incubated overnight at 37 ºC. The following morning the numbers of blue plaques were counted and the phage titer was reported as plaque forming units (PFU) per 10 µL.

Isolation and Characterization of Binding Clones

The phage titer of the unamplified pools was monitored for a sharp increase in PFU between rounds to indicate when consensus sequences had been reached. This indication of sequence homology was observed at Round 6 of both the Initial Positive and the Initial Negative Selections. An overnight culture of ER2738 in LB-tet was diluted 1:100 in LB. The diluted stock was aliquoted 96 x 1 mL into 5 mL culture tubes. Sterilized toothpicks were used to pick plaques from the unamplified titer plates (only on plates with less than 100 plaques), which were then placed into the individual culture tubes. Forty-eight plaques were picked from both the Initial Positive and the Initial Negative Selection. The phage were allowed to amplify over the course of 4.5 h at 37 ºC, 200 rpm. After amplification, the samples were then transferred to individual microfuge tubes and centrifuged for 30 sec at 13.2 rcf. Next, 500 µL of the supernatants were transferred to new microfuge tubes and stored at 4 ºC overnight. The following morning 200 µL PEG-NaCl Buffer was added to each of the phage containing supernatants, they were mixed by inversion and allowed to incubate at RT for 10

min. The samples were then centrifuged at 13.2 rcf for 10 min. The supernatants were discarded, the samples were re-spun and the residual supernatants were also removed. The pellets were then suspended thoroughly in 100 µL NaI Buffer, 250 µL 100% ethanol was then added and the samples were incubated at RT for 10 min to induce phage precipitation. The samples were then centrifuged for 10 min at 13.2 rcf, the supernatants were discarded and the pellets were washed with 100 µL 70% ethanol, re-spun and the supernatants removed again. The phage DNA pellets were then dried under vacuum and resuspended in 30 µL TE Buffer. All DNA samples were quantified by UV-Vis absorption at 260 nm and adjusted to a concentration of 1 µg/mL. The DNA samples (3 µL/well) were then transferred into a 96-well edge plate and PCR amplified using -96 gIII sequencing primer (1 µL/well, specific for the anticodon strand) and The Big Dye Kit™ (4 µL/well) in a reaction volume of 10 µL. The well plate was covered with a rubber lid to prevent evaporation and amplified for 30 cycles using hot start PCR of denaturation at 96 ºC, 10 sec; annealing at 50 ºC, 5 sec; and elongation at 60 ºC, 4 min. After PCR amplification of the phage DNA, 5 µL nuclease free water was added to ensure enough volume remained in the event of evaporation. The edge plate was centrifuged at 8.0 rcf for 3 min to remove PCR buffer. The lower filter on the edge plate was then removed and the edge plate was placed on top of another 96-well plate. The sandwiched plates were then centrifuged at 8.0 rcf for 5 min to collect the DNA samples. After heat-sealing the plate with aluminum foil, the 96-well plate was submitted to the Genome Research Laboratory at Partners II for automated DNA sequencing analysis. The DNA sequencing results were analyzed using the BioEdit® Analysis Program. The encoded phage followed the leading sequence of ACC TCC ACC, the next 9 codons were cropped and the reverse complement was determined. Finally, the codons were translated into the corresponding amino acids yielding the sequences of binding cyclic peptides.

```
5'-....GCT TGT NNK NNK NNK NNK NNK NNK NNK TGC GGT GGA GGT TCG
3'-....CGA ACA NNM NNM NNM NNM NNM NNM NNM ACG CCA CCT CCA AGC
       Ala Cys Xxx Xxx Xxx Xxx Xxx Xxx Xxx Cys Gly Gly Gly Ser
```

General Procedure for Linear Peptide Synthesis

Approximately 500 mg of RINK-Amide MBHA Resin (200 – 400 mesh, 0.44 meq/g) was weighed and placed into a SPPS vessel. The resin was expanded and washed three times with ~ 5 mL DCM and subsequently flushed with nitrogen, and washed with ~ 7 mL DMF three times and flushed with nitrogen. A 50% solution of piperidine in DMF was prepared and added to the reaction vessel and allowed to shake for approximately 20 min to deprotect the resin. The deprotection solution was then evacuated from the vessel by positive nitrogen pressure and the resin was washed four times with 5 mL DMF to ensure the removal of all piperidine. The first (and last) amino acid added to all synthesized peptides (Fmoc-L-allylglycine, FLAG) was pre-activated in DMF:DIEA (4:1) with HCTU (4 FLAG: 1 HCTU) with a catalytic amount of DMAP for approximately 5 min. After activation, the solution was added to the resin and allowed to shake for at least 5 hours. The solution was then evacuated with positive nitrogen pressure and washed three times with 5 mL DMF. All free amines were then capped with 1 mL acetic anhydride in 5 mL DMF for 30 min. The solution was evacuated by nitrogen pressure and washed three times with 5 mL DMF. Next, the Fmoc protecting group on the growing peptide was removed by incubation with a 50% solution of piperidine in DMF for 30 min and the resin was washed with 5 mL DMF three times. The consecutive amino acid of the growing peptide was then pre-activated in DMF:DIEA (4:1) with HCTU (4 AA: 1 HCTU) for 5 min, added to the resin and allowed to couple for 1.5 hours. The process continued with alternating Fmoc deprotection and coupling was continued until the ninth and final amino acid (FLAG for all) was coupled to the growing peptide chain and the final Fmoc deprotected. Some of this linear peptide (~80 mg resin) was then globally deprotected and cleaved from the resin simultaneously by mixing with a fresh solution of TFA, H_2O and TIS (98:1:1) for 2 hours. The resin was filtered and the filtrate was reduced in vacuo to approximately 1 mL in volume at which point cold ether (~1-2 mL total) was added dropwise while sonicating to precipitate out the peptide. Occasionally, samples needed to precipitate at -20 ºC for at least an hour. The suspensions were then transferred to a 15 mL conical tube and centrifuged at 4,000 rpm, 4 ºC for 7 min. The supernatant was decanted and

the ether was allowed to evaporate, the peptide was then suspended in 1 mL H_2O, aliquoted into 1.5 mL microfuge tubes and frozen prior to lyophilization on a vacuum centrifuge.

General Procedure of RCM on Olefin-Terminated Peptides

Dichloroethane (DCE) was degassed with argon for 5 – 10 min prior to the addition of resin-bound peptide and then brought to reflux at 84 ºC. Hoveyda Grubbs 2nd Generation Catalyst was then added in 10 mol% portions over the course of 24 hours. Approximately 100 equivalents of DMSO was added to the mixture and allowed to reflux for 12 more hours. After the mixture was cooled to RT, the resin was filtered over a frit and washed with 5 mL DMSO, DMF, DCM and MeOH three times each. The peptide was then globally deprotected and cleaved from the resin simultaneously with the addition of a fresh mixture of TFA, TIS and H_2O (98:1:1). The mixture was allowed to rock at RT for 2 hours, after which the beads were filtered off and the filtrate was reduced in vacuo to a volume of approximately 1 mL. Peptides were then precipitated out with the addition of cold ether (~1-2 mL) while sonicating. The suspension was then transferred to a 15 mL conical and centrifuged at 4,000 rpm for 15 min. The supernatant was decanted and the ether was allowed to evaporate. Three to four mL of H_2O was added to the solid and vortexed to resuspend the peptide, the mixture, which was never fully soluble in water was then aliquotted into 1.5 mL microfuge tubes, frozen and lyophilized on a vacuum centrifuge.

General Procedure of HPLC Purification of RCM Treated Peptides

The cyclized peptides were purified using a C_5 reverse phase column (Aldrich) connected to either a Shimadzu LC 10AD HPLC or a LabAlliance Model 500 HPLC with a H_2O/ACN mobile phase supplemented with 0.1% TFA. A flow rate of 2 mL/min was applied and the mobile phase graduated from 40% ACN to 100% ACN over the course of 1 hour. The UV-Vis detection was measured at 280 nm. Two overlapping peaks were collected after approximately 10 min of elution and were isolated as a mixture of cis/trans isomers that were not purified further.

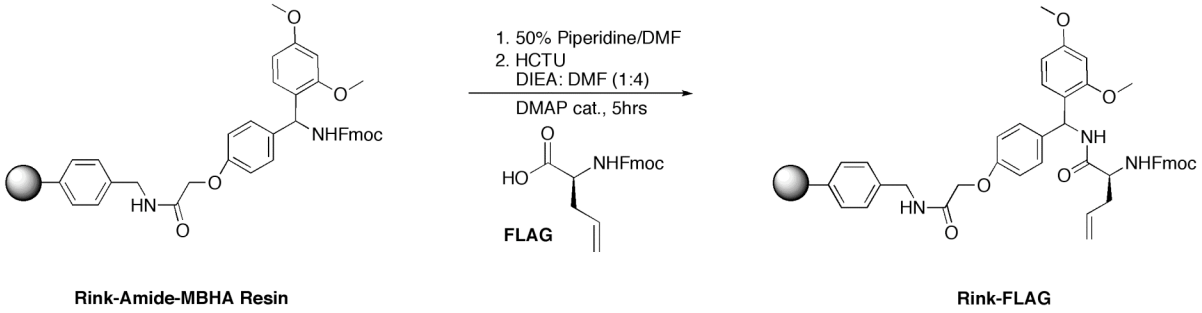

Synthesis of Rink-FLAG

Fmoc-L-allylglycine (FLAG) (300 mg, 0.890 mmol) was preactivated with HCTU (375 mg, 906 mmol) and DMAP (cat.) in 4 mL DMF and 1 mL DIEA for 5 min. It was then added to 500 mg Rink-Amide-MBHA Resin (0.44 meq/g) that had been washed with DCM (3 X 5 mL) and DMF (3 X 7 mL). The coupling reaction was rocked in a Solid Phase Peptide Synthesis reaction vessel for 5 hours. The liquid was then evacuated from the vessel and the resin was washed 4 times with 5 mL DMF. All free amines were then capped with the addition of acetic anhydride (1 mL, 10.6 mmol) in DMF (5 mL) and DIEA (1 mL) for 30 min. The liquid was evacuated from the vessel and the resin was washed with DMF (3 X 5 mL) and DCM (3 X 5 mL) and flushed with nitrogen until dry. Rink-FLAG was stored at 4 ºC until needed for the synthesis of all linear peptides.

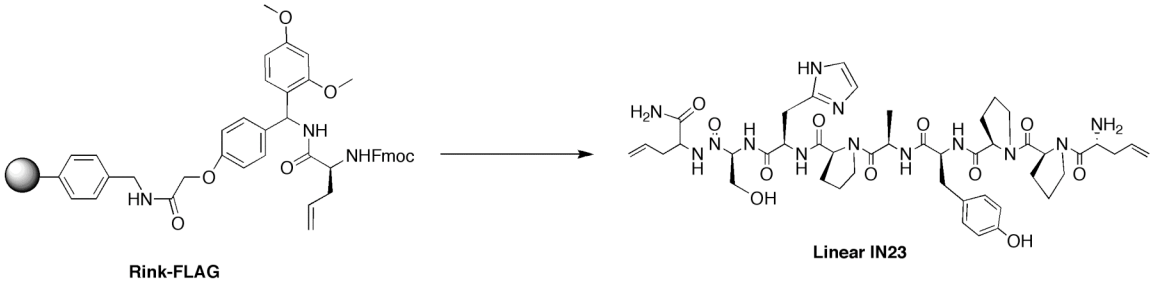

Synthesis of Linear IN23 (allyl-Gly• Pro-Pro-Tyr-Ala-Pro-His-Ser• allyl-Gly)

500 mg of Rink-FLAG was first washed in DCM (3 X 5 mL) then DMF (3 X 5 mL). The Fmoc was then deprotected with a 50% solution of piperidine in DMF (1.5 mL each) for a

period of 20 min. The liquid was then evacuated and the resin was washed with DMF (4 X 6 mL). Fmoc-Ser(tBu)OH (337 mg, 0.880 mmol) was preactivated with HCTU (331 mg, 0.800 mmol) in DMF (4 mL) and DIEA (1 mL) and allowed to couple for 1.5 hours. As outlined in the general peptide synthesis Fmoc deprotection and coupling were alternated until the desired peptide had been synthesized. Couple 2: Fmoc-His(Trt)OH (545 mg, 0.880 mmol) + HCTU (331 mg, 0.800 mmol). Couple 3: Fmoc-Pro-OH (297 mg, 0.880 mmol) + HCTU (331 mg, 0.800 mmol). Couple 4: Fmoc-Ala-OH•H_2O (290 mg, 0.880 mmol) + HCTU (331 mg, 0.800 mmol). Couple 5: Fmoc-Tyr(tBu)OH (404 mg, 0.880 mmol) + HCTU (331 mg, 0.800 mmol). Couple 6: Fmoc-Pro-OH (297 mg, 0.880 mmol) + HCTU (331 mg, 0.800 mmol). Couple 7: Fmoc-Pro-OH (297 mg, 0.880 mmol) + HCTU (331 mg, 0.800 mmol). Couple 8: FLAG (297 mg, 0.880 mmol) + HCTU (331 mg, 0.800 mmol). After final Fmoc deprotection, about 100 mg resin was mixed with a freshly combined solution of TFA (3.92 mL), TIS (40 µL) and H_2O (40 µL) for 2 hours. A white solid was isolated as described in the general method section. H^1 NMR (300 MHz, DMSO) δ 8.96 (s, 1H), δ 8.21 – 7.70 (bm, 5H), δ 7.38 (s, 2H), 7.16 (s, 1H), 6.98 (d, 2H, *J* = 8.1 Hz) 6.61 (d, 2H, *J* = 7.8 Hz) 5.83 – 5.62 (bm, 2H), 5.21 – 4.99 (bm, 4H), 4.59 (bs, 4H), 5.59 – 4.35 (bm, 10 H), 4.28 – 4.05 (bs, 10 H), 3.71 – 3.36 (bm, 13H), 3.11 (m, 2H), 2.98 – 2.89 (bm, 3H), 2.72 (m, 2H), 2.46 – 2.32 (bm, 2H), 1.98 – 1.74 (bm, 16H), 1.29-1.14 (bm, 6H).

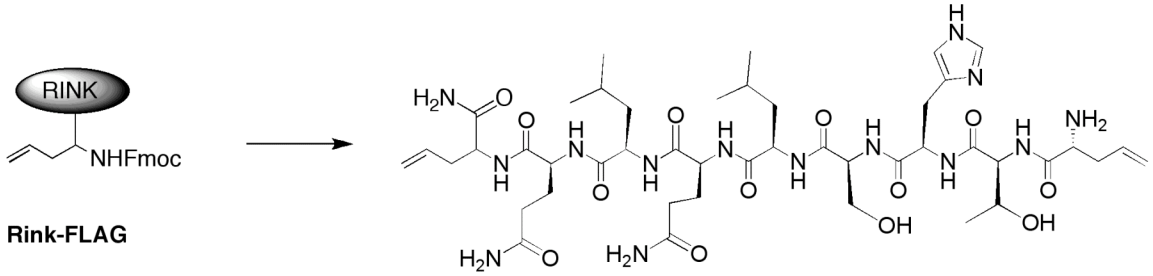

Synthesis of Linear IN8 (allyl-Gly• Thr-His-Ser-Leu-Gln-Leu-Gln• allyl-Gly)

500 mg of Rink-FLAG was first washed in DCM (3 X 5 mL) then DMF (3 X 5 mL). The Fmoc was then deprotected with a 50% solution of piperidine in DMF (1.5 mL each) for a period of 20 min. The liquid was then evacuated and the resin was washed with DMF (4 X 6

mL). Fmoc-Gln(Trt)OH (537 mg, 0.880 mmol) was preactivated with HCTU (331 mg, 0.800 mmol) in DMF (4 mL) and DIEA (1 mL) and allowed to couple for 1.5 hours. As outlined in the general peptide synthesis Fmoc deprotection and coupling were alternated until the desired peptide had been synthesized. Couple 2: Fmoc-Leu-OH (311 mg, 0.880 mmol) + HCTU (331 mg, 0.800 mmol). Couple 3: Fmoc-Gln(Trt)OH (537 mg, 0.880 mmol) + HCTU (331 mg, 0.800 mmol). Couple 4: Fmoc-Leu-OH (311 mg, 0.880 mmol) + HCTU (331 mg, 0.800 mmol). Couple 5: Fmoc-Ser(tBu)OH (337 mg, 0.880 mmol) + HCTU (331 mg, 0.800 mmol). Couple 6: Fmoc-His(Trt)OH (545 mg, 0.880 mmol) + HCTU (331 mg, 0.800 mmol). Couple 7: Fmoc-Thr(tBu)OH (350 mg, 0.880 mmol) + HCTU (331 mg, 0.800 mmol). Couple 8: FLAG (297 mg, 0.880 mmol) + HCTU (331 mg, 0.800 mmol). After final Fmoc deprotection, about 100 mg resin was mixed with a freshly combined solution of TFA (3.92 mL), TIS (40 μL) and H_2O (40 μL) for 2 hours. A white solid was isolated as described in the general method section. H^1 NMR (300 MHz, DMSO) δ 8.96 (s, 1H), δ 8.43 (bs, 1H), δ 8.23 – 8.06 (bm, 6H), 7.94 (s, 2H), 7.80 – 7.60 (bm, 3H), 7.35 – 7.27 (bm, 4H), 7.12 – 7.09 (bm, 2H), 6.81 – 6.78 (bm, 2H), 5.76 – 5.58 (bm, 2H), 5.07 – 4.97 (bm, 4 H), 4.64 (bm, 1 H), 4.31 – 4.19 (bm, 6H), 4.00 – 3.98 (bm, 2H), 3.15 – 3.09 (bm, 2H), 2.88 (s, 2H), 2.72 (s, 2H), 2.45 – 2.27 (bm, 4H), 2.09 – 2.06 (bm, 4H), 1.87 – 1.55 (bm, 9H), 1.43 (s, 5H), 1.25 – 1.10 (bm, 4H), 1.08 (m, 2H), 0.96 (m, 4H), 0.93 – 0.82 (bm, 18H).

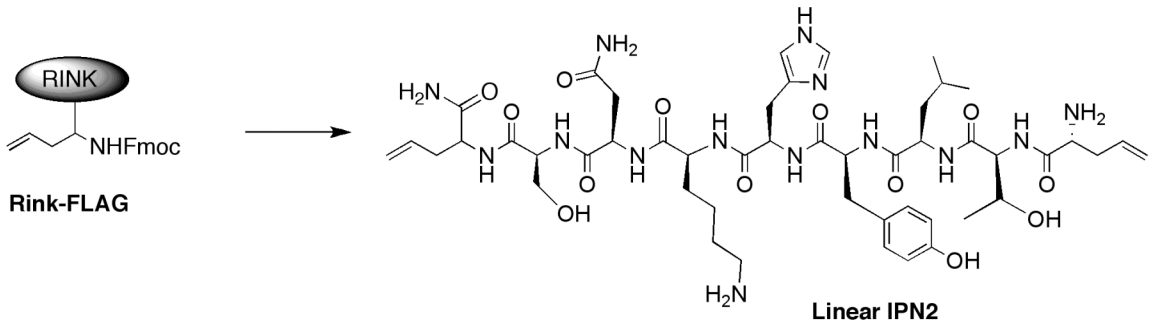

Synthesis of Linear IPN2 (allyl-Gly• Thr-Leu-Tyr-His-Lys-Asn-Ser• allyl-Gly)

500 mg of Rink-FLAG was first washed in DCM (3 X 5 mL) then DMF (3 X 5 mL). The Fmoc was then deprotected with a 50% solution of piperidine in DMF (1.5 mL each) for a

period of 20 min. The liquid was then evacuated and the resin was washed with DMF (4 X 6 mL). Fmoc-Ser(tBu)OH (337 mg, 0.880 mmol) was preactivated with HCTU (331 mg, 0.800 mmol) in DMF (4 mL) and DIEA (1 mL) and allowed to couple for 1.5 hours. As outlined in the general peptide synthesis Fmoc deprotection and coupling were alternated until the desired peptide had been synthesized. Couple 2: Fmoc-Asn(Trt)OH (525 mg, 0.880 mmol) + HCTU (331 mg, 0.800 mmol). Couple 3: Fmoc-Lys(Boc)OH (537 mg, 0.880 mmol) + HCTU (331 mg, 0.800 mmol). Couple 4: Fmoc-His(Trt)OH (545 mg, 0.880 mmol) + HCTU (331 mg, 0.800 mmol). Couple 5: Fmoc-Tyr(tBu)OH (404 mg, 0.880 mmol) + HCTU (331 mg, 0.800 mmol). Couple 6: Fmoc-Leu-OH (311 mg, 0.880 mmol) + HCTU (331 mg, 0.800 mmol). Couple 7: Fmoc-Thr(tBu)OH (350 mg, 0.880 mmol) + HCTU (331 mg, 0.800 mmol). Couple 8: FLAG (297 mg, 0.880 mmol) + HCTU (331 mg, 0.800 mmol). After final Fmoc deprotection, about 100 mg resin was mixed with a freshly combined solution of TFA (3.92 mL), TIS (40 µL) and H_2O (40 µL) for 2 hours. An off white solid was isolated as described in the general method section. H^1 NMR (300 MHz, DMSO) δ 8.96 (s, 1H), δ 8.41 (m, 2H), 8.24 (bm, 4H), 8.00 – 7.94 (m, 3H), 7.80 (bs, 2H), 7.35 (s, 4H), 7.18 – 7.12 (bm, 4H), 7.01 (d, 2H, J = 6.4 Hz), 6.62 (d, 2H, J = 7.8 Hz), 5.69 (m, 2 H), 5.08 – 4.98 (bm, 4 H), 4.56 (m, 2H), 4.28 – 3.92 (bm, 14H), 3.15 – 3.09 (bm, 2H), 2.88 (s, 2H), 2.72 (s, 2H), 2.45 – 2.27 (bm, 4H), 2.09 – 2.06 (bm, 4H), 1.87 – 1.55 (bm, 9H), 1.43 (s, 5H), 1.25 – 1.10 (bm, 4H), 1.08 (m, 2H), 0.96 (m, 4H) 0.93 – 0.82 (bm, 18H).

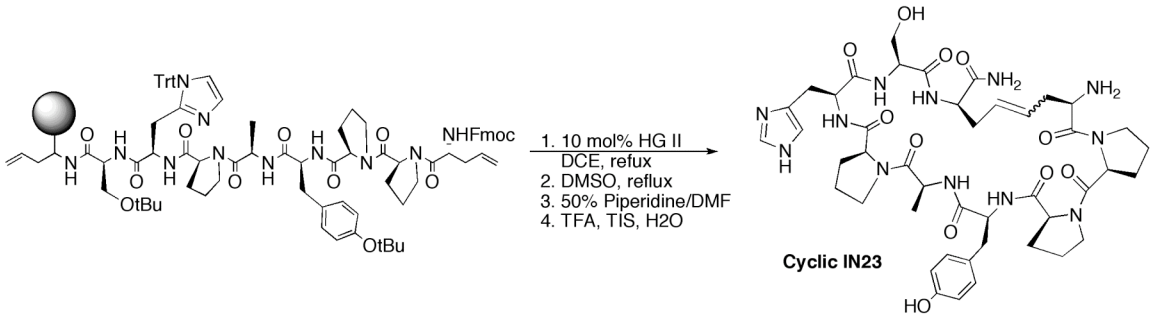

Synthesis of Cyclic IN23

Dichloroethane (4.4 mL) was degassed for 10 min with Ar. Resin bound protected Linear IN23 (110 mg, 48.4 µmol) was added and the suspension was heated to a reflux temperature

of 85 ºC. Hoveyda Grubbs 2nd Generation Catalyst ((1,3-Bis-(2,4,6-trimethylphenyl)-2-imidazolidinylidene)dichloro(*o*-isopropoxyphenylmethylene)ruthen-ium) was added in portions over the course of 24 hrs. Time = 0h, 4 mg, 6.4 µmol; 13h, 3 mg, 4.8 µmol; 15h, 5 mg, 8.0 µmol; 17h, 4 mg, 6.4 µmol; 19h, 2 mg, 3.2 µmol. After 24 hours, DMSO (500 µL, 7.04 mmol) was added and the system maintained reflux for a period of 12 hours. The reaction mixture was cooled to RT and the resin bound peptide was washed over a fritted filter (3 X 15 mL DMF, 3 X 15 mL DCM). During washing, the beads lost most of the original orange color and resembled a very flat brown color when dried under aspiration. The reaction product was then globally deprotected and cleaved from the resin with a fresh cocktail of TFA (3.92 mL, 52.9 mmol), TIS (40 µL, 195 µmol) and H_2O (40 µL, 2.22 mmol) mixed for 2 h. The suspension was filtered over a fritted funnel and rinsed twice with TFA (2 x 1 mL) and the filtrate was concentrated in vacuo until approximately 1 mL of liquid remained. Approximately 3 mL of cold ether was added to precipitate out the peptide. The suspension was transferred to a 15 mL conical and centrifuged at 4,000 rpm for 15 min. The supernatant was then decanted and remaining ether was removed by evaporation.

EMSA of $(CUG)_{54}$ and MBNL-N

Radiolabeled $(CUG)_{54}$ (approximately 5,000 cpm/reaction) was heated to 95 ºC in Annealing Buffer for 5 min and immediately placed on ice to anneal. The reaction was assembled at room temperature with the addition of 1 µL $(CUG)_{54}$, 2.5 µL MBNL-N (various concentrations), 1 µL 10X Binding Buffer and 5.5 µL nuclease free water. The system was allowed to incubate at RT for 30 min. After incubation 10 µL of 2X Native Loading Dye was added, the samples were vortexed briefly and 5 µL was immediately loaded onto an 8% polyacrylamide gel (19:1) prerun for 1 h at 170V in 0.5X TBE. The gel was run for 2 h at 250V, dried for 1 h at 80 ºC and imaged overnight on a phosphor screen (Amersham). The gel was then imaged on a Molecular Dynamics 445-SI phosphorimager.

Competitive EMSA of $(CUG)_{54}$ and MBNL-N with Synthetic Peptides

Radiolabeled $(CUG)_{54}$ was heated to 95 ºC in Annealing Buffer for 5 min and immediately placed on ice to anneal. The reaction was assembled at room temperature with the addition of 1 µL $(CUG)_{54}$, 1 µL peptide, 2.5 µL MBNL, 1 µL 10X Binding Buffer and 4.5 µL nuclease free water. The system was allowed to incubate at RT for 30 min. After incubation 10 µL of 2X Native Loading Dye was added, the samples were vortexed briefly and 5 µL was immediately loaded onto an 8% polyacrylamide gel (19:1) prerun for 1 h at 170V in 0.5X TBE. The gel was run for 2 h at 250V, dried for 1 h at 80 ºC and imaged overnight on a phosphor screen (Amersham). The gel was then imaged on a Molecular Dynamics 445-SI phosphorimager.

REFERENCES

1. H. Steinert, *Dtsch Z Nervenheilkd*, 1909, **37**, 58-104.

2. F. E. Batten and H. P. Gibb, *Brain*, 1909, **32**, 187-205.

3. P. S. Harper, *Myotonic Dystrophy*, W. B. Saunders, London, 2001.

4. E. Gharehbaghi-Schnell, J. Finsterer, I. Korschineck, B. Mamoli and B. R. Binder, *Wien Klin Wochenschr*, 1998, **110**, 7-14.

5. C. Thornton, *Semin Neurol*, 1999, **19**, 25-33.

6. J. D. Brook, M. E. Mccurrach, H. G. Harley, A. J. Buckler, D. Church, H. Aburatani, K. Hunter, V. P. Stanton, J. P. Thirion, T. Hudson, R. Sohn, B. Zemelman, R. G. Snell, S. A. Rundle, S. Crow, J. Davies, P. Shelbourne, J. Buxton, C. Jones, V. Juvonen, K. Johnson, P. S. Harper, D. J. Shaw and D. E. Housman, *Cell*, 1992, **68**, 799-808.

7. Y. H. Fu, A. Pizzuti, R. G. Fenwick, J. King, S. Rajnarayan, P. W. Dunne, J. Dubel, G. A. Nasser, T. Ashizawa, P. Dejong, B. Wieringa, R. Korneluk, M. B. Perryman, H. F. Epstein and C. T. Caskey, *Science*, 1992, **255**, 1256-1258.

8. J. Buxton, P. Shelbourne, J. Davies, C. Jones, T. Vantongeren, C. Aslanidis, P. Dejong, G. Jansen, M. Anvret, B. Riley, R. Williamson and K. Johnson, *Nature*, 1992, **355**, 547-548.

9. M. Mahadevan, C. Tsilfidis, L. Sabourin, G. Shutler, C. Amemiya, G. Jansen, C. Neville, M. Narang, J. Barcelo, K. Ohoy, S. Leblond, J. Earlemacdonald, P. J. Dejong, B. Wieringa and R. G. Korneluk, *Science*, 1992, **255**, 1253-1255.

10. H. G. Harley, J. D. Brook, S. A. Rundle, S. Crow, W. Reardon, A. J. Buckler, P. S. Harper, D. E. Housman and D. J. Shaw, *Nature*, 1992, **355**, 545-546.

11. S. J. Tapscott, *Science*, 2000, **289**, 1701-1702.

12. M. Maeda, C. S. Taft, E. W. Bush, E. Holder, W. M. Bailey, H. Neville, M. B. Perryman and R. D. Bies, *J Biol Chem*, 1995, **270**, 20246-20249.

13. B. Tian, R. J. White, T. B. Xia, S. Welle, D. H. Turner, M. B. Mathews and C. A. Thornton, *Rna*, 2000, **6**, 79-87.

14. K. L. Taneja, M. Mccurrach, M. Schalling, D. Housman and R. H. Singer, *J Cell Biol*, 1995, **128**, 995-1002.

15. B. M. Davis, M. E. McCurrach, K. L. Taneja, R. H. Singer and D. E. Housman, *P Natl Acad Sci USA*, 1997, **94**, 7388-7393.

16. L. T. Timchenko, J. W. Miller, N. A. Timchenko, D. R. DeVore, K. V. Datar, L. J. Lin, R. Roberts, C. T. Caskey and M. S. Swanson, *Nucleic Acids Res*, 1996, **24**, 4407-4414.

17. A. V. Philips, L. T. Timchenko and T. A. Cooper, *Science*, 1998, **280**, 737-741.

18. X. H. Lu, N. A. Timchenko and L. T. Timchenko, *Hum Mol Genet*, 1999, **8**, 53-60.

19. J. W. Miller, C. R. Urbinati, P. Teng-umnuay, M. G. Stenberg, B. J. Byrne, C. A. Thornton and M. S. Swanson, *Embo J*, 2000, **19**, 4439-4448.

20. R. S. Savkur, A. V. Philips and T. A. Cooper, *Nat Genet*, 2001, **29**, 40-47.

21. J. D. Amack, A. P. Paguio and M. S. Mahadevan, *Hum Mol Genet*, 1999, **8**, 1975-1984.

22. A. Mankodi, E. Logigian, L. Callahan, C. McClain, R. White, D. Henderson, M. Krym and C. A. Thornton, *Science*, 2000, **289**, 1769-1772.

23. S. Michalowski, J. W. Miller, C. R. Urbinati, M. Paliouras, M. S. Swanson and J. Griffith, *Nucleic Acids Res*, 1999, **27**, 3534-3542.

24. M. Fardaei, K. Larkin, J. D. Brook and M. G. Hamshere, *Nucleic Acids Res*, 2001, **29**, 2766-2771.

25. T. H. Ho, N. Charlet-B, M. G. Poulos, G. Singh, M. S. Swanson and T. A. Cooper, *Embo J*, 2004, **23**, 3103-3112.

26. M. Fardaei, M. T. Rogers, H. M. Thorpe, K. Larkin, M. G. Hamshere, P. S. Harper and J. D. Brook, *Hum Mol Genet*, 2002, **11**, 805-814.

27. R. N. Kanadia, K. A. Johnstone, A. Mankodi, C. Lungu, C. A. Thornton, D. Esson, A. M. Timmers, W. W. Hauswirth and M. S. Swanson, *Science*, 2003, **302**, 1978-1980.

28. P. C. Gareiss, K. Sobczak, B. R. McNaughton, P. B. Palde, C. A. Thornton and B. L. Miller, *J Am Chem Soc*, 2008, **130**, 16254-16261.

29. B. R. McNaughton and B. L. Miller, *Org Lett*, 2006, **8**, 1803-1806.

30. J. F. Arambula, S. R. Ramisetty, A. M. Baranger and S. C. Zimmerman, *P Natl Acad Sci USA*, 2009, **106**, 16068-16073.

31. H. Kessler, *Angew Chemie Int Ed*, 1982, **21**, 512-523.

32. Y. Yuan, S. A. Compton, K. Sobczak, M. G. Stenberg, C. A. Thornton, J. D. Griffith and M. S. Swanson, *Nucleic Acids Res*, 2007, **35**, 5474-5486.

33. Y. Kino, D. Mori, Y. Oma, Y. Takeshita, N. Sasagawa and S. Ishiura, *Hum Mol Genet*, 2004, **13**, 495-507.

34. M. B. Warf and J. A. Berglund, *Rna*, 2007, **13**, 2238-2251.

APPENDIX

Buffer and Media Recipes

0.7% Agarose Gel Mix: 1.4 g Agarose, 20 mL 10X TBE, 180 mL Millipore purified water. Heat in microwave until agarose has completely dissolved, allow to cool to about 45 ºC and add 50 µL ethidium bromide.

10% APS: 1 g Ammonium Persulfate, 10 mL Millipore purified water

1X Annealing Buffer: 66 mM NaCl, 6.7 mM $MgCl_2$, 27 mM Tris-HCl pH 7.5

1X Protein Storage Buffer: 25 mM Tris, 192 mM Glycine, 1 mM EDTA, 50% glycerol, 0.02% NaN_3

1X TBE Buffer: 89 mM Tris, 89 mM Boric acid, 2 mM EDTA

1X TE Buffer: 10 mM Tris, 1 mM EDTA

1X Tris-Glycine: 25 mM Tris, 192 mM Glycine, pH 8.3

6% RNA/DNA Purification Gel Mix: 240 g Urea (8 M), 75 mL 40% Acrylamide (19:1), 25 mL 10 X TBE, fill to 500 mL with Millipore purified water, place in 37 ºC water bath to dissolve urea and store at 4 ºC.

8% Native EMSA Gel Mix: 2 mL 40% Acrylamide (19:1), 0.5 mL 10X TBE, 7.5 mL Millipore purified water, mix well and polymerize using 100 µL 10% APS and 10 µL TEMED.

8% SDS-PAGE Gel Mix: 2 mL 40% Acrylamide (19:1), 1 mL 10X Tris-Glycine-SDS, 7 mL Millipore purified water, 100 µL 10% APS, 10 µL TEMED

Agarose Top: 20 g/ L LB, 1 g/L $MgCl_2 \cdot 6\ H_2O$, 7 g/L Agarose. Autoclave, store in 50 mL aliquots at RT.

Ampicillin Stock: 10 mg/mL in dd H_2O. Filter sterilize, store at 4ºC.

Binding Buffer: 20 mM Tris-HCl pH = 7.6, 100 mM KCl, 5 mM $MgCl_2$, 0.1 % Triton-X 100

Blocking Buffer: 100 mM $NaHCO_3$ pH = 8.6, 5 mg/ml BSA, 0.02 % NaN_3

Carbenicillin Stock: 50 mg/mL in dd H_2O, Filter sterilize. Store 1 mL aliquots at -20 ºC.

Elution Buffer: 200 mM Glycine-HCl pH = 2.2, 1 mg/ml BSA, filter sterilize and store at 4 ºC

IPTG/XGal Solution: 1.25 g IPTG, 1 g XGal, 25 mL DMF, store in dark at -20 ºC

LB Medium: 10 g Bacto-Tryptone, 5 g Yeast Extract, 5 g NaCl

LB Medium Modified: 10 g Bacto-Tryptone, 5 g Yeast Extract, 10 g NaCl

LB-Agar Amp Plates: 100 mL LB Medium, 1.5 g Agar. Autoclave, cool to 55 ºC. Add 1 mL Ampicillin Stock. Wrap plates in parafilm, store at 4 ºC.

LB-Agar IPTG/XGal Plates: 100 mL LB Medium, 1.5 g Agar. Autoclave, cool to 55 ºC. Add 100 µL IPTG/XGal Solution. Parafilm, store at RT, in dark.

LB-Agar Tet Plates: 100 mL LB Medium, 1.5 g Agar, Autoclave, cool to 55 ºC. Add 100 µL Tetracycline Stock Solution. Parafilm, store at 4 ºC.

NaI Buffer: 10 mM Tris-HCl pH = 8.0, 1 mM EDTA, 4 M NaI. Store at RT in dark.

Neutralizing Solution: 1 M Tris-HCl pH = 9.1

PEG-8000 NaCl Buffer: 20 % (w/v) PEG 8000, 2.5 M NaCl, autoclave, store at RT

TBS Buffer: 50 mM Tris-HCl pH = 7.5, 150 mM NaCl

TBSA Buffer: 50 mM Tris HCl pH = 7.5, 150 mM NaCl, 0.02 % NaN_3

Tetracycline Stock: 20 mg/mL suspension in ethanol, store at -20 ºC.

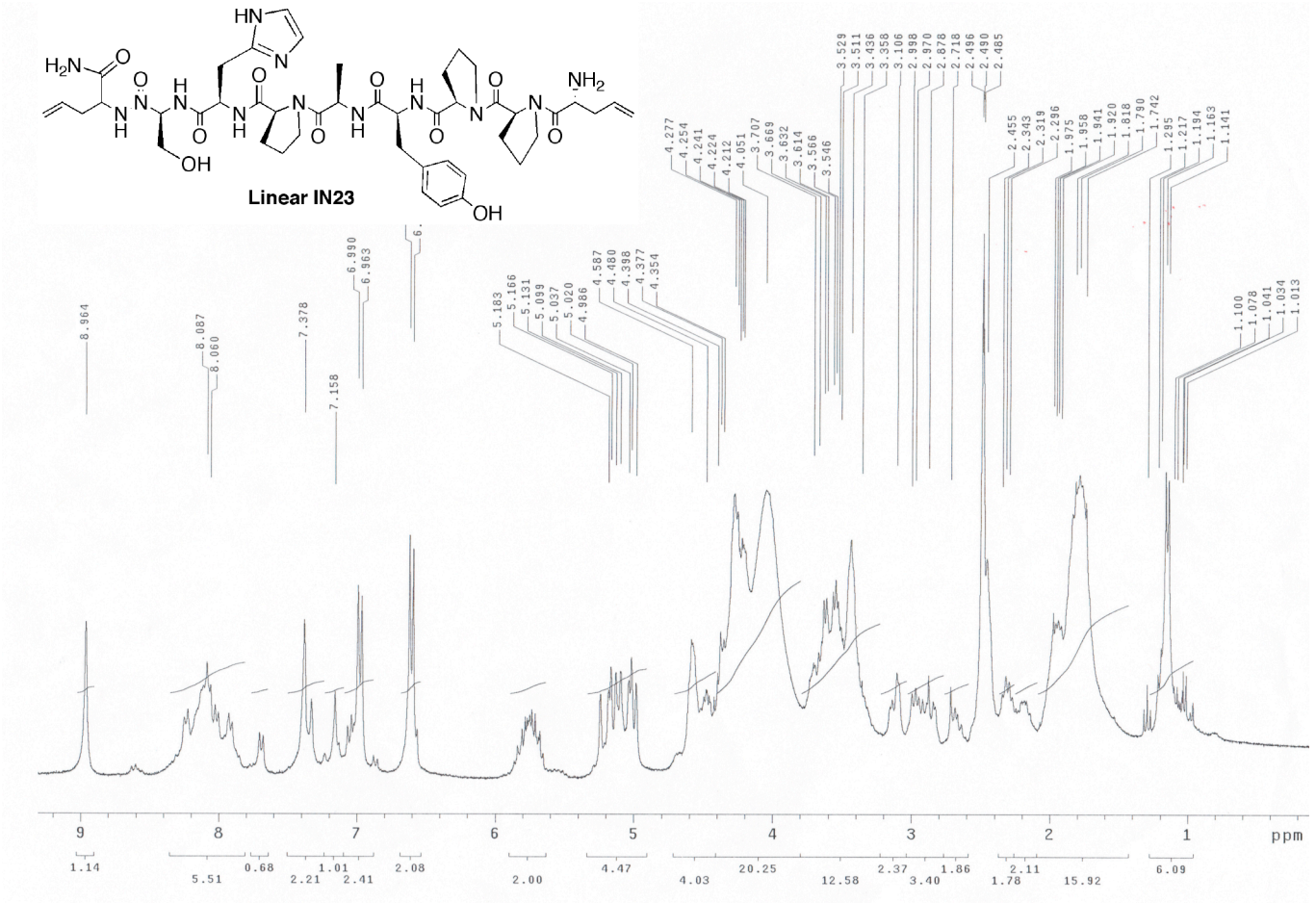
Linear IN23
8.964
8.087
8.060
7.378
7.158
6.990
6.963
5.183
5.166
5.131
5.099
5.037
5.020
4.986
4.587
4.480
4.398
4.377
4.354
4.277
4.254
4.241
4.224
4.212
4.051
3.707
3.669
3.632
3.614
3.566
3.546
3.529
3.511
3.436
3.358
3.106
2.998
2.970
2.878
2.718
2.496
2.490
2.485
2.455
2.343
2.319
2.296
1.975
1.958
1.941
1.920
1.818
1.790
1.742
1.295
1.217
1.194
1.163
1.141
1.100
1.078
1.041
1.034
1.013
9
8
7
6
5
4
3
2
1
ppm
1.14
5.51
0.68
2.21
1.01
2.41
2.08
2.00
4.47
4.03
20.25
12.58
2.37
3.40
1.86
1.78
2.11
15.92
6.09

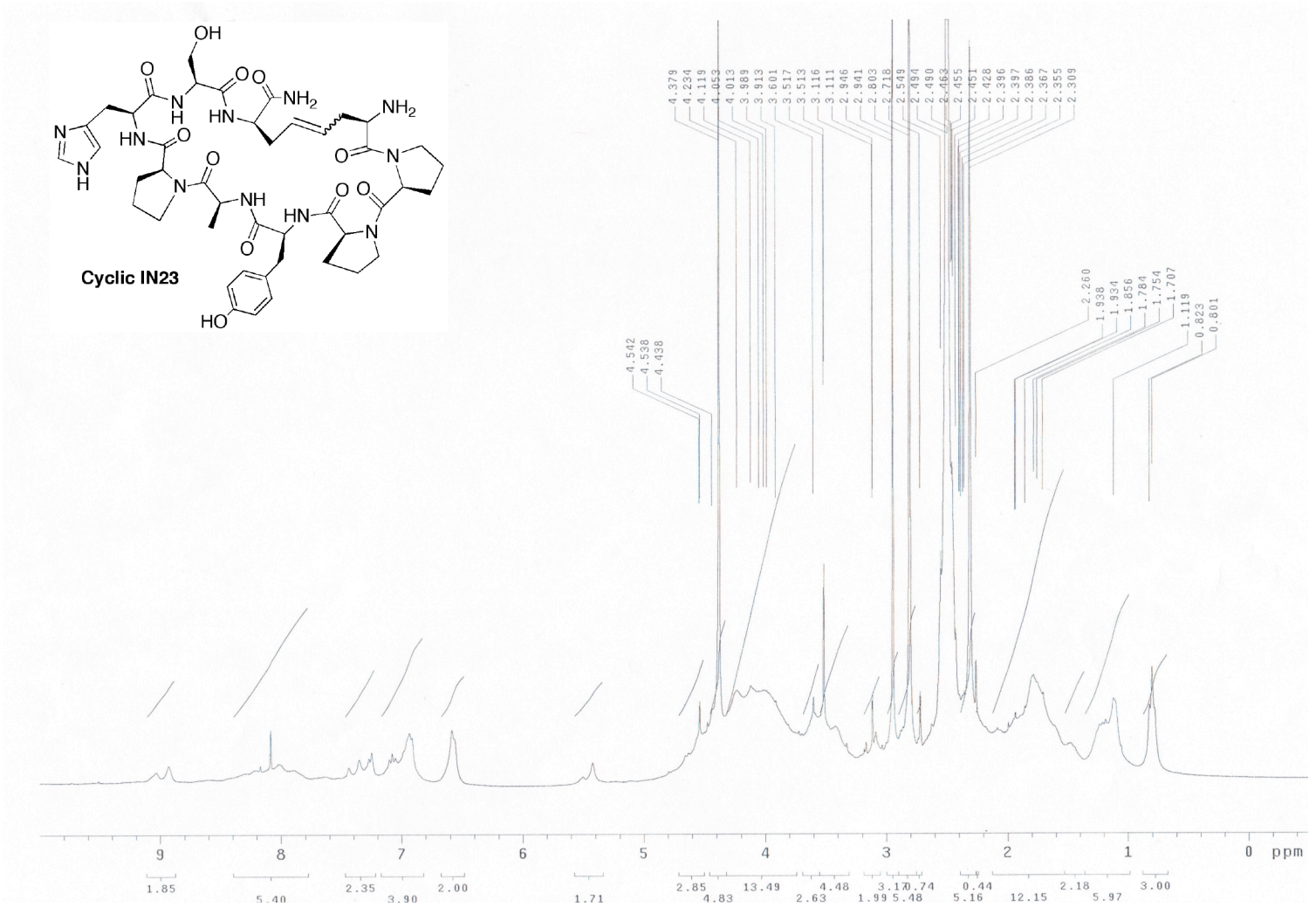
Cyclic IN23
4.379
4.234
4.119
4.053
4.013
3.989
3.913
3.601
3.517
3.513
3.116
3.111
2.946
2.941
2.803
2.718
2.549
2.494
2.490
2.463
2.455
2.451
2.428
2.396
2.397
2.386
2.367
2.355
2.309
4.542
4.538
4.438
2.260
1.938
1.934
1.856
1.784
1.754
1.707
1.119
0.823
0.801
9
8
7
6
5
4
3
2
1
0 ppm
1.85
5.40
2.35
3.90
2.00
1.71
2.85
4.83
13.49
4.48
2.63
3.10
1.99
0.74
5.48
0.44
5.16
2.18
12.15
5.97
3.00

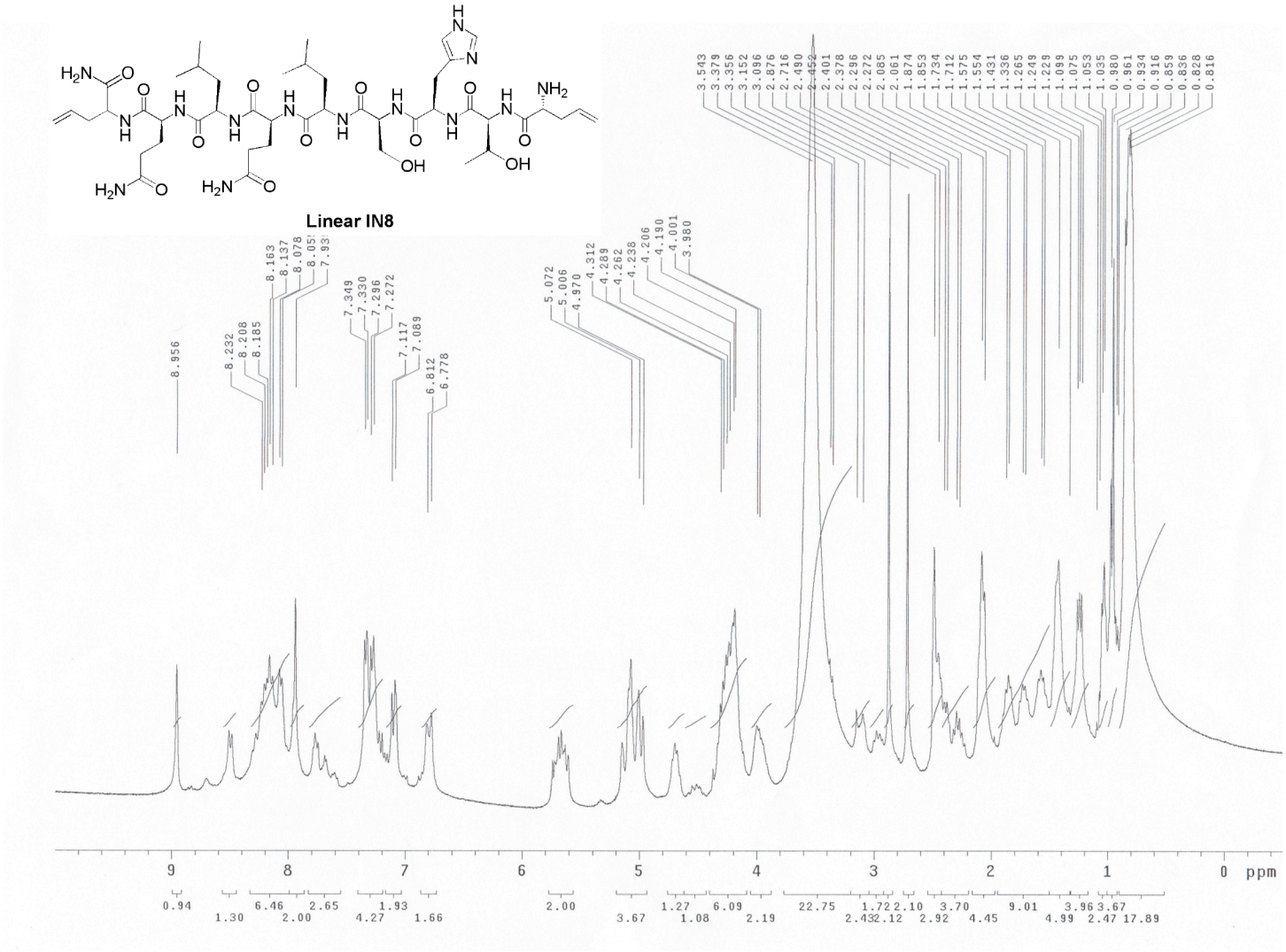
Linear IN8
8.956
8.232
8.208
8.185
8.163
8.137
8.078
8.051
7.933
7.349
7.330
7.296
7.272
7.117
7.089
6.812
6.778
5.072
5.006
4.970
4.312
4.289
4.262
4.238
4.206
4.190
4.001
3.980
3.543
3.379
3.356
3.152
3.096
2.876
2.716
2.490
2.452
2.401
2.378
2.296
2.272
2.085
2.061
1.874
1.853
1.734
1.712
1.575
1.554
1.431
1.336
1.265
1.249
1.229
1.099
1.075
1.053
1.035
0.980
0.961
0.934
0.916
0.859
0.836
0.828
0.816
9
8
7
6
5
4
3
2
1
0
ppm
0.94
1.30
6.46
2.00
2.65
4.27
1.93
1.66
2.00
3.67
1.27
1.08
6.09
2.19
22.75
2.43
1.72
2.12
2.10
2.92
3.70
4.45
9.01
4.99
3.96
2.47
3.67
17.89

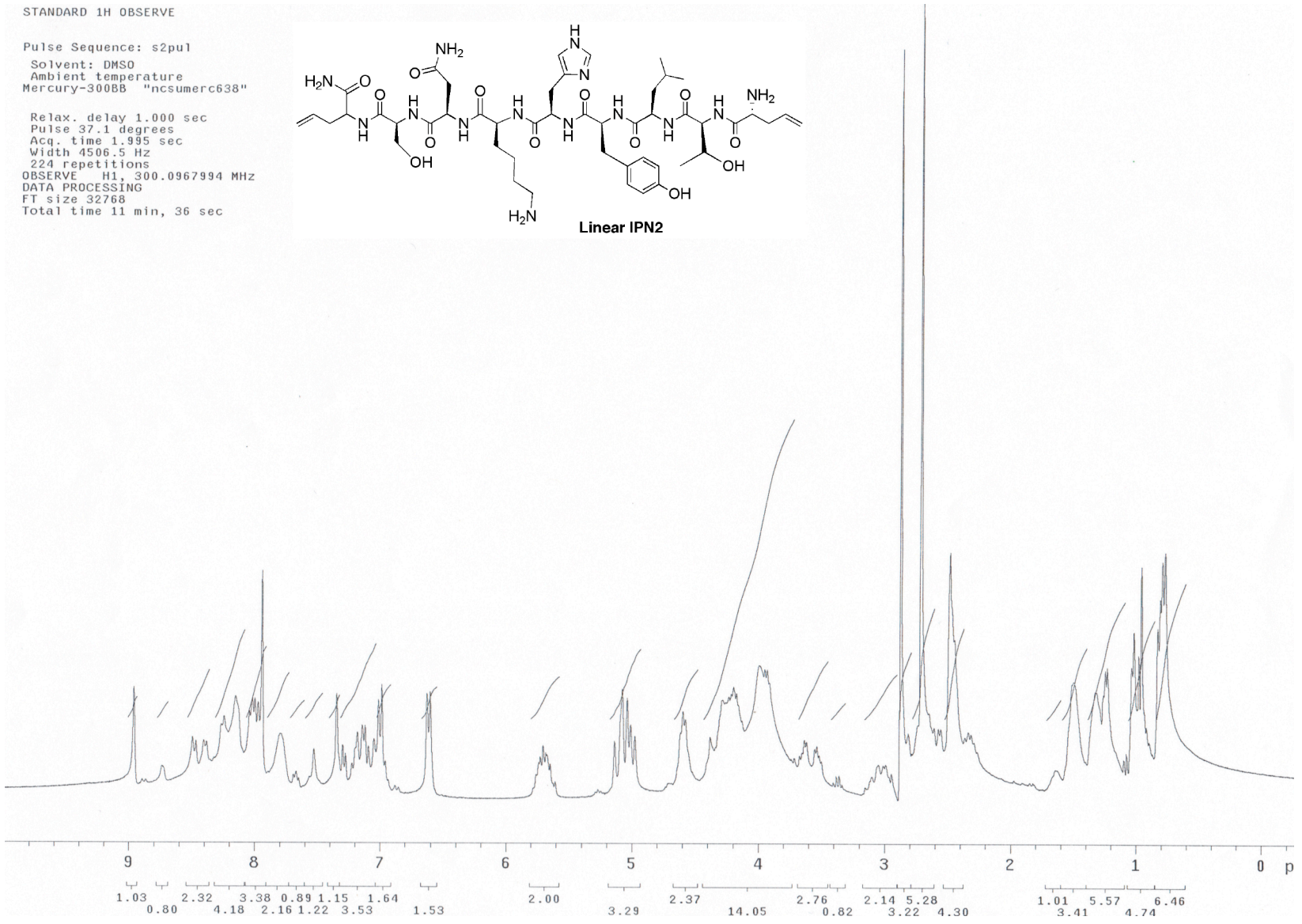
STANDARD 1H OBSERVE
Pulse Sequence: s2pul
Solvent: DMSO
Ambient temperature
Mercury-300BB "ncsumerc638"
Relax. delay 1.000 sec
Pulse 37.1 degrees
Acq. time 1.995 sec
Width 4506.5 Hz
224 repetitions
OBSERVE H1, 300.0967994 MHz
DATA PROCESSING
FT size 32768
Total time 11 min, 36 sec
Linear IPN2
9 8 7 6 5 4 3 2 1 0 p
1.03 0.80 2.32 4.18 3.38 2.16 0.89 1.15 1.22 1.64 3.53 1.53 2.00 3.29 2.37 14.05 2.76 0.82 2.14 5.28 3.22 4.30 1.01 3.41 5.57 4.74 6.46

CHAPTER 2

Kinamycin D Mediated DNA Cleavage

2.1 Introduction

The kinamycins (**Figure 8**) are a complex class of natural products characterized by an uncommon diazobenzo[*b*]fluorene skeleton. Upon isolation of kinamycins A – D from *Streptomyces murayamaensis* in 1970[1] these secondary metabolites were characterized as cyanobenzo[*b*]carbazoles.[2] The structural assignments were later revised to diazobenzo[*b*]fluorenes only after attempts at total synthesis yielded spectral data that did not coincide with that of the isolated natural products.[3, 4] This structural motif was recognized again after the isolation and characterization of the lomaiviticin natural products, which are glycosylated diazobenzo[*b*]fluorene dimers.[5] This discovery promoted an intensified interest in the total synthesis and mechanism by which these classes of natural products elicit their biological activity.

Both families of natural products were discovered to possess potent antibiotic and antitumor activities. Upon isolation, kinamycins A – D were found to be effective antibiotics against gram-positive bacteria and to a lesser extent, gram-negative bacteria.[1] Kinamycin A and C possess anti-proliferative activity against Chinese hamster ovary (CHO) and K562 cell lines.[6] In addition, previous work in this laboratory has shown that simple electronically tuned diazofluorene analogs possess antiproliferative activity against HeLa cells.[7] Similarly potent biological activity is seen in the dimeric lomaiviticin family as well. A cytotoxicity profile[5] of lomaiviticin A shown in **Table 2** indicates a wide range of cancer cell lines that are effected by lomaiviticin A with inhibitory concentrations at 50% (IC_{50}) ranging from 7 pM to 49 nM.

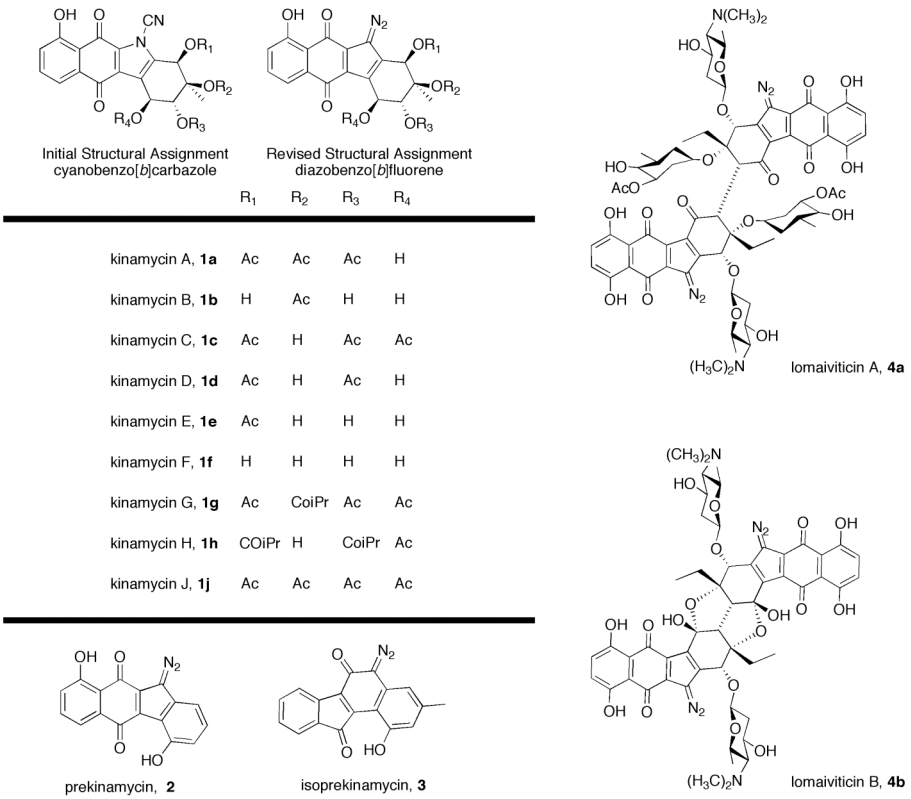

Figure 8. Representative kinamycins and lomaiviticins.

Table 2. Cytotoxicity profile of lomaiviticin A.[5]

Cell Line	IC_{50} (ng/mL)	Cell Line	IC_{50} (ng/mL)	Cell Line	IC_{50} (ng/mL)
colon cancer		*ovarian cancer*		*brain cancer*	
MCF7	36	A2780DDP	6.5	T47D	25
CCL228	8.9	A2780S	0.01	B7474	37
SW948	62	HTB161	0.01	SKBR3	35
LS174T	0.97	*prostate cancer*		*lung cancer*	
HCT15	8.2	LNCAP	0.55	A549	4.8
CACO2	98	RC3	70	LX1	7.4
CX1	80	DU145	0.92	*leukemia*	
COLO205	13	*melanoma*		CCRFCEM	0.5
SW620	6.3	SKMEL303	10	HL60	0.9
MIP	34	LOX	3.1		

2.2 Previous MOA Studies: Model Systems

The uniqueness and potency of the diazo containing natural products has attracted many theories regarding their biological mode of action (MOA). Upon the discovery of their DNA cleaving potential many researchers developed mechanistic proposals to account for this behavior. Early work included thermal and light induced decomposition and activation with cuprous salts. Although these explanations offered mechanistic insight into the behavior of diazo containing molecules, they could not explain the antibacterial and cytotoxic biological properties where these activators are not present.

2.2.1 Oxidative Activation Mechanism

Arya and Jebartanam originally speculated an oxidative activation to account for DNA damage when treated with diazo-containing small molecules. This hypothesis was tested by employing a plasmid relaxation assay by incubating pBR322 DNA with two model kinamycin substrates in the presence or absence of $Cu(OAc)_2$, AgOAc, $Tl(OAc)_3$ and $Hg(OAc)_2$. Both 9-diazofluorene **5** and β-napthylphenyl diazomethane **6** were observed to generate DNA cleavage, but only when treated with cupric acetate. This result supported their mechanistic proposal that Cu(II) could oxidize the diazo substrate and through the loss

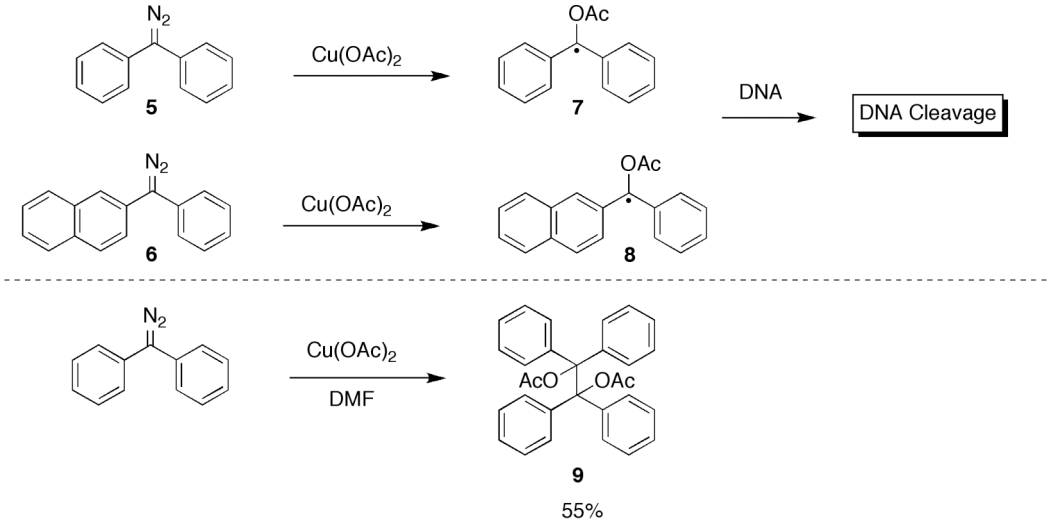

Scheme 3. Jebartanam's oxidative activation hypothesis.

of N_2 yield a fluorenyl acetate radical that could lead to DNA damage (**Scheme 3**). This theory was supported by earlier work which indicated that the dimerization product of this radical, a fluoreneone pinacol diacetate, was the major reaction product of metal catalyzed decomposition of **5**.[8]

2.2.2 Electrophilic Activation Mechanism

Dmietrienko offered the second kinamycin MOA postulate as a manifestation of the electrophilicity of the diazo group. Through comparison of calculated IR stretching frequencies for various diazo compounds they speculated a trend of enhanced diazonium ion character with the availability of an intramolecular hydrogen-bonding network. To this end, they tested the relative electrophilicities of the diazo group of isoprekinamycin (**10**) and **11** by treating them with β-naphthol and Cs_2CO_3. As shown in **Scheme 4**, both substrates were subjects of nucleophilic attack; however, only **10** underwent H atom abstraction. They rationalized that the enhanced electrophilicity of the kinamycin diazo group could provide a substrate for nucleophilic attack by DNA purines, which upon decomposition would lead to radical formation and DNA strand scission through known pathways.[9, 10]

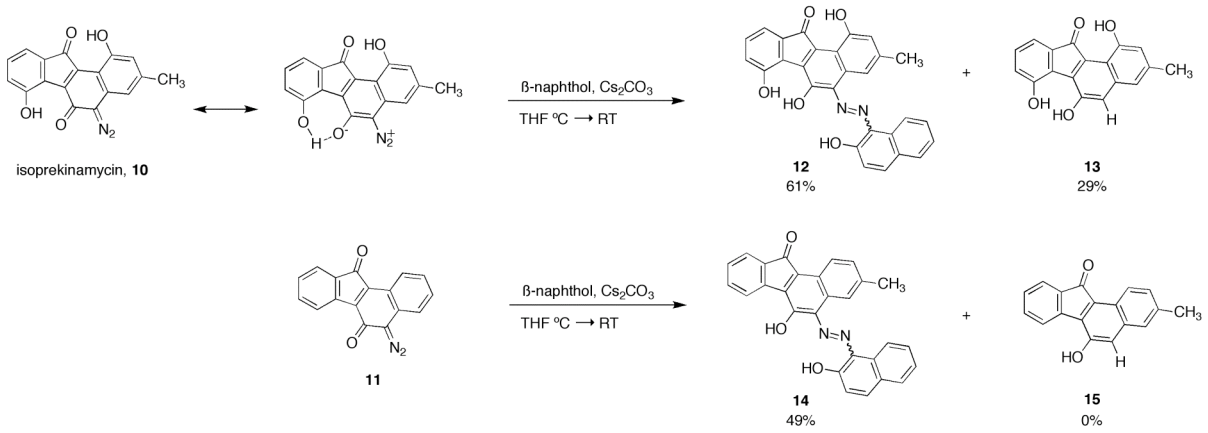

Scheme 4. Dmietrienko's supporting data for an electrophilic activation.

2.2.3 Reductive Activation Mechanism

Feldman and Eastman provided an alternative hypothesis that reductive activation of the kinamycins accounted for their biological activity. They speculated a single electron

reduction to the corresponding semiquinone and concomitant loss of N_2 to provide a cyclopentenyl radical that could be capable of H atom abstraction to an orthoquinone methide and subsequent DNA base alkylation (**Figure 9**).

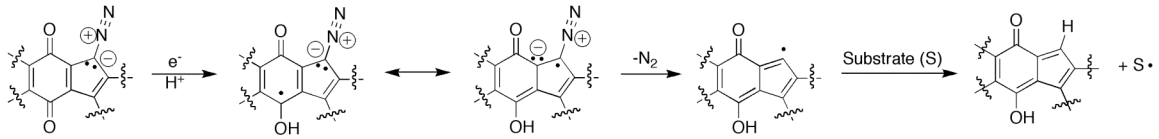

Figure 9. Feldman's reductive activation mechanism.

They observed the single electron reductive chemistry of prekinamycin (**16**) upon treatment with the radical initiator AIBN and Bu_3SnH in refluxing deuterobenzene (**Scheme 5**). To their surprise, they did not isolate an orthoquinone methide unit, but a radically trapped deuterobenzene at the reactive center instead. Given, the very modest reactivity of benzene, they could not differentiate the mechanistic rationale (carbene, carbocation/orthoquinone methide equivalent or radical) for the reactive intermediate. They attempted to further elucidate the role of the reactive intermediate by employing selenium and sulfur nucleophiles as a supplement to their reaction conditions. One example is depicted below in **Scheme 5** where prekinamycin derivative **17** was reacted with Se_2Ph_2 in benzene. The product distribution shows a radical trapped arene product (**20**) as observed previously in addition to a phenylselenyl adduct they infer as evidence of an orthoquinone methide reactive intermediate. Although reductive activation seems a likely trigger for biological activity, the reactivity demonstrated in this work could only be accomplished with the use of aromatic solvents. While this provides further knowledge of the reductive chemistry of diazoparaquinones, there is no biological basis for the methods employed in this investigation.

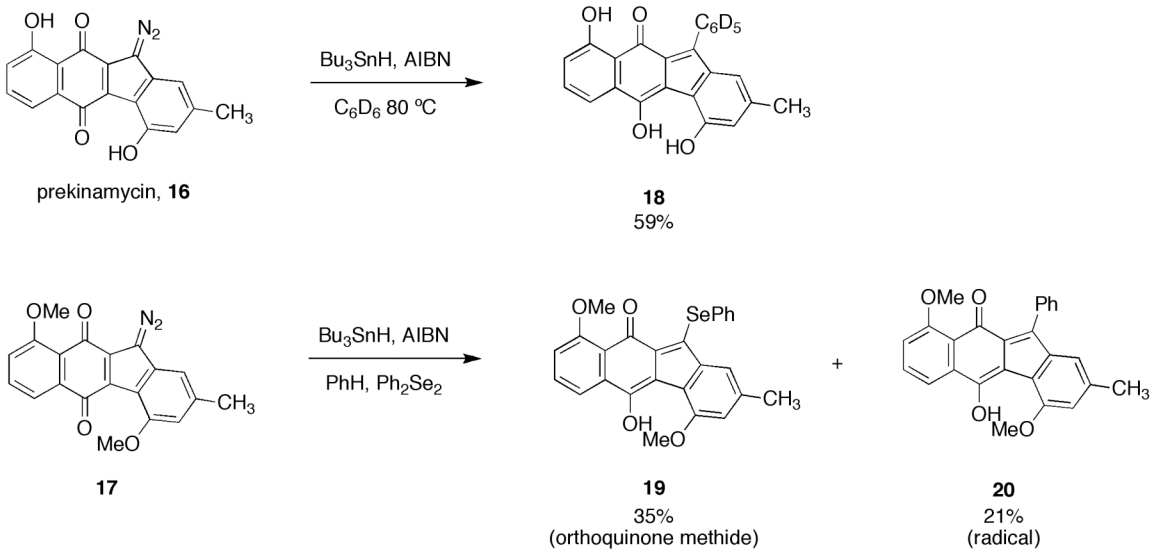

Scheme 5. Feldman's reductive activation supporting data.

2.3 Previous MOA Studies: Biomimetic Approaches

Although the postulates presented in connection with the diazo model studies described above had insightful rationale, none of them were directly applicable to a biological environment. The initial report disclosing the isolation of lomaiviticin A also revealed the ability of lomaiviticin A to cleave DNA under reducing conditions; however, experimental details were not presented.[5] Given this result and considering components of the cellular environment, it seemed more reasonable that biological thiols (e.g. glutathione, GSH) were capable of inducing a $2H^+/2e^-$ reduction from diazoparaquinones to the corresponding hydroquinones to initiate the biological cascade of activity.

2.3.1 Biomimetic DNA Cleavage Mediated by Kinamycin D

Dr. T. Eric Ballard, a former student in the Melander laboratory, performed the initial biomimetic investigations into kinamycin mediated DNA cleavage. In addition to recapitulating DNA cleavage activity with simple electronically tuned diazofluorenes,[7] he was able to report the first account of biomimetic DNA cleavage mediated by kinamycin D using a plasmid relaxation assay.[11] Ballard demonstrated that kinamycin D was able to nick pBR322 DNA in the presence of both GSH and dithiothreitol (DTT) at 37 ºC during 24 – 48

hour periods. Control experiments using only GSH/DTT or kinamycin D demonstrated no evidence of DNA cleavage, supporting a $2H^+/2e^-$ reduction *in vivo*. Two mechanistic possibilities were proposed to account for the observed DNA cleavage mediated by a $2H^+/2e^-$ reduction of kinamycin D treated with GSH/DTT (**Figure 10**), which paralleled the previously proposed mechanisms. One possibility (**Figure 10**, Route A) proposed the resultant hydroquinone would be activated towards nucleophilic attack on the terminal diazo nitrogen, this nucleophilic adduct would then undergo homolytic bond cleavage to provide a carbon centered radical that could elicit DNA damage. The alternative possibility (**Figure 10**, Route B) proposed that protonation would promote the formation of an orthoquinone methide reactive intermediate with concomitant loss of N_2.

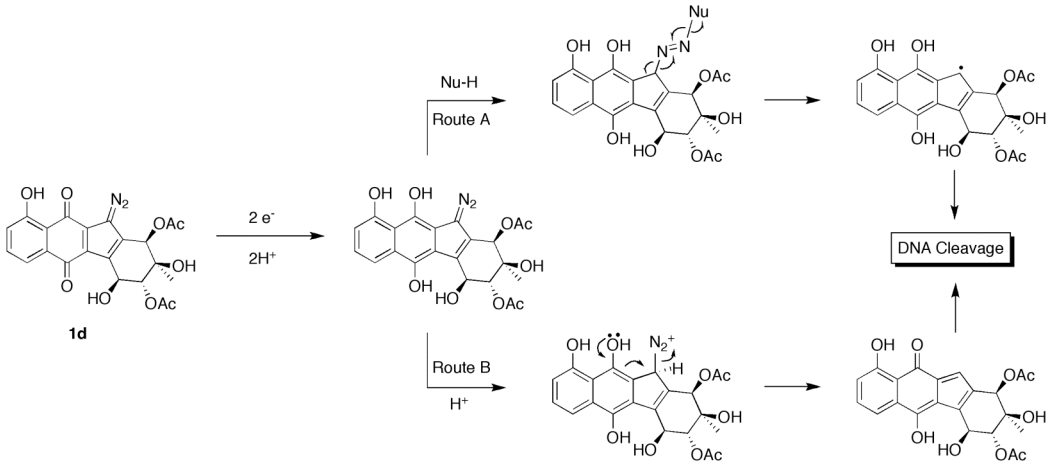

Figure 10. Potential routes to DNA cleavage.

2.3.2 Biomimetic DNA Cleavage Mediated by Kinamycin F

Recently, in an extensive *in vivo* study,[12] Hasinoff demonstrated that kinamycin F was also able to cleave DNA when treated with cellularly relevant concentrations of GSH. Furthermore, the DNA-cleavage exhibited upon treatment of kinamycin F with GSH was determined occur in an iron-, H_2O_2- and hydroxyl-radical-dependent manner. Kinamycin F was also found to induce DNA strand cleavage in cell culture experiments with K562 cells. Finally, EPR studies indicated that kinamycin F was capable of generating air-stable free

radicals in the presence of GSH. These results appear consistent with the $2H^+/2e^-$ reduction followed by nucleophilic activation mechanism originally proposed (**Figure 10**, Route A).

2.4 Current MOA Examination of Kinamycin D Mediated DNA Cleavage

The revelation that GSH and DTT could both promote kinamycin D mediated DNA cleavage prompted us to investigate the mechanistic consequences upon diazoparaquinone reduction. In order to further elucidate the mechanism by which the kinamycins mediate DNA damage, we employed manual DNA sequencing gel electrophoresis to analyze the pattern of kinamycin D mediated DNA cleavage under a variety of conditions. Given that proton transfer is involved in both mechanisms we recently proposed (**Figure 10**), we first chose to confirm the effect of pH on the ability of kinamycin D to cleave DNA under reducing conditions. Previous results from our group have demonstrated that both DTT and GSH promote kinamycin D mediated DNA cleavage in an identical manner; therefore, we chose to simply employ DTT in this study.[11] Phosphate buffered solutions containing 5.7 mM DTT were incubated with 100 μM kinamycin D and a 175-mer radiolabeled DNA (approximately 10,000 cpm/reaction) at a pH range of 5.5 – 8.0 at 37 ºC. The results of this assay (**Figure 11**, Gel A) clearly illustrate the reaction is favored in acidic media as indicated by the sharp decrease in the amount of full length DNA as pH is lowered. At the two lowest pH's tested (5.5 and 6.0) the extent of DNA damage was so severe that only a small amount of full length DNA template remained intact, while the majority of the DNA was cleaved multiple times into small fragments that ran at the bottom/off of the gel. Given that tumors can have acidic microenvironments in comparison to surrounding tissue,[13] we found this result promising for the use of kinamycin D as a cancer therapeutic.

Given that DNA sequencing gel electrophoresis relies on generating single strand breaks into subpopulations of DNA, the extensive DNA damage observed at 37 ºC and pH 5.5 made reaction analysis difficult to interpret. Therefore, reactions were also performed at room

temperature and the general reaction pH was chosen as 6.0 to facilitate interpretation of the electrophoretic radiograms.

After confirming that DNA cleavage preferentially occurred at acidic pH, we sought to investigate the lower limit of kinamycin D concentration that could elicit a measurable cleavage response. Incubations were performed in 5 mM phosphate buffer, 50 mM DTT at pH 6.0 with kinamycin D concentrations ranging from 50 μM – 1 μM. Significant DNA cleavage was observed when treated with as little as 10 μM kinamycin D, and minimal observable cleavage was promoted with 1 μM Kinamycin D (**Figure 11**, Gel B).

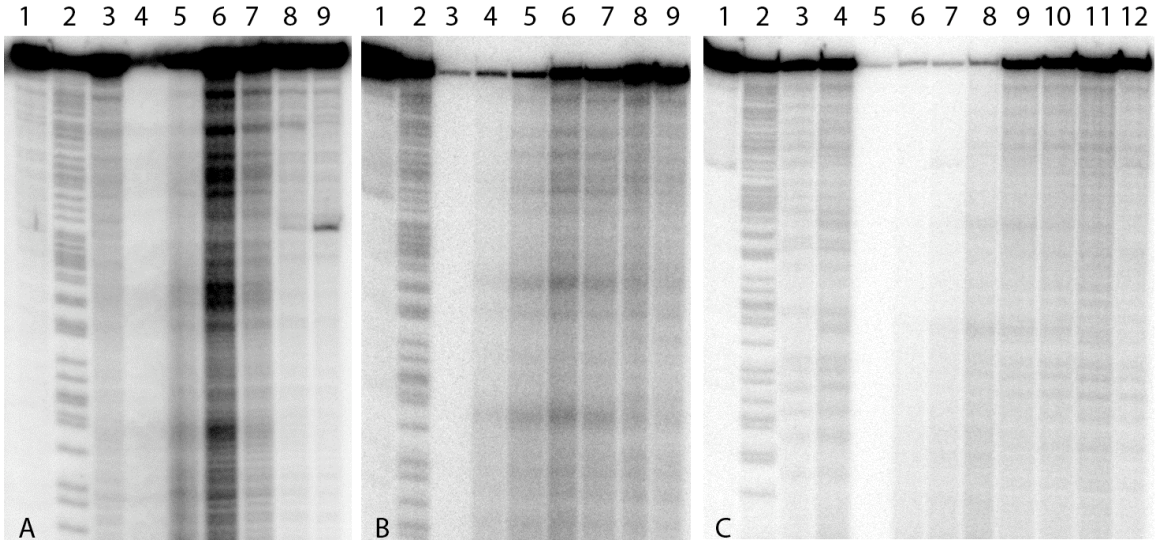

Figure 11. DNA sequencing gel electrophoretic radiograms. **A.** pH Dependence of DNA Cleavage. Lane 1: DNA, Lane 2: G+A ladder, Lane 3: DNA + 5.7 mM DTT, Lane 4: DNA + 5.7 mM DTT + 100 μM Kin D (standard rxn) pH 5.5, Lane 5: standard rxn pH 6.0, Lane 6: standard rxn pH 6.5, Lane 7: standard rxn pH 7.0, Lane 8: standard rxn pH 7.5, Lane 9: standard rxn pH 8.0. **B.** Effect of [Kin D] on DNA Cleavage at 50 mM DTT, pH 6.0 37 ºC 16 h. Lane 1: DNA stock, Lane 2: G+A, Lane 3: 50 μM Kin D + DTT, Lane 4: 20 μM Kin D + DTT, Lane 5: 10 μM Kin D + DTT, Lane 6: 5 μM Kin D + DTT, Lane 7: 2 μM Kin D + DTT, Lane 8: 1 μM Kin D + DTT, Lane 9: DNA + DTT only. Gel C: Effect of [DTT] on DNA Cleavage at 50 μM Kin D pH 6.0 37 ºC 15 h. Lane 1: DNA stock, Lane 2: G+A, Lane 3: 500 mM DTT, Lane 4: 500 mM DTT + Kin D, Lane 5: 50 mM DTT + Kin D, Lane 6: 20 mM DTT + Kin D, Lane 7: 10 mM DTT + Kin D, Lane 8: 5 mM DTT + Kin D, Lane 9: 2 mM DTT + Kin D, Lane 10: 1 mM DTT + Kin D, Lane 11: 500 μM DTT + Kin D, Lane 12: Kin D.

In addition to exploring the effects of kinamycin D concentration we wanted to reconfirm the effect DTT concentration had upon the cleavage reactions. Therefore, we chose to investigate

a wide range of thiol concentrations from 500 mM – 500 μM. We discovered that DTT concentrations as low as 5 mM were effective at promoting cleavage of the majority of DNA template when treated with 50 μM kinamycin D. However, the upper limit of 500 mM DTT was actually shown to inhibit DNA cleavage (**Figure 11**, Gel C). This result also parallels the recent work of Hasinoff, which indicated that reduced intracellular GSH levels increased the cytotoxicity of Kinamycin F and increased GSH levels decreased cytotoxicity.[12] The concentration dependent cleavage trend we observe with DTT coupled with Hasinoff's EPR studies suggest that kinamycin D mediates DNA cleavage via a radical based mechanism, where low concentrations of DTT can promote the formation of a reactive radical intermediate, whereas at higher concentrations it is capable of quenching the activity of the reactive intermediates capable of inducing DNA damage.

The radical based mechanism postulated is also supported by the lack of sequence specific DNA cleavage products. Although the electrophoretic radiograms indicate general DNA cleavage at every position in the oligonucleotide, these observations could not rule out the possibility that kinamycin D could alkylate DNA as well. Therefore, we subjected the reaction products to heat lability and hot piperidine treatment to generate strand breaks on any DNA base modified through alkylation as shown previously with quinone methides.[14] These experiments did not promote the formation of any additional DNA cleavage products demonstrating that kinamycin D does not appear to alkylate DNA under our reaction conditions (**Figure 12**, Gel A).

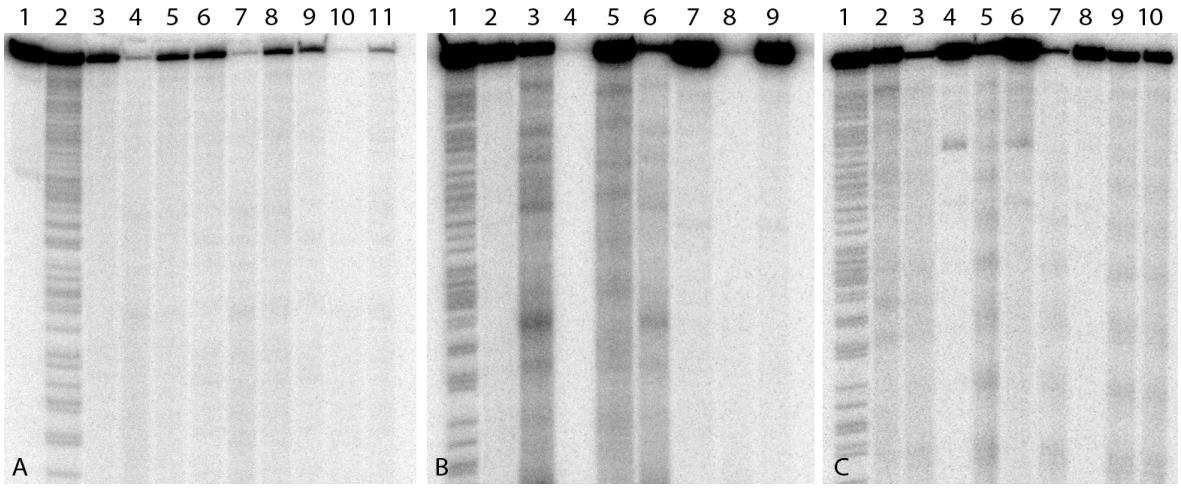

Figure 12. DNA sequencing gel electrophoretic radiograms. **A.** Piperidine and Heat Lability Assay for DNA Alkylation @ 5 mM DTT, 100 µM Kin D, pH 6.0, 37 ºC, 15h. Lane 1: DNA, Lane 2: G+A, Lane 3: Kin D only, Lane 4: Kin D + DTT, Lane 5: DTT only, Lane 6: Kin D, 70 ºC, 2h, Lane 7: Kin D + DTT, 70 ºC, 2h, Lane 8: DTT, 70 ºC, 2h, Lane 9: Kin D, piperidine, Lane 10: Kin D + DTT + piperidine, Lane 11: DTT + piperidine. **B.** Hydroxyl Radical Scavenger Assay. Hydroxyl Radical Scavenger Assay. Lane 1: G + A ladder, Lane 2: DNA + 100 µM Kin D + 50 mM DTT (standard rxn pH 6.0) + 100 mM NaN_3, Lane 3: standard rxn + 100 mM MeOH, Lane 4: standard rxn + 100 mM glycerol, Lane 5: standard rxn + 100 mM thiourea, Lane 6: standard rxn + 100 mM DMSO, Lane 7: standard rxn + 100 µM desferoxamine, Lane 8: standard rxn, Lane 9: DNA + DTT. **C.** ROS Assay. Lane 1: G+A ladder, Lane 2: DNA + 50 mM DTT, Lane 3: DNA + 100 µM Kin D + 50 mM DTT (standard rxn), Lane 4: standard rxn + 1 U CAT, Lane 5: standard rxn + 3 U SOD, Lane 6: standard rxn + CAT (95 ºC, 10 m), Lane 7: standard rxn + SOD (95 ºC 10 m), Lane 8: standard rxn + CAT-trypsin, Lane 9: standard rxn + SOD-trypsin, Lane 10: standard rxn + trypsin.

Given the generic DNA cleavage pattern exhibited with kinamycin D under our reaction conditions and Hasinoff's earlier results indicating that trace iron is important for kinamycin F mediated DNA cleavage, we hypothesized that the general DNA cleavage promoted by kinamcyin D under reducing and acidic conditions was symptomatic of a general diffusible reactive oxygen species (ROS). To test this hypothesis, we first explored the effects of introducing EDTA, a generic metal chelator, to the reaction system. At the lowest concentration tested, 20 µM EDTA was able to completely suppress DNA degradation when treated with 100 µM kinamycin D and 50 mM DTT at pH 6.0 incubated for 14 h at 37 ºC. The ability of EDTA to suppress this reaction through chelation seemed promising; however, it did not reveal which trace metal was responsible for catalyzing this behavior. Therefore we introduced desferoxamine, an Fe^{3+} chelator to our reaction system to indicate whether iron

has a specific role in promoting DNA damage (**Figure 12**, Gel B). Paralleling the results with kinamycin F, kinamycin D did not induce any amount of DNA cleavage when treated with 50 μM desferoxamine, highlighting the importance of trace iron and the catalytic role it plays in kinamycin D mediated DNA cleavage. A variety of hydroxyl radical scavengers (100 mM) were also employed to further clarify the reaction mechanism.[15] Glycerol was the only scavenger shown to have no inhibitory effect while DMSO had modest inhibitory activity; however sodium azide prevented nearly all DNA degradation and thiourea and methanol, prevented a majority of degradation as well. The ability of these hydroxyl radical scavengers to inhibit DNA cleavage further supports the involvement of ROS.

Given that the ROS in our reaction system is most likely superoxide and or hydrogen peroxide and kinamyicin F mediated DNA cleavage is inhibited by catalase, we explored the necessity of either species to mediate DNA cleavage. The enzymes catalase (CAT) and superoxide dismutase (SOD) catalyze the dismutation of hydrogen peroxide (1) and superoxide (2) respectively.

(1) $H_2O_2 \rightarrow H_2O + ½\ O_2$

(2) $H_2O + O_2^- \rightarrow H_2O_2 + ½\ O_2$

As with kinamycin F, CAT completely inhibited DNA cleavage when treated with 100 μM kinamycin D and 50 mM DTT at pH 6.0 emphasizing that the production of hydrogen peroxide is crucial in generating DNA damage (**Figure 12**, Gel C). Superoxide dismutase was shown to slightly inhibit the cleavage reaction; however the optimum pH for SOD activity is 8.0, which could explain the limited DNA cleavage seen upon SOD treatment. When each enzyme was heated to 95 ºC for 10 min, CAT retained the ability to prevent DNA cleavage (unlike kinamycin F) suggesting a possible nonspecific interaction between the enzyme and the DNA template. However, heat-treated SOD showed enhanced DNA cleavage over the kinamycin only control indicating a role for superoxide in kinamycin D

mediated DNA cleavage under our conditions. Trypsin digest controls were performed to investigate the possibility of a nonspecific interaction between CAT and our DNA template; however, these results were inconclusive because trypsin itself inhibited DNA cleavage. This result suggested the possibility of alternative biological targets for kinamycin D in addition to DNA.

Given the result that: 1) acidic media affords enhanced DNA cleavage under reducing conditions in the presence of kinamycin D, 2) there is no cleavage in the absence of thiol and 3) there is considerable evidence for a radical based reactive intermediate, we have augmented our initial mechanistic proposal. Based on the evidence presented herein it seems probable that protonation promotes reduction and/or facilitates nucleophilic attack. The resulting adduct could form with the electrophilic diazo nitrogen and upon homolytic bond cleavage provide a cyclopentenyl radical capable of eliciting DNA damage through oxygen mediated pathways (**Figure 13**).

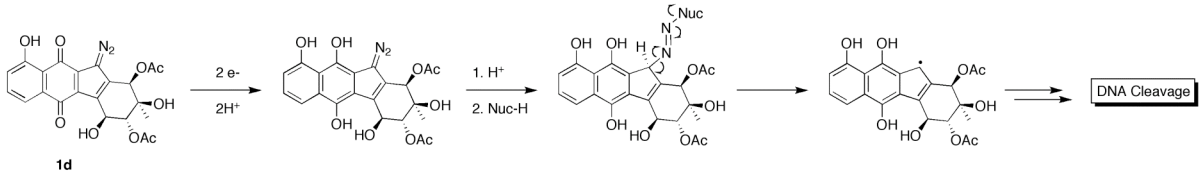

Figure 13. Revised mechanistic rationale for DNA cleavage.

2.5 Conclusion

In conclusion, we have been able to demonstrate the important role pH plays in reaction progress, highlighting the necessity of acidic media to promote kinamycin D mediated DNA cleavage under reducing conditions. Furthermore, we have shown that trace iron and hydroxyl radicals are critical for DNA cleavage. It appears that the kinamycins may mediate DNA cleavage through similar mechanisms even though their D-ring substitution patterns differ. This study also raises the possibility for biological targets in addition to DNA.

2.6 Experimental

All reagents were obtained from Fisher Scientific unless otherwise noted and used as received without further purification. Kinamycin D was isolated by Dr. T. Eric Ballard as previously described from *S. murayamaensis* (ATCC 21414) and dissolved in DMF.[16]

Preparation of DNA Template for Sequencing

pUC18 DNA (Stratagene) was used as a PCR template to generate the 175-nt DNA fragment for sequencing analysis (forward primer: ggcgctttctcatagctcac; reverse primer gcctacatacctcgctctgc (Sigma Genosys)). The forward primer was enzymatically end-labeled with γ-^{32}P-ATP (4500 Ci/mmol, MPBiomedicals) and T4 PNK (New England Biolabs) for 30 min at 37 ºC. The radiolabeled primer was purified on a Sephadex-G25 column (IBI Scientific); the eluate was immediately precipitated with 3 volumes of ice-cold isopropanol and 1/3 volume of 5 M NH_4OAc. The primer was centrifuged at 4 ºC, 13.2 rcf for 20 min, the supernatant was removed and the pellet was washed with 100 µL 70% EtOH. The pellet was centrifuged briefly, the supernatant was removed and the pellet was allowed to air dry. The pellet was resuspended in nuclease free water and immediately used in PCR. The DNA was amplified via hot-start PCR consisting of 40 cycles of: denaturation at 95 ºC, 15 s; annealing at 64 ºC, 15 s, and elongation at 72 ºC, 45s; with a final elongation time of 5 min. The amplified DNA template was immediately purified on an 8% native polyacrylamide (19:1) gel in 0.5X TBE run for 2 h at 200 V. After the gel was imaged and developed using X-ray film, the desired band of DNA was cut from the gel slab, crushed in a microfuge tube and eluted overnight in 400 µL 5 M NH_4OAc. The following day the microfuge tube was centrifuged for 10 min at 4 ºC, 13.2 rcf and the eluate was carefully separated from the crushed gel pieces (using a P-1000 micropipette tip lodged inside a P-200 micropipette tip) and transferred to another microfuge tube. The DNA was then isopropanol precipitated and washed as described above and after air-drying, was resuspended in nuclease free water. DNA radioactivity was counted using a liquid scintillation counter and adjusted to 10,000 cpm/µL.

DNA Cleavage Reactions

All reactions were performed in 5 mM sodium phosphate buffered solutions at the designated pH and [DTT]. All reaction buffers were prepared fresh daily. DNA and kinamycin D were added to opposite sides of a microfuge tube and spun down to the reaction buffer (total volume 20 μL) to initiate DNA cleavage. After the designated reaction time, 10 μL of stop solution was added to quench the reaction. Stop solution was prepared fresh daily and included 80 μL 4 M NaCl, 20 μL glycogen (20 mg/ml), 20 μL calf thymus DNA (100 mM base pairs) and 20 μL nuclease free water. The DNA was then isopropanol precipitated as described above. DNA was washed with 100 μL 70% EtOH and air-dried. After drying, 7 μL of formamide loading buffer was added to DNA samples, which were heated at 95 ºC for 5 min, and immediately placed on iced. The samples were then loaded onto an 8 M Urea, 6% polyacrylamide (19:1) DNA sequencing gel that had been pre-run at 35 W for 1 hour in 0.5X TBE. Gels were run at 35 W for 70 minutes, subsequently dried and exposed to a phosphor screen overnight. Gels were imaged using a Molecular Dynamics 445-SI phosphorimager.

Piperidine and Heat Lability Alkylation Assay

The piperidine and heat lability assay was performed after cleavage reactions had been quenched with stop solution. One set of reactions was heated to 70 ºC for 2 h to promote cleavage at alkylation sites. Piperidine treatment included the addition of 125 μL nuclease free water and 15 μL piperidine. After vortexing, the solutions were heated to 95 ºC for 15 min and then immediately placed on ice. The microfuge tubes were centrifuged for 5 min and the solution was transferred to a new microfuge tube and precipitated with isopropanol as described above.

G + A Sequencing Reaction

Thirty μL radiolabeled DNA template was heated to 37 ºC for 25 min with 3 μL 4% formic acid in a microfuge tube. After heating the sample was chilled on ice. Piperidine (45 μL) was mixed with nuclease free H_2O (375 μL) and added to the chilled sample of DNA. The

mixture was heated to 95 ºC for 25 min and immediately cooled on ice. The microfuge tube was centrifuged briefly and the supernatant was transferred to another microfuge tube to remove debris. The G + A DNA ladder was then isolated via isopropanol precipitation with 20 µL 4 M NaCl, 600 µL isopropanol (-20 ºC) and 1 µL glycogen (20 mg/mL). The DNA pellet was washed with 100 µL 70% ethanol, respun and allowed to air dry. The G + A ladder was then dissolved in 60 µL of 2X formamide loading dye and stored at -20 ºC.

REFERENCES

1. S. Ito, T. Matsuya, S. Omura, M. Otani, A. Nakagawa, Takeshim.H, Y. Iwai, M. Ohtani and T. Hata, *J Antibiot*, 1970, **23**, 315.

2. T. Hata, S. Omura, Y. Iwai, A. Nakagawa, M. Otani, S. Ito and T. Matsuya, *J Antibiot*, 1971, **24**, 353.

3. S. J. Gould, N. Tamayo, C. R. Melville and M. C. Cone, *J Am Chem Soc*, 1994, **116**, 2207-2208.

4. S. W. Mithani, C.; Taylor, J.; Dmitrienko, G. I., *J Am Chem Soc*, 1994, **116**, 2209-2210.

5. H. Y. He, W. D. Ding, V. S. Bernan, A. D. Richardson, C. M. Ireland, M. Greenstein, G. A. Ellestad and G. T. Carter, *J Am Chem Soc*, 2001, **123**, 5362-5363.

6. B. B. Hasinoff, X. Wu, J. C. Yalowich, V. Goodfellow, R. S. Laufer, O. Adedayo and G. I. Dmitrienko, *Anti-Cancer Drug*, 2006, **17**, 825-837.

7. W. Zeng, T. E. Ballard, A. G. Tkachenko, V. A. Burns, D. L. Feldheim and C. Melander, *Bioorg Med Chem Lett*, 2006, **16**, 5148-5151.

8. T. Shirafuj, Y. Yamamoto and H. Nozaki, *Tetrahedron*, 1971, **27**, 5353.

9. H. Zollinger, *Acc Chem Res*, 1973, **6**, 335-341.

10. J. Stubbe and J. W. Kozarich, *Chem Rev*, 1987, **87**, 1107-1136.

11. T. E. Ballard and C. Melander, *Tetrahedron Lett*, 2008, **49**, 3157-3161.

12. K. A. O'hara, X. Wu, D. Patel, H. Liang, J. C. Yalowich, N. Chen, V. Goodfellow, O. Adedayo, G. I. Dmitrienko and B. B. Hasinoff, *Free Radical Bio Med*, 2007, **43**, 1132-1144.

13. I. F. Tannock and D. Rotin, *Cancer Res*, 1989, **49**, 4373-4384.

14. Q. B. Zhou, P. Pande, A. E. Johnson and S. E. Rokita, *Bioorg Med Chem*, 2001, **9**, 2347-2354.

15. L. M. Dorfman and G. E. Adams, *Nat Stand Ref Data Sys*, 1973, **46**, 1-59.

16. M. C. Cone, P. J. Seaton, K. A. Halley and S. J. Gould, *J Antibiot*, 1989, **42**, 179-188.

CHAPTER 3

Osteoclastogenesis Inhibition using Substituted 1,4-Triazoles

3.1 Introduction

Osteoclastic bone resorption is implicated in a variety of skeletal diseases including osteoporosis,[1, 2] Paget's disease,[3-5] Rheumatoid Arthritis[6] (RA) and metastatic bone disease.[7] Osteoclasts are bone resorptive multinucleated cells, which differentiate from monocyte/macrophage hematopoeitic stem cell (HSC) lineages.[8] Bone density and architecture are regulated by the interplay between osteoclasts and osteoblasts (cells which deposit bone tissue). Imbalances in this relationship, which favor osteoclastogenic activity, are the basis for the aforementioned, associated skeletal disease pathologies.

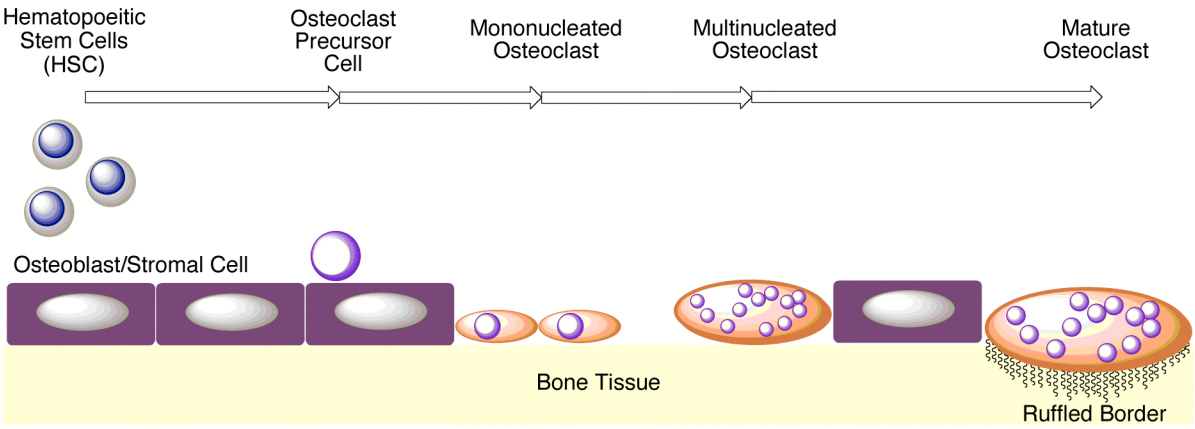

Figure 14. Osteoclast maturation pathway.

Osteoclasts are in essence specialized macrophages, which form from differentiation of monocyte/macrophage precursors at bone surfaces. A close spatial relationship between stromal cells and bone marrow is essential for osteoclastogenic activity. This system produces two crucial hematopoeitic factors for osteoclastogenesis: 1) the receptor activator nuclear factor κB (RANK) ligand (RANKL) and 2) the macrophage colony stimulating factor (M-CSF),[9, 10] which activates RANK at the surface of HSCs.[10-12] These cytokines act in

concert to direct expression of cathepsin K and tartrate resistant acid phosphatase (TRAP),[10] which aid in the development of mature osteoclasts. During bone resorption, mature osteoclasts form tightly sealed compartments on bone surfaces, whereby lysosomes such as cathepsin K and subsequently TRAP are released through the ruffled border, resulting in dissolution of the bone matrix forming a resorption pit (**Figure 14**).[13] After phagocytosis is complete, solubilized calcium, phosphate and collagen are then released into the extracellular environment.

Advances in our understanding of bone biology and the osteoclast/osteoblast relationship have been furthered mostly through studying molecules known or designed to prevent bone loss. Molecules capable of inhibiting osteoclastogenesis have the potential for therapeutic intervention as well as providing further insight into the bone remodeling process.

3.2 Known Inhibitors of Osteoclastogenesis

A variety of strategies have been employed to inhibit osteoclastogenesis with several degrees of success in clinical trials. Some successful anti-resorption methods include cathespin K inhibitors,[14] selective estrogen receptor modulators (SERMs),[15] RANK/RANKL disruptors,[16] and bisphosphonates.

3.2.1 Bisphosphonates

The current hallmark therapy for osteoporosis and other osteoclast mediated diseases is treatment with bisphosphonates (BPs).[17] Nitrogen containing bisphosphonates (NBPs) are an especially potent antiresorptive therapy for osteoporosis, bone pain and Paget's disease with IC_{50} values ranging from the low micromolar to high nanomolar range.[18] Although both BPs and NBPs are both effective towards osteoclastogenesis inhibition, they elicit their activity through differing modes of action. BPs are known to inhibit osteoclastogenesis and induce apoptosis in osteoclasts by displacing the terminal pyrophosphate in ATP forming a nonfunctional complex which competes with ATP during cellular metabolism.[19] NBPs

however, act by disrupting the mevalonate pathway through inhibition of protein prenylation.[20, 21] It is speculated that the disruption of protein prenylation affects the signal transduction proteins (Ras, Rho and Rac) responsible for maintaining the ruffled border of osteoclasts. Although there have been many generations of clinically prescribed BPs and NBPs, they suffer from extremely poor bioavailability; typically less than 1% of BPs and NBPs are absorbed after oral administration.[17] In addition, the high polarity of these molecules leads to pronounced gastrointestinal complications in approximately half of all patients prescribed them for treatment.[22] Furthermore, BPs and NBPs are known to cause irreversible osteonecrosis of the bone in the lower jaw.[23-26]

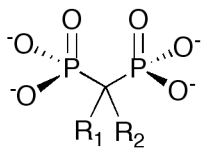

Name	R_1	R_2
clodronate	Cl	Cl
etidronate	OH	Me
tiludronate	H	S-*p*-PhCl
pamidronate	OH	$(CH_2)_2NH_2$
neridronate	OH	$(CH_2)_6NH_2$
olpadronate	OH	$(CH_2)_2N(CH_3)_2$
aldendronate	OH	$(CH_2)_3NH_2$
ibandronate	OH	$(CH_3)_2N$ with Me and $(CH_2)_4CH_3$

Figure 15. Common bisphosphonates and nitrogen-containing bisphosphonates.

3.2.2 Selective Estrogen Receptor Modulators

Osteoprotegrin (OPG) is a member of the tumor necrosis factor (TNF) family of receptors (like RANKL) and acts as the natural decoy ligand for RANK. OPG inhibits RANKL binding to RANK preventing osteoclast maturation as well as inducing apoptosis. Hormone

replacement therapy was initially prescribed to increase OPG production; however, the high risks of developing breast and endometrial cancer have mostly terminated this therapeutic avenue as a first line treatment.[27]

An improvement on this strategy utilizes selective estrogen receptor modulators (SERMs). Raloxifene (**Figure 16**) is currently the only clinically approved SERM for therapeutic use and possesses IC_{50} values in the high nanomolar range.[15, 28] Raloxifene works as an estrogen agonist on bones, reducing the number and activity of osteoclasts thus increasing bone mineral density.[15, 28] Additionally, raloxifene works as an estrogen antagonist on breast and endometrial tissues and poses no known risk for developing breast or uterine cancers unlike traditional hormone replacement therapy. However, like hormone replacement therapy, raloxifene has a high propensity for the formation of vein thrombosis.

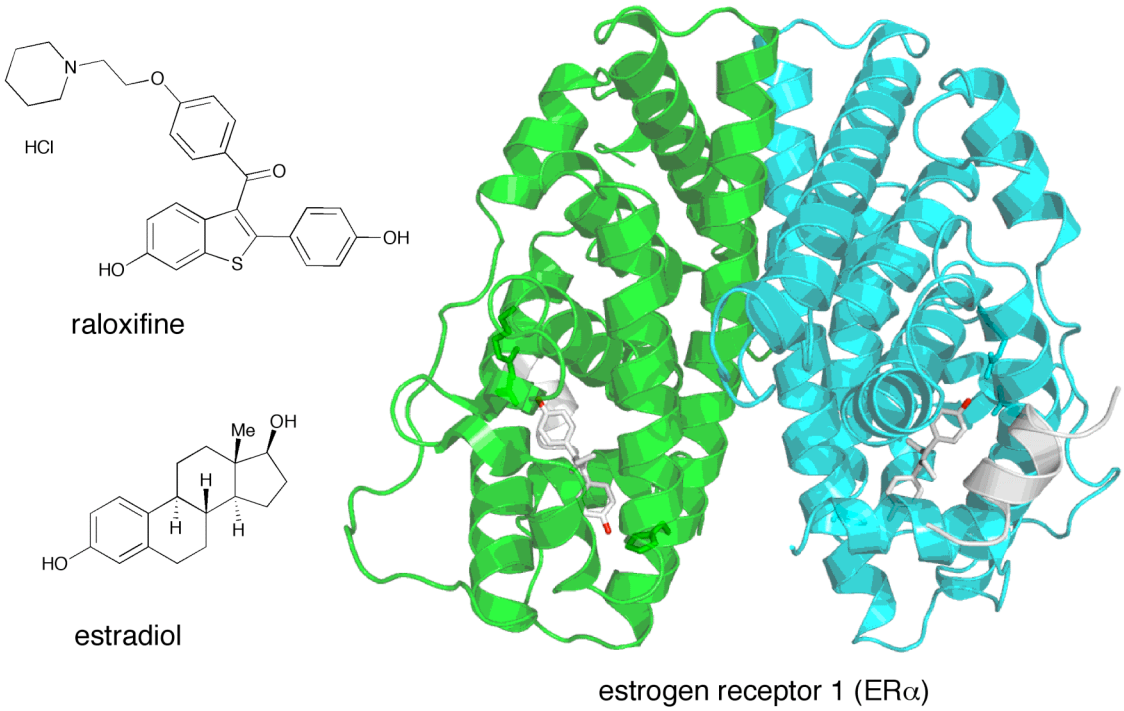

Figure 16. Comparison of raloxifine, estradiol and estrogen receptor 1.

3.3 Library Design

Although various strategies toward targeting osteoclasts have had degrees of success, there still exist many limitations and disadvantages for these therapeutic treatments. In addition, small molecules that can inhibit the formation of osteoclasts can also provide deeper knowledge of the osteoclast/osteoblast relationship as well as other regulators of bone biology. Toward this end, Steven Rogers (a current Melander group member) synthesized a variety of triazolyl-2-aminoimidazole conjugates (**Figure 17**), which were originally slated for biofilm inhibition assays in the context of oral bacteria in collaboration with Dr. Hui Wu at the University of Alabama. Dr. Wu, in addition to exploring their activity as anti-biofilm agents, subjected them to an osteoclast formation screen.

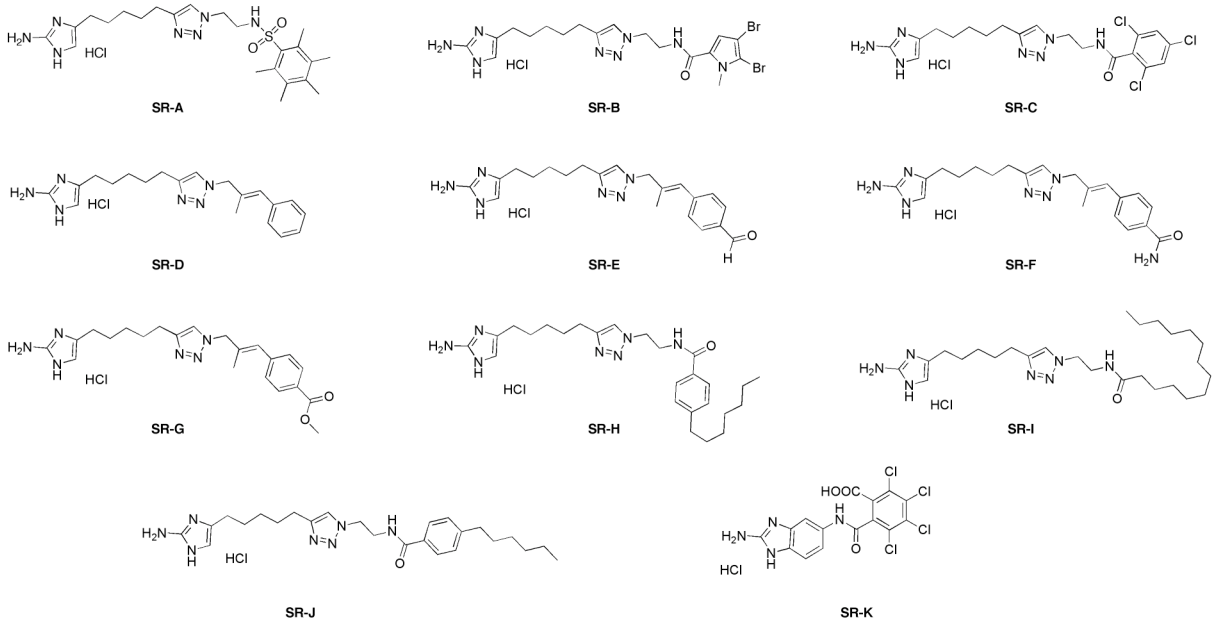

Figure 17. First generation 2-aminoimidazole-triazole library for osteoclastogenesis inhibition.

This initial screen revealed many of these small molecules induced global cell death; however, three promising leads for analog development were identified. Given that each of these molecules contained a triazole and a 2-aminoimidazole moiety, we first investigated the necessity of the 2-aminoimidazole subunit by synthesizing and screening a pilot library of

triazoles without a 2-aminoimidazle substituent for the ability to inhibit osteoclastogenesis. A simple triazole library has the advantage of facile synthesis by employing the Huisgen 1,3-dipolar cycloaddition reaction of terminal azides and alkynes, commonly referred to as "Click Chemistry".

The second-generation library was based on the three promising leads synthesized by Rogers (**SR-A**, **SR-B**, **SR-C**) and included: 1) pentamethylbenzenesulfonamide, 2) 4,5-dibromo-1-methylpyrrole-3-carboxamide and 3) 2,4,6-tricholorobenzamide functionalities. We envisioned a facile route to 1,4-substituted triazoles could be accomplished by performing a 1,3-dipolar cycloaddition reaction between commercially available alkynes and functionally modified azides. The functionalized azides could be accessed by acylating 2-azidoethylamine with commercially available acid or sulfonyl chlorides. (**Figure 18**).

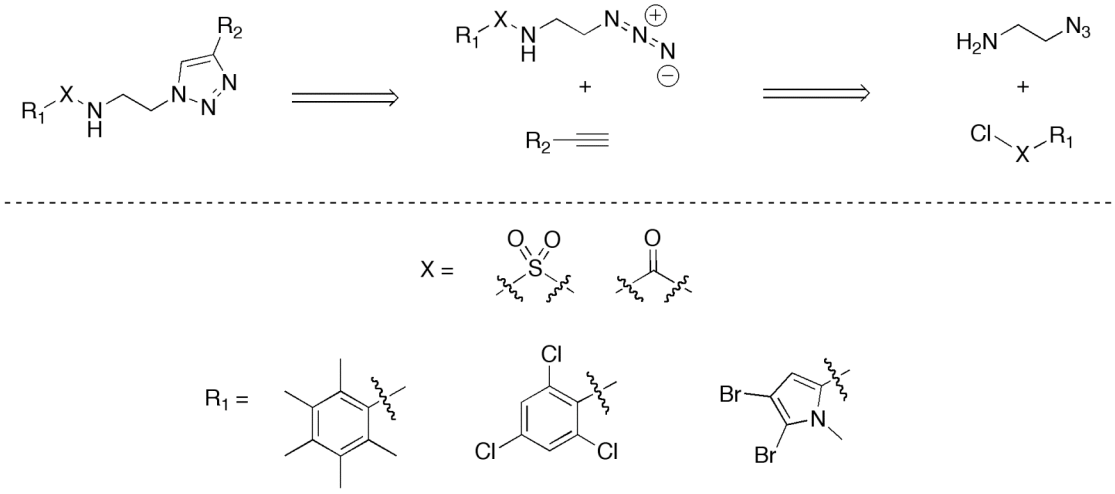

Figure 18. Retrosynthetic analysis of triazole library.

3.3.1 Synthesis of Second Generation Triazole Library

The initial step in completing the second-generation triazole library began with the synthesis of 2-azidoethylamine (**21**), which was accessed via a known literature procedure (**Scheme 6**). The requisite, functionalized azides **22** and **23** were then synthesized through acylation of **21**

with pentamethylbenzenesulfonyl chloride and 2,4,6-trichlorobenzoyl chloride. Steven Rogers generously provided the azido precursor **24**.

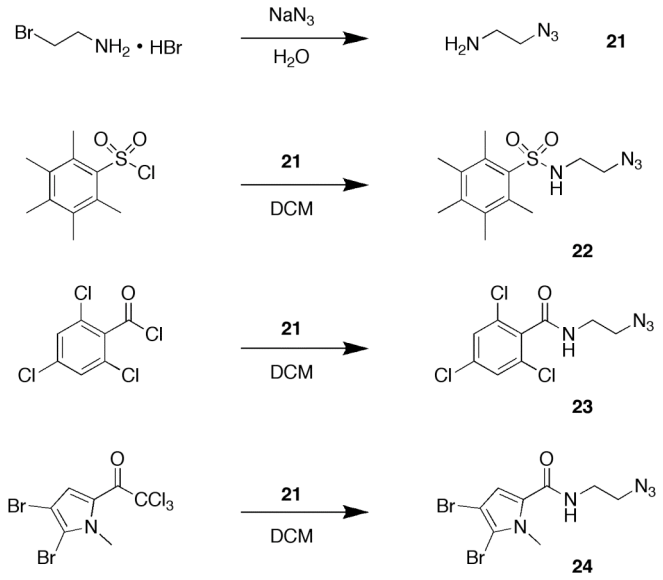

Scheme 6. Synthesis of azido precursors.

Once the functionalized azides **22** – **24** were in hand we employed a Cu(I)-catalyzed 1,3-dipolar cycloaddition reaction with various commercially available alkynes to generate a simple, synthetically diverse 1,4-substitued triazole library in moderate to good yields in two steps from literature precedents (**Scheme 7**).

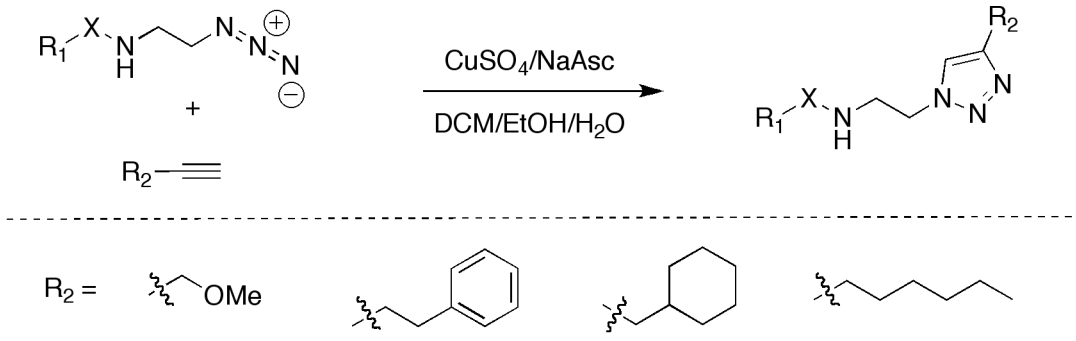

Scheme 7. Synthesis of 1,4-substituted triazoles for second-generation library.

The complete second-generation triazole library is depicted below in **Figure 19**.

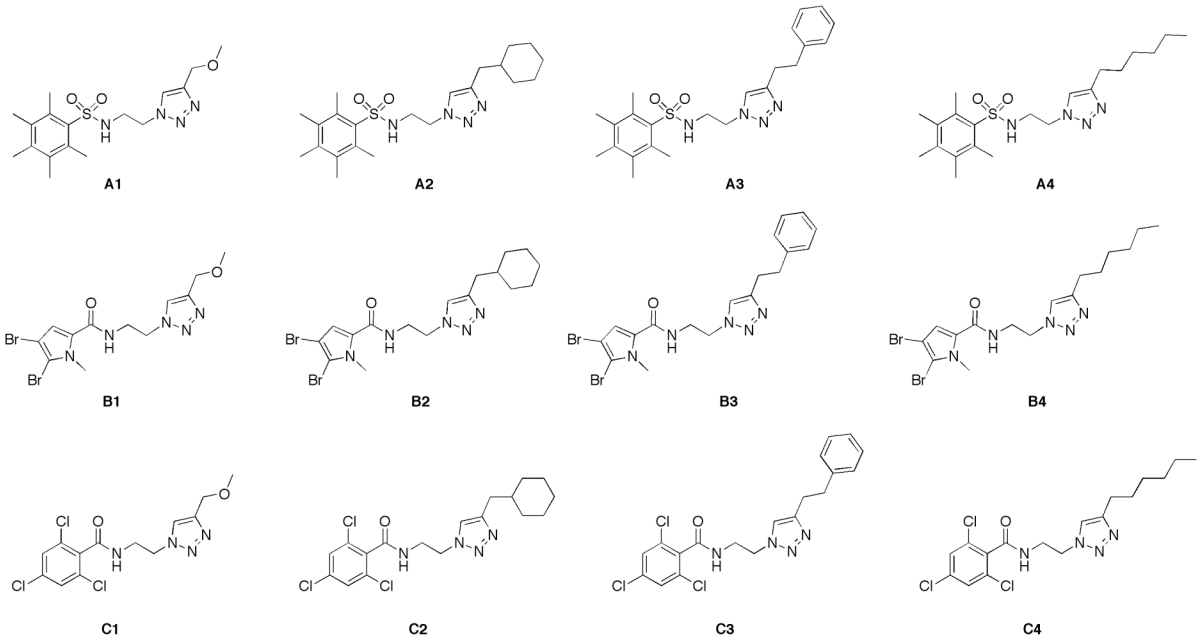

Figure 19. Complete second generation triazole library.

3.3.2 Osteoclastogenesis Inhibition Screen of Second Generation Triazole Library

Upon the successful synthesis of our pilot triazole library, each molecule was screened for osteoclastogenesis inhibition by Dr. Wu's laboratory at UAB. The qualitative results of this screen are described by the microscopic images in **Figure 20**. These photographs represent various stages in the formation of large, mature osteoclasts. As depicted, Stage 0 represents the RANKL-negative control, whereby the formation of osteoclasts is inhibited. Stage 1 illustrates cells that are not currently producing TRAP, indicating that no osteoclasts have formed yet. Stage 2 shows the formation of very small osteoclasts, where most of the cells present are expressing TRAP. Stages 3 through 5 indicate the progressive growth and abundance of osteoclasts from many small osteoclasts to many large, mature osteoclasts.

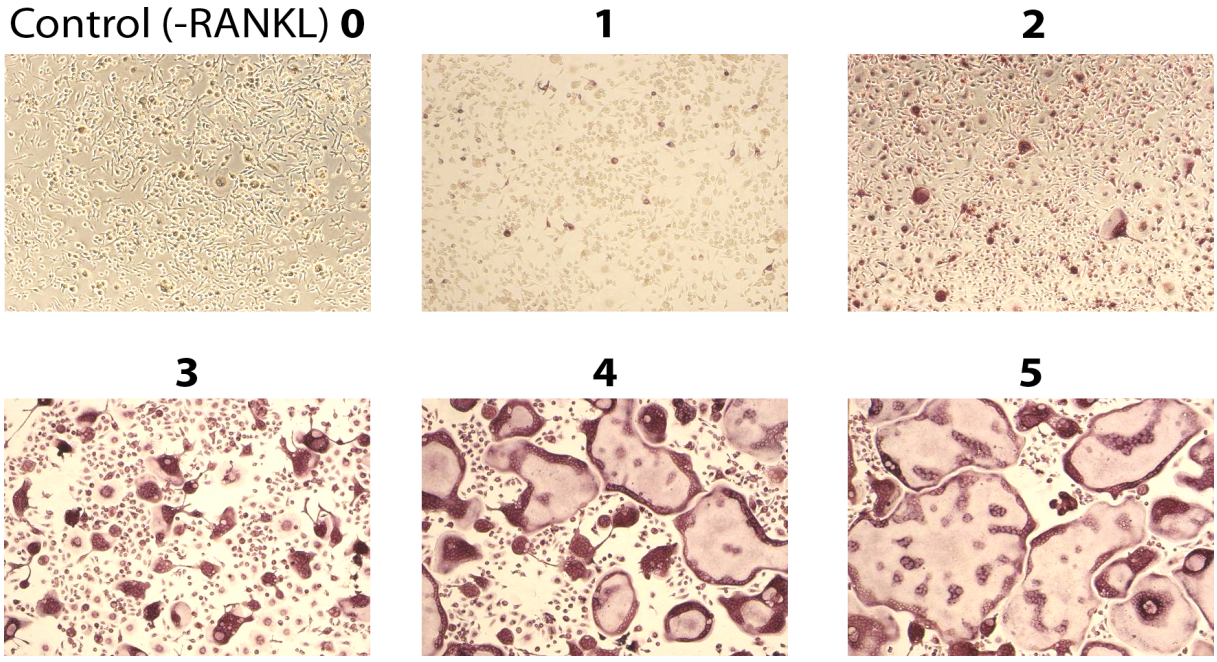

Figure 20. Stages of osteoclast development for analysis of triazole library mediation of osteoclast formation. Stage 0: Control, Stage 1: No osteoclasts, Stage 2: A few small osteoclasts, Stage 3: Many small osteoclasts, Stage 4: Many large osteoclasts, Stage 5: Many large, mature osteoclasts.

A comparative analysis of six of these compounds is shown in **Table 3**. Evaluation of these small molecules at a variety of concentrations indicated that 2,4,6-trichlorobenzamide containing triazoles (C series) were especially capable of inhibiting osteoclastogenesis. Analogs **C2** and **C4** possessed the highest efficacy by preventing the formation of any osteoclasts at a concentration of 10 μM. The B series (aside from analog **B2)**, and the A series of the second-generation triazole library did not prove to appreciably inhibit osteoclastogenesis; therefore, they were not investigated further for future library derivations.

Table 3. Evaluation of second-generation library by osteoclast formation stages.

Compound/Concentration	20 μM	10 μM	5 μM	1 μM
A1	4	5	NA	NA
B2	1	1	3	4
C1	2	4	4	5
C2	1	1	2	4
C3	1	2	3	4
C4	1	1	2	4

3.3.3 Synthesis of Third Generation Library

Evaluation of the library screen for osteoclastogenesis inhibition revealed both 2,4,6-trichlorobenzamide and the cyclohexylmethyl pendant group as the most promising leads for future library development. Therefore two third generation libraries were synthesized based on each of these terminal functionalities (**Figure 21**). Dr. Daniel Whitehead, a post-doctoral associate in the Melander Laboratory performed the synthesis of the majority of the cyclohexylmethyl-triazole analogs; whereas I synthesized a third generation library based off the 2,4,6-trichlorobenzamide pendant group.

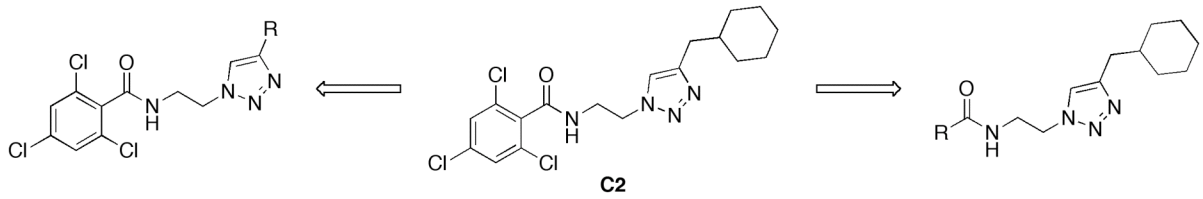

Figure 21. C2 as a scaffold for third generation triazole libraries.

3.3.3.1 2,4,6-Trichlorobenzamide Third Generation Library

The 2,4,6-trichlorobenzamide (C-series) third-generation library was readily accessed by employing the Huisgen 1,3-dipolar cycloaddition reaction with **23** and various commercially available alkynes (**Scheme 8**). In order to gain mechanistic insight towards osteoclastogenesis inhibition, we chose alkynes with aliphatic rings and chains of various lengths and substitution patterns as well as multiply substituted aromatic functionalities.

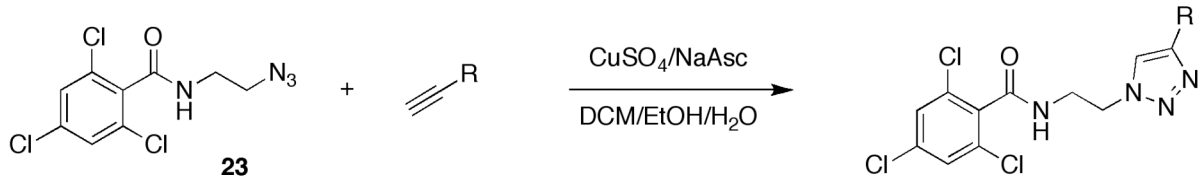

Scheme 8. Synthesis of C-series third generation library

The complete third generation library based on the 2,4,6-trichlorobenzamide pendant group is shown in **Figure 22**.

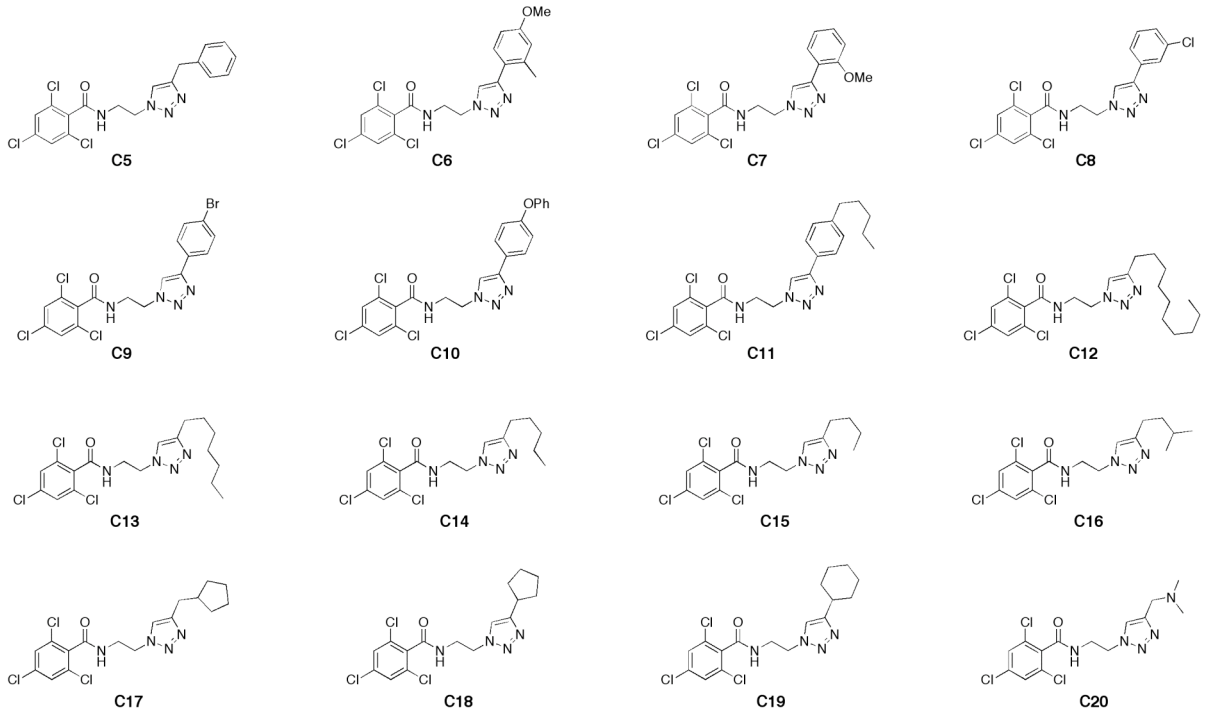

Figure 22. Third generation triazole library based on 2,4,6-trichlorobenzamide (C-series).

3.3.3.2 Osteoclastogenesis Inhibition Results of Third Generation C-Series Library

After the successful synthesis of the third-generation C-series library, these compounds were subjected to an osteoclast inhibitory screen by Dr. Wu's laboratory. The screening protocol utilized is described in **Figure 20**. The screening results of the 2,4,6-trichlorobenzamide-triazole library are summarized in **Table 4**.

Table 4. Evaluation of third-generation C-series library by osteoclast formation stages.

Compound/Concentration	20 μM	5 μM	1 μM
C5	3	5	5
C6	3	5	5
C8	1	4	5
C9	1	4	5
C11	4	5	5
C12	1	4	5
C13	2	4	5
C14	3	5	5
C15	4	5	5
C16	4	5	5
C17	4	5	5
C18	4	5	5
C19	3	4	5
C20	2	5	5

The third generation triazole library based on 2,4,6-trichlorobenzamide in general was not as successful as the results of the second generation C series library subset. Analogs **C8**, **C9** and **C12** were the most successful exhibiting no osteoclast formation at a concentration of 20 μM. Interestingly, sliding the cyclohexyl group of the lead compound **C2** one carbon closer

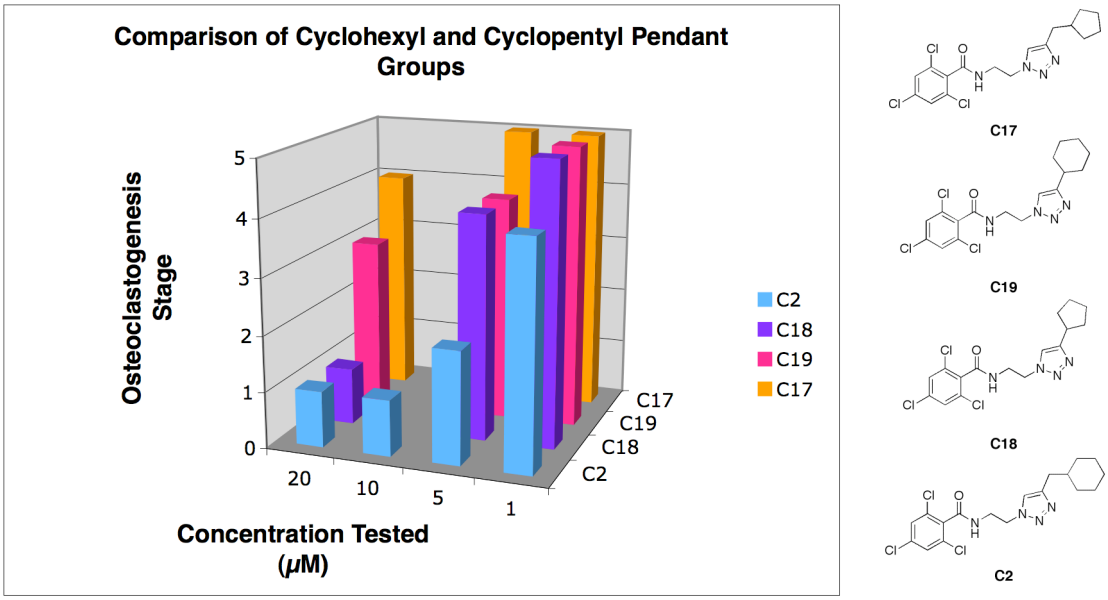

Figure 23. Comparison of cyclohexyl and cyclopentyl pendant groups on osteoclastogenesis inhibition.

to the triazole (**C19**) showed a marked decrease in osteoclastogenesis. Furthermore, substitution of the cyclohexyl pendant group in **C2** and **C19** with a cylopentyl functionality (**C17** and **C18** respectively) also severely decreased the inhibition of osteoclast formation (**Figure 23**).

Upon comparison of varying the aliphatic chain length of lead compound **C4** the results are not as dramatic, but follow the trend of **C4** > **C12** > **C13** > **C14** > **C15** (hexyl > decyl > heptyl > pentyl > butyl) where aside from the hexyl outlier, decreasing aliphatic pendant group chain length decreases the propensity for osteoclastogenesis inhibition. The only doubly aromatic analogs capable of inhibiting osteoclastogenesis were **C8** and **C9,** both halogenated (*meta* and *para* respectively) phenyl pendant groups. All other substituted phenyl pendant groups were not able to appreciably suppress osteoclast formation.

3.3.3.3 Cylclohexylmethyl Third Generation Library

The third generation cyclohexylmethyl pendant group library (2-series) was synthesized via a 1,3-dipolar cycloaddition reaction between 3-cyclohexyl-1-propyne and various azides, which had been accessed through the acylation of **21** with commercially available acid chlorides (**Scheme 9**). The available acid chlorides chosen for this third generation library subset spanned an assortment of substituted aromatic functionalities in order to delineate possible structural activity relationships for this substituent. The complete third-generation cyclohexylmethyl library is illustrated in **Figure 24**.

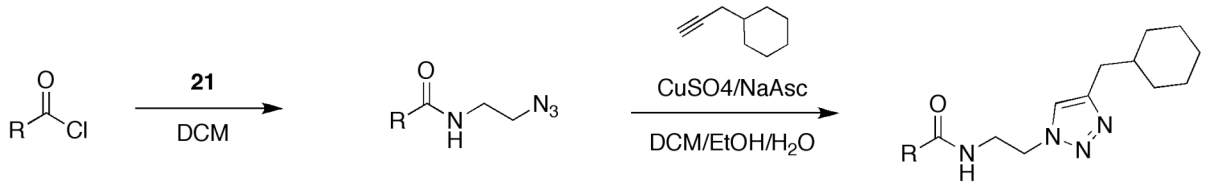

Scheme 9. Synthesis of cyclohexylmethyl (2-series) third generation library.

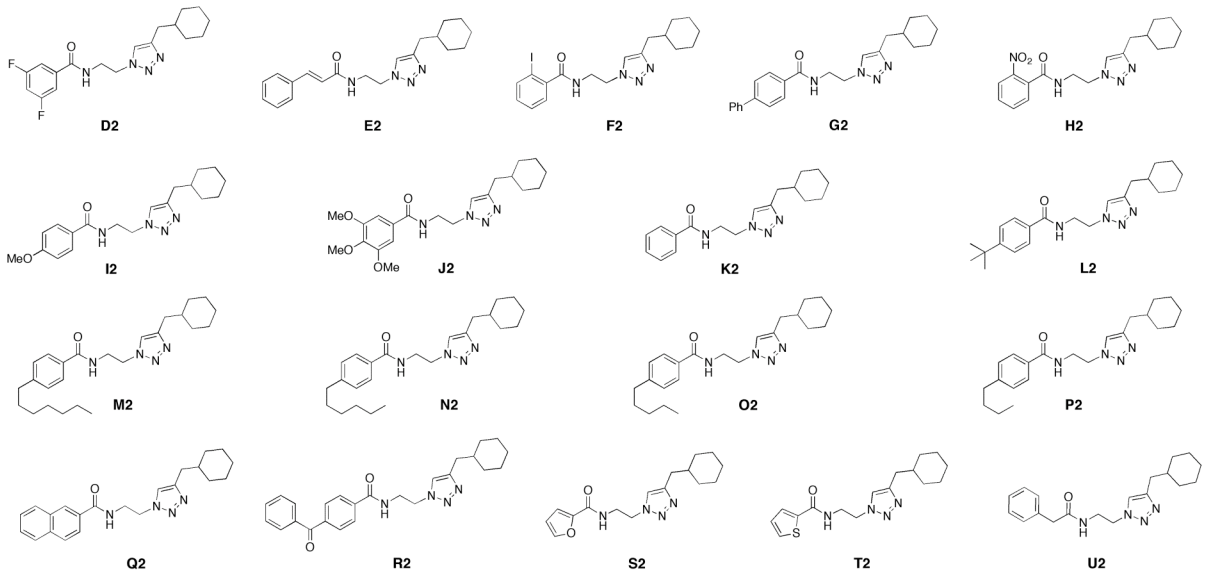

Figure 24. Third-generation cyclohexylmethyl-triazole library (2-series).

3.3.3.4 Osteoclastogenesis Inhibition Results of Third Generation 2-Series Library

The cyclohexylmethyl-triazole library was also subjected to an osteoclast formation screen as described in **Figure 20**. The results of this assay are presented in **Table 5**.

Table 5. Evaluation of third-generation cyclohexylmethyl library by osteoclast formation stages.

Compound/Concentration	20 μM	5 μM	1 μM
D2	4	5	5
E2	3	5	5
F2	1	3	5
H2	1	3	5
I2	3	5	5
J2	1	3	5
K2	4	5	5
L2	1	5	5
M2	1	4	5
N2	1	3	5
P2	1	4	5
Q2	2	5	5
S2	5	5	5
T2	3	5	5
U2	4	5	5

The osteoclastogenesis inhibition assay of the cyclohexylmethyl-triazole third generation library revealed numerous compounds that successfully inhibited osteoclastogenesis at 20 μM. The more successful benzamides from this library included electron-withdrawing groups (EWG) at the *ortho* position (e.g. **F2**, *ortho*-iodo and **H2** *ortho*-nitro) of which **C2** qualifies as well. Substitution of electron-withdrawing groups at the *meta* position (e.g. *meta*-difluorobenzamide **D2**); however, show a marked decrease in osteoclast inhibition activity. Additionally, benzamides lacking any substituents (**K2**) off the phenyl moiety were unable to inhibit osteoclastogenesis to any functional degree at the same concentrations. A comparison of these variously substituted benzamides is charted in **Figure 25**.

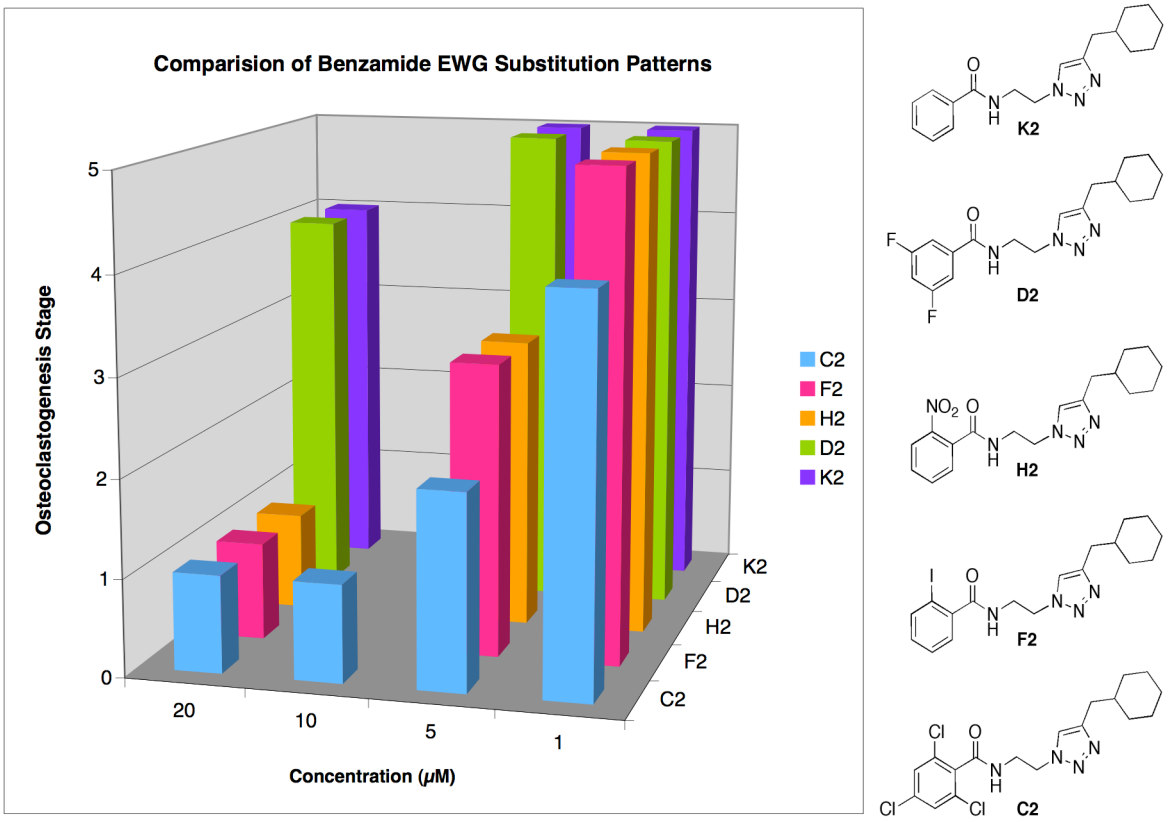

Figure 25. Comparison of various benzamide EWG substitution patterns on osteoclastogenesis inhibition.

The osteoclast inhibition screening also revealed a number of inhibitors with aliphatic substituents *para* to the benzamide functionality. Upon comparison with **K2,** which has no

substituents off the phenyl moiety, the addition of any of these aliphatic functionalities had a dramatic effect on osteoclastogenesis inhibition when treated at a concentration of 20 µM (**Figure 26**). The most effective aliphatic benzamide was the *para*-hexyl derivative **N2**; the heptyl, butyl and *tert*-butyl derivaties were also effective, but to a lesser extent at lower concentrations.

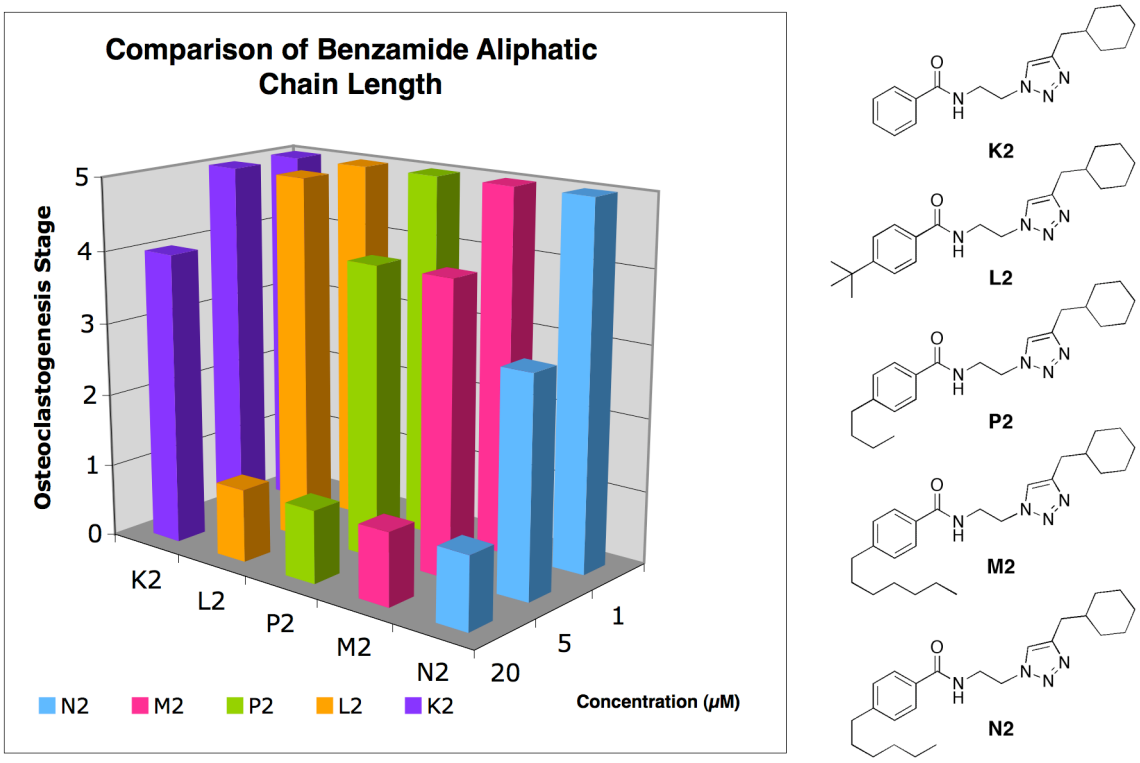

Figure 26. Comparison of benzamide aliphatic substituents on osteoclastogenesis inhibition.

The compilation of screening data for each of these third generation libraries coupled with the results of the second generation library reveal an especially important role for the cyclohexyl pendant group. Three substituted cyclohexylmethyl-triazoles were found to have the same osteoclast inhibition profile where no osteoclast formation occurred with 20 µM dosing and Stage 3 osteoclast formation was visible at 5 µM dosing. These promising compounds are shown in **Figure 27**.

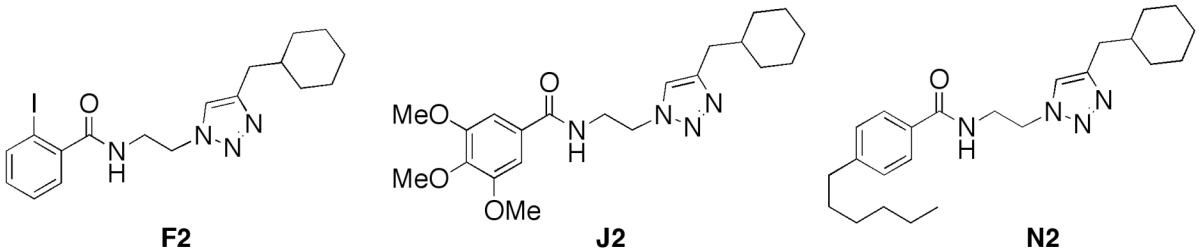

Figure 27. Most successful compounds from cyclohexylmethyl triazole library.

Although the third generation cyclohexylmethyl-triazole library produced three promising compounds towards osteoclastogenesis inhibition, the current lead molecules of these libraries remain **C2** and **C4**. Additionally, these molecules currently comprise the most potent known inhibitors of osteoclastogenesis ever disclosed. Logical future extensions of these libraries include synthesizing the 1,5-substituted triazole analogs, varying the amide-triazole linker length, in addition to immobilizing the lead compounds for pull-down assay identification of biological targets.

3.4 Conclusion

A variety of substituted 1,4-triazoles were synthesized and investigated for osteoclastogenesis inhibition activity. These libraries revealed a number of small molecules capable of inhibiting the formation of osteoclasts, as well as the most potent known inhibitors of osteoclastogenesis to date. The common features of the most active triazoles include substituted benzamides coupled with a C-4-substituted cyclohexylmethyl pendant group. These promising results serve as the basis for future library designs as well as screening assays to identify the biological targets through which these small molecules elicit their anti-osteoclastic activity.

3.5 Experimental

All ^{1}H NMR (400 MHz or 300 MHz) and ^{13}C NMR (400 MHz or 300 MHz) spectra were recorded at 25.0 ºC on a Varian Mercury spectrometer. Chemical shifts (δ) are given in ppm relative to $CDCl_3$; coupling constants (*J*) are in hertz. Abbreviations used are s = singlet, bs =

broad singlet, d = doublet, dd = doublet of doublets, t = triplet, dt = doublet of triplets, m = multiplet, and b = broad. Electrospray Ionization (ESI) exact mass measurements were carried out on an Agilent Technologies 6210 LC-TOF mass spectrometer. The sample matrix used was a H_2O/MeOH (1:3) mixture with 0.1% formic acid. Silica gel (40 μm average particle size) was used for flash column chromatography.

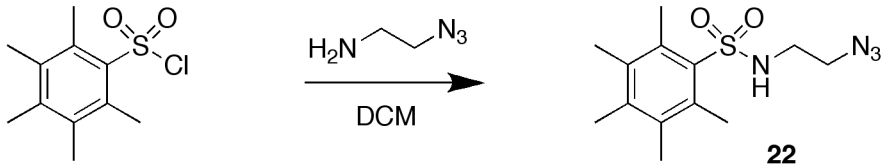

22

N-(2-azidoethyl)-2,3,4,5,6-pentamethylbenzenesulfonamide (22). 2-azidoethylamine (**21**) (241 μL, 3.12 mmol) was dissolved in DCM (10 mL) and cooled to 0 ºC. Pentamethylbenzenesulfonyl chloride (610 mg, 2.47 mmol) was added dropwise slowly. The solution was allowed to warm to RT overnight with a total reaction time of 28 h. The solvent was reduced in vacuo and the product was purified via flash column chromatography with 100% DCM mobile phase (R_r ~ 0.33). The product (282 mg, 39%) was isolated as an eggshell colored powder. ^{1}H NMR (400 MHz, $CDCl_3$) δ 5.13 (1H, t, *J* = 5.2 Hz) 3.38 (2H, t, *J* = 5.6 Hz), 3.06 (2H, dt, *J* = 5.6 Hz, 5.2 Hz), 2.61 (6H, s), 2.30 (3H, s), 2.27 (6H, s); ^{13}C NMR (400 MHz, $CDCl_3$) δ 135.2, 134.2, 51.1, 42.3, 19.1, 18.0, 17.2; HRMS (ESI) *m/z*, ([M + H]$^+$, $C_{13}H_{20}N_4O_2S$): theoretical 297.1380, observed 297.1381.

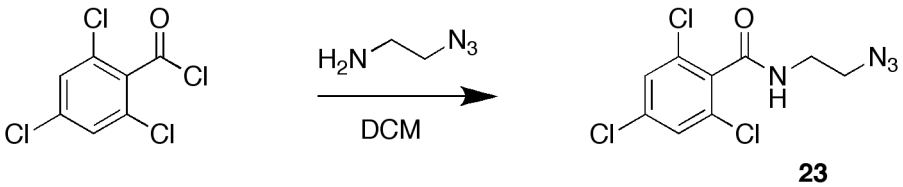

23

***N*-(2-azidoethyl)-2,4,6-trichlorobenzamide (23).** Reagent **21** (206 μL, 2.67 mmol) was dissolved in DCM (10 mL) and cooled to 0 ºC. 2,4,6-trichlorobenzoyl chloride (316 μL, 2.47 mmol) was added dropwise slowly. The solution was then allowed to warm to RT with a total reaction time of 8 h. The solvent was extracted with H_2O (2 x 10 mL), the combined

H_2O layers was extracted with DCM (2 x 20 mL) and the combined organic phase was dried over Na_2SO_4, filtered and reduced in vacuo. The product was purified using flash column chromatography with a 100% DCM mobile phase (R_f ~ 0.4). The product (198 mg, 35%) was isolated as a cream colored powder. ^{1}H NMR (400 MHz, $CDCl_3$) 7.30 (2H, s), 6.05 (1H), 3.56 (4H, s); ^{13}C NMR (400 MHz, $CDCl_3$) δ 164.5, 136.1, 134.4, 133.0, 128.3, 122.8, 49.4, 39.7, 38.2, 33.4, 33.2, 26.5, 26.3; HRMS (ESI) *m/z*, ($[M + H]^+$, $C_9H_7Cl_3N_4O$): theoretical 292.9758, observed 292.9757.

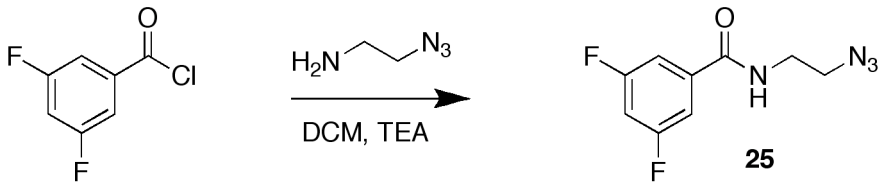

***N*-(2-azidoethyl)-3,5-difluorobenzamide (25).** Reagent **21** (201 µL, 2.66 mmol) and TEA (660 µL, 4.74 mmol) were dissolved in DCM (10 mL) and cooled to 0 ºC. 3,5-difluorobenzoyl chloride (419 mg, 2.37 mmol) was added slowly in small portions. The solution was then allowed to warm to RT with a total reaction time of 3.5 h. The solvent was extracted reduced in vacuo and immediately purified via flash chromatography with a DCM/MeOH mobile phase (9:1). The product (198 mg, 35%) was isolated as a white powder. ^{1}H NMR (400 MHz, $CDCl_3$) δ 7.31 (2H, m), 6.99 (1H, m), 6.34 (1H, bs), 3.65 – 3.57 (4H, bm); ^{13}C NMR (400 MHz, $CDCl_3$) δ 110.6, 110.4, 107.4, 51.0, 39.8; HRMS (ESI) *m/z*, ($[M + H]^+$, $C_9H_8F_2N_4O$): theoretical 227.0739, observed 227.0745.

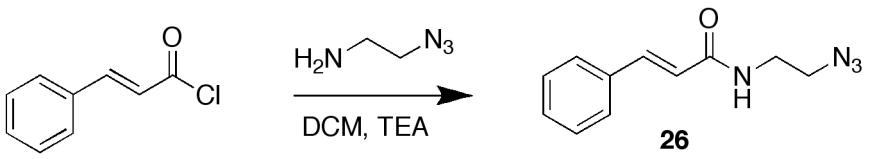

***N*-(2-azidoethyl)cinnamamide (26).** Reagent **21** (296 µL, 4.22 mmol) and TEA (700 µL, 5.02 mmol) were dissolved in DCM and cooled to 0 ºC. Cinnamoyl chloride (416 mg, 2.50 mmol) was added dropwise and allowed to warm to RT over the course of 24 h. The solvent was removed in vacuo and immediately purified through flash column chromatography using

a DCM mobile phase (R_f ~ 0.6 in 5% MeOH/DCM). The product was isolated as a viscous yellow oil (437 mg, 81%). ^{1}H NMR (300 MHz, $CDCl_3$) 7.65 (1H, d, *J* = 15.6 Hz), 7.50 (2H, m), 7.34 (3H, m), 6.40 (1H, d, *J* = 15.6 Hz), 5.90 (1H, bs), 3.61 – 2.52 (4H, bm); ^{13}C NMR (400 MHz, $CDCl_3$) δ 166.3, 141.9, 134.8, 130.1, 129.5, 128.1, 120.4, 51.2, 39.2; HRMS (ESI) *m/z*, ($[M + H]^+$, $C_{11}H_{12}N_4O$): theoretical 217.1084, observed 217.1080.

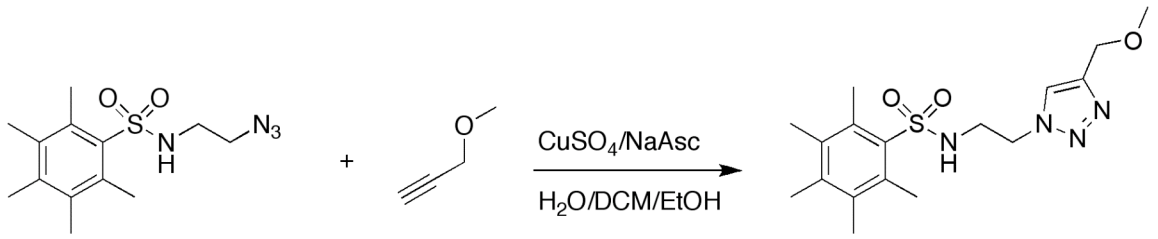

22 **A1**

***N*-(2-(4-(methoxymethyl)-1*H*-1,2,3-triazol-1-yl)ethyl)-2,3,4,5,6-pentamethylbenzene sulfonamide (A1).** DCM (500 µL), EtOH (500 µL) and H_2O (500 µL) were added into a vial. Methylpropargyl ether (5.26 µL, 106 µmol) and **22** (31 mg, 105 µmol) were then added, followed by sodium ascorbate (11 mg, 55.5 µmol) and 1 M $CuSO_4$ (15.7 µL, 15.7 µmol). The reaction was stirred at RT for 16 h, DCM (3 mL) and H_2O (5 mL) were added and the H_2O layer was extracted with DCM (2 x 5 mL). The organic layer was dried over Na_2SO_4, filtered and reduced in vacuo. The product was purified via flash column chromatography using a DCM/MeOH (99:1) mobile phase (R_f ~ 0.3) and isolated as a filmy beige solid (29 mg, 89%). ^{1}H NMR (400 MHz, $CDCl_3$) 7.54 (1H, s), 5.51 (1H, m), 4.53 (2H, m), 4.42 (2H, t, *J* = 5.6 Hz), 3.38 (2H, m), 3.05 (1H, m), 2.59 (3H, s), 2.54 (6H, s), 2.28 (6H, s), 2.25 (3H, m); ^{13}C NMR (400 MHz, $CDCl_3$) δ 145.2, 139.9, 136.1, 135.9, 135.1, 134.2, 134.2, 124.1, 65.9, 58.6, 51.1, 49.2, 42.5, 42.2, 41.6, 19.1, 17.9, 17.2; HRMS (ESI) *m/z*, ($[M + H]^+$, $C_{17}H_{26}N_4O_3S$): theoretical 367.1805, observed 367.1819.

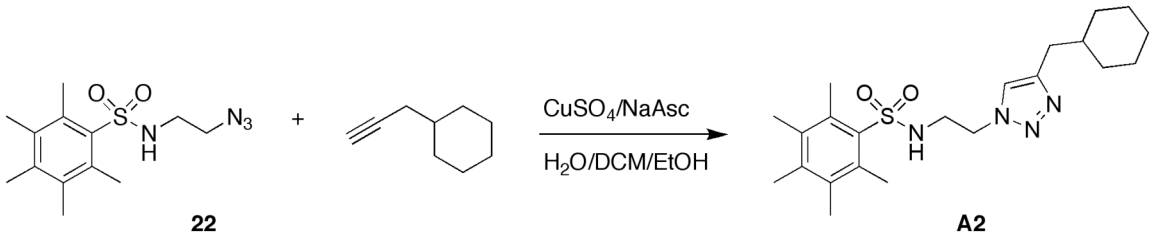

22 A2

***N*-(2-(4-(cyclohexylmethyl)-1*H*-1,2,3-triazol-1-yl)ethyl)-2,3,4,5,6-pentamethyl benzenesulfonamide (A2).** DCM (500 µL), EtOH (500 µL) and H_2O (500 µL) were added into a vial. 3-cyclohexyl-1-propyne (10.75 µL, 74.32 µmol) and **22** (22 mg, 74 µmol) were then added, followed by sodium ascorbate (8 mg, 0.04 mmol) and 1 M $CuSO_4$ (11.2 µL, 11.2 µmol). The reaction was stirred at RT for 21 h, DCM (3 mL) and H_2O (5 mL) were added and the H_2O layer was extracted with DCM (2 x 5 mL). The organic layer was dried over Na_2SO_4, filtered and reduced in vacuo. The product was purified via flash column chromatography using a DCM/MeOH (99:1) mobile phase ($R_f \sim 0.3$) and isolated as an off-white solid (18 mg, 58%). ^{1}H NMR (400 MHz, $CDCl_3$) δ 5.42 (1H, m), 4.39 (2H, m), 3.42 (2H, m), 2.54 (8H, s), 2.27 (3H, s), 2.23 (6H, s), 1.70 (6H, m) 1.32 – 1.12 (4H, bm), 0.98, (2H, bm) ^{13}C NMR (300 MHz, $CDCl_3$) δ 139.9, 136.0, 135.1, 134.2, 122.8, 50.2, 42.5, 38.3, 33.5, 33.2, 26.6, 26.3, 19.1, 17.9, 17.2; HRMS (ESI) *m/z*, ($[M + H]^+$, $C_{22}H_{34}N_4O_2S$): theoretical 419.2481, observed 419.2484.

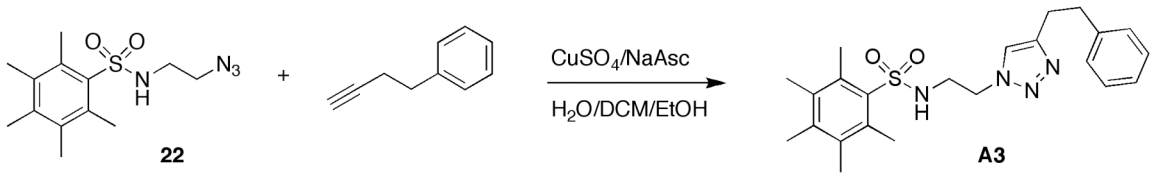

22 A3

2,3,4,5,6-pentamethyl-*N*-(2-(4-phenethyl-1*H*-1,2,3-triazol-1-yl)ethyl)benzene sulfonamide (A3). DCM (500 µL), EtOH (500 µL) and H_2O (500 µL) were added into a vial. 4-phenyl-1-butyne (9.02 µL, 64.2 µmol) and **22** (19 mg, 64 µmol) were then added, followed by sodium ascorbate (7 mg, 0.04 mmol) and 1 M $CuSO_4$ (9.63 µL, 9.63 µmol). The reaction was stirred at RT for 21 h, DCM (3 mL) and H_2O (5 mL) were added and the H_2O layer was extracted with DCM (2 x 5 mL). The organic layer was dried over Na_2SO_4, filtered

and reduced in vacuo. The product was purified via flash column chromatography using a DCM/MeOH gradient (100:0 to 99:1) mobile phase (R_f ~ 0.5 in 7% MeOH/DCM) and isolated as an off-white solid (16 mg, 59%). ^{1}H NMR (400 MHz, $CDCl_3$) δ 7.28 (2H, m), 7.17 (3H, m), 5.39 (bm, 1H), 4.36 (2H, m), 3.40 (2H, m) 3.00 (4H, m), 2.55 (6H, s), 2.74 (3H, s), 2.23 (6H, s); ^{13}C NMR (400 MHz, $CDCl_3$) δ 147.4, 141.2 139.9, 135.9, 135.1, 134.2, 128.6, 128.6, 126.4, 122.6, 50.2, 42.5, 35.7, 27.6, 19.1, 17.9, 17.2; HRMS (ESI) *m/z*, ([M + H]$^+$, $C_{23}H_{30}N_4O_2S$): theoretical 427.2162, observed 427.2156.

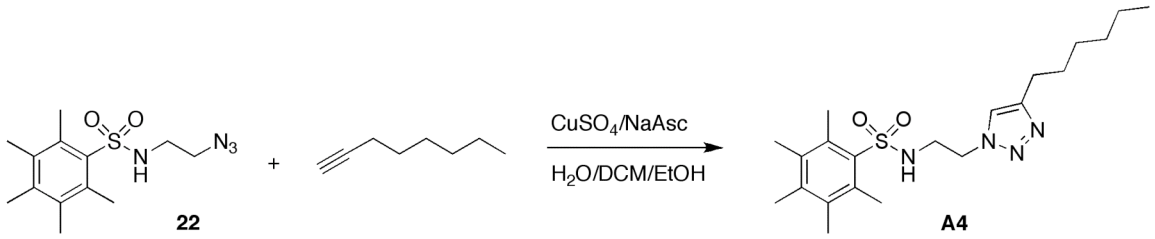

***N*-(2-(4-hexyl-1*H*-1,2,3-triazol-1-yl)ethyl)-2,3,4,5,6-pentamethylbenzenesulfonamide (A4).** DCM (2.3 mL), EtOH (2.3 mL) and H_2O (2.3 mL) were added into a vial. 1-octyne (20.48 µL, 139.3 µmol) and **22** (41.2 mg, 139 µmol) were then added, followed by sodium ascorbate (14.4 mg, 72.7 µmol) and 1 M $CuSO_4$ (20.85 µL, 20.85 µmol). The reaction was stirred at RT for 16 h, DCM (3 mL) and H_2O (5 mL) were added and the H_2O layer was extracted with DCM (2 x 5 mL). The organic layer was dried over Na_2SO_4, filtered and reduced in vacuo. The product was purified via flash column chromatography using a DCM/MeOH gradient (100:0 to 9:1) mobile phase (R_f ~ 0.7 in 10% MeOH/DCM) and isolated as an off-white solid (49 mg, 69%). ^{1}H NMR (400 MHz, $CDCl_3$) δ 0.90 (5H, m), 1.27 (3H, s), 1.33 (8H, m), 1.56 (2H, s); HRMS (ESI) *m/z*, ([M + H]$^+$, $C_{21}H_{34}N_4O_2S$): theoretical 407.2475, observed 407.2473.

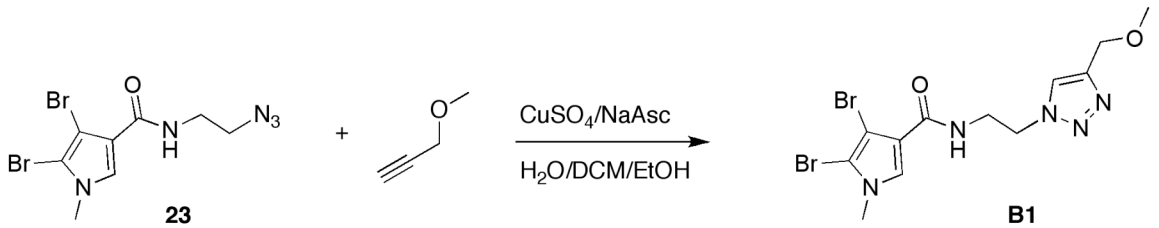

4,5-dibromo-*N*-(2-(4-(methoxymethyl)-1*H*-1,2,3-triazol-1-yl)ethyl)-1-methyl-1*H*-pyrrole-3-carboxamide (B1). DCM (500 µL), EtOH (500 µL) and H_2O (500 µL) were added into a vial. Methylpropargyl ether (7.0 µL, 139 µmol) and **23** (42.0 mg, 120 µmol) were then added, followed by sodium ascorbate (12 mg, 60.6 µmol) and 1 M $CuSO_4$ (17.9 µL, 17.9 µmol). The reaction was stirred at RT for 15 h, DCM (3 mL) and H_2O (5 mL) were added and the H_2O layer was extracted with DCM (2 x 5 mL). The organic layer was dried over Na_2SO_4, filtered and reduced in vacuo. The product was purified via flash column chromatography using a DCM/MeOH (98:2) mobile phase (R_f ~ 0.3) and isolated as a filmy white solid (32 mg, 64%). ^{1}H NMR (400 MHz, $CDCl_3$) δ 7.51 (1H, s), 7.02 (1H, bs), 6.71 (1H, s), 4.53 (4H, m), 3.94 (3H, s), 3.86 (2H, m), 3.39 (3H, s); ^{13}C NMR (400 MHz, $CDCl_3$) δ 123.7, 114.7, 66.0, 58.6, 49.8, 39.6, 35.9; HRMS (ESI) *m/z*, ($[M + H]^+$, $C_{12}H_{15}Br_2N_5O_2$): theoretical 421.9651, observed 421.9661.

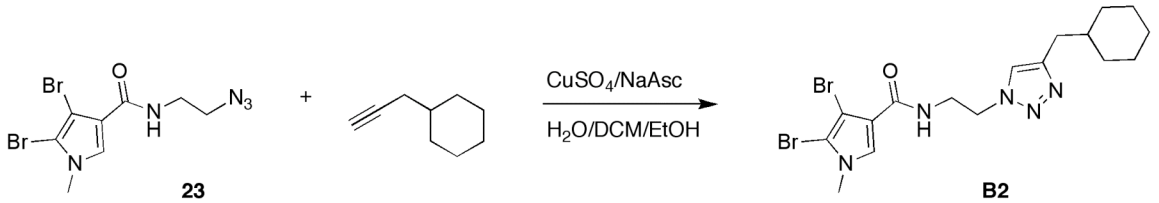

4,5-dibromo-*N*-(2-(4-(cyclohexylmethyl)-1*H*-1,2,3-triazol-1-yl)ethyl)-1-methyl-1*H*-pyrrole-3-carboxamide (B2). DCM (500 µL), EtOH (500 µL) and H_2O (500 µL) were added into a vial. 3-cyclohexyl-1-propyne (14.4 µL, 99.6 µmol) and **23** (30.0 mg, 85.5 µmol) were then added, followed by sodium ascorbate (11 mg, 56 µmol) and 1 M $CuSO_4$ (12.8 µL, 12.8 µmol). The reaction was stirred at RT for 21 h, DCM (3 mL) and H_2O (5 mL) were added and the H_2O layer was extracted with DCM (2 x 5 mL). The organic layer was dried

over Na_2SO_4, filtered and reduced in vacuo. The product was purified via flash column chromatography using a DCM/MeOH (98:2) mobile phase (R_f ~ 0.3) and isolated as an off-white solid (30 mg, 75%). ^{1}H NMR (400 MHz, $CDCl_3$) δ 7.24 (1H, m), 7.03 (1H, bm), 6.66 (1H, m), 4.50 (2H, m), 3.90 (2H, m), 3.83 (2H, m), 2.51 (2H, m), 1.66 – 1.52 (bm), 1.19 – 1.14 (4H, bm), 0.90 (2H, m); ^{13}C NMR (300 MHz, $CDCl_3$) δ 161.0, 134.4, 127.2, 114.6, 112.3, 100.4, 98.3, 38.3, 33.5, 33.2, 33.2, 26.6, 26.5, 26.3, 26.3; HRMS (ESI) *m/z*, ($[M + H]^+$, $C_{17}H_{23}Br_2N_5O$): theoretical 474.0328, observed 474.0336.

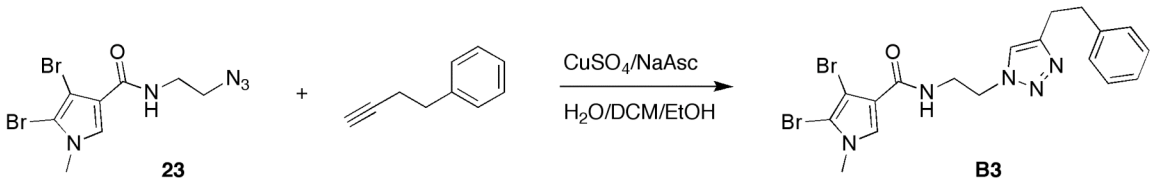

4,5-dibromo-1-methyl-*N*-(2-(4-phenethyl-1*H*-1,2,3-triazol-1-yl)ethyl)-1*H*-pyrrole-3-carboxamide (B3). DCM (500 µL), EtOH (500 µL) and H_2O (500 µL) were added into a vial. 4-phenyl-1-butyne (11.71 µL, 83.30 µmol) and **23** (32.0 mg, 91.2 µmol) were then added, followed by sodium ascorbate (9.0 mg, 45 µmol) and 1 M $CuSO_4$ (12.5 µL, 12.5 µmol). The reaction was stirred at RT for 15 h, DCM (3 mL) and H_2O (5 mL) were added and the H_2O layer was extracted with DCM (3 x 5 mL). The organic layer was dried over Na_2SO_4, filtered and reduced in vacuo. The product was purified via flash column chromatography using a DCM/MeOH (97:3) mobile phase (R_f ~ 0.5 5% MeOH/DCM) and isolated as an off-white solid (35 mg, 81%). %). ^{1}H NMR (400 MHz, $CDCl_3$) δ 7.27 (2H, m), 7.16, (4H, m), 6.93 (1H, t, *J* = 6.0 Hz), 6.70 (1H, s), 4.46 (2H, t, *J* = 5.2 Hz), 3.94 (3H, s), 3.83 (2H, dt, *J* = 5.2 Hz, 6.0 Hz), 3.03 – 2.93 (4H, bm); ^{13}C NMR (400 MHz, $CDCl_3$) δ 161.0, 147.4, 141.0, 128.6, 127.2, 126.4, 122.3, 114.6, 112.3, 98.3, 49.6, 39.6, 35.9, 35.6, 27.5; HRMS (ESI) *m/z*, ($[M + H]^+$, $C_{18}H_{19}Br_2N_5O$): theoretical 480.0035, observed 480.0029.

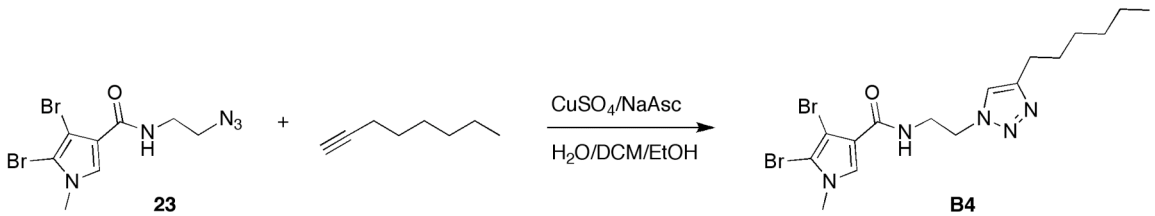

4,5-dibromo-*N*-(2-(4-hexyl-1*H*-1,2,3-triazol-1-yl)ethyl)-1-methyl-1*H*-pyrrole-3-carboxamide (B4). DCM (500 µL), EtOH (500 µL) and H_2O (500 µL) were added into a vial. 1-octyne (12.6 µL, 85.6 µmol) and **23** (33.0 mg, 94.1 µmol) were then added, followed by sodium ascorbate (9.0 mg, 45 µmol) and 1 M $CuSO_4$ (12.9 µL, 12.9 µmol). The reaction was stirred at RT for 15 h, DCM (3 mL) and H_2O (5 mL) were added and the H_2O layer was extracted with DCM (3 x 5 mL). The organic layer was dried over Na_2SO_4, filtered and reduced in vacuo. The product was purified via flash column chromatography using a DCM/MeOH (98:2) mobile phase (R_f ~ 0.45 5% MeOH/DCM) and isolated as an off-white solid (36 mg, 84%). ^{1}H NMR (400 MHz, $CDCl_3$) δ 7.25 (1H, s), 7.17, (1H, t, *J* = 6.0 Hz), 6.74 (1H, s), 4.49 (2H, t, *J* = 5.2 Hz), 3.95 (3H, s), 3.86 (2H, dt, *J* = 5.2 Hz, 6.0 Hz), 2.64 (2H, t, *J* = 7.6 Hz) 1.60 (2H, m), 1.33 – 1.24 (7H, bm) 0.86 (3H, t, *J* = 6.8 Hz); ^{13}C NMR (300 MHz, $CDCl_3$) δ 161.0, 127.2, 122.0, 114.7, 112.2, 98.3, 49.6, 39.6, 35.9, 31.7, 29.6, 29.1, 25.8, 22.7, 14.3; HRMS (ESI) *m/z*, ($[M + H]^+$, $C_{16}H_{23}Br_2N_5O$): theoretical 460.0342, observed 460.0347.

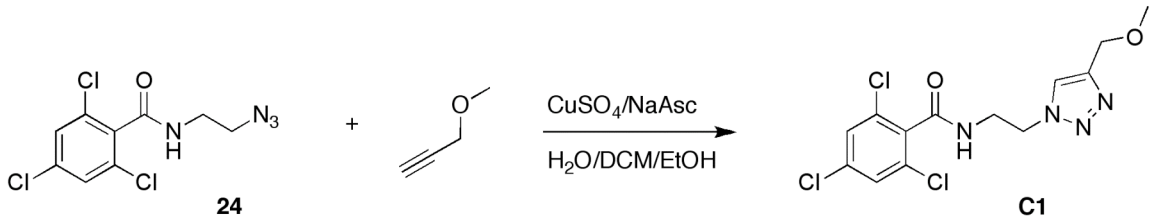

2,4,6-trichloro-*N*-(2-(4-(methoxymethyl)-1*H*-1,2,3-triazol-1-yl)ethyl)benzamide (C1). DCM (500 µL), EtOH (500 µL) and H_2O (500 µL) were added into a vial. Methylpropargyl ether (5.77 µL, 115 µmol) and **24** (29.0 mg, 105 µmol) were then added, followed by sodium ascorbate (10.0 mg, 50.5 µmol) and 1 M $CuSO_4$ (15.7 µL, 15.7 µmol). The reaction was stirred at RT for 15 h, DCM (3 mL) and H_2O (5 mL) were added and the H_2O layer was

extracted with DCM (3 x 5 mL). The organic layer was dried over Na_2SO_4, filtered and reduced in vacuo. The product was purified via flash column chromatography using a DCM/MeOH gradient (100:0 to 96:4) mobile phase (R_f ~ 0.5 5% MeOH/DCM) and isolated as an off-white solid (19 mg, 45%). ^{1}H NMR (400 MHz, $CDCl_3$) δ 7.57 (1H, s), 7.30 (1H, s), 7.23 (1H, s), 6.97 (1H, bm), 4.55 (2H, t, *J* = 5.3 Hz), 4.40 (2H, s), 3.87 (2H, dt, *J* = 5.2 Hz, 6.0 Hz), 3.31 (3H s); ^{13}C NMR (400 MHz, $CDCl_3$) δ 164.5, 145.1, 136.1, 134.2, 133.0, 128.3, 128.3, 123.8, 65.9, 58.5, 50.0, 39.7, 39.4; HRMS (ESI) *m/z*, ($[M + H]^+$, $C_{13}H_{13}Cl_3N_4O_2$): theoretical 363.0183, observed 363.0194.

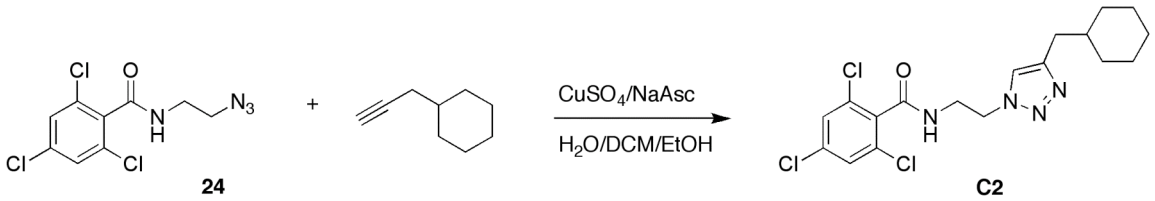

2,4,6-trichloro-*N*-(2-(4-(cyclohexylmethyl)-1*H*-1,2,3-triazol-1-yl)ethyl)benzamide (C2). DCM (500 µL), EtOH (500 µL) and H_2O (500 µL) were added into a vial. 3-cyclohexyl-1-propyne (22.9 µL, 158 µmol) and **24** (44.0 mg, 159 µmol) were then added, followed by sodium ascorbate (14.0 mg, 70.7 µmol) and 1 M $CuSO_4$ (23.8 µL, 23.8 µmol). The reaction was stirred at RT for 17 h, DCM (3 mL) and H_2O (5 mL) were added and the H_2O layer was extracted with DCM (3 x 5 mL). The organic layer was dried over Na_2SO_4, filtered and reduced in vacuo. The product was purified via flash column chromatography using a DCM/MeOH (98:2) mobile phase (R_f ~ 0.3) and isolated as a white solid (35 mg, 54%). ^{1}H NMR (400 MHz, $CDCl_3$) δ 7.76 (1H, m), 7.28 (2H, m), 4.52 (2H, t, *J* = 5.6 Hz), 4.01 (2H, dt, *J* = 5.6 Hz, 5.2 Hz), 2.29 (2H, d, *J* = 6.8 Hz), 1.65 (3H, bs), 1.54 (2H, m), 1.16 (1H, m), 1.13 (3H, m), 0.79 (2H, m); ^{13}C NMR (400 MHz, $CDCl_3$) δ 164.5, 136.1, 134.4, 133.0, 128.3, 122.8, 49.4, 39.7, 38.2, 33.3, 33.2, 26.5, 26.3; HRMS (ESI) *m/z*, ($[M + H]^+$, $C_{18}H_{21}Cl_3N_4O$): theoretical 415.0860, observed 415.0868.

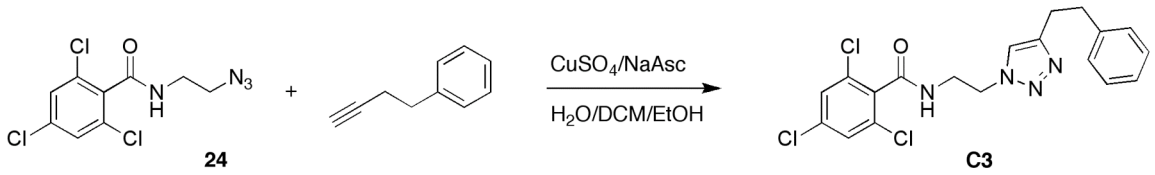

2,4,6-trichloro-*N*-(2-(4-phenethyl-1*H*-1,2,3-triazol-1-yl)ethyl)benzamide (C3). DCM (500 µL), EtOH (500 µL) and H_2O (500 µL) were added into a vial. 4-phenyl-1-butyne (15.6 µL, 111 µmol) and **24** (28.0 mg, 101 µmol) were then added, followed by sodium ascorbate (11.0 mg, 55.5 µmol) and 1 M $CuSO_4$ (15.1 µL, 15.1 µmol). The reaction was stirred at RT for 17 h, DCM (3 mL) and H_2O (5 mL) were added and the H_2O layer was extracted with DCM (3 x 5 mL). The organic layer was dried over Na_2SO_4, filtered and reduced in vacuo. The product was purified via flash column chromatography using a DCM/MeOH (98:2) mobile phase (R_f ~ 0.3) and isolated as a white solid (34 mg, 74%). ^{1}H NMR (400 MHz, $CDCl_3$) δ 7.25 (2H, m), 7.18 – 7.10 (5H, m), 4.49 (2H, t, *J* = 5.2 Hz), 3.96 (2H, dt, *J* = 5.2 Hz), 2.86 (4H, s); ^{13}C NMR (300 MHz, $CDCl_3$) δ 164.5, 141.0, 136.1, 134.3, 133.0, 128.6, 128.6, 128.3, 126.4, 122.4, 49.4, 39.8, 35.4, 27.3; HRMS (ESI) *m/z*, ($[M + H]^+$, $C_{19}H_{17}Cl_3N_4O$): theoretical 423.0547, observed 423.0540.

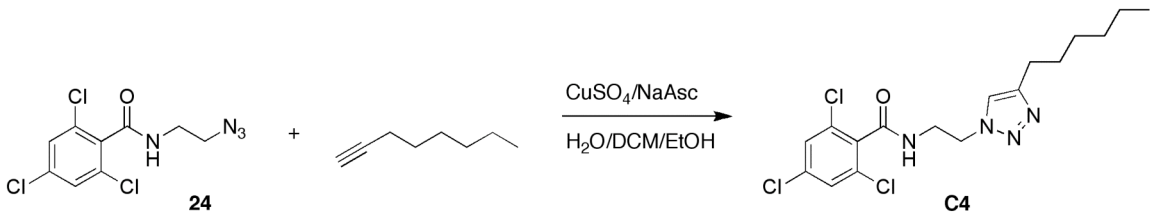

2,4,6-trichloro-*N*-(2-(4-hexyl-1*H*-1,2,3-triazol-1-yl)ethyl)benzamide (C4). DCM (500 µL), EtOH (500 µL) and H_2O (500 µL) were added into a vial. 1-octyne (15.2 µL, 103 µmol) and **24** (26.0 mg, 94.0 µmol) were then added, followed by sodium ascorbate (8.0 mg, 40 µmol) and 1 M $CuSO_4$ (14.1 µL, 14.1 µmol). The reaction was stirred at RT for 17 h, DCM (3 mL) and H_2O (5 mL) were added and the H_2O layer was extracted with DCM (3 x 5 mL). The organic layer was dried over Na_2SO_4, filtered and reduced in vacuo. The product was purified via flash column chromatography using a DCM/MeOH (98:2) mobile phase (R_f ~ 0.3) and isolated as a white solid (24 mg, 59%). ^{1}H NMR (400 MHz, $CDCl_3$) δ 7.40 (1H, m),

7.28 (1H, m), 4.50 (2H, t, J = 5.2 Hz), 3.99 (2H, dt, J = 5.2 Hz, 6.0 Hz), 2.44 (2H, t, J = 7.6 Hz), 1.47 (2H, m), 1.24 (6H, m), 0.85 (3H, t, J = 6.8 Hz); ^{13}C NMR (300 MHz, $CDCl_3$) δ 164.5, 136.0, 134.4, 133.0, 128.3, 122.1 49.4, 39.7, 31.7, 29.4, 29.1, 25.6, 22.8, 14.3; HRMS (ESI) *m/z*, ($[M + H]^+$, $C_{17}H_{21}Cl_3N_4O$): theoretical 403.0866, observed 403.0857.

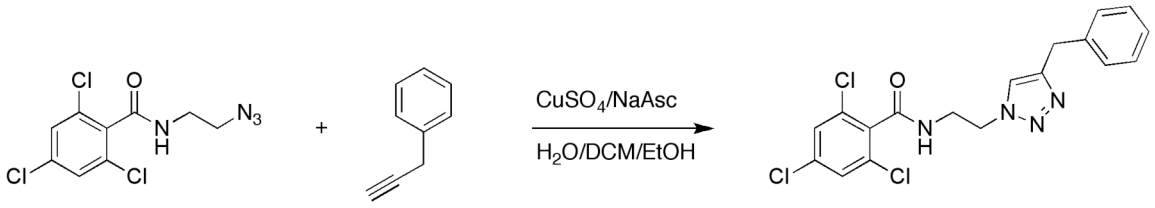

24 **C5**

***N*-(2-(4-benzyl-1*H*-1,2,3-triazol-1-yl)ethyl)-2,4,6-trichlorobenzamide (C5).** DCM (1 mL), EtOH (1 mL) and H_2O (1 mL) were added into a vial. 3-phenyl-1-propyne (25 µL, 201 µmol) and **24** (55.2 mg, 199 µmol) were then added, followed by sodium ascorbate (20.2 mg, 102 µmol) and 1 M $CuSO_4$ (31.0 µL, 31.0 µmol). The reaction was stirred at RT for 14 h, DCM (6 mL) and H_2O (8 mL) were added and the H_2O layer was extracted with DCM (3 x 8 mL). The organic layer was dried over Na_2SO_4, filtered and reduced in vacuo. The product was purified via flash column chromatography using a DCM/MeOH (100:1) mobile phase (R_f ~ 0.3) and isolated as an off-white solid (44 mg, 53%). ^{1}H NMR (400 MHz, $CDCl_3$) δ 7.58 (1H, s), 7.29 (3H, m), 7.16 (2H, m), 4.52 (2H, t, J = 5.6 Hz), 3.99 (2H, dt, J = 5.6 Hz, 5.2 Hz), 3.89 (2H, s); ^{13}C NMR (300 MHz, $CDCl_3$) δ 164.6, 138.8, 136.0, 134.4, 132.9, 128.9, 128.7, 128.2, 126.9, 123.1, 49.4, 39.8, 32.1, 29.9; HRMS (ESI) *m/z*, ($[M + H]^+$, $C_{18}H_{15}Cl_3N_4O$): theoretical 409.0384, observed 409.0388.

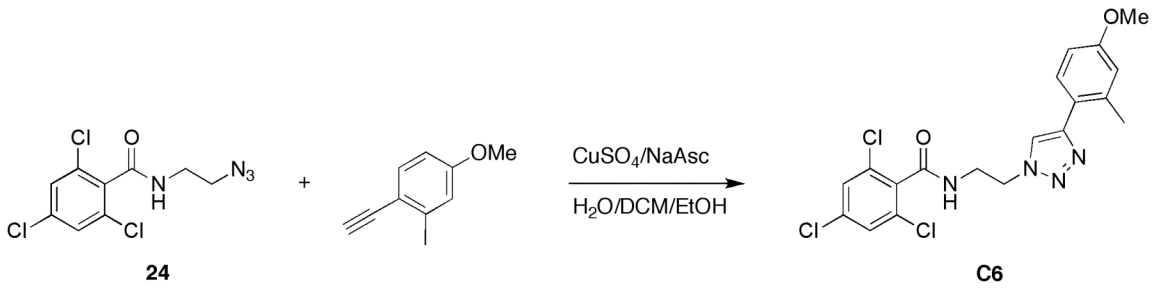

24 **C6**

2,4,6-trichloro-*N*-(2-(4-(4-methoxy-2-methylphenyl)-1*H*-1,2,3-triazol-1-yl)ethyl)benzamide (C6). DCM (1 mL), EtOH (1 mL) and H_2O (1 mL) were added into a vial. 1-ethynyl-4-methoxy-2-methylbenzene (24.4 mg, 166 µmol) and **24** (44.3 mg, 159 µmol) were then added, followed by sodium ascorbate (16.9 mg, 85.1 µmol) and 1 M $CuSO_4$ (24.0 µL, 24.0 µmol). The reaction was stirred at RT for 6 h, DCM (6 mL) and H_2O (8 mL) were added and the H_2O layer was extracted with DCM (3 x 8 mL). The organic layer was dried over Na_2SO_4, filtered and reduced in vacuo. The product was purified via flash column chromatography using a DCM/MeOH (99:1) mobile phase (R_f ~ 0.3) and isolated as a white solid (65 mg, 92%). ^{1}H NMR (400 MHz, $CDCl_3$) δ 8.03 (1H, m), 7.64, (1H, s), 7.29 (1H, m) 6.71 – 6.65 (2H, bm), 4.63 (2H, t, *J* = 5.6 Hz), 4.11 (2H, dt, *J* = 5.6 Hz, 5.2 Hz), 3.85 (3H, s), 2.17 (3H, s); HRMS (ESI) *m/z*, ($[M + H]^+$, $C_{19}H_{17}Cl_3N_4O_2$): theoretical 439.0490, observed 439.0496.

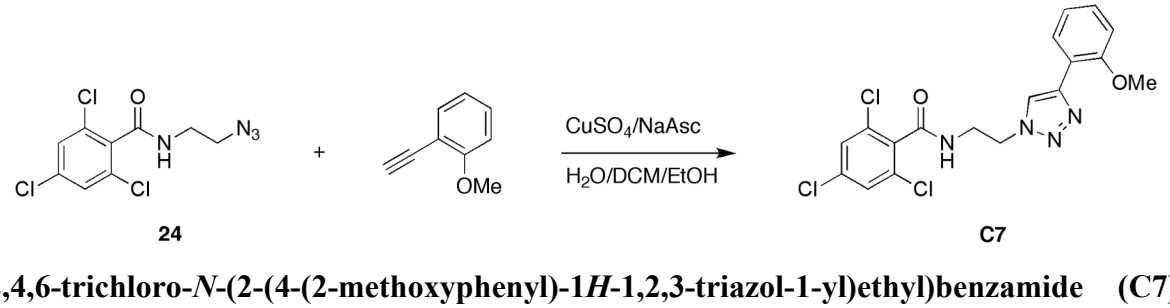

24 **C7**

2,4,6-trichloro-*N*-(2-(4-(2-methoxyphenyl)-1*H*-1,2,3-triazol-1-yl)ethyl)benzamide (C7). DCM (1 mL), EtOH (1 mL) and H_2O (1 mL) were added into a vial. 2-ethynylanisole (24.0 µL, 186 µmol) and **24** (46.6 mg, 168 µmol) were then added, followed by sodium ascorbate (19.3 mg, 97.4 µmol) and 1 M $CuSO_4$ (30.0 µL, 30.0 µmol). The reaction was stirred at RT for 4 h, DCM (6 mL) and H_2O (8 mL) were added and the H_2O layer was extracted with

DCM (3 x 8 mL). The organic layer was dried over Na_2SO_4, filtered and reduced in vacuo. The product was purified via flash column chromatography using a DCM/MeOH (98:2) mobile phase (R_f ~ 0.3) and isolated as a white solid (70 mg, 98%). ^{1}H NMR (400 MHz, $CDCl_3$) δ 8.08 (1H, s), 7.92 (1H, d, *J* = 7.6 Hz), 7.31 (2H, s), 6.93 (1H, t, *J* = 7.2 Hz), 6.86 (1H, m), 4.63 (2H, s), 4.10 (2H, s), 3.85 (2H, s); ^{13}C NMR (400 MHz, $CDCl_3$) δ 164.5, 155.7, 136.1, 133.1, 129.1, 128.3, 127.2, 124.7, 120.9, 118.9, 110.8, 55.4, 49.7, 40.0; HRMS (ESI) *m/z*, ($[M + H]^+$, $C_{18}H_{15}Cl_3N_4O_2$): theoretical 425.0333, observed 425.0336.

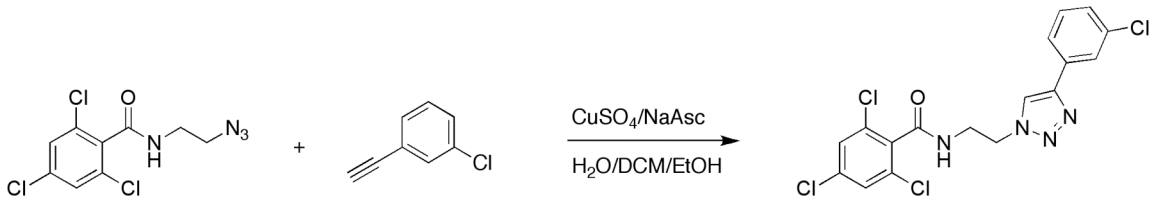

24 **C8**

2,4,6-trichloro-*N*-(2-(4-(3-chlorophenyl)-1*H*-1,2,3-triazol-1-yl)ethyl)benzamide (C8). DCM (1 mL), EtOH (1 mL) and H_2O (1 mL) were added into a vial. 3-chloro-1-ethynylbenzene (23.0 µL, 187 µmol) and **24** (51.3 mg, 185 µmol) were then added, followed by sodium ascorbate (24.7 mg, 125 µmol) and 1 M $CuSO_4$ (28.0 µL, 28.0 µmol). The reaction was stirred at RT for 2.5 h, DCM (6 mL) and H_2O (8 mL) were added and the H_2O layer was extracted with DCM (2 x 8 mL). The organic layer was dried over Na_2SO_4, filtered and reduced in vacuo. The product was purified via flash column chromatography using a DCM/MeOH gradient (100:1 to 96:4) mobile phase (R_f ~ 0.3 4% MeOH/DCM) and isolated as a filmy sand colored solid (47 mg, 59%). ^{1}H NMR (400 MHz, $CDCl_3$) δ 7.83 (1H, s), 7.54 (1H, s), 7.39 (2H, m), 7.29 (2H, s), 7.24 (1H, m), 4.62 (2H, t, *J* = 5.6 Hz), 4.04 (2H, dt, *J* = 5.6 Hz, 5.2 Hz); ^{13}C NMR (400 MHz, $CDCl_3$) δ 164.6, 164,2, 136.2, 135.0, 134.3, 134.2, 133.0, 132.9, 131.9, 130.2, 128.5, 128.3, 125.6, 123.5, 94.5, 50.9, 49.8, 39.8, 39.4; HRMS (ESI) *m/z*, ($[M + H]^+$, $C_{17}H_{12}Cl_4N_4O$): theoretical 428.9838, observed 428.9844.

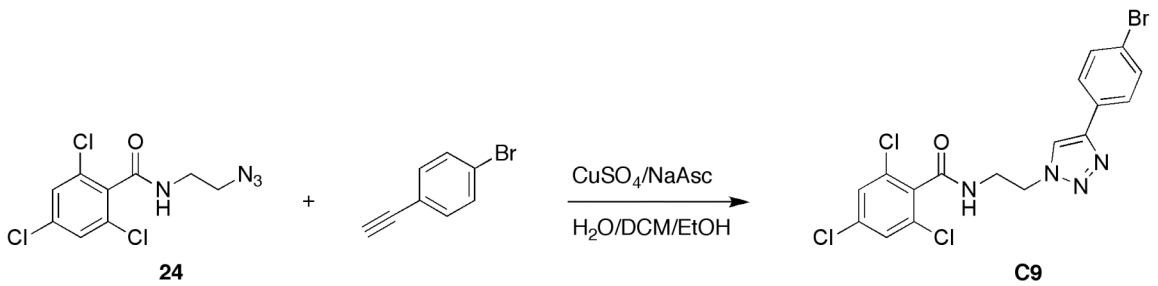

24 C9

***N*-(2-(4-(4-bromophenyl)-1*H*-1,2,3-triazol-1-yl)ethyl)-2,4,6-trichlorobenzamide (C9).** DCM (1 mL), EtOH (1 mL) and H_2O (1 mL) were added into a vial. 1-bromo-4-ethynylbenzene (40.0 mg, 221 µmol) and **24** (49.2 mg, 177 µmol) were then added, followed by sodium ascorbate (17.0 mg, 85.8 µmol) and 1 M $CuSO_4$ (31.0 µL, 31.0 µmol). The reaction was stirred at RT for 14 h, DCM (6 mL) and H_2O (8 mL) were added and the H_2O layer was extracted with DCM (3 x 8 mL). The organic layer was dried over Na_2SO_4, filtered and reduced in vacuo. The product was purified via flash column chromatography using a DCM/MeOH gradient (100:1 to 96:4) mobile phase (R_f ~ 0.4 4% MeOH/DCM) and isolated as an eggshell colored solid (56 mg, 43%). ^{1}H NMR (300 MHz, $CDCl_3$) δ 7.73 (1H, s), 7.52 (1H, bs), 7.33 (2H, d, *J* = 8.1 Hz), 7.20 (2H, d, *J* = 8.1 Hz), 4.57 (2H, t, *J* = 6.0 Hz), 4.03 (2H, dt, *J* = 6.0 Hz, 5.1 Hz); ^{13}C NMR (300 MHz, $CDCl_3$) δ 164.6, 146.4, 136.2, 134.3, 133.0, 132.1, 129.0, 128.3, 126.8, 122.4, 121.4, 49.9, 39.9; HRMS (ESI) *m/z*, ($[M + H]^+$, $C_{17}H_{12}BrCl_3N_4O$): theoretical 472.9333, observed 472.9335.

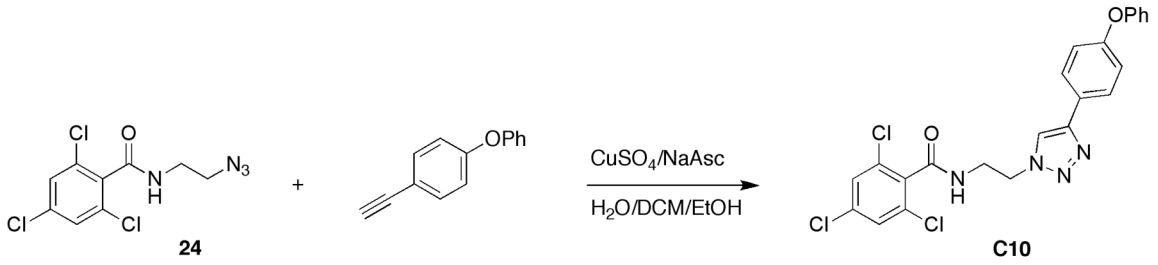

24 C10

2,4,6-trichloro-*N*-(2-(4-(4-phenoxyphenyl)-1*H*-1,2,3-triazol-1-yl)ethyl)benzamide (C10). DCM (1 mL), EtOH (1 mL) and H_2O (1 mL) were added into a vial. 1-ethynyl-4-phenoxybenzene (27.0 µL, 149 µmol) and **24** (40.1 mg, 145 µmol) were then added, followed by sodium ascorbate (17.6 mg, 88.8 µmol) and 1 M $CuSO_4$ (22.0 µL, 22.0 µmol).

The reaction was stirred at RT for 20 h, DCM (6 mL) and H_2O (8 mL) were added and the H_2O layer was extracted with DCM (2 x 8 mL). The organic layer was dried over Na_2SO_4, filtered and reduced in vacuo. The product was purified via flash column chromatography using a DCM/MeOH gradient (99:1 to 96:4) mobile phase (R_f ~ 0.3 4% MeOH/DCM) and isolated as a white solid (60 mg, 85%). ^{1}H NMR (300 MHz, $CDCl_3$) δ 7.78 (1H, m), 7.72 – 7.30 (4H, bm), 7.15 (1H, m), 7.02 (2H, d, *J* = 7.8 Hz), 6.87 (2H, d, *J* = 8.7 Hz), 4.60 (2H, t, *J* = 5.4 Hz), 4.07 (2H, dt, *J* = 5.4 Hz, 4.8 Hz); ^{13}C NMR (300 MHz, $CDCl_3$) δ 175.1, 164.6, 157.7, 156.8, 146.9, 136.1, 134.4, 133.0, 130.1, 128.3, 126.8, 125.0, 124.0, 121.0, 119.5, 118.8, 49,9, 40.0; HRMS (ESI) *m/z*, ($[M + H]^+$, $C_{23}H_{17}Cl_3N_4O_2$): theoretical 487.0490, observed 487.0487.

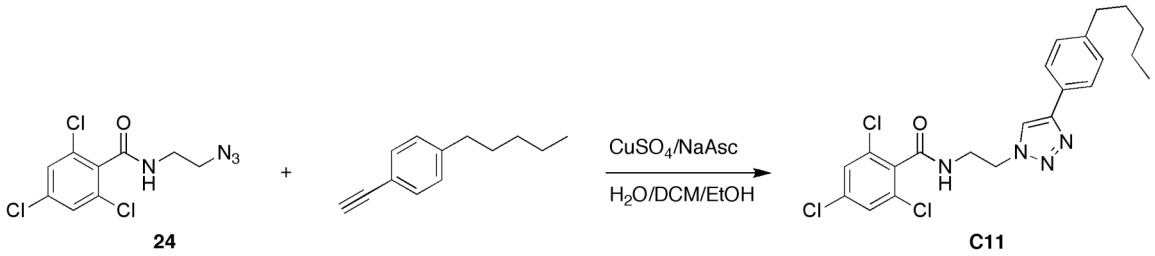

2,4,6-trichloro-*N*-(2-(4-(4-pentylphenyl)-1*H*-1,2,3-triazol-1-yl)ethyl)benzamide (C11). DCM (1 mL), EtOH (1 mL) and H_2O (1 mL) were added into a vial. 4-pentylphenylacetylene (30.0 µL, 154 µmol) and **24** (42.5 mg, 153 µmol) were then added, followed by sodium ascorbate (18.0 mg, 90.8 µmol) and 1 M $CuSO_4$ (23.0 µL, 23.0 µmol). The reaction was stirred at RT for 5 h, DCM (6 mL) and H_2O (8 mL) were added and the H_2O layer was extracted with DCM (2 x 8 mL). The organic layer was dried over Na_2SO_4, filtered and reduced in vacuo. The product was purified via flash column chromatography using a DCM/MeOH (100:1) mobile phase (R_f ~ 0.6 4% MeOH/DCM) and isolated as a filmy off-white solid (64 mg, 90%). %). ^{1}H NMR (400 MHz, $CDCl_3$) δ 7.96 (1H, s), 7.71 (1H, s), 7.25 (2H, m), 7.03 (2H, d, *J* = 6.8 Hz), 4.57 (2H, m), 4.04 (2H, m), 2.58 (2H, t, *J* = 7.6 Hz), 1.62 (2H, m), 1.33 (4H, m), 0.92 (3H, t, *J* = 4.8 Hz); ^{13}C NMR (300 MHz, $CDCl_3$) δ 164.6, 159.4, 146.3, 137.1, 135.8, 134.4, 132.9, 129.6, 128.1, 122.9, 122.1, 116.4, 111.4, 100.4, 55.4, 53.3,

49.7, 48.8, 39.8, 29.9, 21.5; HRMS (ESI) *m/z*, ([M + H]$^+$, $C_{22}H_{23}Cl_3N_4O$): theoretical 465.1016, observed 465.1015.

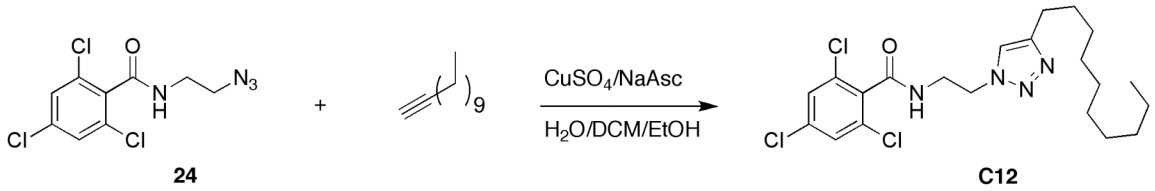

24 **C12**

2,4,6-trichloro-*N*-(2-(4-decyl-1*H*-1,2,3-triazol-1-yl)ethyl)benzamide (C12). DCM (1 mL), EtOH (1 mL) and H_2O (1 mL) were added into a vial. 1-dodecyne (39.0 µL, 182 µmol) and **24** (49.4 mg, 178 µmol) were then added, followed by sodium ascorbate (17.7 mg, 89.3 µmol) and 1 M $CuSO_4$ (28.0 µL, 28.0 µmol). The reaction was stirred at RT for 5 h, DCM (6 mL) and H_2O (8 mL) were added and the H_2O layer was extracted with DCM (2 x 8 mL). The organic layer was dried over Na_2SO_4, filtered and reduced in vacuo. The product was purified via flash column chromatography using a DCM/MeOH (100:1) mobile phase (R_f ~ 0.6 2% MeOH/DCM) and isolated as an eggshell colored solid (72 mg, 88%). ^{1}H NMR (400 MHz, $CDCl_3$) δ 7.83 (1H, s), 7.29 (1H, s), 4.50 (2H, t, *J* = 5.6 Hz), 3.99 (2H, dt, *J* = 5.6 Hz, 5.2 Hz), 2.38 (2H, t, *J* = 7.6 Hz), 1.45 (2H, m), 1.24 (14H, m), 0.86 (3H, d, *J* = 6.8 Hz); ^{13}C NMR (300 MHz, $CDCl_3$) δ 164.5, 135.8, 134.5, 133.0, 128.2, 122.2, 100.0, 49.4, 39.8, 32.1, 29.8, 29.8, 29.6, 29.5, 29.4, 25.5, 22.8, 14.3; HRMS (ESI) *m/z*, ([M + H]$^+$, $C_{17}H_{19}Cl_3N_4O$): theoretical 459.1480, observed 459.1480.

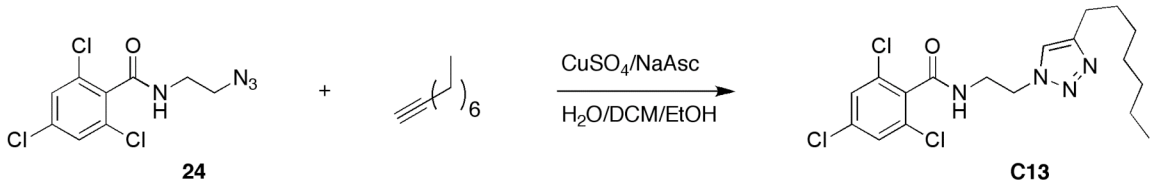

24 **C13**

2,4,6-trichloro-*N*-(2-(4-heptyl-1*H*-1,2,3-triazol-1-yl)ethyl)benzamide (C13). DCM (1 mL), EtOH (1 mL) and H_2O (1 mL) were added into a vial. 1-nonyne (32.0 µL, 195 µmol) and **24** (52.7 mg, 190 µmol) were then added, followed by sodium ascorbate (18.9 mg, 95.8 µmol) and 1 M $CuSO_4$ (28.5 µL, 28.5 µmol). The reaction was stirred at RT for 4 h, DCM (6

mL) and H_2O (8 mL) were added and the H_2O layer was extracted with DCM (2 x 8 mL). The organic layer was dried over Na_2SO_4, filtered and reduced in vacuo. The product was purified via flash column chromatography using a DCM/MeOH (99:1) mobile phase (R_f ~ 0.4 2% MeOH/DCM) and isolated as a white solid (56 mg, 70%). ^{1}H NMR (400 MHz, $CDCl_3$) δ 7.83 (1H, s), 7.29 (1H, s) 4.50 (2H, t, *J* = 5.6 Hz), 3.99 (2H, dt, *J* = 5.6 Hz, 5.2 Hz), 2.38 (2H, t, *J* = 7.6 Hz), 1.45 (2H, m), 1.26 (8H, m), 0.86 (3H, t, 6.8 Hz); ^{13}C NMR (400 MHz, $CDCl_3$) δ 164.5, 148.2, 136.0, 134.5, 133.0, 128.3, 122.2, 49.4, 39.8, 32.0, 29.5, 29.4, 29.2, 25.6, 22.8, 14.3; HRMS (ESI) *m/z*, ($[M + H]^+$, $C_{18}H_{23}Cl_3N_4O$): theoretical 417.1010, observed 417.1014.

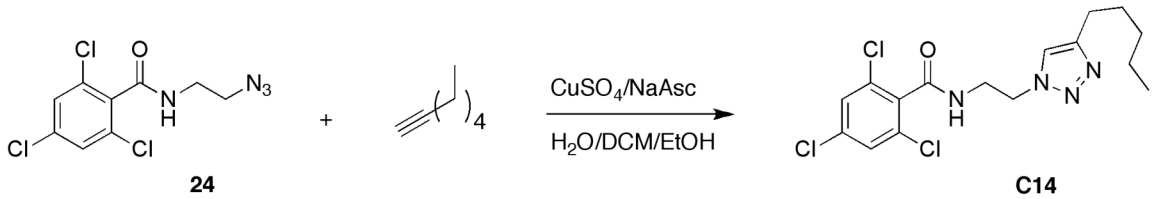

2,4,6-trichloro-*N*-(2-(4-pentyl-1*H*-1,2,3-triazol-1-yl)ethyl)benzamide (C14). DCM (1 mL), EtOH (1 mL) and H_2O (1 mL) were added into a vial. 1-heptyne (26.6 µL, 203 µmol) and **24** (56.3 mg, 203 µmol) were then added, followed by sodium ascorbate (19.2 mg, 96.9 µmol) and 1 M $CuSO_4$ (30.0 µL, 30.0 µmol). The reaction was stirred at RT for 17 h, DCM (6 mL) and H_2O (8 mL) were added and the H_2O layer was extracted with DCM (2 x 8 mL). The organic layer was dried over Na_2SO_4, filtered and reduced in vacuo. The product was purified via flash column chromatography using a DCM/MeOH (100:1) mobile phase (R_f ~ 0.4 1% MeOH/DCM) and isolated as an off-white solid (62 mg, 86%). ^{1}H NMR (400 MHz, $CDCl_3$) δ 7.71 (1H, s), 7.29 (1H, s), 4.50 (2H, t, *J* = 5.6 Hz), 3.98 (2H, dt, *J* – 5.6 Hz, 5.2 Hz), 2.40 (2H, t, *J* = 7.6 Hz), 1.47 (2H, m), 1.23 (5H, bm), 0.86 (3H, t, *J* = 6.8 Hz); ^{13}C NMR (400 MHz, $CDCl_3$) δ 164.5, 136.0, 135.9, 134.5, 133.0, 128.2, 49.4, 39.7, 31.6, 29.9, 29.1, 25.6, 22.6, 14.2; HRMS (ESI) *m/z*, ($[M + H]^+$, $C_{16}H_{19}Cl_3N_4O$): theoretical 389.0697, observed 389.0694.

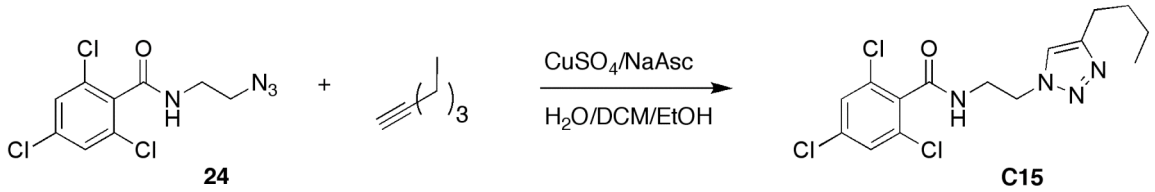

24 **C15**

***N*-(2-(4-butyl-1*H*-1,2,3-triazol-1-yl)ethyl)-2,4,6-trichlorobenzamide (C15).** DCM (1 mL), EtOH (1 mL) and H_2O (1 mL) were added into a vial. 1-hexyne (23.3 µL, 207 µmol) and **24** (57.4 mg, 207 µmol) were then added, followed by sodium ascorbate (21.9 mg, 111 µmol) and 1 M $CuSO_4$ (31.0 µL, 31.0 µmol). The reaction was stirred at RT for 16 h, DCM (6 mL) and H_2O (8 mL) were added and the H_2O layer was extracted with DCM (2 x 8 mL). The organic layer was dried over Na_2SO_4, filtered and reduced in vacuo. The product was purified via flash column chromatography using a DCM/MeOH (100:1) mobile phase (R_f ~ 0.5 1% MeOH/DCM) and isolated as an off-white solid (22 mg, 67%). ^{1}H NMR (400 MHz, $CDCl_3$) δ 7.72 (1H, t, *J* = 5.6 Hz), 7.29 (1H, s), 4.50 (2H, t, *J* = 6.0 Hz), 3.98 (2H, dt, *J* = 5.6 Hz, 6.0 Hz), 2.40 (2H, t, *J* = 7.6 Hz), 1.43 (2H, dt, *J* = 7.6 Hz, 7.2 Hz), 1.25 (2H, m), 0.86 (3H, t, *J* = 7.6 Hz); ^{13}C NMR (300 MHz, $CDCl_3$) δ 164.5, 135.9, 134.5, 133.0, 128.2, 128.2, 49.4, 39.8, 31.5, 25.2, 22.5, 14.0; HRMS (ESI) *m/z*, ($[M + H]^+$, $C_{15}H_{17}Cl_3N_4O$): theoretical 375.0541, observed 375.0543.

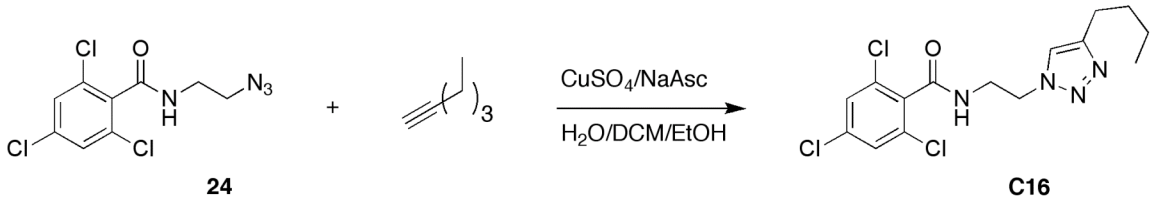

24 **C16**

2,4,6-trichloro-*N*-(2-(4-isopentyl-1*H*-1,2,3-triazol-1-yl)ethyl)benzamide (C16). DCM (1 mL), EtOH (1 mL) and H_2O (1 mL) were added into a vial. 5-methyl-1-hexyne (28.0 µL, 212 µmol) and **24** (58.4 mg, 210 µmol) were then added, followed by sodium ascorbate (38.0 mg, 192 µmol) and 1 M $CuSO_4$ (38.0 µL, 38.0 µmol). The reaction was stirred at RT for 14 h, DCM (6 mL) and H_2O (8 mL) were added and the H_2O layer was extracted with DCM (2 x 8 mL). The organic layer was dried over Na_2SO_4, filtered and reduced in vacuo. The product was purified via flash column chromatography using a DCM/MeOH (99:1) mobile phase (R_f

~ 0.3 1% MeOH/DCM) and isolated as an off-white solid (65 mg, 82%). ^{1}H NMR (400 MHz, $CDCl_3$) δ 7.96 (1H, s), 7.27 (1H, s), 4.52 (2H, s), 4.00 (2H, s) 2.41 (2H, s) 1.50 (1H, m), 1.37 (2H, s), 0.88 (6H, d, 6.4 Hz; ^{13}C NMR (300 MHz, $CDCl_3$) δ 164.5, 136.0, 134.4, 133.0, 128.3, 49.5, 39.7, 38.4, 27.8, 23.5, 22.5; HRMS (ESI) *m/z*, ($[M + H]^+$, $C_{16}H_{19}Cl_3N_4O$): theoretical 389.0697, observed 389.0705.

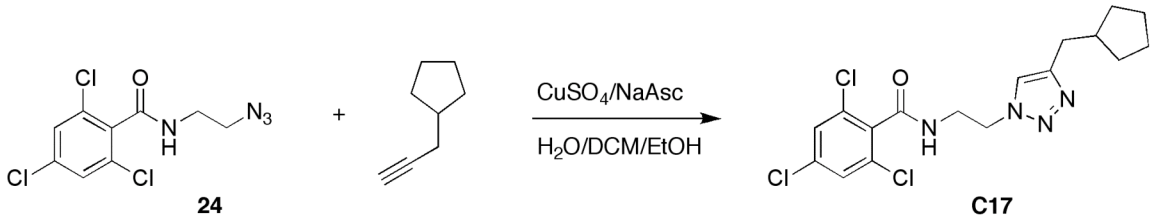

2,4,6-trichloro-*N*-(2-(4-(cyclopentylmethyl)-1*H*-1,2,3-triazol-1-yl)ethyl)benzamide (C17). DCM (1 mL), EtOH (1 mL) and H_2O (1 mL) were added into a vial. 3-cyclopentyl-1-propyne (24.8 µL, 190 µmol) and **24** (52.5 mg, 189 µmol) were then added, followed by sodium ascorbate (20.3 mg, 102 µmol) and 1 M $CuSO_4$ (29.0 µL, 29.0 µmol). The reaction was stirred at RT for 16 h, DCM (6 mL) and H_2O (8 mL) were added and the H_2O layer was extracted with DCM (2 x 8 mL). The organic layer was dried over Na_2SO_4, filtered and reduced in vacuo. The product was purified via flash column chromatography using a DCM/MeOH (100:1) mobile phase (R_f ~ 0.4 1% MeOH/DCM) and isolated as an off-white solid (52 mg, 69%). ^{1}H NMR (400 MHz, $CDCl_3$) δ 7.80 (1H, s), 7.28 (1H, m), 4.50 (2H, t, *J* = 5.6 Hz), 3.99 (2H, dt, *J* = 5.6 Hz, 5.2 Hz), 2.39 (2H, d, *J* = 7.6 Hz), 1.91 (1H, m), 1.64 – 1.45 (6H, bm), 1.08 – 1.01 (2H, bm); ^{13}C NMR (400 MHz, $CDCl_3$) δ 202.2, 164.6, 135.9, 134.6, 133.1, 128.2, 49.5, 40.0, 39.8, 32.7, 31.7, 29.9, 25.2; HRMS (ESI) *m/z*, ($[M + H]^+$, $C_{17}H_{19}Cl_3N_4O$): theoretical 401.0697, observed 401.0700.

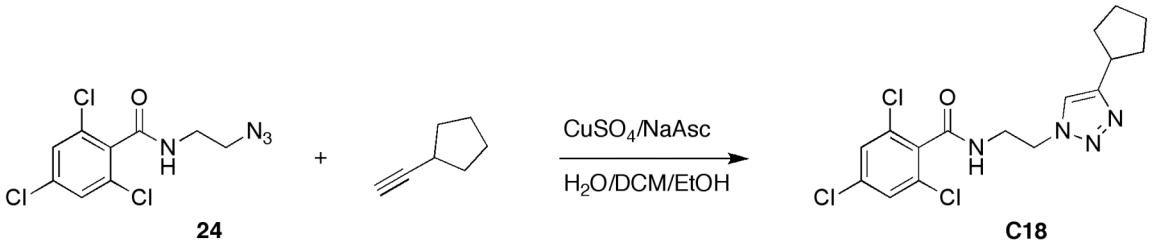

24 **C18**

2,4,6-trichloro-*N*-(2-(4-cyclopentyl-1*H*-1,2,3-triazol-1-yl)ethyl)benzamide (C18). DCM (1 mL), EtOH (1 mL) and H_2O (1 mL) were added into a vial. cyclopentylacetylene (22.4 mg, 223 µmol) and **24** (61.8 mg, 238 µmol) were then added, followed by sodium ascorbate (37.0 mg, 187 µmol) and 1 M $CuSO_4$ (34.0 µL, 34.0 µmol). The reaction was stirred at RT for 16 h, DCM (6 mL) and H_2O (8 mL) were added and the H_2O layer was extracted with DCM (3 x 8 mL). The organic layer was dried over Na_2SO_4, filtered and reduced in vacuo. The product was purified via flash column chromatography using a DCM/MeOH (100:1) mobile phase (R_f ~ 0.4 2% MeOH/DCM) and isolated as an off-white solid (68 mg, 78%). ^{1}H NMR (400 MHz, $CDCl_3$) δ 7.78 (1H, s), 7.25 (1H, s), 4.53 (2H, s), 4.02 (2H, s), 2.85 (1H, s) 1.90 (2H, s), 1.64 (4H, m), 1.44 (2H, s); ^{13}C NMR (300 MHz, $CDCl_3$) δ 164.6, 135.9, 134.5, 133.0, 128.2, 39.7, 32.9, 29.9, 25.1, 23.3, 14.3; HRMS (ESI) *m/z*, ($[M + H]^+$, $C_{16}H_{17}Cl_3N_4O$): theoretical 387.0541, observed 387.0544.

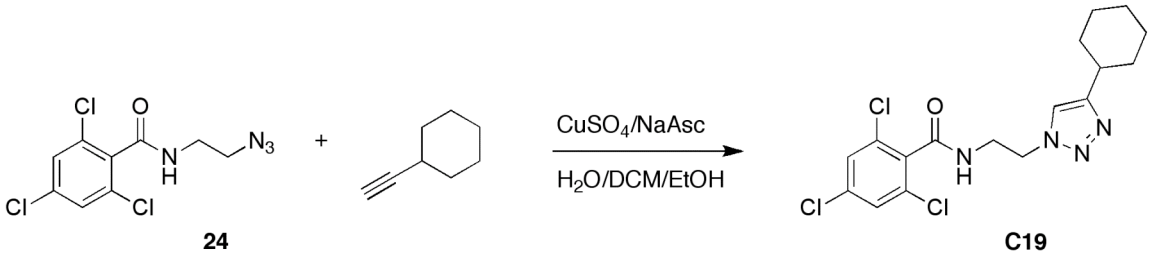

24 **C19**

2,4,6-trichloro-*N*-(2-(4-cyclohexyl-1*H*-1,2,3-triazol-1-yl)ethyl)benzamide (C19). DCM (1 mL), EtOH (1 mL) and H_2O (1 mL) were added into a vial. Cyclohexylacetylene (24.8 µL, 192 µmol) and **24** (53.3 mg, 192 µmol) were then added, followed by sodium ascorbate (22.4 mg, 113 µmol) and 1 M $CuSO_4$ (29.0 µL, 29.0 µmol). The reaction was stirred at RT for 17 h, DCM (6 mL) and H_2O (8 mL) were added and the H_2O layer was extracted with DCM (3 x 8 mL). The organic layer was dried over Na_2SO_4, filtered and reduced in vacuo. The product

was purified via flash column chromatography using a DCM/MeOH (100:1) mobile phase (R_f ~ 0.5 2% MeOH/DCM) and isolated as an off-white solid (60 mg, 78%). ^{1}H NMR (400 MHz, $CDCl_3$) δ 7.97 (1H, t, *J* = 5.2 Hz), 7.25 (2H, s), 4.50 (1H, t, *J* = 5.6 Hz), 4.00 (2H, dt, *J* = 5.6 Hz, 5.2 Hz), 2.37 (1H, m), 1.76 – 1.30 (5H, bm), 1.29 – 1.08 (7H, bm); ^{13}C NMR (300 MHz, $CDCl_3$) δ 202.3, 164.6, 153.1, 135.9, 134.5, 133.0, 128.1, 121.1, 49.4, 39.9, 35.2, 32.9, 29.9, 26.2, 26.1; HRMS (ESI) *m/z*, ($[M + H]^+$, $C_{17}H_{19}Cl_3N_4O$): theoretical 401.0697, observed 401.0697.

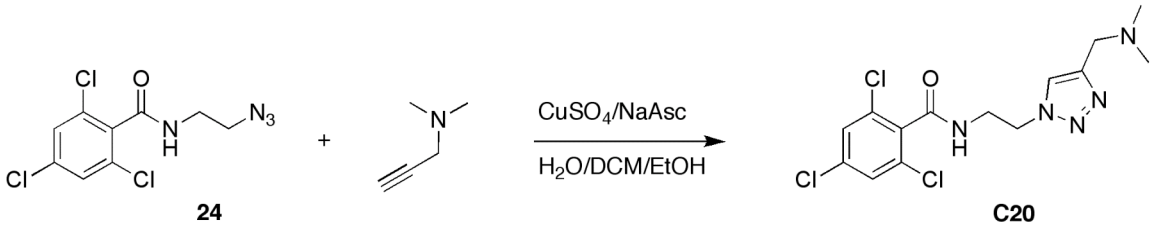

24 **C20**

2,4,6-trichloro-*N*-(2-(4-((dimethylamino)methyl)-1*H*-1,2,3-triazol-1-yl)ethyl) benzamide (C20). DCM (1 mL), EtOH (1 mL) and H_2O (1 mL) were added into a vial. Cyclohexylacetylene (24.8 µL, 192 µmol) and **24** (53.3 mg, 192 µmol) were then added, followed by sodium ascorbate (22.4 mg, 113 µmol) and 1 M $CuSO_4$ (29.0 µL, 29.0 µmol). The reaction was stirred at RT for 37 h, DCM (6 mL) and H_2O (8 mL) were added and the H_2O layer was extracted with DCM (3 x 8 mL). The organic layer was dried over Na_2SO_4, filtered and reduced in vacuo. The product was purified via flash column chromatography using a DCM/MeOH gradient (100:1 to 96:4) mobile phase (R_f ~ 0.3 4% MeOH/DCM), however the product was difficult to elute off of the column. DCM/NH_3 (sat.) MeOH (9:1 to 8:2) was added to flush product through the silica. All fractions were collected, evaporated in vacuo and recrystallized in $CDCl_3$. The product was isolated as a white needle-shaped solid (18 mg, 22%). ^{1}H NMR (400 MHz, $CDCl_3$) δ 7.55 (1H, s), 7.22 (1H, s), 4.55 (2H, m), 3.99 (2H, m), 3.47 (2H, s); ^{13}C NMR (300 MHz, $CDCl_3$) δ 164.547, 147.8, 143.4, 136.2, 134.3, 133.0, 129.0, 128.4, 127.5, 125.5, 120.8, 49.8, 39.9, 35.9, 31.7, 31.3, 22.8, 14.3; HRMS (ESI) *m/z*, ($[M + H]^+$, $C_{14}H_{16}Cl_3N_5O$): (inconclusive) theoretical 376.0500, observed 301.1413, 361.2348, 405.2618, 537.3401.

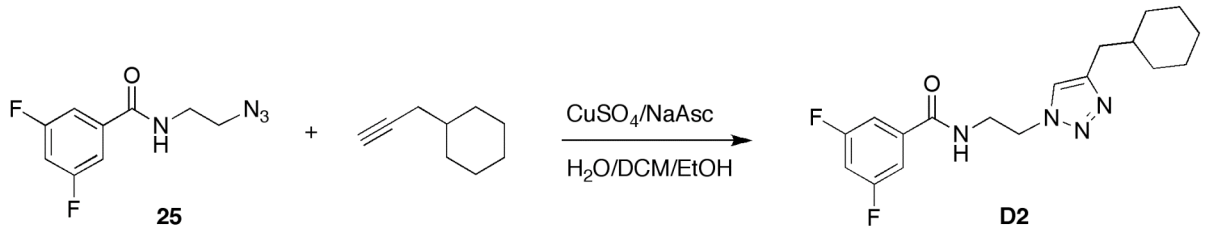

***N*-(2-(4-(cyclohexylmethyl)-1*H*-1,2,3-triazol-1-yl)ethyl)-3,5-difluorobenzamide (D2).** DCM (500 µL), EtOH (500 µL) and H_2O (500 µL) were added into a vial. 3-cyclohexyl-1-propyne (28.5 µL, 197 µmol) and **25** (47.7 mg, 179 µmol) were then added, followed by sodium ascorbate (16.8 mg, 84.8 µmol) and 1 M $CuSO_4$ (26.9 µL, 26.9 µmol). The reaction was stirred at RT for 7 h, DCM (6 mL) and H_2O (8 mL) were added and the H_2O layer was extracted with DCM (3 x 8 mL). The organic layer was dried over Na_2SO_4, filtered and reduced in vacuo. The product was purified via flash column chromatography using a DCM/MeOH (96:4) mobile phase (R_f ~ 0.5 5% MeOH/DCM). The product was isolated as an off white solid (55 mg, 62%). ^{1}H NMR (400 MHz, $CDCl_3$) δ 8.08 (1H, s), 7.44 (2H, m), 6.92 (1H, m), 4.56 (2H, d, *J* = 5.6 Hz), 3.99 (2H, m), 2.46 (2H, d, *J* = 7.2 Hz) 1.56 (5H, m), 1.46 (1H, m), 1.09 (3H, m), 0.84 (2H, m); HRMS (ESI) *m/z*, ($[M + H]^+$, $C_{18}H_{22}F_2N_4O$): theoretical 349.1841, observed 349.1845.

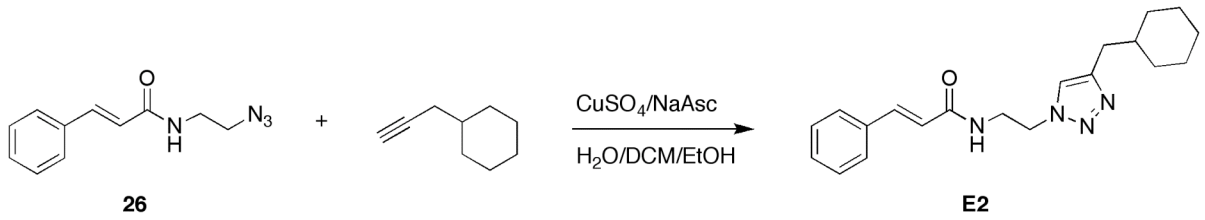

***N*-(2-(4-(cyclohexylmethyl)-1*H*-1,2,3-triazol-1-yl)ethyl)cinnamamide (E2).** DCM (500 µL), EtOH (500 µL) and H_2O (500 µL) were added into a vial. 3-cyclohexyl-1-propyne (44.2 µL, 306 µmol) and **26** (60.0 mg, 278 µmol) were then added, followed by sodium ascorbate (25.0 mg, 126 µmol) and 1 M $CuSO_4$ (41.6 µL, 41.6 µmol). The reaction was stirred at RT for 19 h, DCM (4 mL) and H_2O (6 mL) were added and the H_2O layer was extracted with

DCM (3 x 8 mL). The organic layer was dried over Na_2SO_4, filtered and reduced in vacuo. The product was purified via flash column chromatography using a DCM/MeOH (97:3) mobile phase (R_f ~ 0.4 5% MeOH/DCM). The product was isolated as an off white solid (66 mg, 70%). ^{1}H NMR (400 MHz, $CDCl_3$) δ 7.55 (1H, d, *J* = 15.6 Hz), 7.40 (2H, s), 7.21 (3H, m), 6.44 (1H, d, *J* = 15.6 Hz), 4.46 (2H, s), 3.82 (2H, s), 2.45 (2H, m), 1.57 (5H, m), 1.06 (3H, m), 0.84 (2H, m); ^{13}C NMR (400 MHz, $CDCl_3$) δ 166.8, 147.0, 141.5, 134.8, 129.9, 129.0, 128.0, 122.7, 120.5, 49.4, 39.7, 38.2, 33.5, 33.2, 26.5, 26.3; HRMS (ESI) *m/z*, ($[M + H]^+$, $C_{20}H_{26}N_4O$): theoretical 339.2186, observed 339.2188.

REFERENCES

1. S. L. Teitelbaum, *Science*, 2000, **289**, 1504-1508.

2. S. C. Manolagas, *Endocr Rev*, 2000, **21**, 115-137.

3. A. Demulder, S. Takahashi, F. R. Singer, D. J. Hosking and G. D. Roodman, *Endocrinology*, 1993, **133**, 1978-1982.

4. G. D. Roodman, *Bone*, 1996, **19**, 209-212.

5. W. Wuyts, L. Van Wesenbeeck, A. Morales-Piga, S. Ralston, L. Hocking, F. Vanhoenacker, R. Westhovens, L. Verbruggen, D. Anderson, A. Hughes and W. Van Hul, *Bone*, 2001, **28**, 104-107.

6. H. Takayanagi, H. Iizuka, T. Juji, T. Nakagawa, A. Yamamoto, T. Miyazaki, Y. Koshihara, H. Oda, K. Nakamura and S. Tanaka, *Arthritis Rheum*, 2000, **43**, 259-269.

7. R. E. Coleman, *Cancer Treat Rev*, 2001, **27**, 165-176.

8. T. Suda, N. Takahashi and T. J. Martin, *Endocr Rev*, 1992, **13**, 66-80.

9. H. Yasuda, N. Shima, N. Nakagawa, K. Yamaguchi, M. Kinosaki, S. Mochizuki, A. Tomoyasu, K. Yano, M. Goto, A. Murakami, E. Tsuda, T. Morinaga, K. Higashio, N. Udagawa, N. Takahashi and T. Suda, *P Natl Acad Sci USA*, 1998, **95**, 3597-3602.

10. D. L. Lacey, E. Timms, H. L. Tan, M. J. Kelley, C. R. Dunstan, T. Burgess, R. Elliott, A. Colombero, G. Elliott, S. Scully, H. Hsu, J. Sullivan, N. Hawkins, E. Davy, C. Capparelli, A. Eli, Y. X. Qian, S. Kaufman, I. Sarosi, V. Shalhoub, G. Senaldi, J. Guo, J. Delaney and W. J. Boyle, *Cell*, 1998, **93**, 165-176.

11. N. Nakagawa, M. Kinosaki, K. Yamaguchi, N. Shima, H. Yasuda, K. Yano, T. Morinaga and K. Higashio, *Biochem Bioph Res Co*, 1998, **253**, 395-400.

12. H. L. Hsu, D. L. Lacey, C. R. Dunstan, I. Solovyev, A. Colombero, E. Timms, H. L. Tan, G. Elliott, M. J. Kelley, I. Sarosi, L. Wang, X. Z. Xia, R. Elliott, L. Chiu, T. Black, S. Scully, C. Capparelli, S. Morony, G. Shimamoto, M. B. Bass and W. J. Boyle, *P Natl Acad Sci USA*, 1999, **96**, 3540-3545.

13. W. J. Boyle, W. S. Simonet and D. L. Lacey, *Nature*, 2003, **423**, 337-342.

14. S. A. Stoch, S. Zajic, J. Stone, D. L. Miller, K. Van Dyck, M. J. Gutierrez, M. De Decker, L. Liu, Q. Liu, B. B. Scott, D. Panebianco, B. Jin, L. T. Duong, K. Gottesdiener and J. A. Wagner, *Clin Pharmacol Ther*, 2009, **86**, 175-182.

15. A. Taranta, M. Brama, A. Teti, V. De Luca, R. Scandurra, G. Spera, D. Agnusdei, J. D. Termine and S. Migliaccio, *Bone*, 2002, **30**, 368-376.

16. M. R. McClung, E. M. Lewiecki, S. B. Cohen, M. A. Bolognese, G. C. Woodson, A. H. Moffett, M. Peacock, P. D. Miller, S. N. Lederman, C. H. Chesnut, D. Lain, A. J. Kivitz, D. L. Holloway, C. Zhang, M. C. Peterson, P. J. Bekker and A. B. L. S. Grp, *New Engl J Med*, 2006, **354**, 821-831.

17. R. G. G. Russell and M. J. Rogers, *Bone*, 1999, **25**, 97-106.

18. M. J. Rogers, A. J. Roelofs and F. P. Coxon, *Clin Exp Metastas*, 2008, **25**, 27-28.

19. J. C. Frith, J. Monkkonen, G. M. Blackburn, R. G. G. Russell and M. J. Rogers, *J Bone Miner Res*, 1997, **12**, 1358-1367.

20. E. van Beek, C. Lowik, G. van der Pluijm and S. Papapoulos, *J Bone Miner Res*, 1999, **14**, 722-729.

21. E. R. van Beek, L. H. Cohen, I. M. Leroy, F. H. Ebetino, C. W. G. M. Lowik and S. E. Papapoulos, *Bone*, 2003, **33**, 805-811.

22. P. C. deGroen, D. F. Lubbe, L. J. Hirsch, A. Daifotis, W. Stephenson, D. Freedholm, S. PryorTillotson, M. J. Seleznick, H. Pinkas and K. K. Wang, *New Engl J Med*, 1996, **335**, 1016-1021.

23. S. Pozzi, R. Marcheselli, S. Sacchi, G. Quarta, P. Musto, G. Caparrotti, D. Natale, G. Pianezze, G. Polimeno, V. Pitini, L. Ponchio, C. Broglia, M. Spriano, M. Musso, L. Masini, A. Donelli, D. Dini, G. Leonardi, S. Luminari and G. Pollastri, *Blood*, 2005, **106**, 346B-346B.

24. C. Walter, B. Al-Nawas, K. A. Grotz, C. Thomas, J. W. Thuroff, V. Zinser, H. Gamm, J. Beck and W. Wagner, *European Urology*, 2008, **54**, 1066-1072.

25. A. A. Khan, G. K. B. Sandor, E. Dore, A. D. Morrison, M. Alsahli, F. Amin, E. Peters, D. A. Hanley, S. R. Chaudry, B. Lentle, D. W. Dempster, F. H. Glorieux, A. J. Neville, R. M. Talwar, C. M. Clokie, M. Al Mardini, T. Paul, S. Khosla, R. G. Josse, S. Sutherland, D. K. Lam, R. P. Carmichael, N. Blanas, D. Kendler, S. Petak, L. G.

Ste-Marie, J. Brown, A. W. Evans, L. Rios and J. E. Compston, *Journal of Rheumatology*, 2009, **36**, 478-490.

26. P. N. Sambrook, *Nature Clinical Practice Rheumatology*, 2009, **5**, 6-7.

27. G. K. Reeves, V. Beral, J. Green, T. Gathani, D. Bull and M. W. S. Collaborators, *Lancet Oncol*, 2006, **7**, 910-918.

28. B. Ettinger, D. M. Black, B. H. Mitlak, R. K. Knickerbocker, T. Nickelsen, H. K. Genant, C. Christiansen, P. D. Delmas, J. R. Zanchetta, J. Stakkestad, C. C. Gluer, K. Krueger, F. J. Cohen, S. Eckert, K. E. Ensrud, L. V. Avioli, P. Lips, S. R. Cummings and M. O. R. Evaluation, *Jama-J Am Med Assoc*, 1999, **282**, 637-645.

APPENDIX

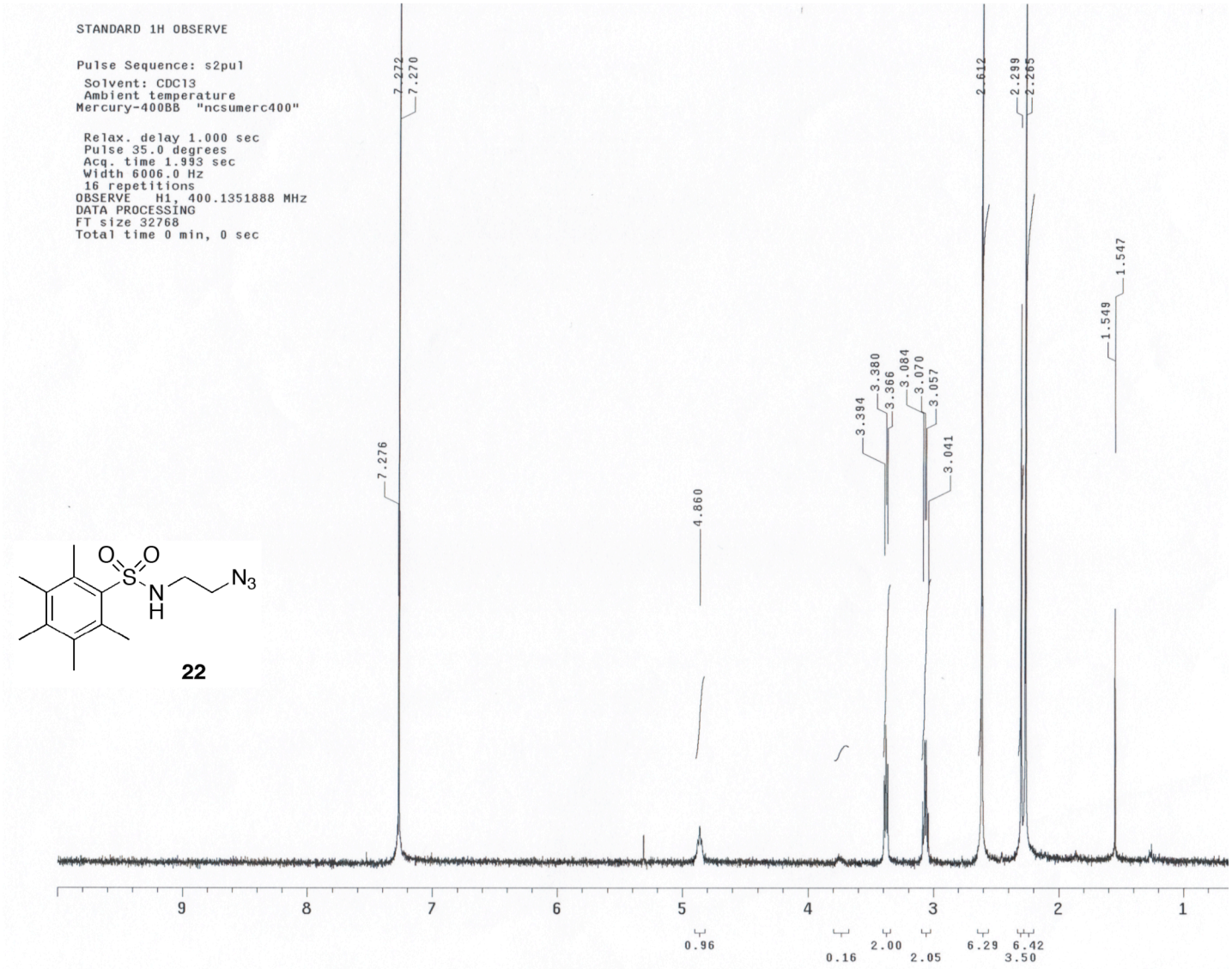
STANDARD 1H OBSERVE
Pulse Sequence: s2pul
Solvent: CDCl3
Ambient temperature
Mercury-400BB "ncsumerc400"
Relax. delay 1.000 sec
Pulse 35.0 degrees
Acq. time 1.993 sec
Width 6006.0 Hz
16 repetitions
OBSERVE H1, 400.1351888 MHz
DATA PROCESSING
FT size 32768
Total time 0 min, 0 sec
7.272
7.270
7.276
4.860
3.394
3.380
3.366
3.084
3.070
3.057
3.041
2.612
2.299
2.285
1.549
1.547
O
O
S
N
H
N3
22
9
8
7
6
5
4
3
2
1
0.96
0.16
2.00
2.05
6.29
6.42
3.50

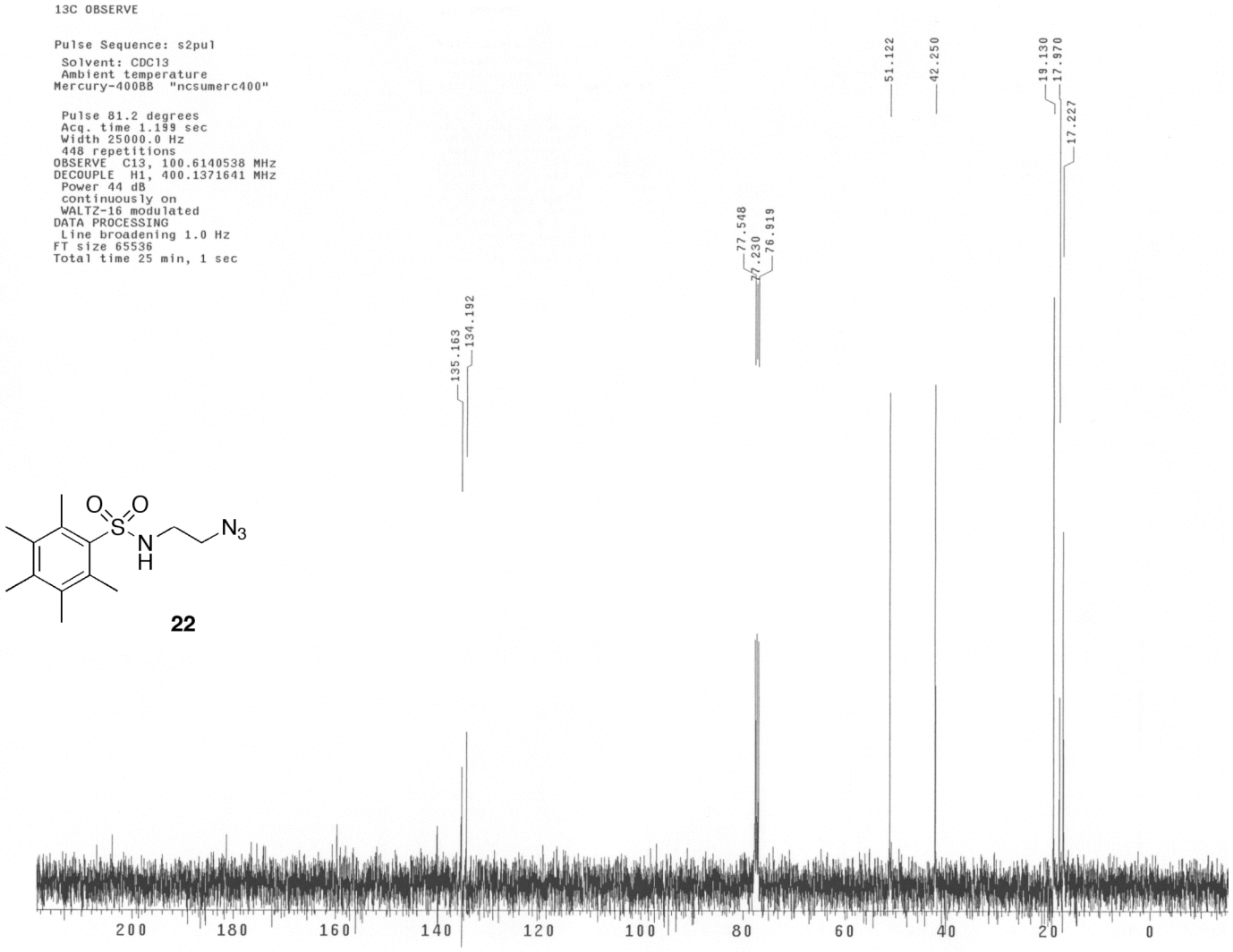
13C OBSERVE
Pulse Sequence: s2pul
Solvent: CDCl3
Ambient temperature
Mercury-400BB "ncsumerc400"
Pulse 81.2 degrees
Acq. time 1.199 sec
Width 25000.0 Hz
448 repetitions
OBSERVE C13, 100.6140538 MHz
DECOUPLE H1, 400.1371641 MHz
Power 44 dB
continuously on
WALTZ-16 modulated
DATA PROCESSING
Line broadening 1.0 Hz
FT size 65536
Total time 25 min, 1 sec
135.163
134.192
77.548
77.230
76.919
51.122
42.250
19.130
17.970
17.227
200
180
160
140
120
100
80
60
40
20
0

22

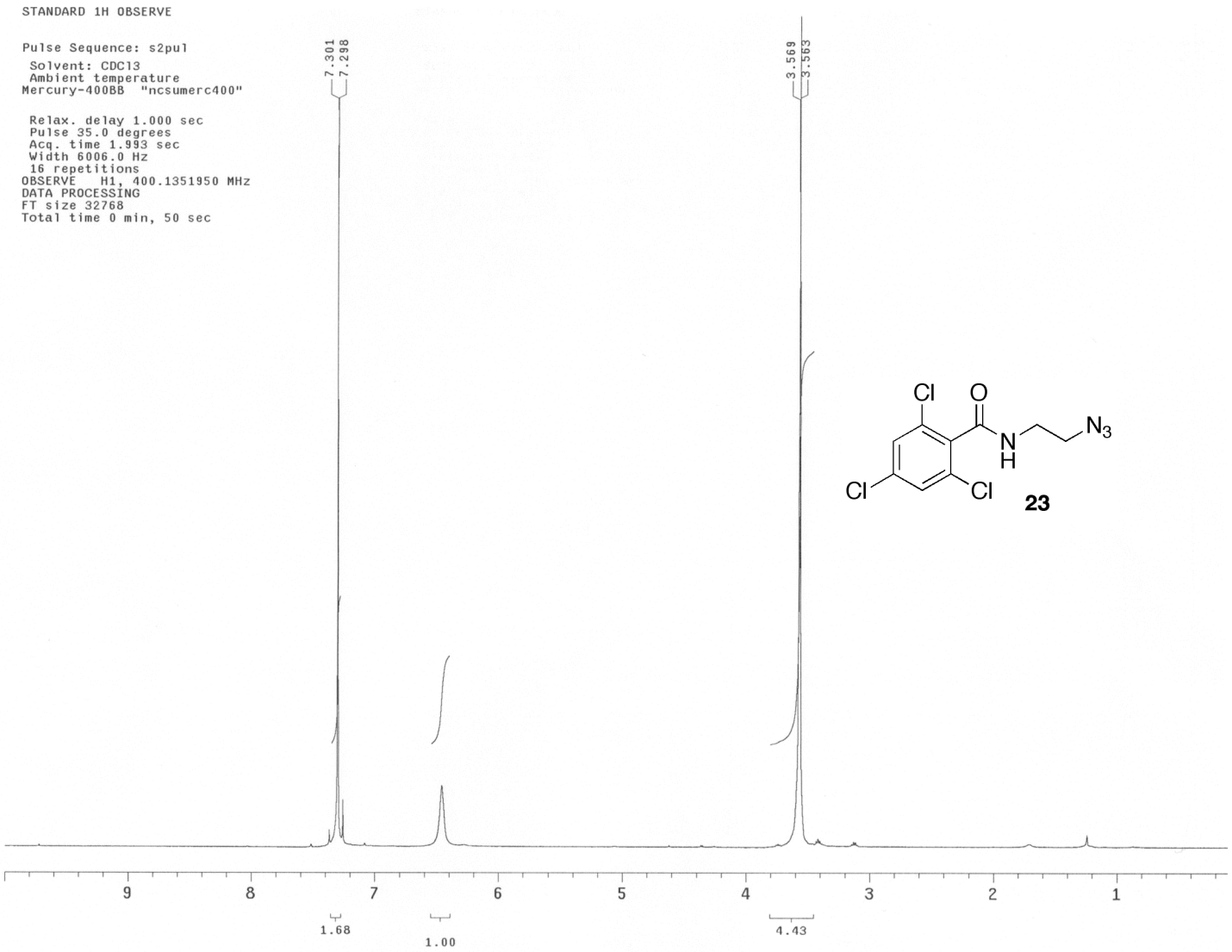
STANDARD 1H OBSERVE
Pulse Sequence: s2pul
Solvent: CDCl3
Ambient temperature
Mercury-400BB "ncsumerc400"
Relax. delay 1.000 sec
Pulse 35.0 degrees
Acq. time 1.993 sec
Width 6006.0 Hz
16 repetitions
OBSERVE H1, 400.1351950 MHz
DATA PROCESSING
FT size 32768
Total time 0 min, 50 sec
7.301
7.298
3.569
3.563
Cl
O
N
H
N3
Cl
Cl
23
9
8
7
6
5
4
3
2
1
1.68
1.00
4.43

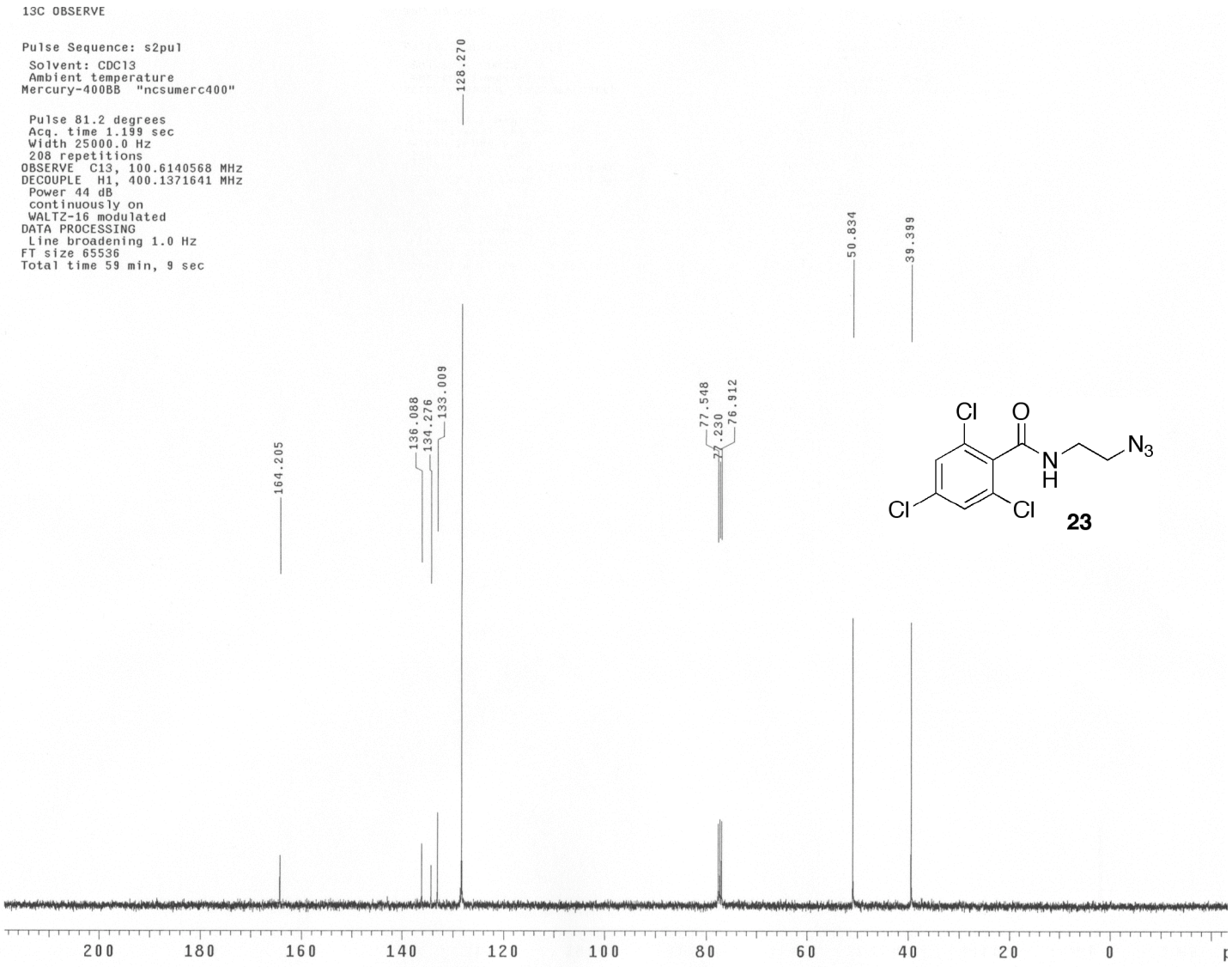
13C OBSERVE
Pulse Sequence: s2pul
Solvent: CDCl3
Ambient temperature
Mercury-400BB "ncsumerc400"
Pulse 81.2 degrees
Acq. time 1.199 sec
Width 25000.0 Hz
208 repetitions
OBSERVE C13, 100.6140568 MHz
DECOUPLE H1, 400.1371641 MHz
Power 44 dB
continuously on
WALTZ-16 modulated
DATA PROCESSING
Line broadening 1.0 Hz
FT size 65536
Total time 59 min, 9 sec
128.270
50.834
39.399
77.548
77.230
76.912
136.088
134.276
133.009
164.205
Cl
O
N
H
N3
Cl
Cl
23
200
180
160
140
120
100
80
60
40
20
0

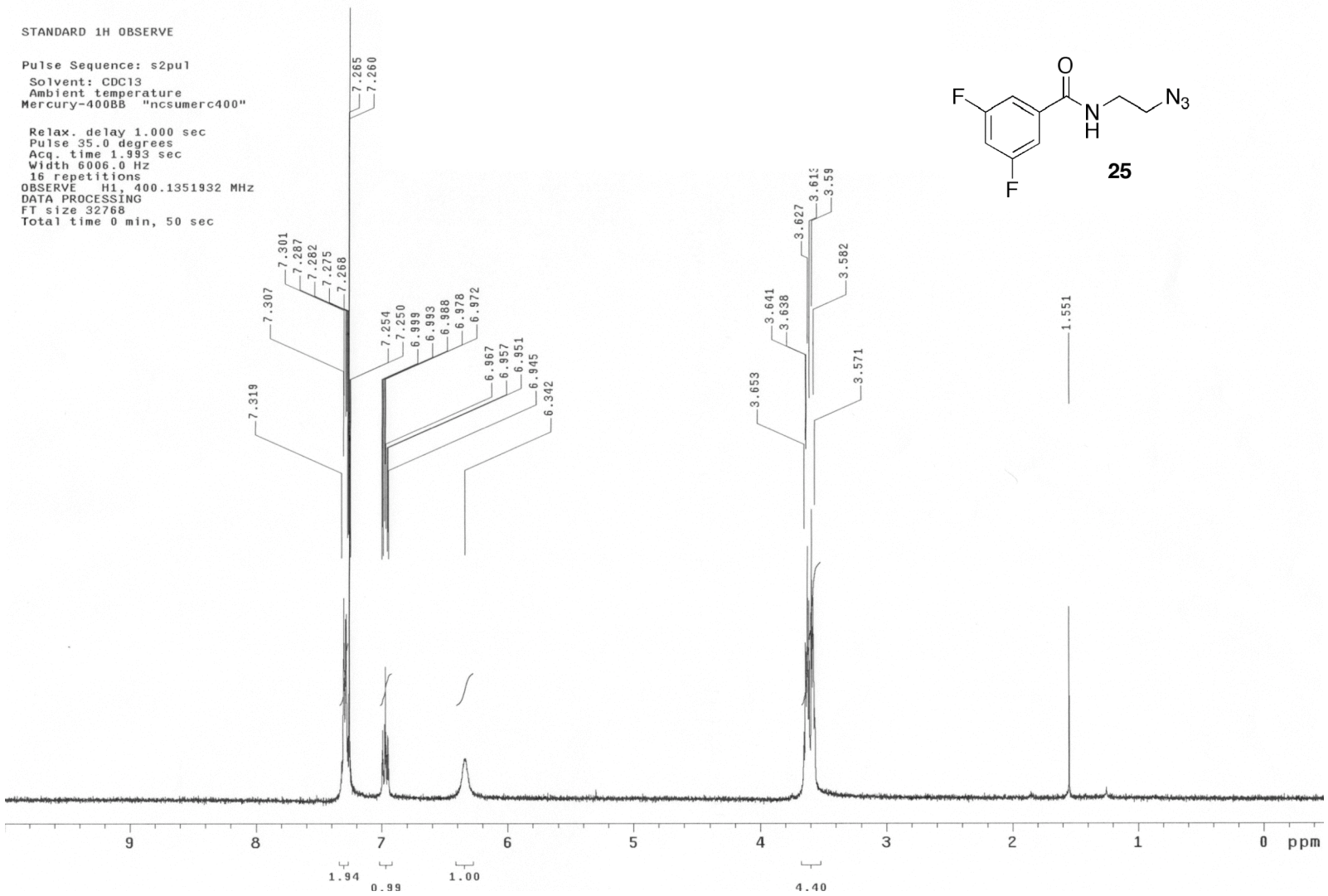
STANDARD 1H OBSERVE
Pulse Sequence: s2pul
Solvent: CDCl3
Ambient temperature
Mercury-400BB "ncsumerc400"
Relax. delay 1.000 sec
Pulse 35.0 degrees
Acq. time 1.993 sec
Width 6006.0 Hz
16 repetitions
OBSERVE H1, 400.1351932 MHz
DATA PROCESSING
FT size 32768
Total time 0 min, 50 sec
7.265
7.260
7.301
7.287
7.282
7.275
7.268
7.307
7.319
7.254
7.250
6.999
6.993
6.988
6.978
6.972
6.967
6.957
6.951
6.945
6.342
3.627
3.582
3.641
3.638
3.653
3.571
1.551
F
O
N
H
N3
F
25
9
8
7
6
5
4
3
2
1
0
ppm
1.94
0.99
1.00
4.40

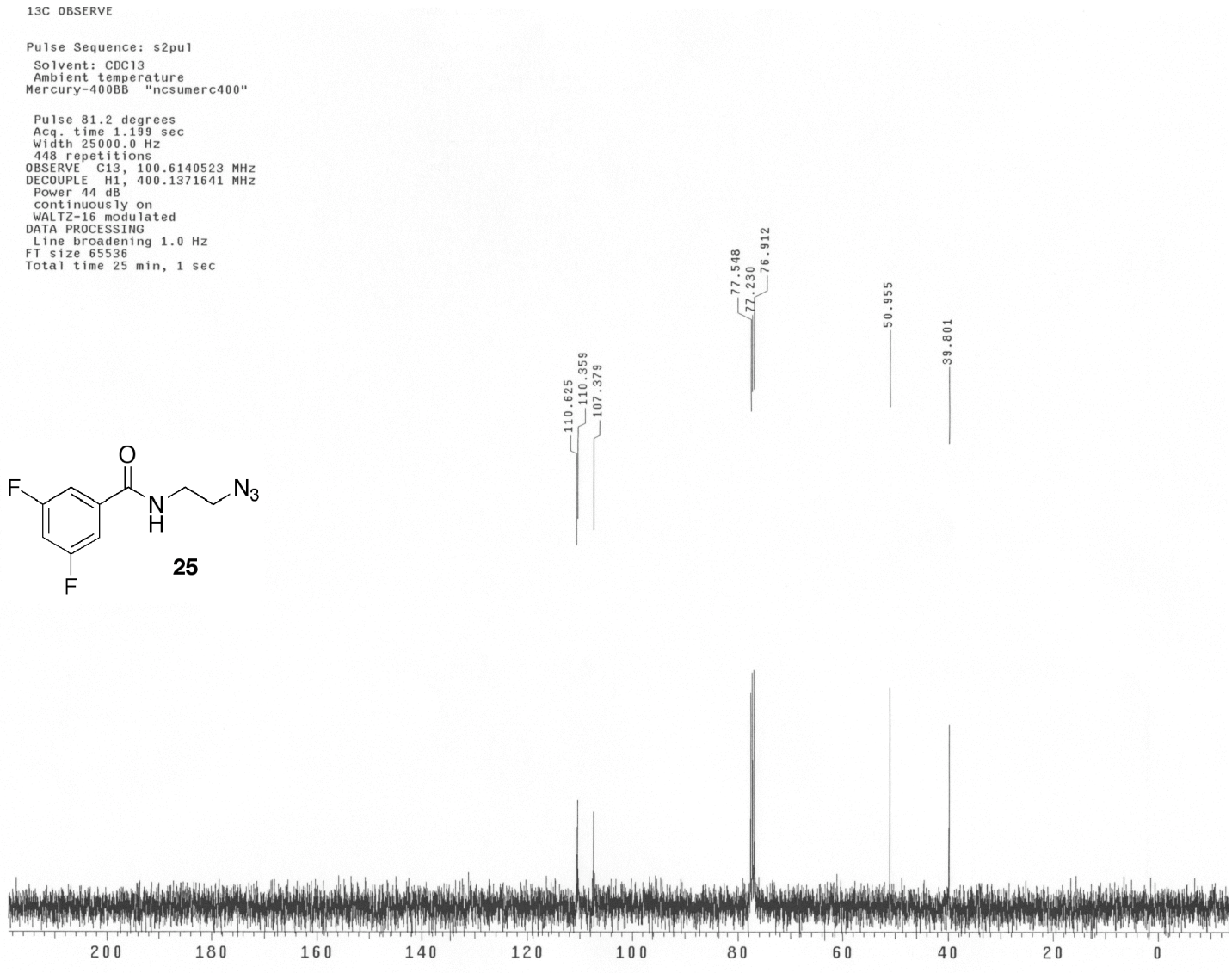
13C OBSERVE
Pulse Sequence: s2pul
Solvent: CDCl3
Ambient temperature
Mercury-400BB "ncsumerc400"
Pulse 81.2 degrees
Acq. time 1.199 sec
Width 25000.0 Hz
448 repetitions
OBSERVE C13, 100.6140523 MHz
DECOUPLE H1, 400.1371641 MHz
Power 44 dB
continuously on
WALTZ-16 modulated
DATA PROCESSING
Line broadening 1.0 Hz
FT size 65536
Total time 25 min, 1 sec
110.625
110.359
107.379
77.548
77.230
76.912
50.955
39.801
F
O
N
H
N3
F
25
200
180
160
140
120
100
80
60
40
20
0

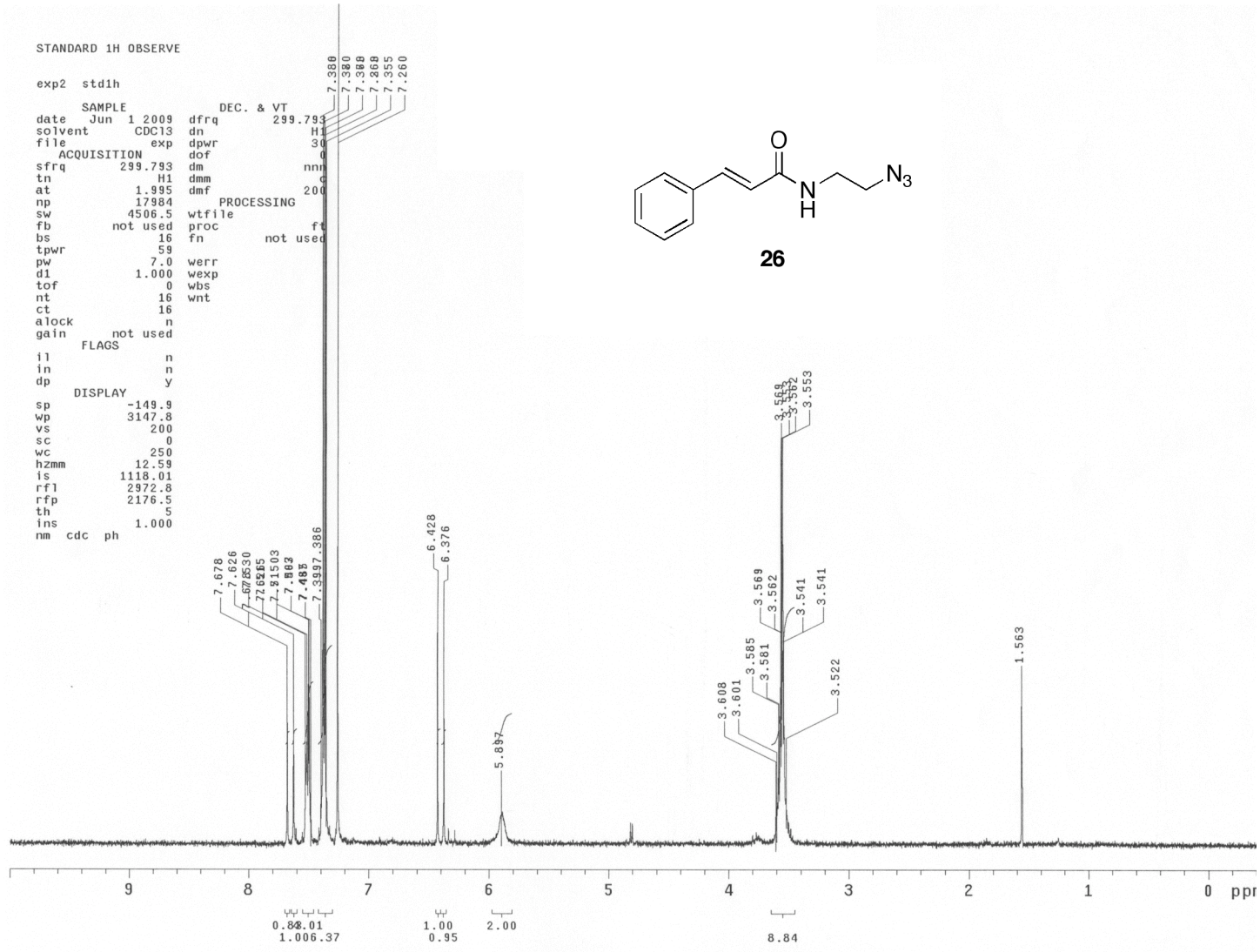
STANDARD 1H OBSERVE
exp2 std1h
SAMPLE
date Jun 1 2009
solvent CDCl3
file exp
ACQUISITION
sfrq 299.793
tn H1
at 1.995
np 17984
sw 4506.5
fb not used
bs 16
tpwr 59
pw 7.0
d1 1.000
tof 0
nt 16
ct 16
alock n
gain not used
FLAGS
il n
in n
dp y
DISPLAY
sp -149.9
wp 3147.8
vs 200
sc 0
wc 250
hzmm 12.59
is 1118.01
rfl 2972.8
rfp 2176.5
th 5
ins 1.000
nm cdc ph
DEC. & VT
dfrq 299.793
dn H1
dpwr 30
dof 0
dm nnn
dmm c
dmf 200
PROCESSING
wtfile
proc ft
fn not used
werr
wexp
wbs
wnt
7.380
7.380
7.388
7.368
7.355
7.260
7.678
7.626
7.397
7.386
6.428
6.376
5.887
3.608
3.601
3.585
3.581
3.569
3.562
3.553
3.541
3.541
3.522
1.563
9
8
7
6
5
4
3
2
1
0 ppm
0.84
8.01
1.00
2.00
1.00
6.37
0.95
8.84

O
N
H
N3

26

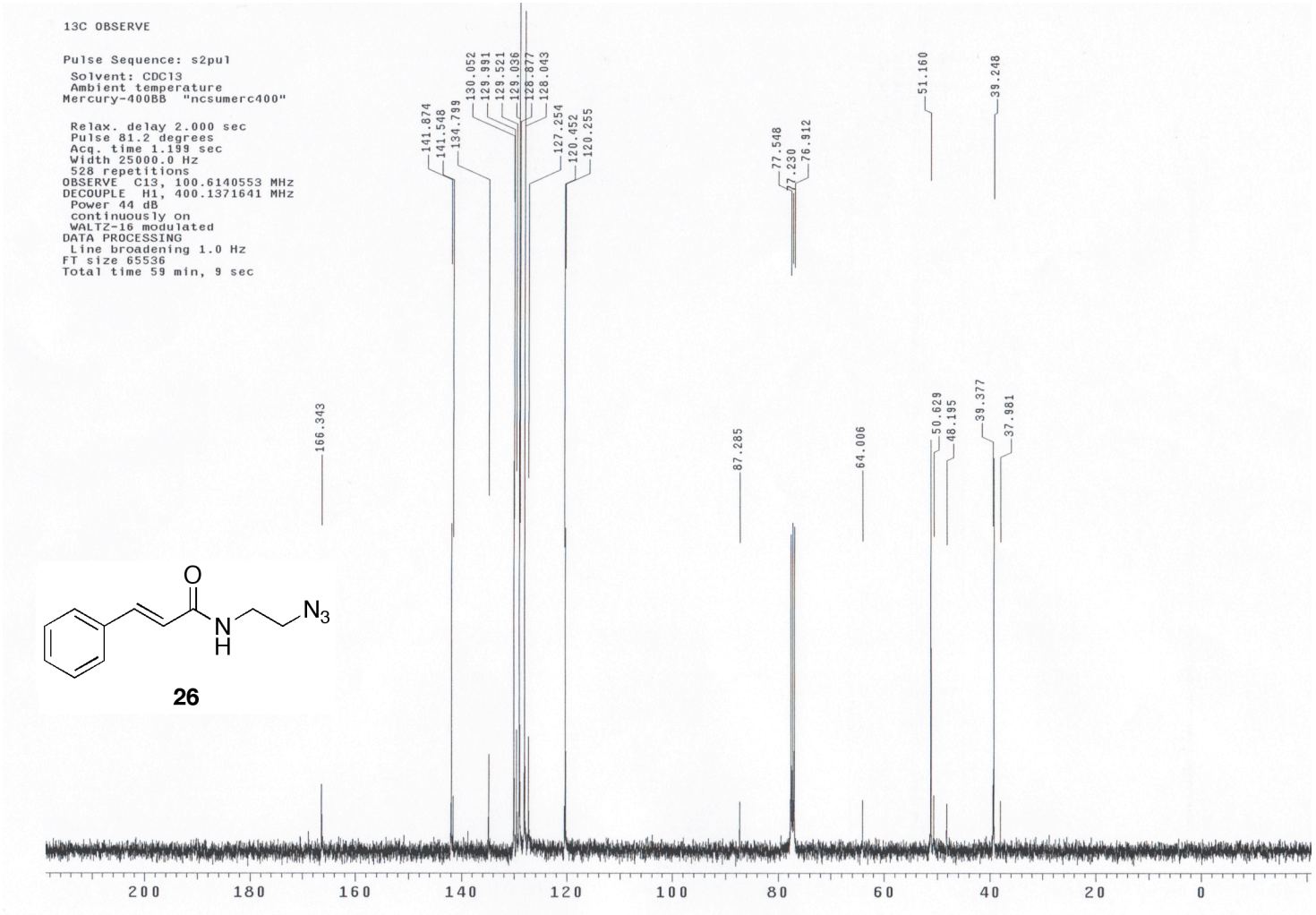
13C OBSERVE
Pulse Sequence: s2pul
Solvent: CDCl3
Ambient temperature
Mercury-400BB "ncsumerc400"
Relax. delay 2.000 sec
Pulse 81.2 degrees
Acq. time 1.199 sec
Width 25000.0 Hz
528 repetitions
OBSERVE C13, 100.6140553 MHz
DECOUPLE H1, 400.1371641 MHz
Power 44 dB
continuously on
WALTZ-16 modulated
DATA PROCESSING
Line broadening 1.0 Hz
FT size 65536
Total time 59 min, 9 sec
166.343
141.874
141.548
134.799
130.052
129.991
129.521
129.036
128.877
128.043
127.254
120.452
120.255
87.285
77.548
77.230
76.912
64.006
51.160
50.629
48.195
39.377
39.248
37.981
O
N
H
N3
26
200
180
160
140
120
100
80
60
40
20
0

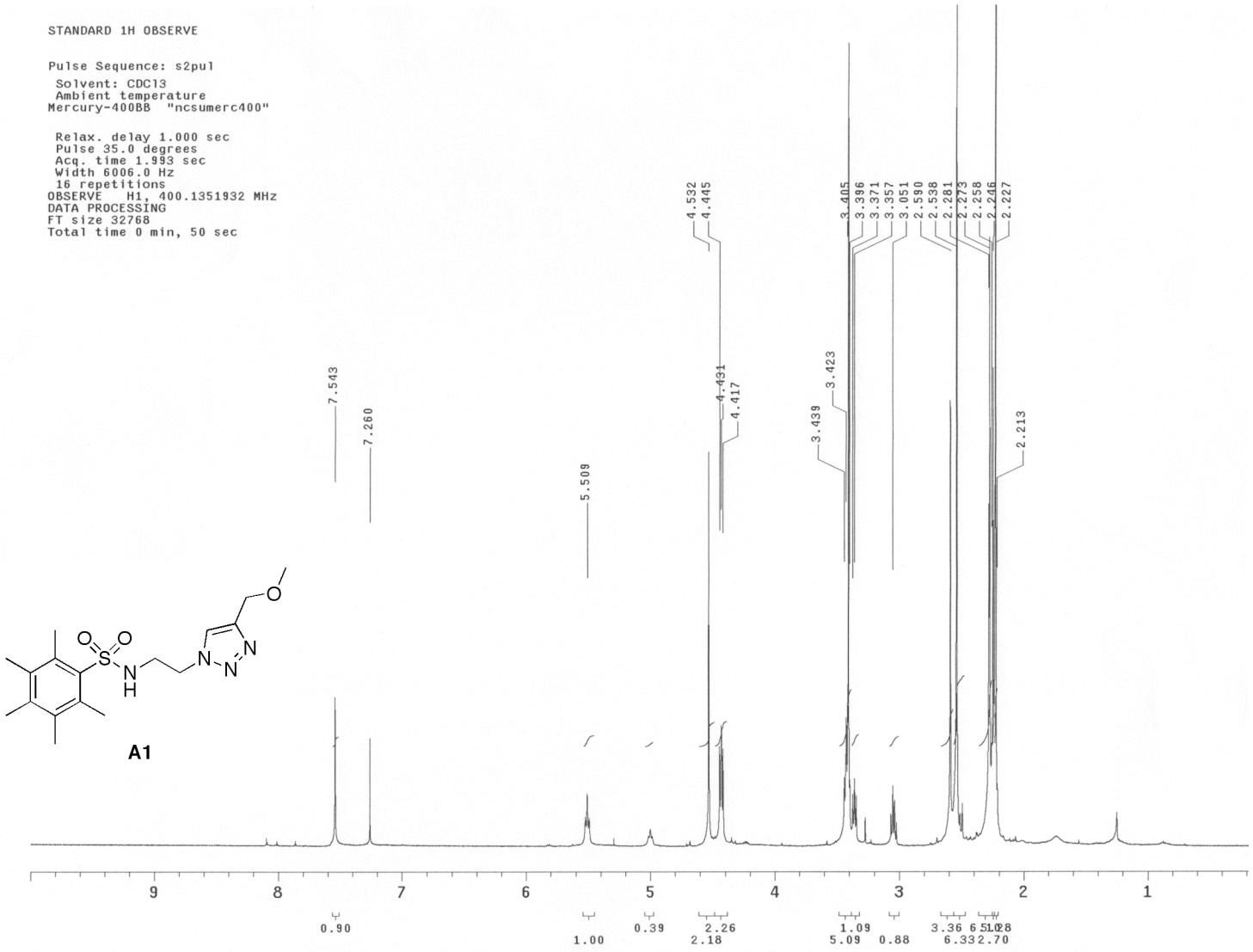
STANDARD 1H OBSERVE
Pulse Sequence: s2pul
Solvent: CDCl3
Ambient temperature
Mercury-400BB "ncsumerc400"
Relax. delay 1.000 sec
Pulse 35.0 degrees
Acq. time 1.993 sec
Width 6006.0 Hz
16 repetitions
OBSERVE H1, 400.1351932 MHz
DATA PROCESSING
FT size 32768
Total time 0 min, 50 sec
7.543
7.260
5.509
4.532
4.445
4.431
4.417
3.439
3.423
3.405
3.396
3.371
3.357
3.051
2.590
2.538
2.281
2.273
2.258
2.246
2.227
2.213
A1
9
8
7
6
5
4
3
2
1
0.90
1.00
0.39
2.26
2.18
1.09
5.09
0.88
3.36
6.33
2.70

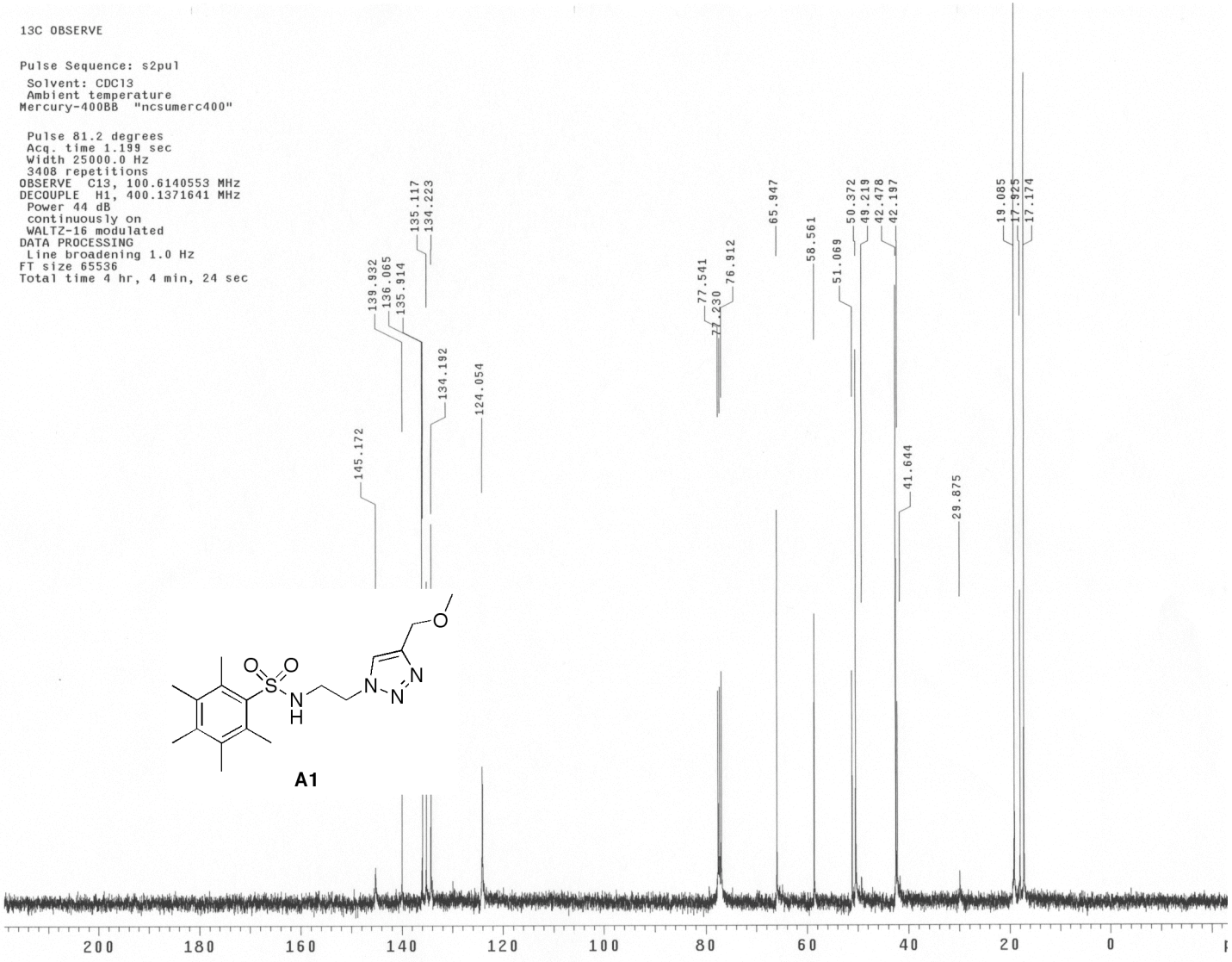
13C OBSERVE
Pulse Sequence: s2pul
Solvent: CDCl3
Ambient temperature
Mercury-400BB "ncsumerc400"
Pulse 81.2 degrees
Acq. time 1.199 sec
Width 25000.0 Hz
3408 repetitions
OBSERVE C13, 100.6140553 MHz
DECOUPLE H1, 400.1371641 MHz
Power 44 dB
continuously on
WALTZ-16 modulated
DATA PROCESSING
Line broadening 1.0 Hz
FT size 65536
Total time 4 hr, 4 min, 24 sec
145.172
139.932
136.065
135.914
135.117
134.223
134.192
124.054
77.541
77.230
76.912
65.947
58.561
51.069
50.372
49.219
42.478
42.197
41.644
29.875
19.085
17.925
17.174
A1
200
180
160
140
120
100
80
60
40
20
0

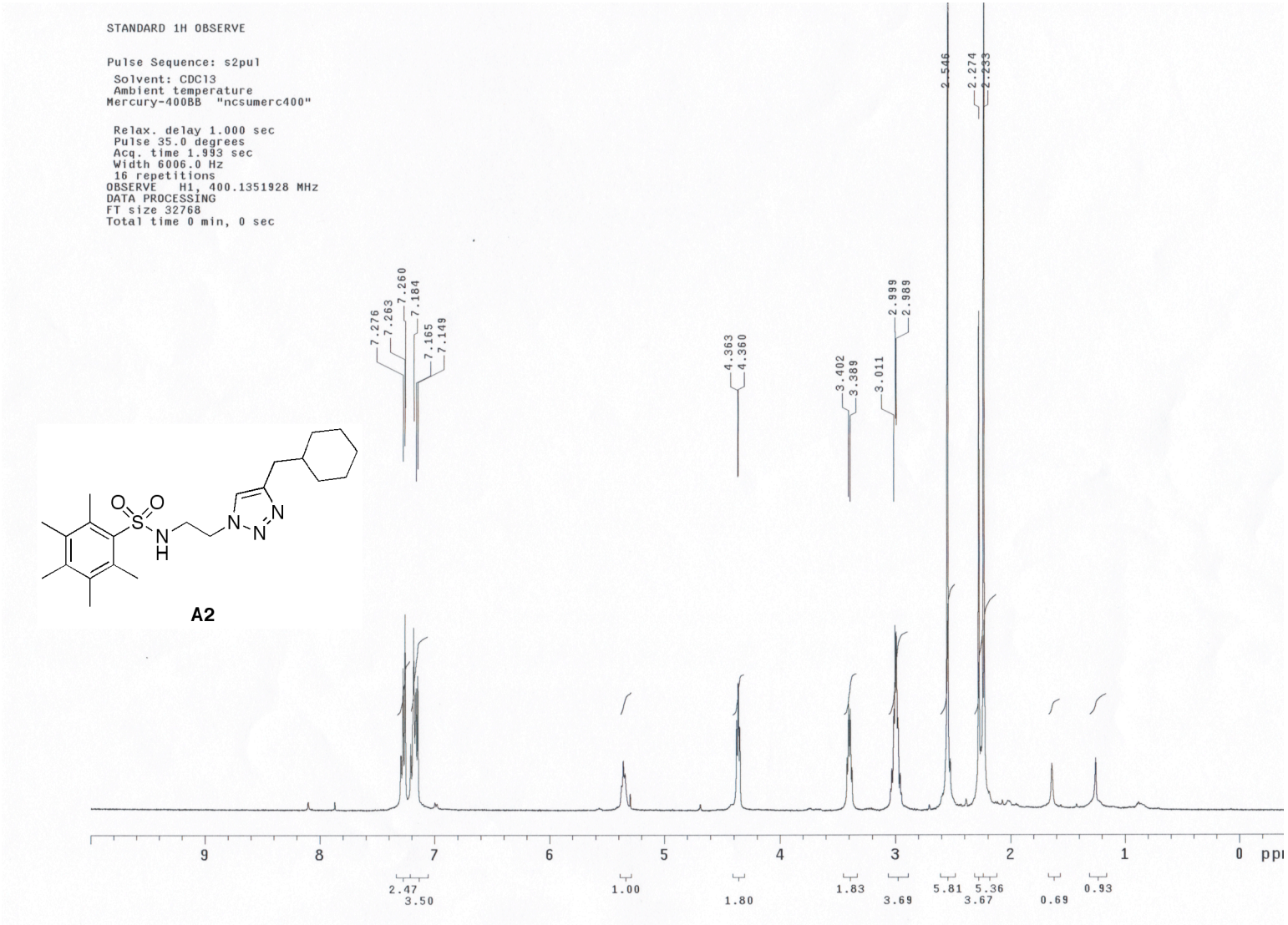
STANDARD 1H OBSERVE
Pulse Sequence: s2pul
Solvent: CDCl3
Ambient temperature
Mercury-400BB "ncsumerc400"
Relax. delay 1.000 sec
Pulse 35.0 degrees
Acq. time 1.993 sec
Width 6006.0 Hz
16 repetitions
OBSERVE H1, 400.1351928 MHz
DATA PROCESSING
FT size 32768
Total time 0 min, 0 sec
7.276
7.263
7.260
7.184
7.165
7.149
4.363
4.360
3.402
3.389
3.011
2.999
2.989
2.546
2.274
2.233
A2
9
8
7
6
5
4
3
2
1
0
ppm
2.47
3.50
1.00
1.80
1.83
3.69
5.81
5.36
3.67
0.69
0.93

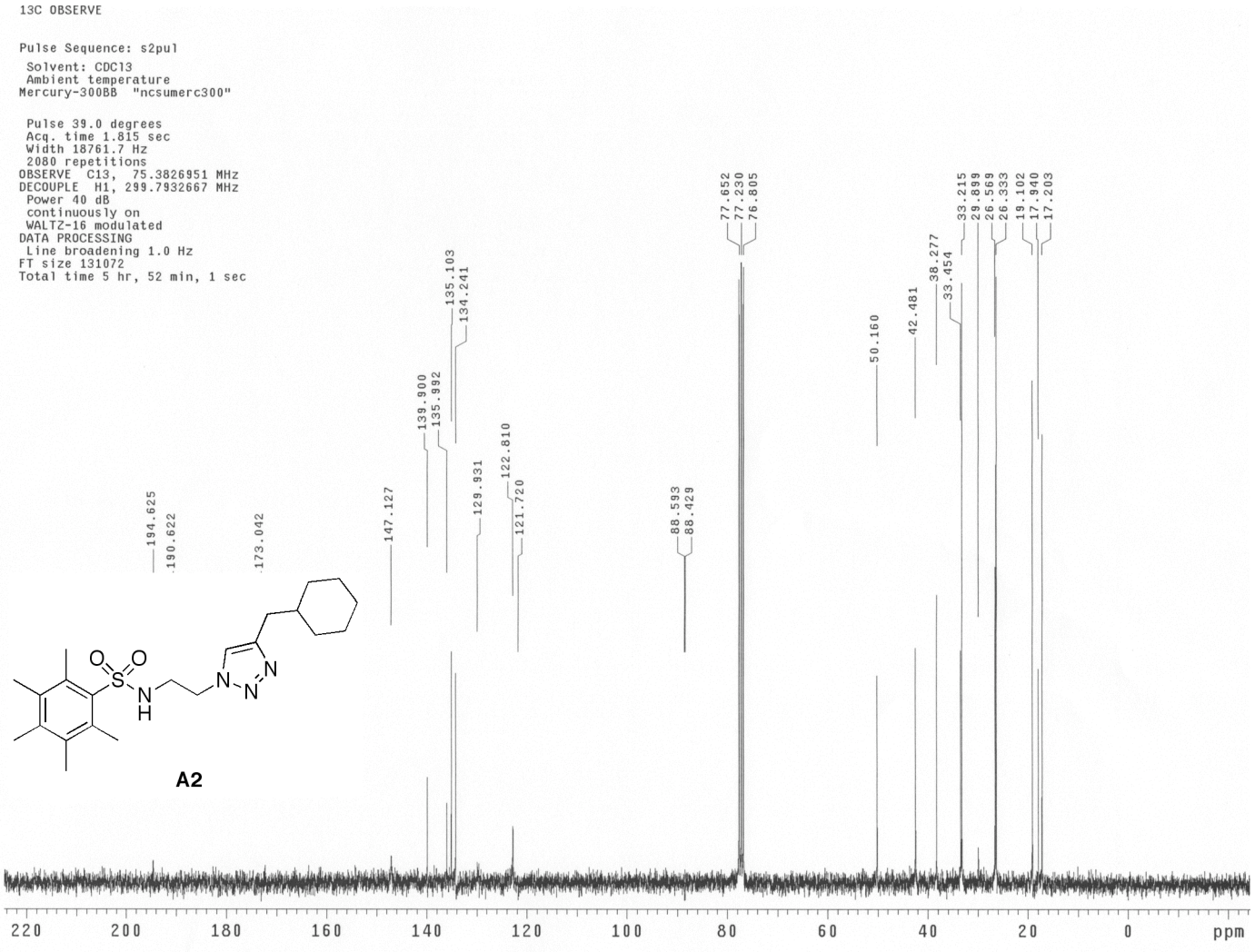
13C OBSERVE
Pulse Sequence: s2pul
Solvent: CDCl3
Ambient temperature
Mercury-300BB "ncsumerc300"
Pulse 39.0 degrees
Acq. time 1.815 sec
Width 18761.7 Hz
2080 repetitions
OBSERVE C13, 75.3826951 MHz
DECOUPLE H1, 299.7932667 MHz
Power 40 dB
continuously on
WALTZ-16 modulated
DATA PROCESSING
Line broadening 1.0 Hz
FT size 131072
Total time 5 hr, 52 min, 1 sec
194.625
190.622
173.042
147.127
139.900
135.992
135.103
134.241
129.931
122.810
121.720
88.593
88.429
77.652
77.230
76.805
50.160
42.481
38.277
33.454
33.215
29.899
26.569
26.333
19.102
17.940
17.203
A2
220
200
180
160
140
120
100
80
60
40
20
0
ppm

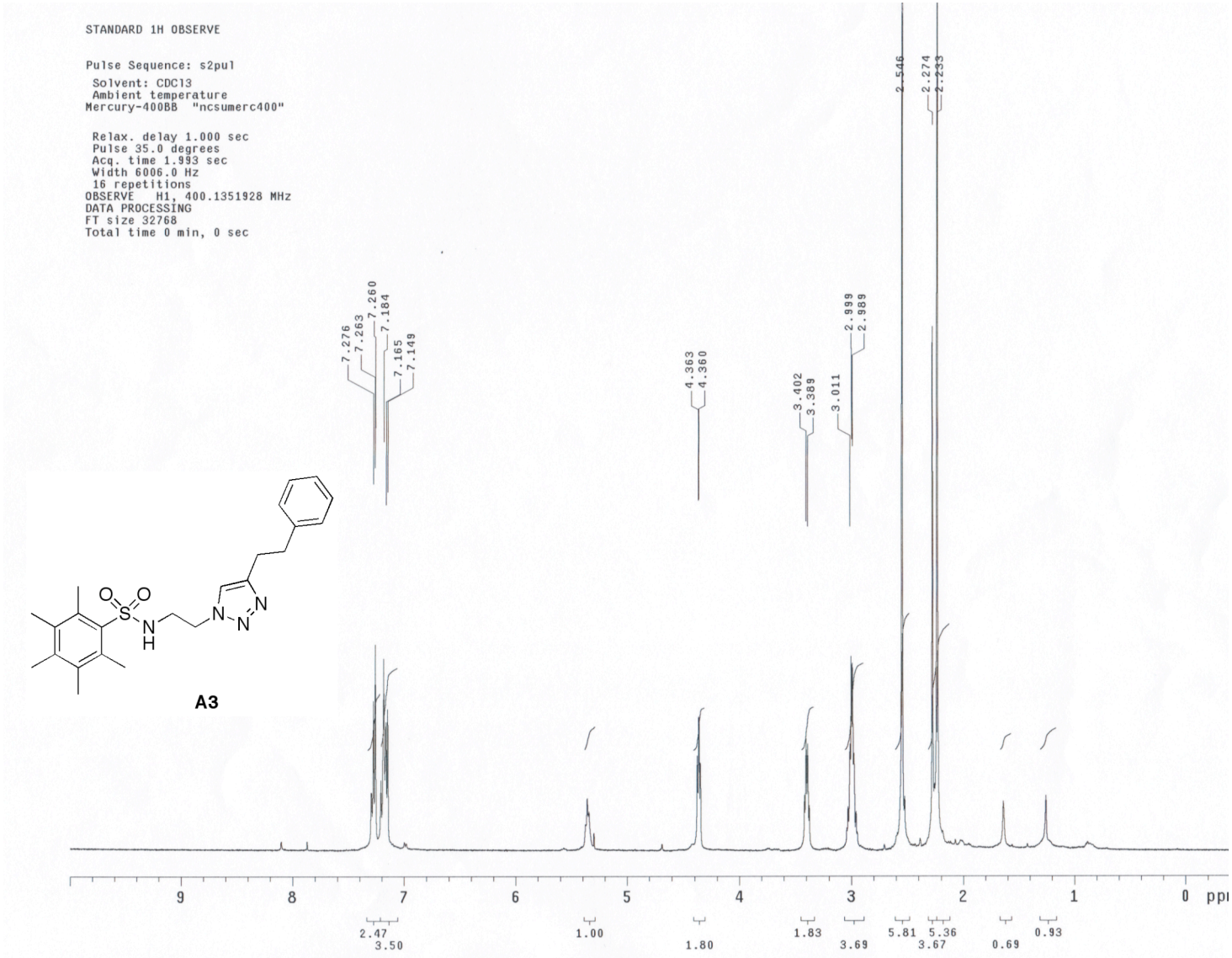
STANDARD 1H OBSERVE
Pulse Sequence: s2pul
Solvent: CDCl3
Ambient temperature
Mercury-400BB "ncsumerc400"
Relax. delay 1.000 sec
Pulse 35.0 degrees
Acq. time 1.993 sec
Width 6006.0 Hz
16 repetitions
OBSERVE H1, 400.1351928 MHz
DATA PROCESSING
FT size 32768
Total time 0 min, 0 sec
7.276
7.263
7.260
7.184
7.165
7.149
4.363
4.360
3.402
3.389
3.011
2.999
2.989
2.546
2.274
2.233
A3
9
8
7
6
5
4
3
2
1
0 ppm
2.47
3.50
1.00
1.80
1.83
3.69
5.81
5.36
3.67
0.69
0.93

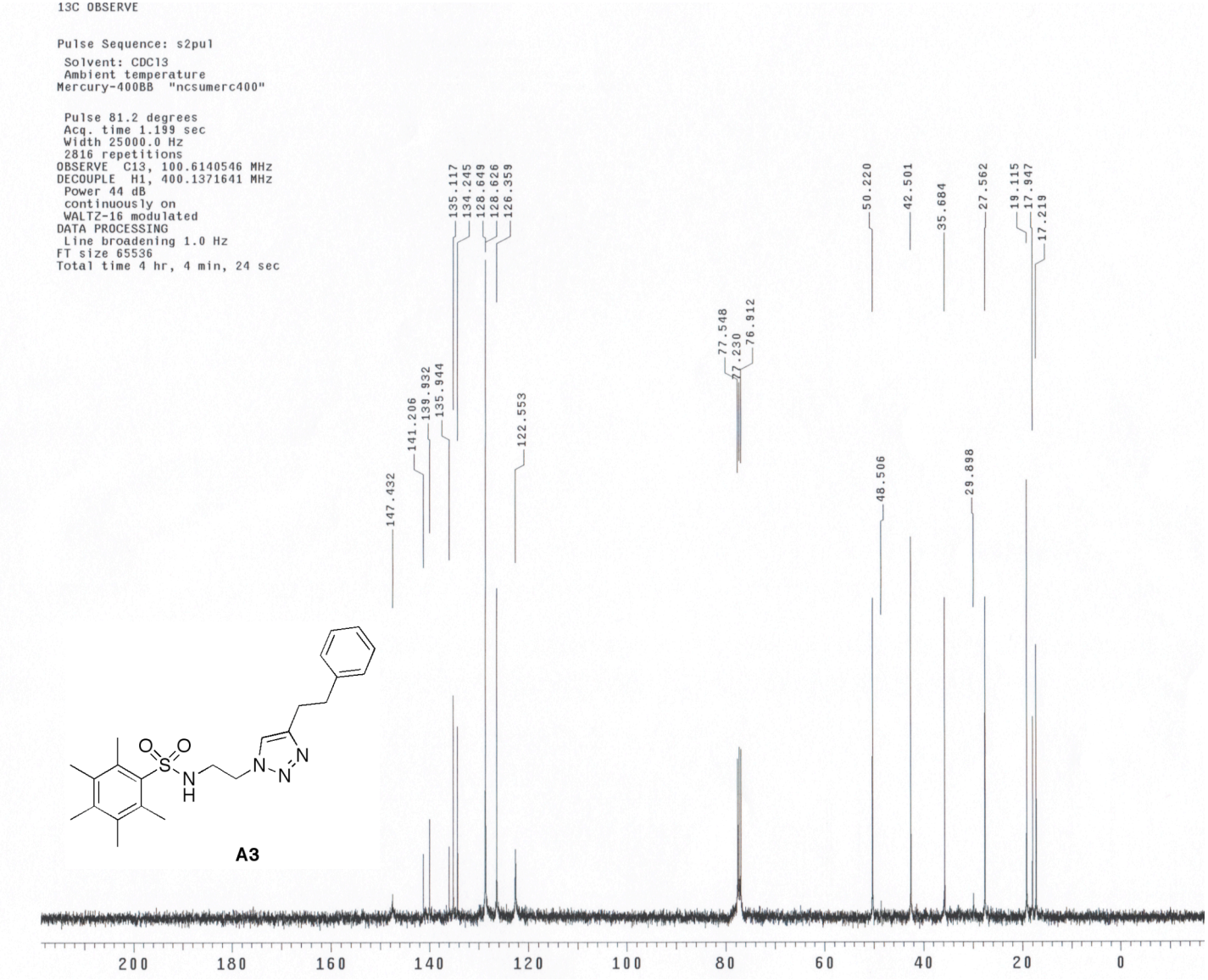
13C OBSERVE
Pulse Sequence: s2pul
Solvent: CDCl3
Ambient temperature
Mercury-400BB "ncsumerc400"
Pulse 81.2 degrees
Acq. time 1.199 sec
Width 25000.0 Hz
2816 repetitions
OBSERVE C13, 100.6140546 MHz
DECOUPLE H1, 400.1371641 MHz
Power 44 dB
continuously on
WALTZ-16 modulated
DATA PROCESSING
Line broadening 1.0 Hz
FT size 65536
Total time 4 hr, 4 min, 24 sec
147.432
141.206
139.932
135.944
135.117
134.245
128.649
128.626
126.359
122.553
77.548
77.230
76.912
50.220
48.506
42.501
35.684
29.898
27.562
19.115
17.947
17.219
A3
200
180
160
140
120
100
80
60
40
20
0

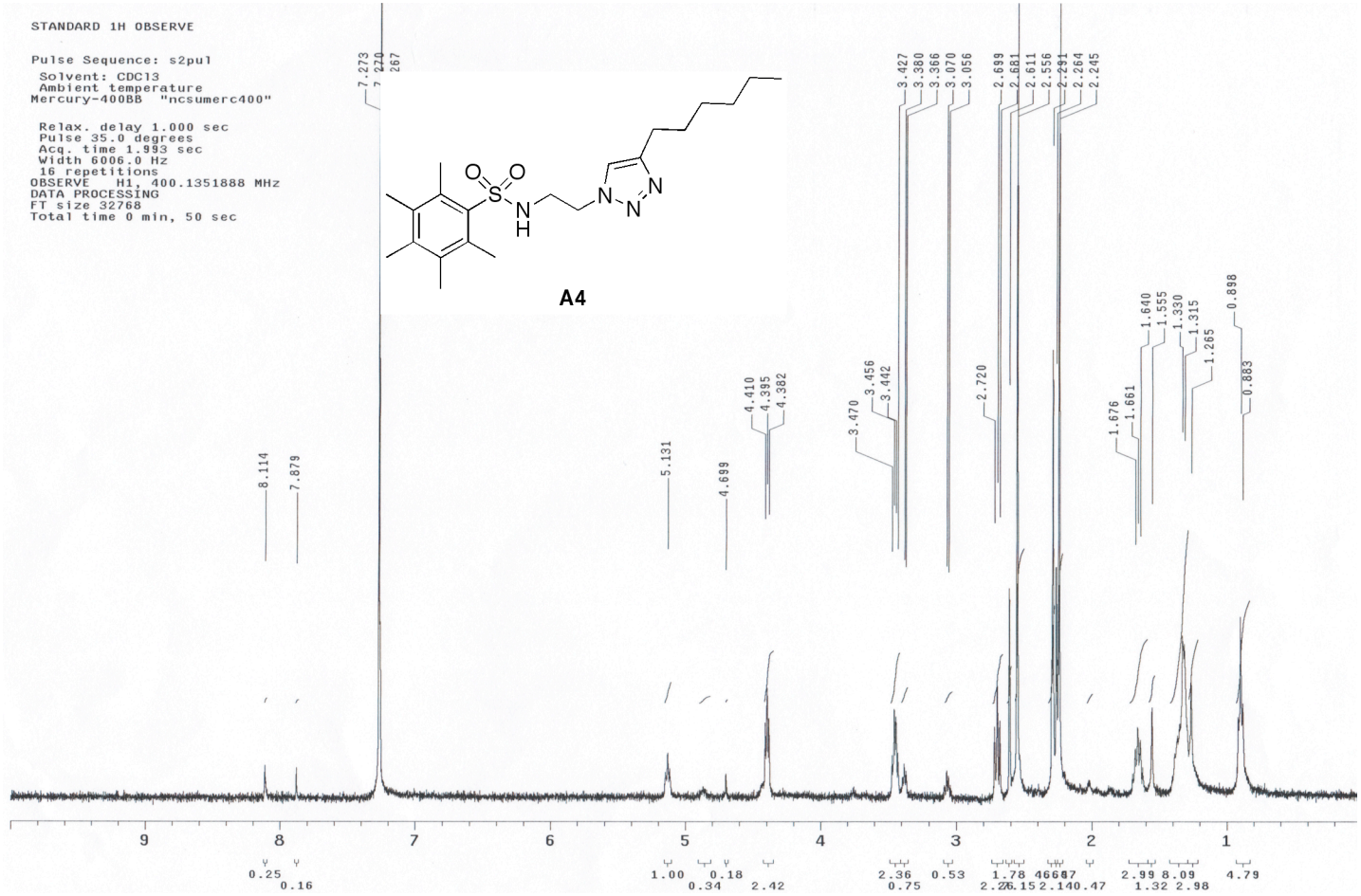
STANDARD 1H OBSERVE
Pulse Sequence: s2pul
Solvent: CDCl3
Ambient temperature
Mercury-400BB "ncsumerc400"
Relax. delay 1.000 sec
Pulse 35.0 degrees
Acq. time 1.993 sec
Width 6006.0 Hz
16 repetitions
OBSERVE H1, 400.1351888 MHz
DATA PROCESSING
FT size 32768
Total time 0 min, 50 sec
A4

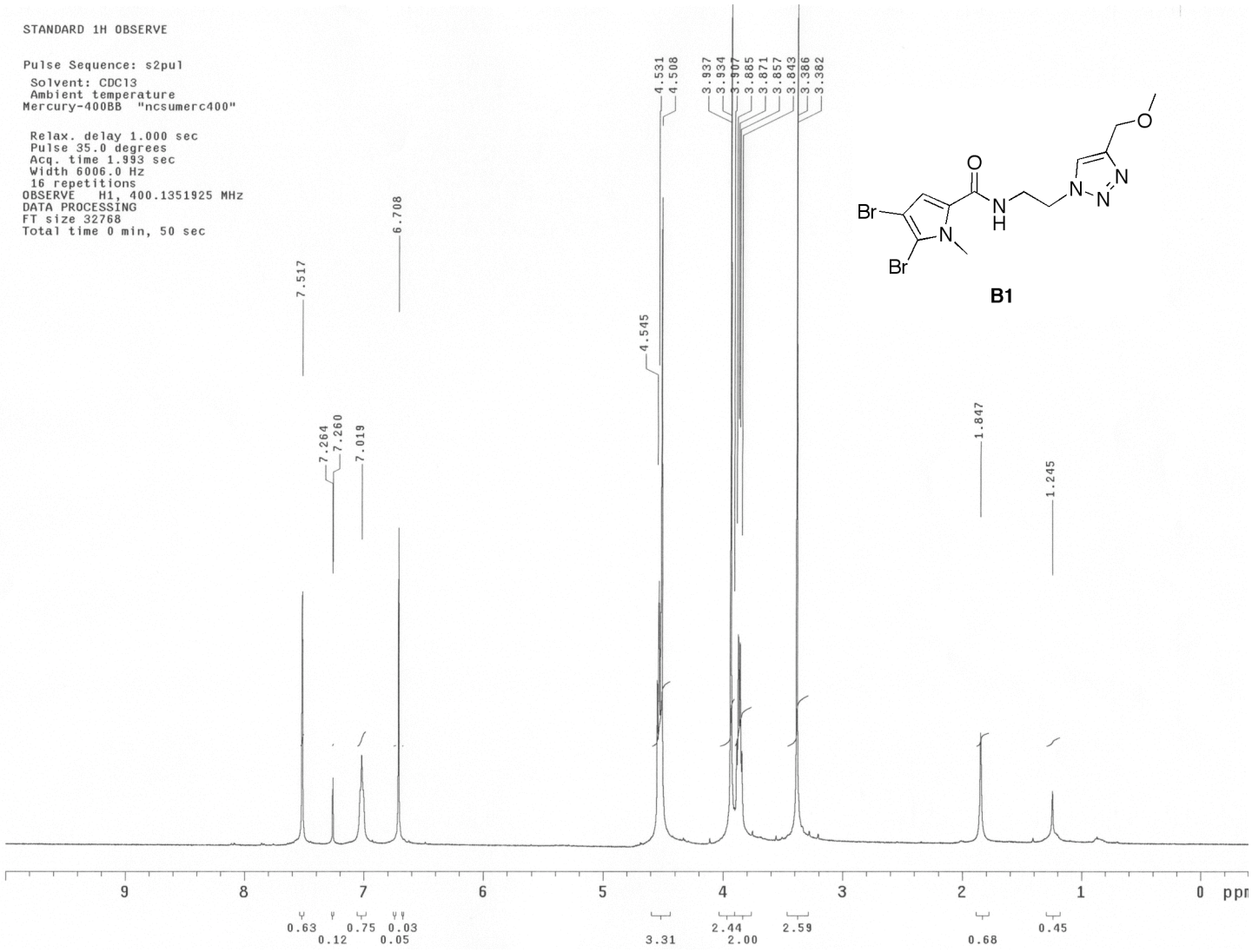
STANDARD 1H OBSERVE
Pulse Sequence: s2pul
Solvent: CDCl3
Ambient temperature
Mercury-400BB "ncsumerc400"
Relax. delay 1.000 sec
Pulse 35.0 degrees
Acq. time 1.993 sec
Width 6006.0 Hz
16 repetitions
OBSERVE H1, 400.1351925 MHz
DATA PROCESSING
FT size 32768
Total time 0 min, 50 sec
7.517
7.264
7.260
7.019
6.708
4.545
4.531
4.508
3.937
3.934
3.907
3.885
3.871
3.857
3.843
3.386
3.382
1.847
1.245
Br
Br
N
O
N
H
N
N
N
O
B1
9
8
7
6
5
4
3
2
1
0 ppm
0.63
0.12
0.75
0.05
0.03
3.31
2.44
2.00
2.59
0.68
0.45

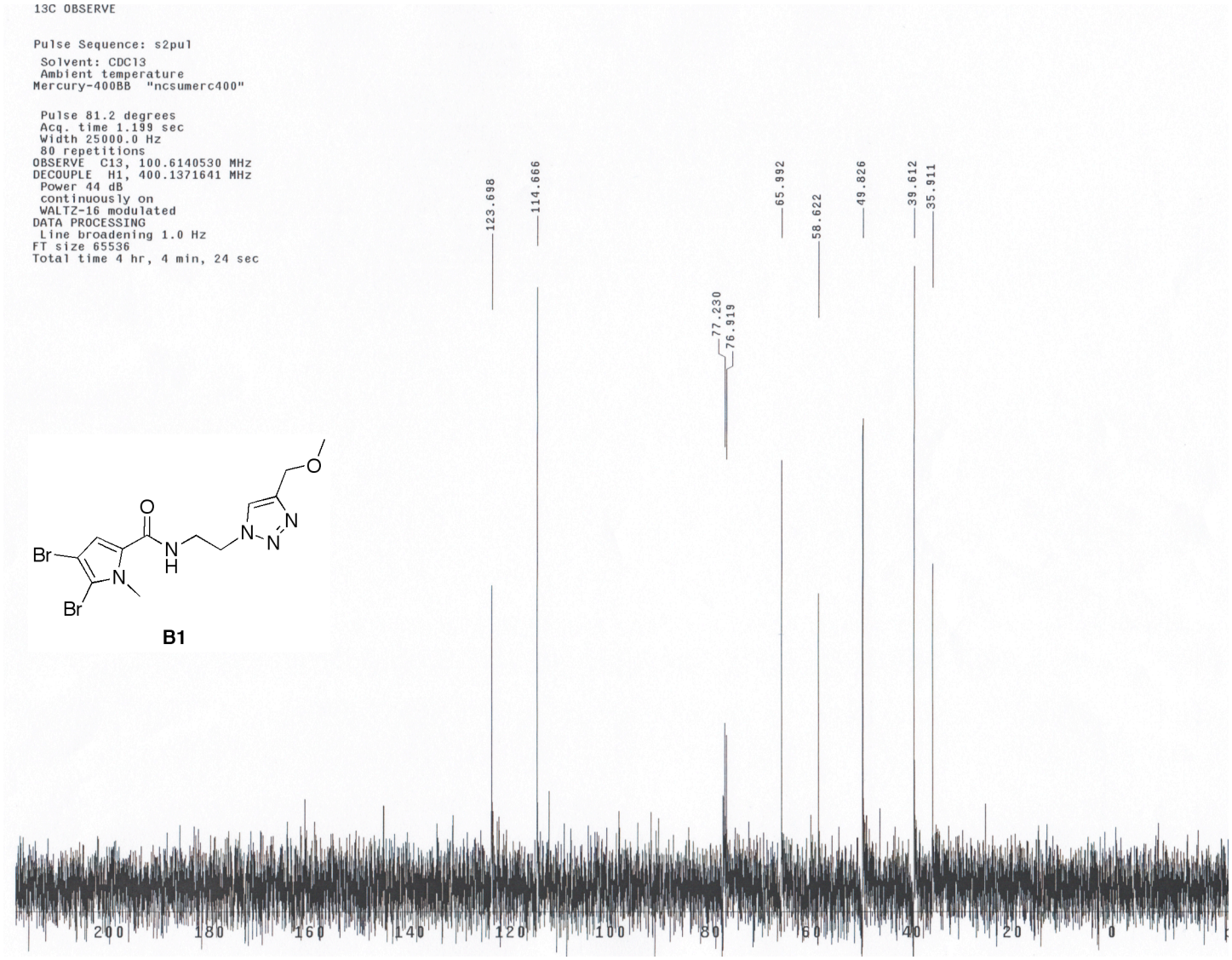
13C OBSERVE
Pulse Sequence: s2pul
Solvent: CDCl3
Ambient temperature
Mercury-400BB "ncsumerc400"
Pulse 81.2 degrees
Acq. time 1.199 sec
Width 25000.0 Hz
80 repetitions
OBSERVE C13, 100.6140530 MHz
DECOUPLE H1, 400.1371641 MHz
Power 44 dB
continuously on
WALTZ-16 modulated
DATA PROCESSING
Line broadening 1.0 Hz
FT size 65536
Total time 4 hr, 4 min, 24 sec
123.698
114.666
77.230
76.919
65.992
58.622
49.826
39.612
35.911
200
180
160
140
120
100
80
60
40
20
0
Br
Br
N
O
N
H
N
N
N
O

B1

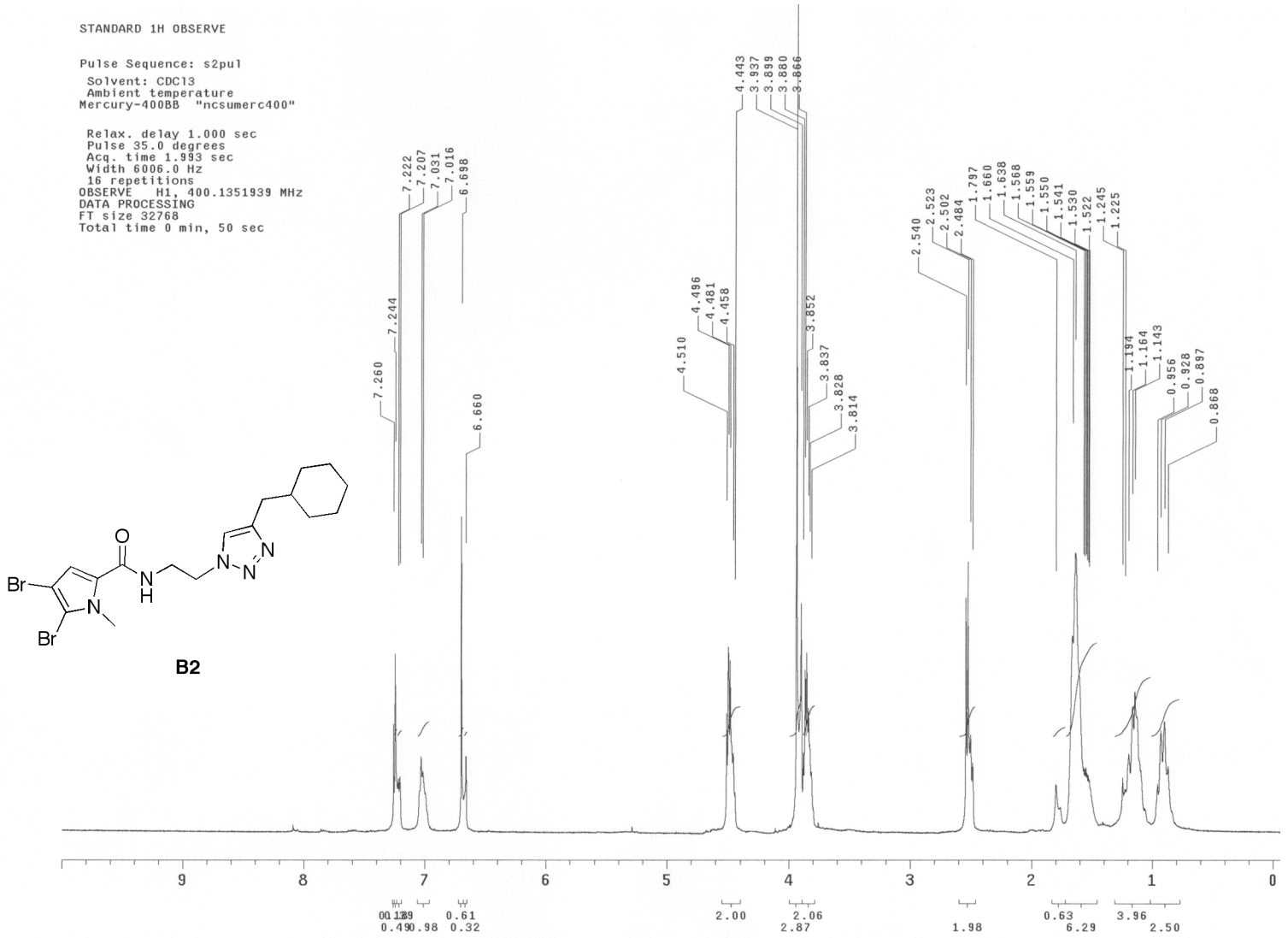
STANDARD 1H OBSERVE
Pulse Sequence: s2pul
Solvent: CDCl3
Ambient temperature
Mercury-400BB "ncsumerc400"
Relax. delay 1.000 sec
Pulse 35.0 degrees
Acq. time 1.993 sec
Width 6006.0 Hz
16 repetitions
OBSERVE H1, 400.1351939 MHz
DATA PROCESSING
FT size 32768
Total time 0 min, 50 sec
7.260
7.244
7.222
7.207
7.031
7.016
6.698
6.660
4.510
4.496
4.481
4.458
4.443
3.937
3.899
3.880
3.866
3.852
3.837
3.828
3.614
2.540
2.523
2.502
2.484
1.797
1.660
1.638
1.568
1.559
1.550
1.541
1.530
1.522
1.245
1.225
1.194
1.164
1.143
0.956
0.928
0.897
0.868
9
8
7
6
5
4
3
2
1
0
0.49
0.98
0.32
2.00
2.87
1.98
6.29
2.50
Br
Br
O
N
H
N
N
N
B2

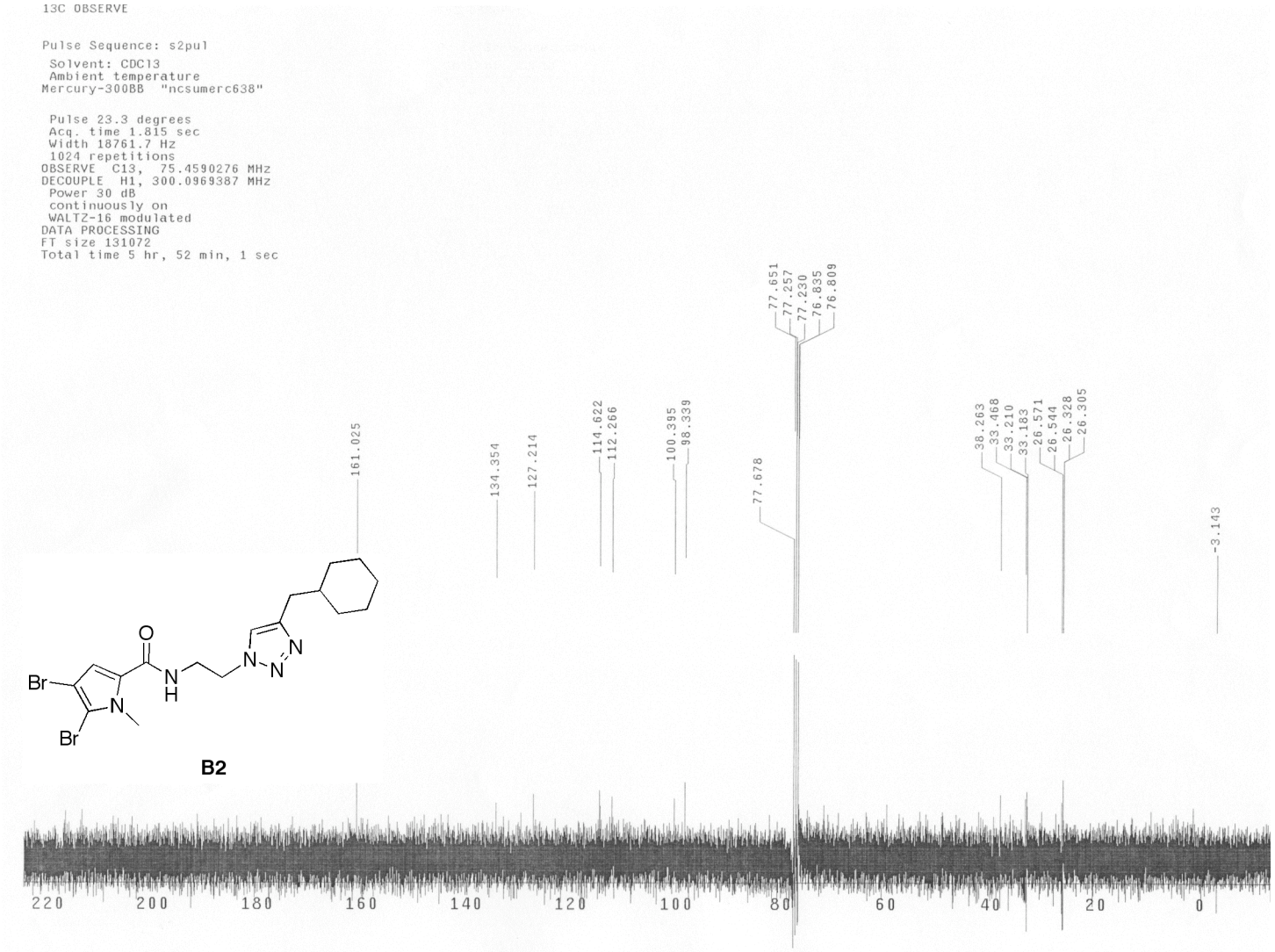
13C OBSERVE
Pulse Sequence: s2pul
Solvent: CDCl3
Ambient temperature
Mercury-300BB "ncsumerc638"
Pulse 23.3 degrees
Acq. time 1.815 sec
Width 18761.7 Hz
1024 repetitions
OBSERVE C13, 75.4590276 MHz
DECOUPLE H1, 300.0969387 MHz
Power 30 dB
continuously on
WALTZ-16 modulated
DATA PROCESSING
FT size 131072
Total time 5 hr, 52 min, 1 sec
161.025
134.354
127.214
114.622
112.266
100.395
98.339
77.678
77.651
77.257
77.230
76.835
76.809
38.263
33.468
33.210
33.183
26.571
26.544
26.328
26.305
-3.143
220
200
180
160
140
120
100
80
60
40
20
0

B2

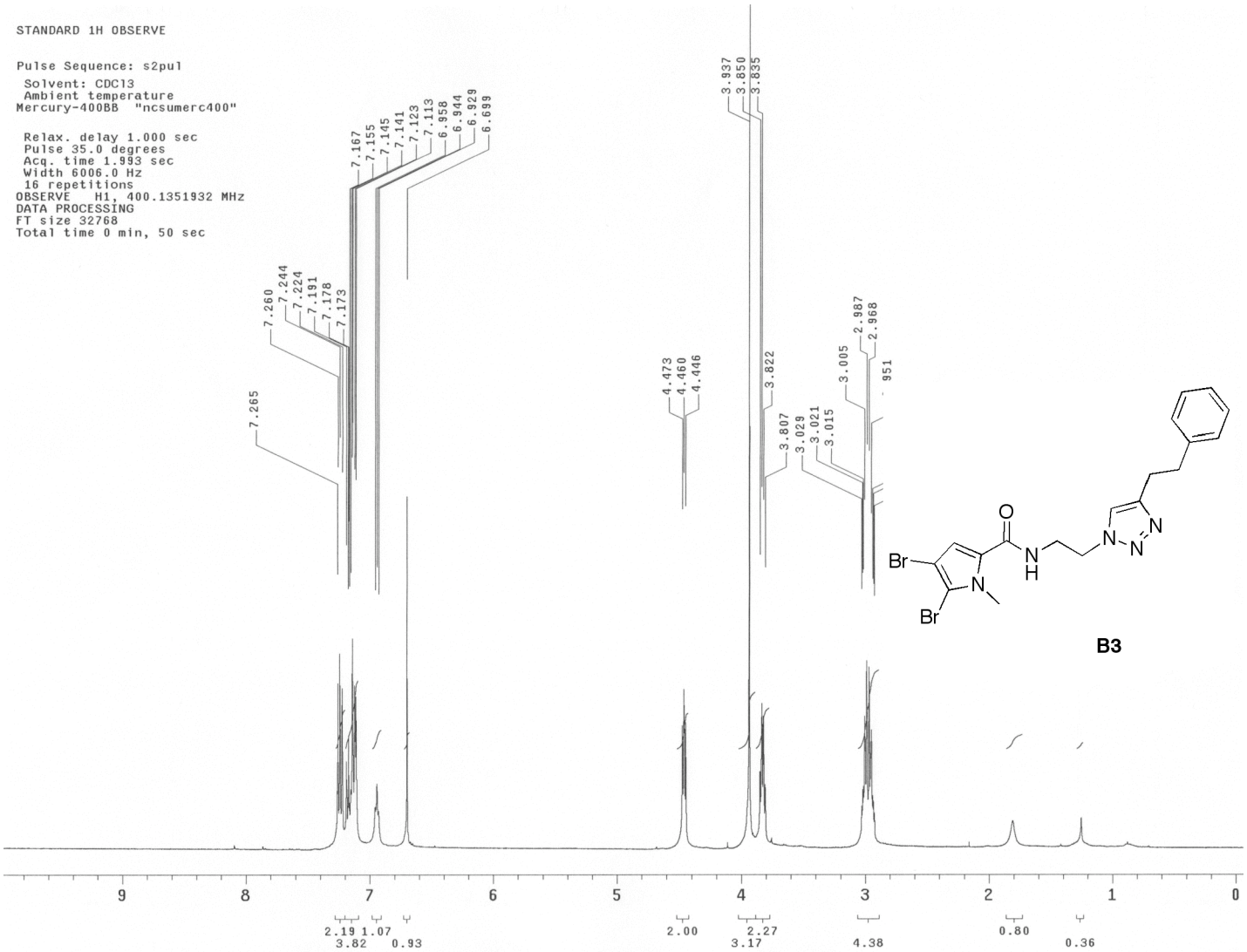
STANDARD 1H OBSERVE
Pulse Sequence: s2pul
Solvent: CDCl3
Ambient temperature
Mercury-400BB "ncsumerc400"
Relax. delay 1.000 sec
Pulse 35.0 degrees
Acq. time 1.993 sec
Width 6006.0 Hz
16 repetitions
OBSERVE H1, 400.1351932 MHz
DATA PROCESSING
FT size 32768
Total time 0 min, 50 sec
7.265
7.260
7.244
7.224
7.191
7.178
7.173
7.167
7.155
7.145
7.141
7.123
7.113
6.958
6.944
6.929
6.699
4.473
4.460
4.446
3.937
3.850
3.835
3.822
3.807
3.029
3.021
3.015
3.005
2.987
2.968
951
Br
Br
N
O
N
H
N
N
N
B3
9
8
7
6
5
4
3
2
1
0
2.19
1.07
0.93
3.82
2.00
2.27
3.17
4.38
0.80
0.36

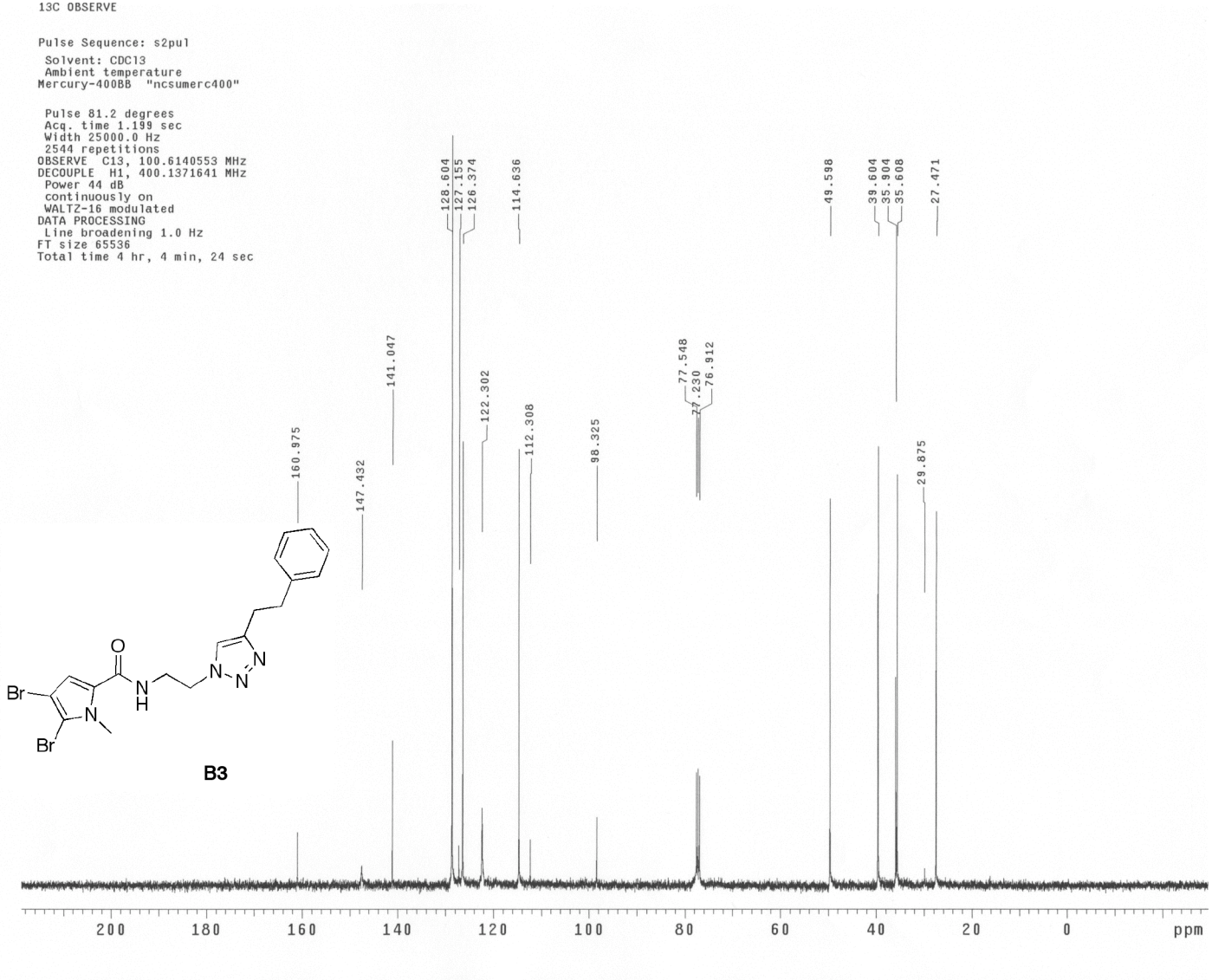
13C OBSERVE
Pulse Sequence: s2pul
Solvent: CDCl3
Ambient temperature
Mercury-400BB "ncsumerc400"
Pulse 81.2 degrees
Acq. time 1.199 sec
Width 25000.0 Hz
2544 repetitions
OBSERVE C13, 100.6140553 MHz
DECOUPLE H1, 400.1371641 MHz
Power 44 dB
continuously on
WALTZ-16 modulated
DATA PROCESSING
Line broadening 1.0 Hz
FT size 65536
Total time 4 hr, 4 min, 24 sec
160.975
147.432
141.047
128.604
127.155
126.374
122.302
114.636
112.308
98.325
77.548
77.230
76.912
49.598
39.604
35.904
35.608
29.875
27.471
B3
200
180
160
140
120
100
80
60
40
20
0
ppm

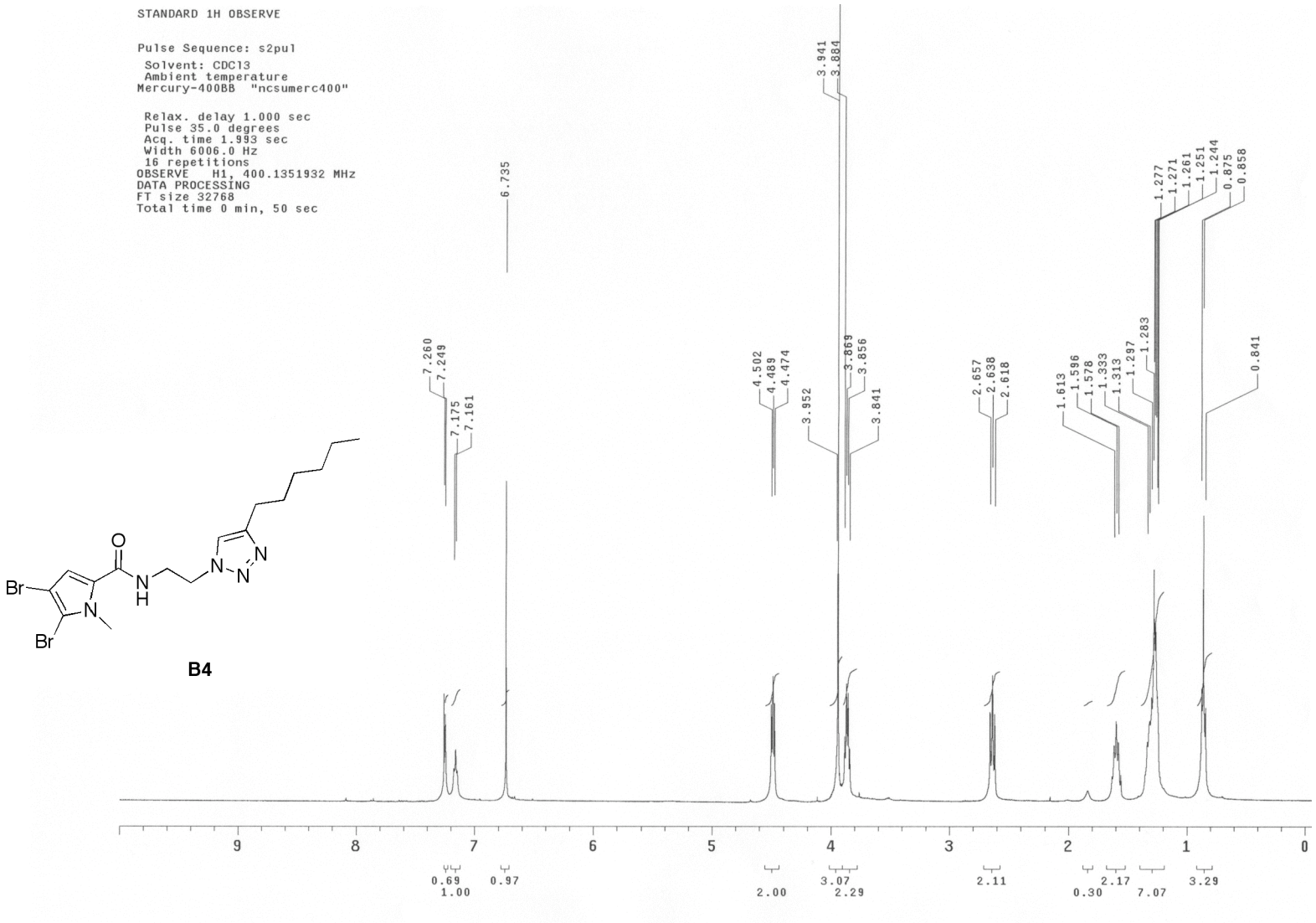
STANDARD 1H OBSERVE
Pulse Sequence: s2pul
Solvent: CDCl3
Ambient temperature
Mercury-400BB "ncsumerc400"
Relax. delay 1.000 sec
Pulse 35.0 degrees
Acq. time 1.993 sec
Width 6006.0 Hz
16 repetitions
OBSERVE H1, 400.1351932 MHz
DATA PROCESSING
FT size 32768
Total time 0 min, 50 sec
B4

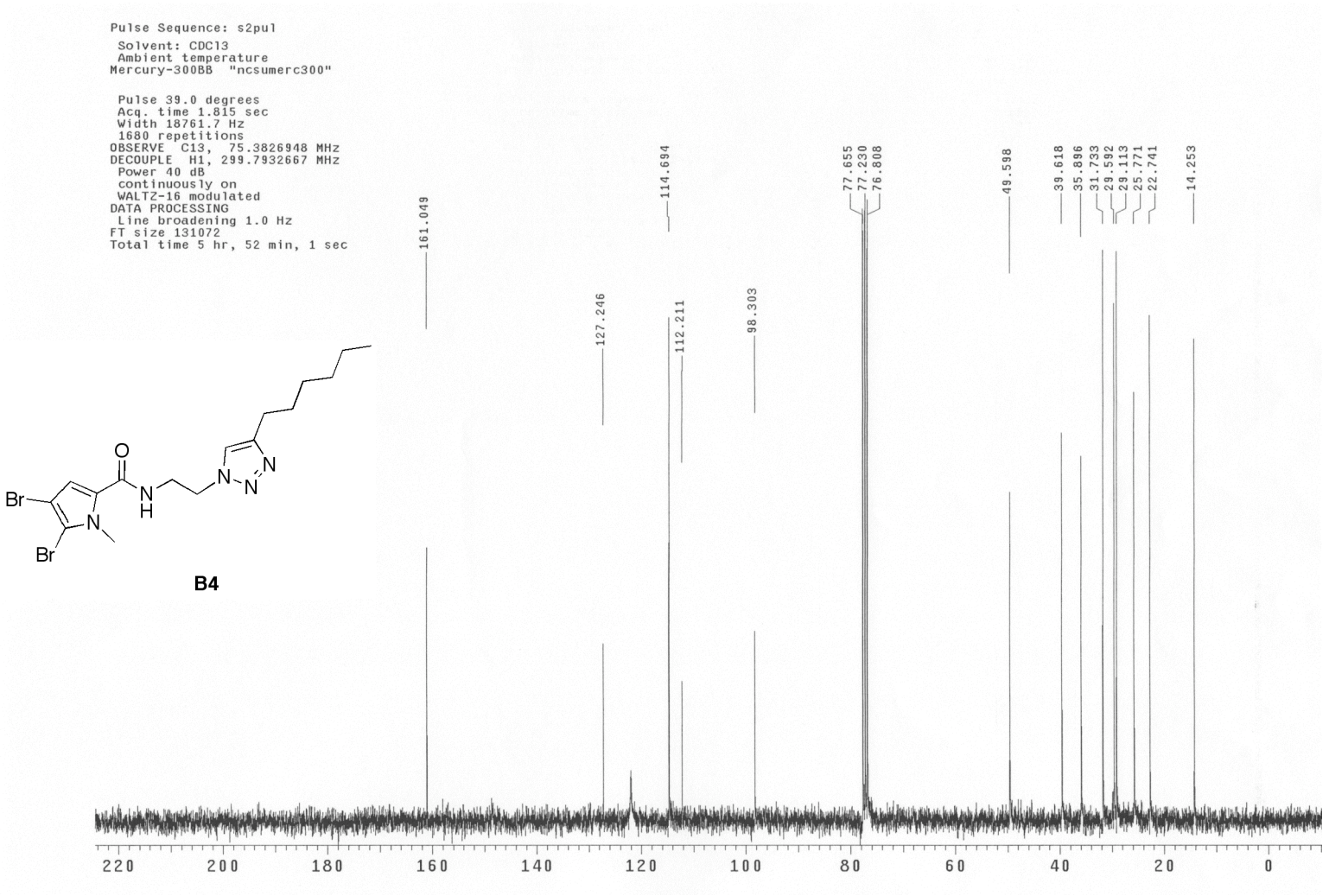
Pulse Sequence: s2pul
Solvent: CDCl3
Ambient temperature
Mercury-300BB "ncsumerc300"
Pulse 39.0 degrees
Acq. time 1.815 sec
Width 18761.7 Hz
1680 repetitions
OBSERVE C13, 75.3826948 MHz
DECOUPLE H1, 299.7932667 MHz
Power 40 dB
continuously on
WALTZ-16 modulated
DATA PROCESSING
Line broadening 1.0 Hz
FT size 131072
Total time 5 hr, 52 min, 1 sec
161.049
127.246
114.694
112.211
98.303
77.655
77.230
76.808
49.598
39.618
35.896
31.733
29.592
29.113
25.771
22.741
14.253
220
200
180
160
140
120
100
80
60
40
20
0
Br
Br
O
N
H
N
N
N
B4

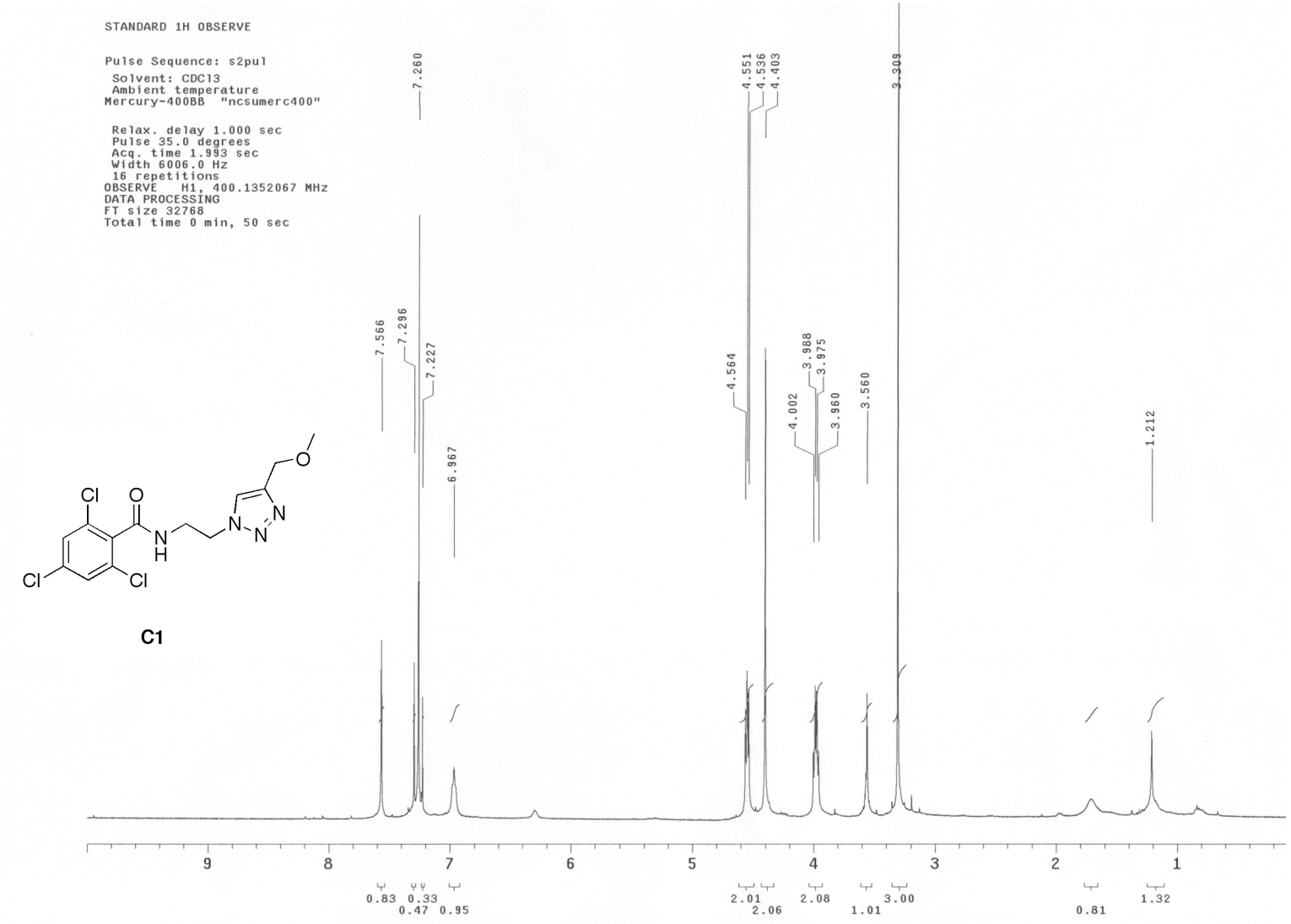
STANDARD 1H OBSERVE
Pulse Sequence: s2pul
Solvent: CDCl3
Ambient temperature
Mercury-400BB "ncsumerc400"
Relax. delay 1.000 sec
Pulse 35.0 degrees
Acq. time 1.993 sec
Width 6006.0 Hz
16 repetitions
OBSERVE H1, 400.1352067 MHz
DATA PROCESSING
FT size 32768
Total time 0 min, 50 sec
7.566
7.296
7.260
7.227
6.967
4.564
4.551
4.536
4.403
4.002
3.988
3.975
3.960
3.560
3.309
1.212
0.83
0.33
0.47
0.95
2.01
2.06
2.08
1.01
3.00
0.81
1.32

C1

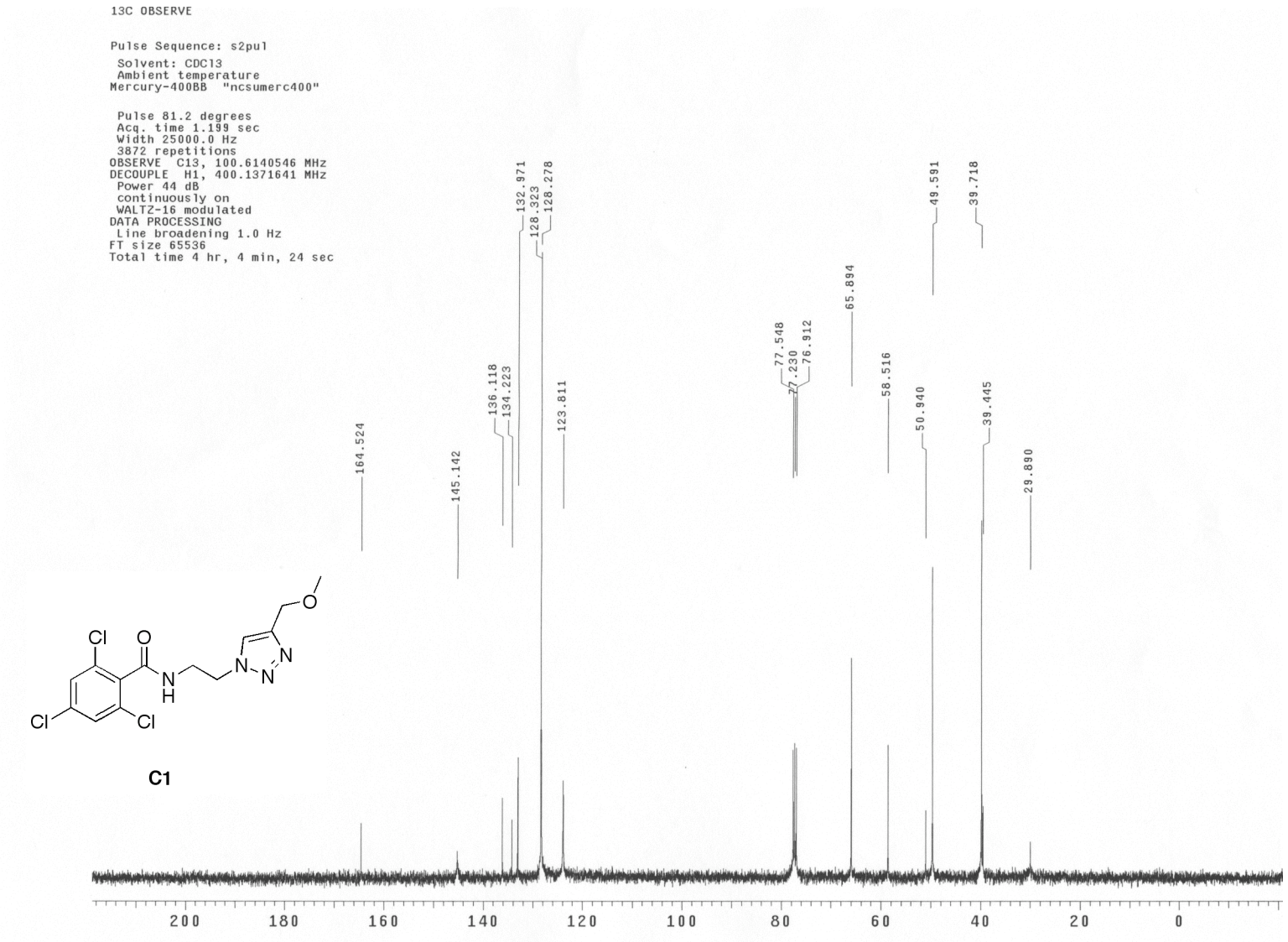
13C OBSERVE
Pulse Sequence: s2pul
Solvent: CDCl3
Ambient temperature
Mercury-400BB "ncsumerc400"
Pulse 81.2 degrees
Acq. time 1.199 sec
Width 25000.0 Hz
3872 repetitions
OBSERVE C13, 100.6140546 MHz
DECOUPLE H1, 400.1371641 MHz
Power 44 dB
continuously on
WALTZ-16 modulated
DATA PROCESSING
Line broadening 1.0 Hz
FT size 65536
Total time 4 hr, 4 min, 24 sec
164.524
145.142
136.118
134.223
132.971
128.323
128.278
123.811
77.548
77.230
76.912
65.894
58.516
50.940
49.591
39.718
39.445
29.890
Cl
O
N
H
N
N
N
O
Cl
Cl
200
180
160
140
120
100
80
60
40
20
0

C1

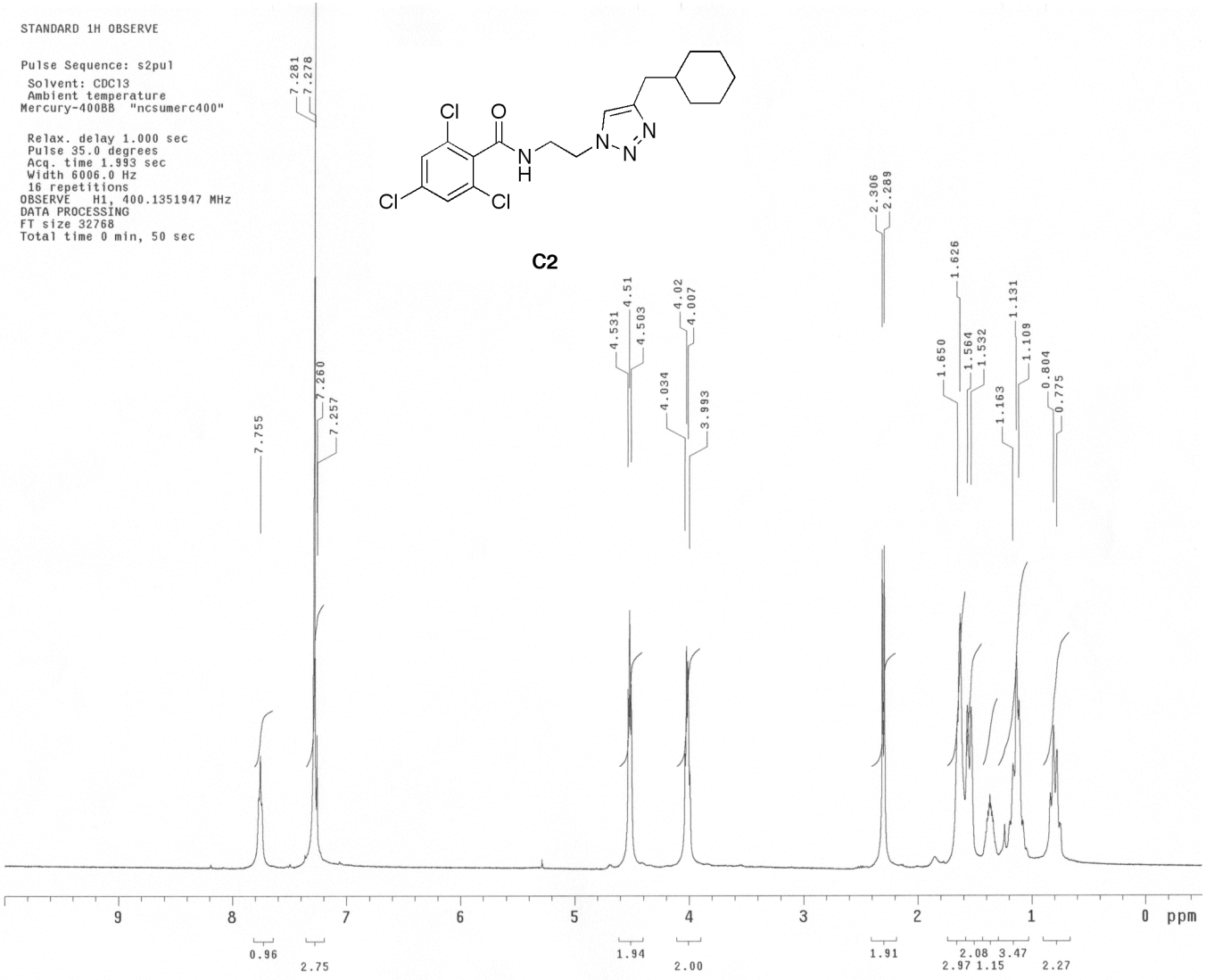
STANDARD 1H OBSERVE
Pulse Sequence: s2pul
Solvent: CDCl3
Ambient temperature
Mercury-400BB "ncsumerc400"
Relax. delay 1.000 sec
Pulse 35.0 degrees
Acq. time 1.993 sec
Width 6006.0 Hz
16 repetitions
OBSERVE H1, 400.1351947 MHz
DATA PROCESSING
FT size 32768
Total time 0 min, 50 sec
C2
7.281
7.278
7.755
7.260
7.257
4.531
4.51
4.503
4.034
4.02
4.007
3.993
2.306
2.289
1.650
1.626
1.564
1.532
1.163
1.131
1.109
0.804
0.775
9
8
7
6
5
4
3
2
1
0
ppm
0.96
2.75
1.94
2.00
1.91
2.08
3.47
2.97
1.15
2.27

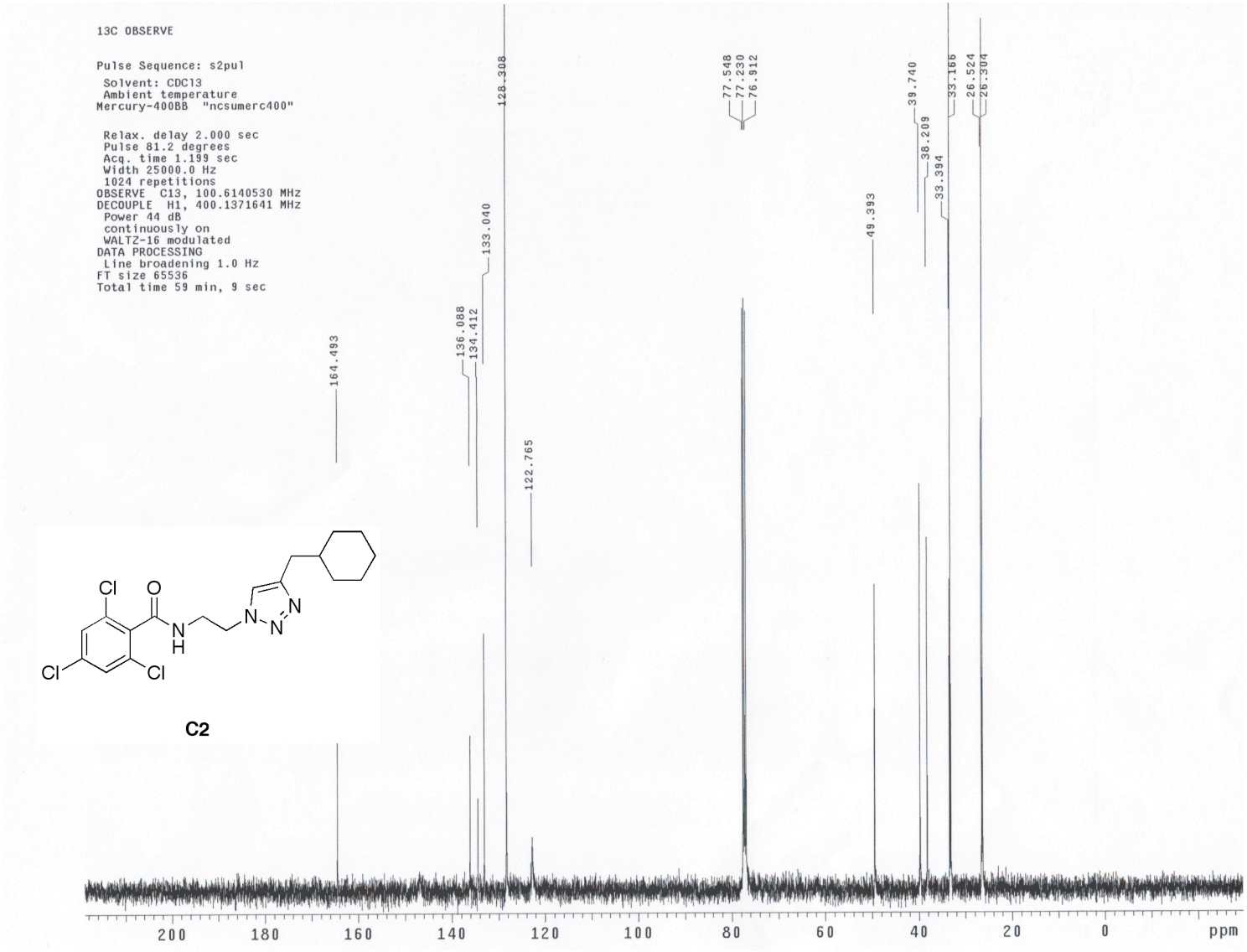
13C OBSERVE
Pulse Sequence: s2pul
Solvent: CDCl3
Ambient temperature
Mercury-400BB "ncsumerc400"
Relax. delay 2.000 sec
Pulse 81.2 degrees
Acq. time 1.199 sec
Width 25000.0 Hz
1024 repetitions
OBSERVE C13, 100.6140530 MHz
DECOUPLE H1, 400.1371641 MHz
Power 44 dB
continuously on
WALTZ-16 modulated
DATA PROCESSING
Line broadening 1.0 Hz
FT size 65536
Total time 59 min, 9 sec
164.493
136.088
134.412
133.040
128.308
122.765
77.548
77.230
76.912
49.393
39.740
38.209
33.394
33.166
26.524
26.304
Cl
O
N
H
N
N
N
Cl
Cl
C2
200
180
160
140
120
100
80
60
40
20
0
ppm

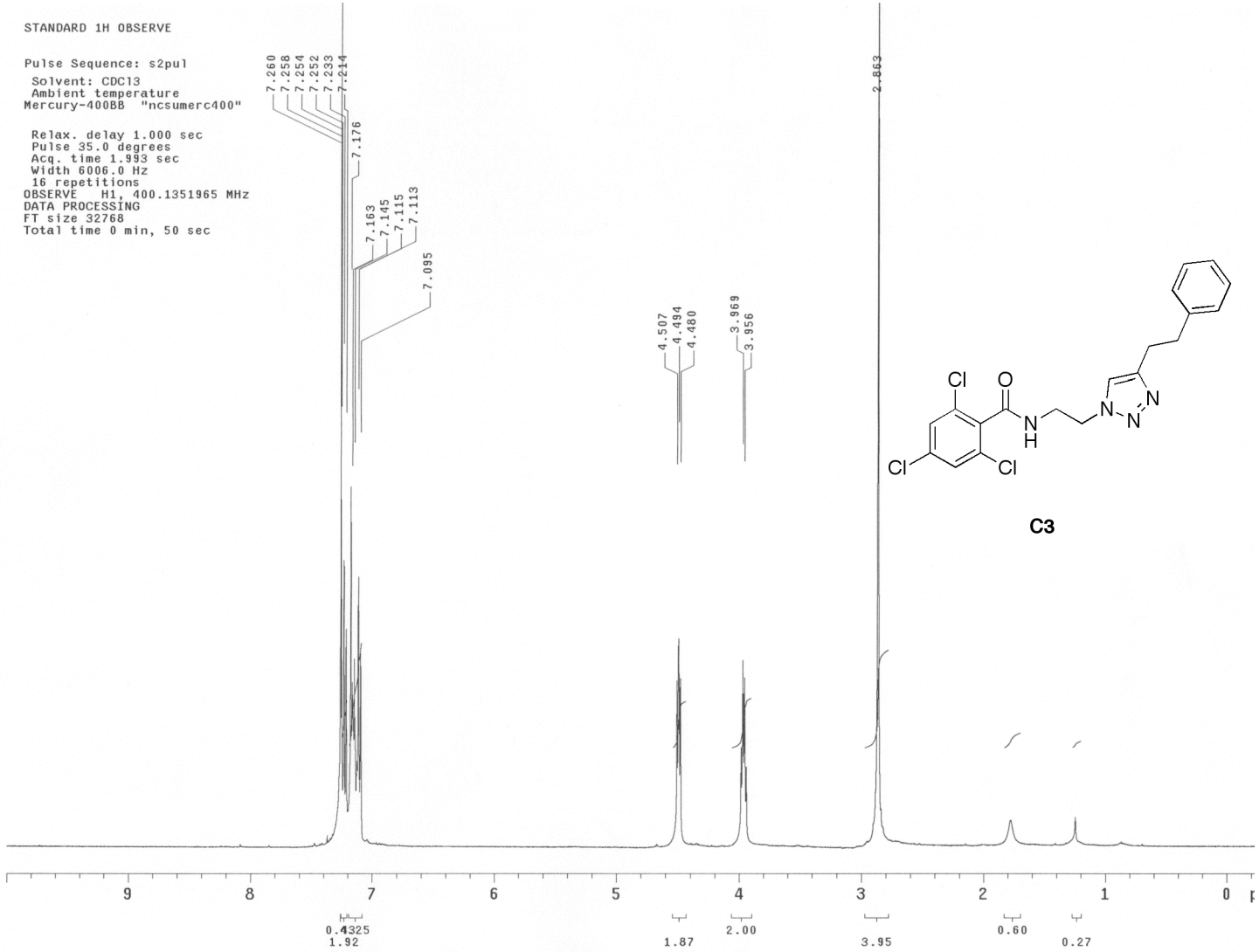
STANDARD 1H OBSERVE
Pulse Sequence: s2pul
Solvent: CDCl3
Ambient temperature
Mercury-400BB "ncsumerc400"
Relax. delay 1.000 sec
Pulse 35.0 degrees
Acq. time 1.993 sec
Width 6006.0 Hz
16 repetitions
OBSERVE H1, 400.1351965 MHz
DATA PROCESSING
FT size 32768
Total time 0 min, 50 sec
7.260
7.258
7.254
7.252
7.233
7.214
7.176
7.163
7.145
7.115
7.113
7.095
4.507
4.494
4.480
3.969
3.956
2.853
Cl
O
N
H
N
N
N
Cl
Cl
9
8
7
6
5
4
3
2
1
0
0.4325
1.92
1.87
2.00
3.95
0.60
0.27

C3

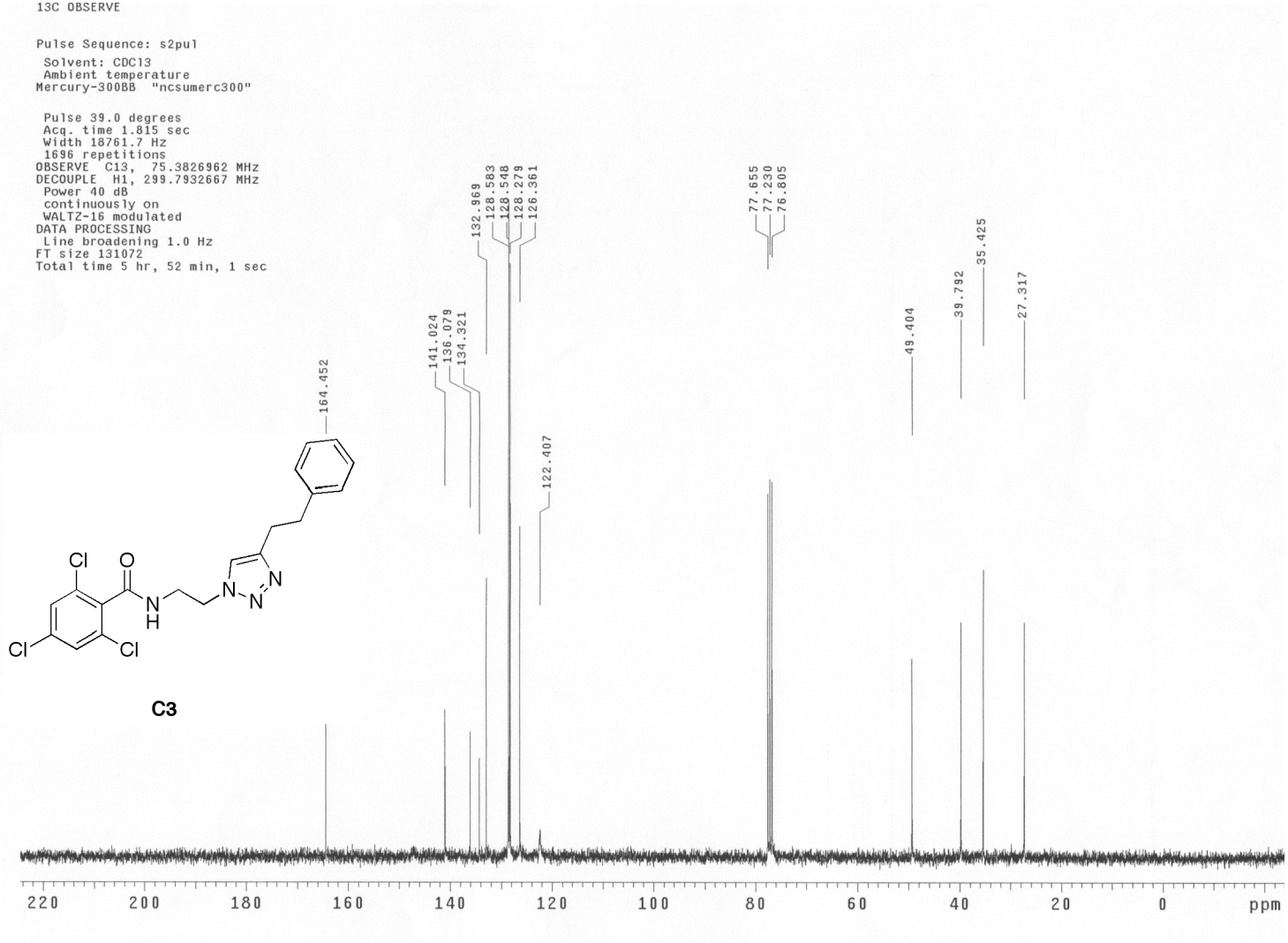
13C OBSERVE
Pulse Sequence: s2pul
Solvent: CDCl3
Ambient temperature
Mercury-300BB "ncsumerc300"
Pulse 39.0 degrees
Acq. time 1.815 sec
Width 18761.7 Hz
1696 repetitions
OBSERVE C13, 75.3826962 MHz
DECOUPLE H1, 299.7932667 MHz
Power 40 dB
continuously on
WALTZ-16 modulated
DATA PROCESSING
Line broadening 1.0 Hz
FT size 131072
Total time 5 hr, 52 min, 1 sec
164.452
141.024
136.079
134.321
132.969
128.583
128.548
128.279
126.361
122.407
77.655
77.230
76.805
49.404
39.792
35.425
27.317
Cl
O
N
H
N
N
N
Cl
Cl
C3
220
200
180
160
140
120
100
80
60
40
20
0
ppm

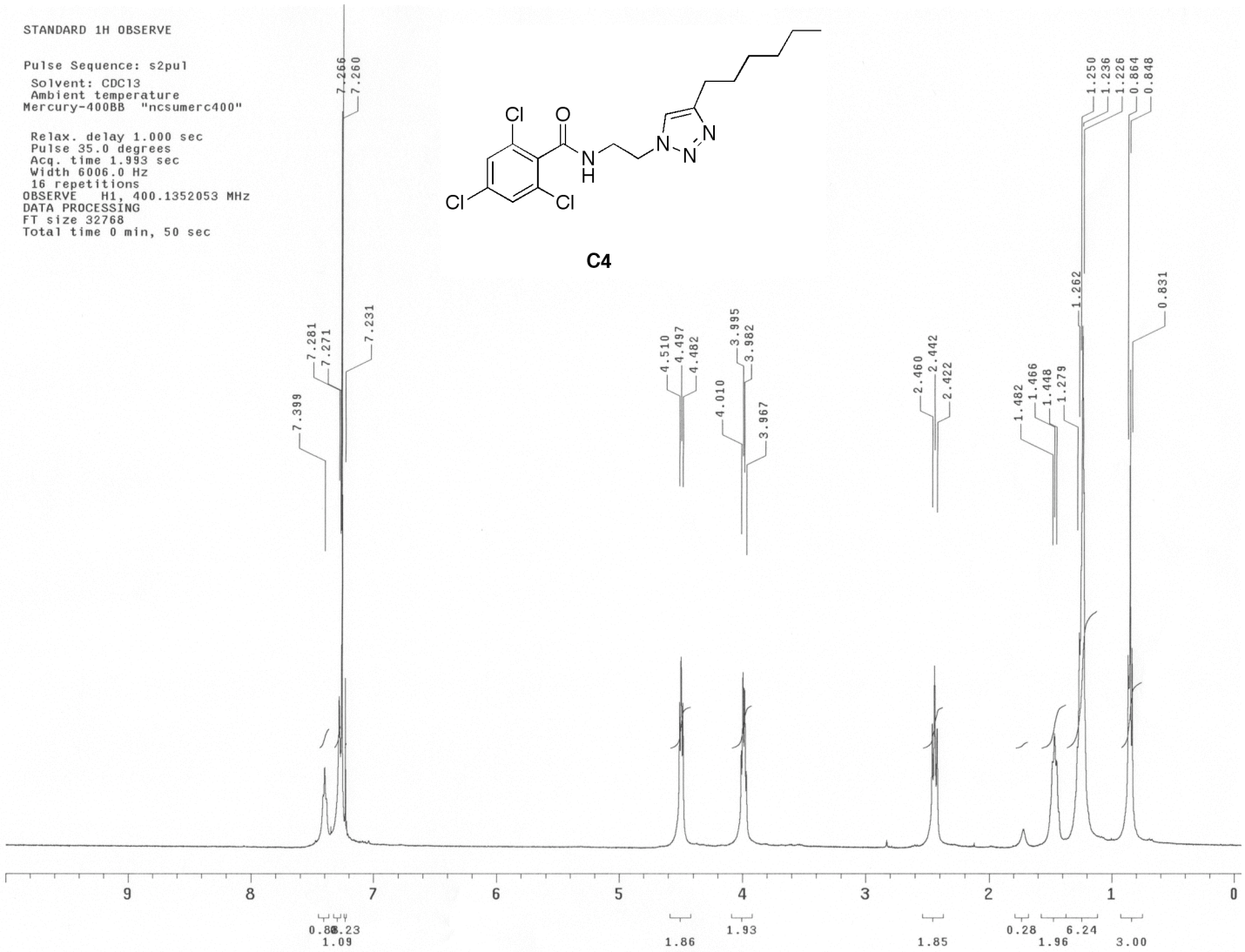
STANDARD 1H OBSERVE
Pulse Sequence: s2pul
Solvent: CDCl3
Ambient temperature
Mercury-400BB "ncsumerc400"
Relax. delay 1.000 sec
Pulse 35.0 degrees
Acq. time 1.993 sec
Width 6006.0 Hz
16 repetitions
OBSERVE H1, 400.1352053 MHz
DATA PROCESSING
FT size 32768
Total time 0 min, 50 sec
Cl
O
N
H
N
N
N
Cl
Cl
C4
7.266
7.260
7.399
7.281
7.271
7.231
4.510
4.497
4.482
4.010
3.995
3.982
3.967
2.460
2.442
2.422
1.482
1.466
1.448
1.279
1.262
1.250
1.236
1.226
0.864
0.848
0.831
9
8
7
6
5
4
3
2
1
0
0.86
0.23
1.09
1.86
1.93
1.85
0.28
6.24
1.96
3.00

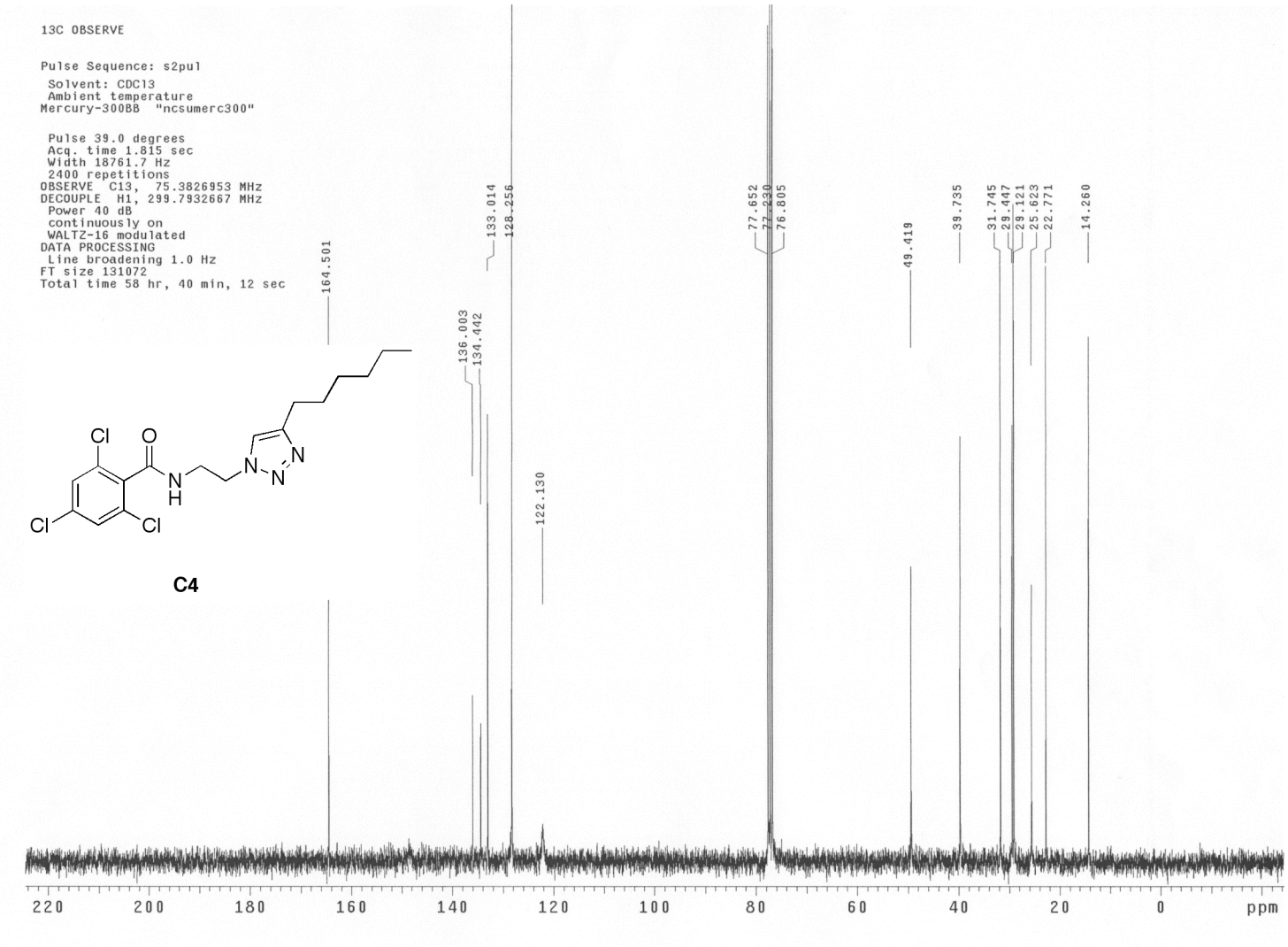
13C OBSERVE
Pulse Sequence: s2pul
Solvent: CDCl3
Ambient temperature
Mercury-300BB "ncsumerc300"
Pulse 39.0 degrees
Acq. time 1.815 sec
Width 18761.7 Hz
2400 repetitions
OBSERVE C13, 75.3826953 MHz
DECOUPLE H1, 299.7932667 MHz
Power 40 dB
continuously on
WALTZ-16 modulated
DATA PROCESSING
Line broadening 1.0 Hz
FT size 131072
Total time 58 hr, 40 min, 12 sec
164.501
136.003
134.442
133.014
128.256
122.130
77.652
77.230
76.805
49.419
39.735
31.745
29.447
29.121
25.623
22.771
14.260
Cl
O
N
H
N
N
N
Cl
Cl
220
200
180
160
140
120
100
80
60
40
20
0
ppm

C4

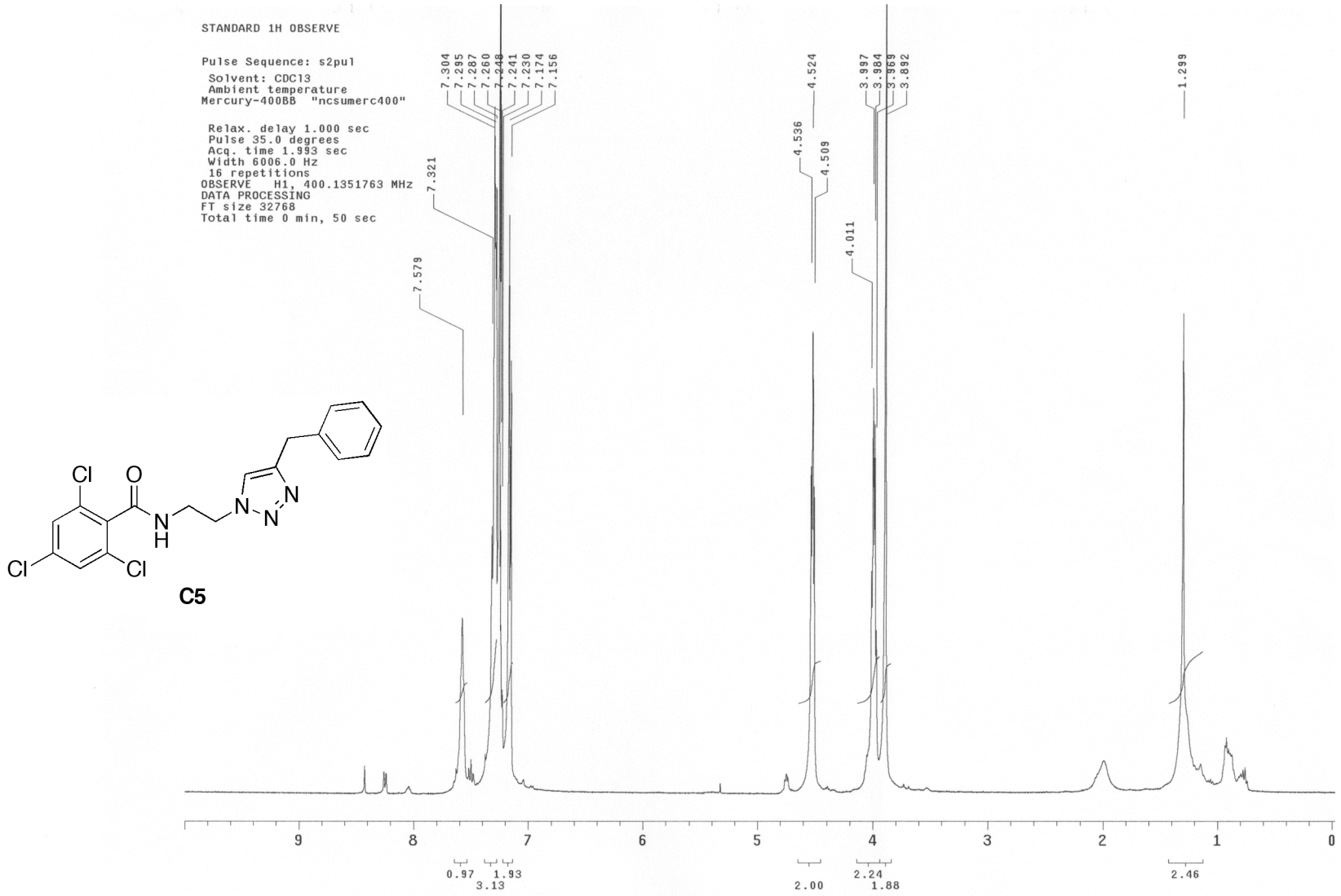
STANDARD 1H OBSERVE
Pulse Sequence: s2pul
Solvent: CDCl3
Ambient temperature
Mercury-400BB "ncsumerc400"
Relax. delay 1.000 sec
Pulse 35.0 degrees
Acq. time 1.993 sec
Width 6006.0 Hz
16 repetitions
OBSERVE H1, 400.1351763 MHz
DATA PROCESSING
FT size 32768
Total time 0 min, 50 sec
7.304
7.295
7.287
7.260
7.248
7.241
7.230
7.174
7.156
7.321
7.579
4.524
4.536
4.509
4.011
3.997
3.984
3.969
3.892
1.299
Cl
O
N
H
N
N
N
Cl
Cl
Cl
C5
9
8
7
6
5
4
3
2
1
0
0.97
1.93
3.13
2.00
2.24
1.88
2.46

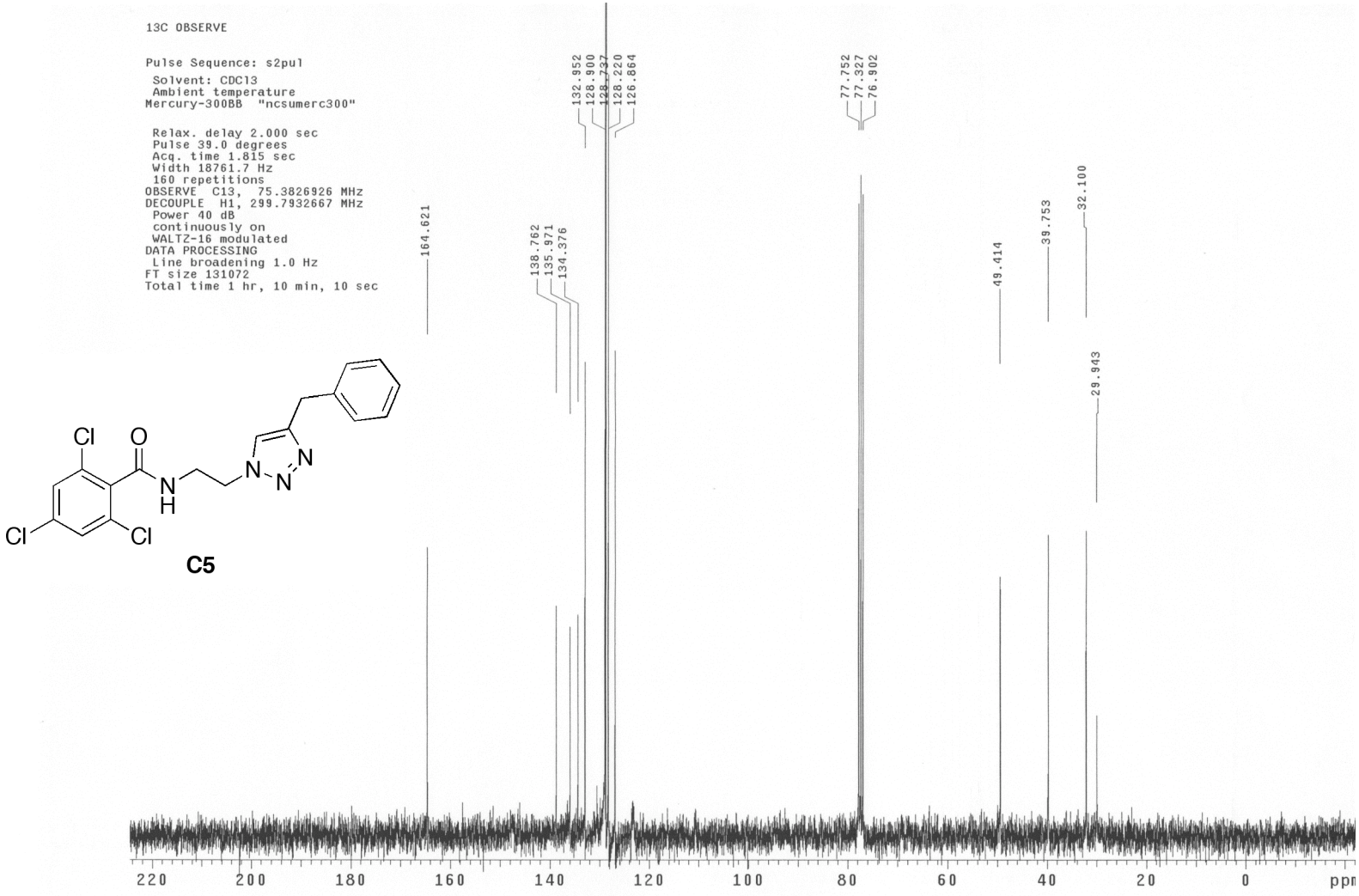
13C OBSERVE
Pulse Sequence: s2pul
Solvent: CDCl3
Ambient temperature
Mercury-300BB "ncsumerc300"
Relax. delay 2.000 sec
Pulse 39.0 degrees
Acq. time 1.815 sec
Width 18761.7 Hz
160 repetitions
OBSERVE C13, 75.3826926 MHz
DECOUPLE H1, 299.7932667 MHz
Power 40 dB
continuously on
WALTZ-16 modulated
DATA PROCESSING
Line broadening 1.0 Hz
FT size 131072
Total time 1 hr, 10 min, 10 sec
164.621
138.762
135.971
134.376
132.952
128.900
128.737
128.220
126.864
77.752
77.327
76.902
49.414
39.753
32.100
29.943
220
200
180
160
140
120
100
80
60
40
20
0
ppm
Cl
O
N
H
N
N
N
Cl
Cl
C5

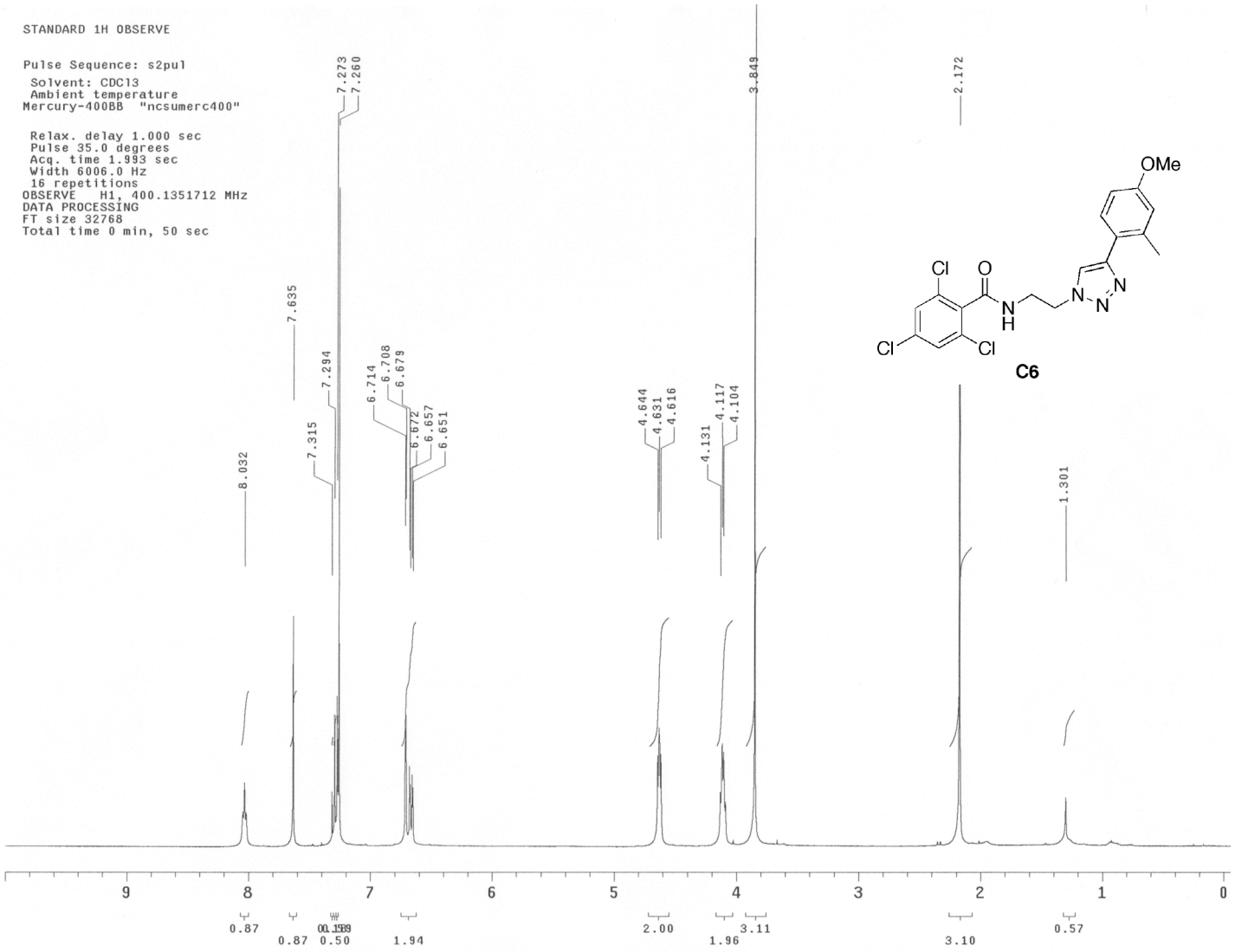
STANDARD 1H OBSERVE
Pulse Sequence: s2pul
Solvent: CDCl3
Ambient temperature
Mercury-400BB "ncsumerc400"
Relax. delay 1.000 sec
Pulse 35.0 degrees
Acq. time 1.993 sec
Width 6006.0 Hz
16 repetitions
OBSERVE H1, 400.1351712 MHz
DATA PROCESSING
FT size 32768
Total time 0 min, 50 sec
8.032
7.635
7.315
7.294
7.273
7.260
6.714
6.708
6.679
6.672
6.657
6.651
4.644
4.631
4.616
4.131
4.117
4.104
3.849
2.172
1.301
OMe
Cl
O
N
H
N
N
N
Cl
Cl
C6
0.87
0.87
0.50
1.94
2.00
1.96
3.11
3.10
0.57

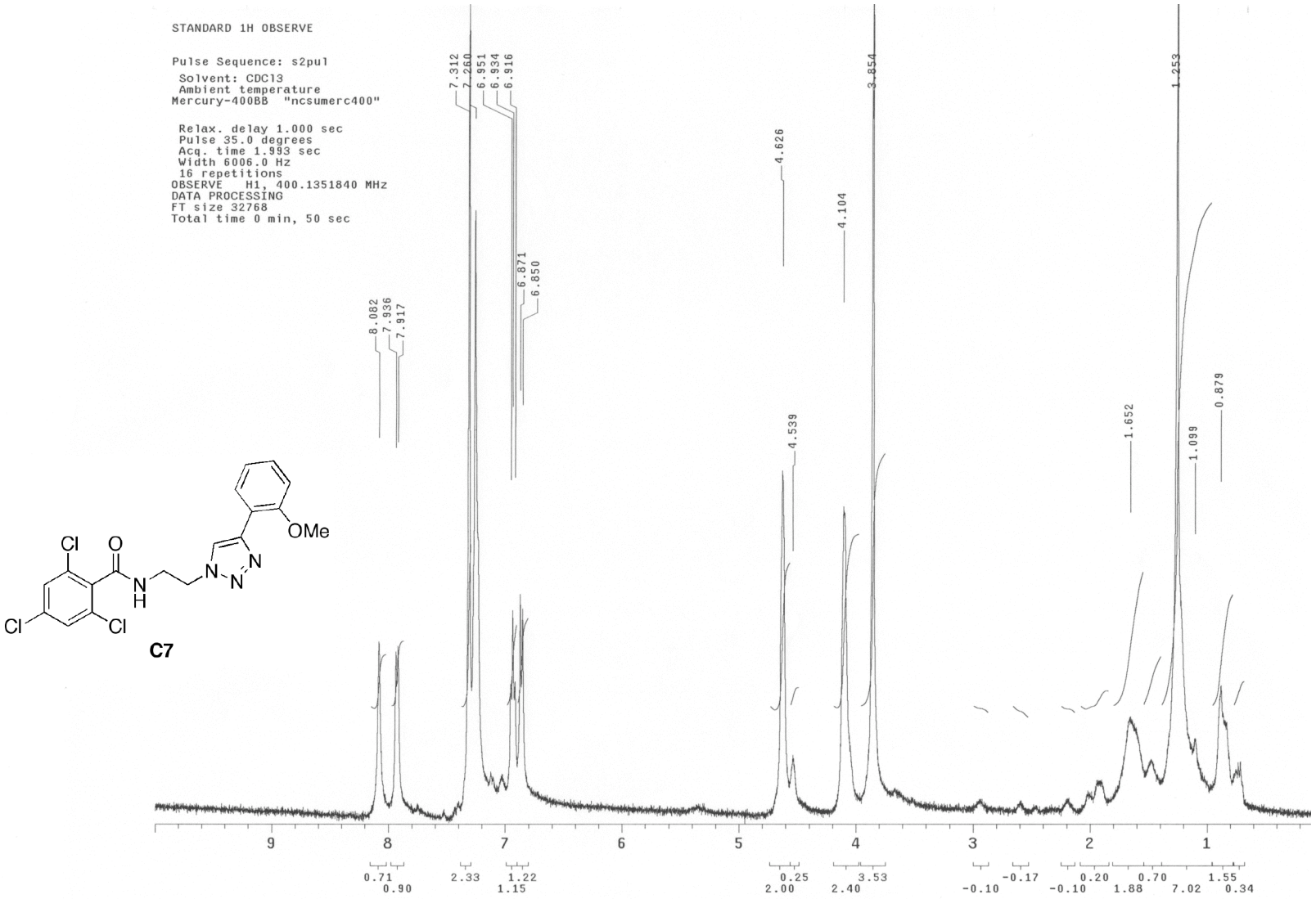
STANDARD 1H OBSERVE
Pulse Sequence: s2pul
Solvent: CDCl3
Ambient temperature
Mercury-400BB "ncsumerc400"
Relax. delay 1.000 sec
Pulse 35.0 degrees
Acq. time 1.993 sec
Width 6006.0 Hz
16 repetitions
OBSERVE H1, 400.1351840 MHz
DATA PROCESSING
FT size 32768
Total time 0 min, 50 sec
7.312
7.260
6.951
6.934
6.916
6.871
6.850
8.082
7.936
7.917
4.626
4.539
4.104
3.854
1.652
1.253
1.099
0.879
Cl
O
N
H
N
N
N
OMe
Cl
Cl
C7
9
8
7
6
5
4
3
2
1
0.71
0.90
2.33
1.22
1.15
0.25
2.00
3.53
2.40
-0.10
-0.17
0.20
-0.10
0.70
1.88
1.55
7.02
0.34

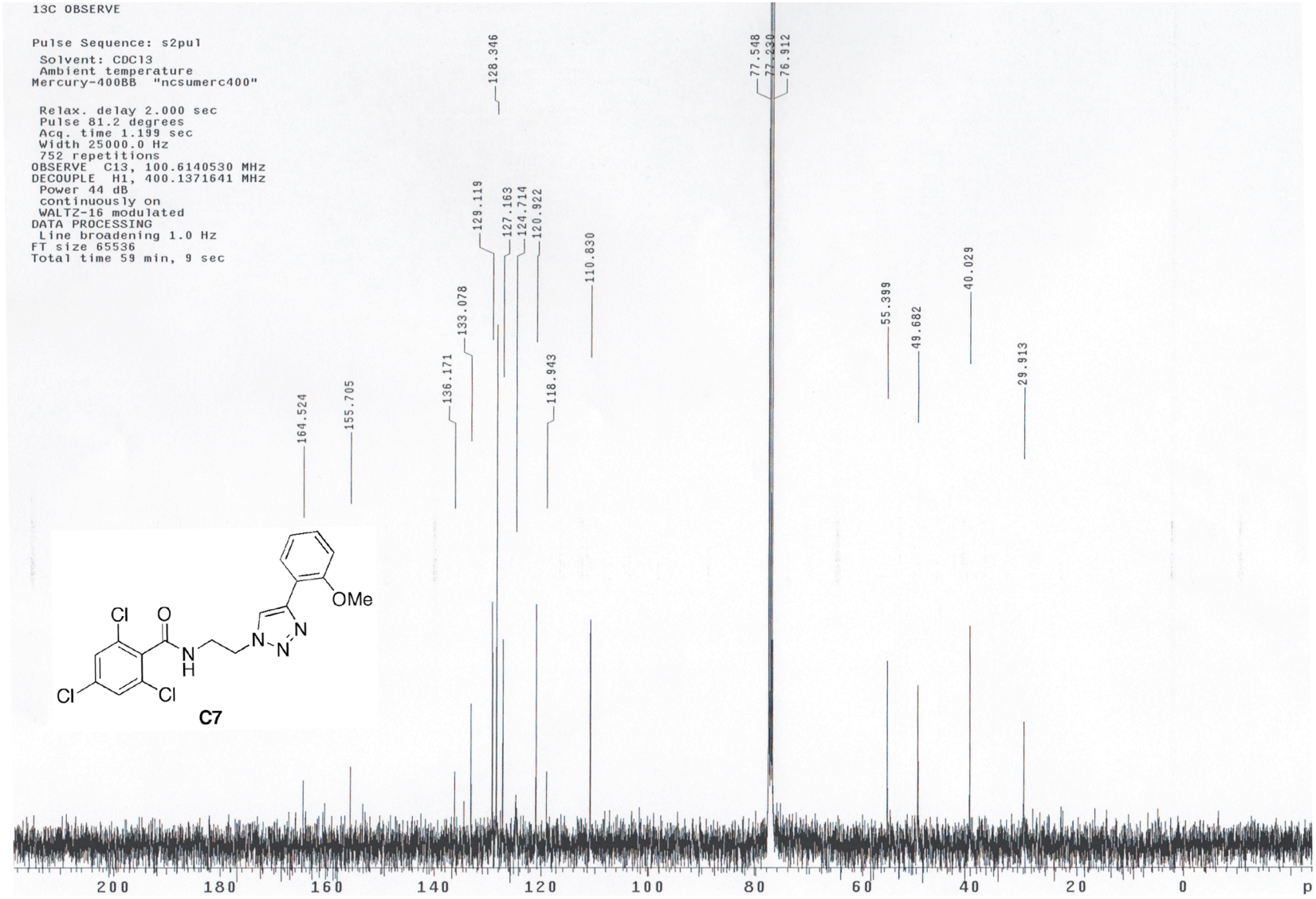
13C OBSERVE
Pulse Sequence: s2pul
Solvent: CDCl3
Ambient temperature
Mercury-400BB "ncsumerc400"
Relax. delay 2.000 sec
Pulse 81.2 degrees
Acq. time 1.199 sec
Width 25000.0 Hz
752 repetitions
OBSERVE C13, 100.6140530 MHz
DECOUPLE H1, 400.1371641 MHz
Power 44 dB
continuously on
WALTZ-16 modulated
DATA PROCESSING
Line broadening 1.0 Hz
FT size 65536
Total time 59 min, 9 sec
164.524
155.705
136.171
133.078
129.119
128.346
127.163
124.714
120.922
118.943
110.830
77.548
77.230
76.912
55.399
49.682
40.029
29.913
Cl
O
N
H
N
N
N
OMe
Cl
Cl
C7
200
180
160
140
120
100
80
60
40
20
0
p

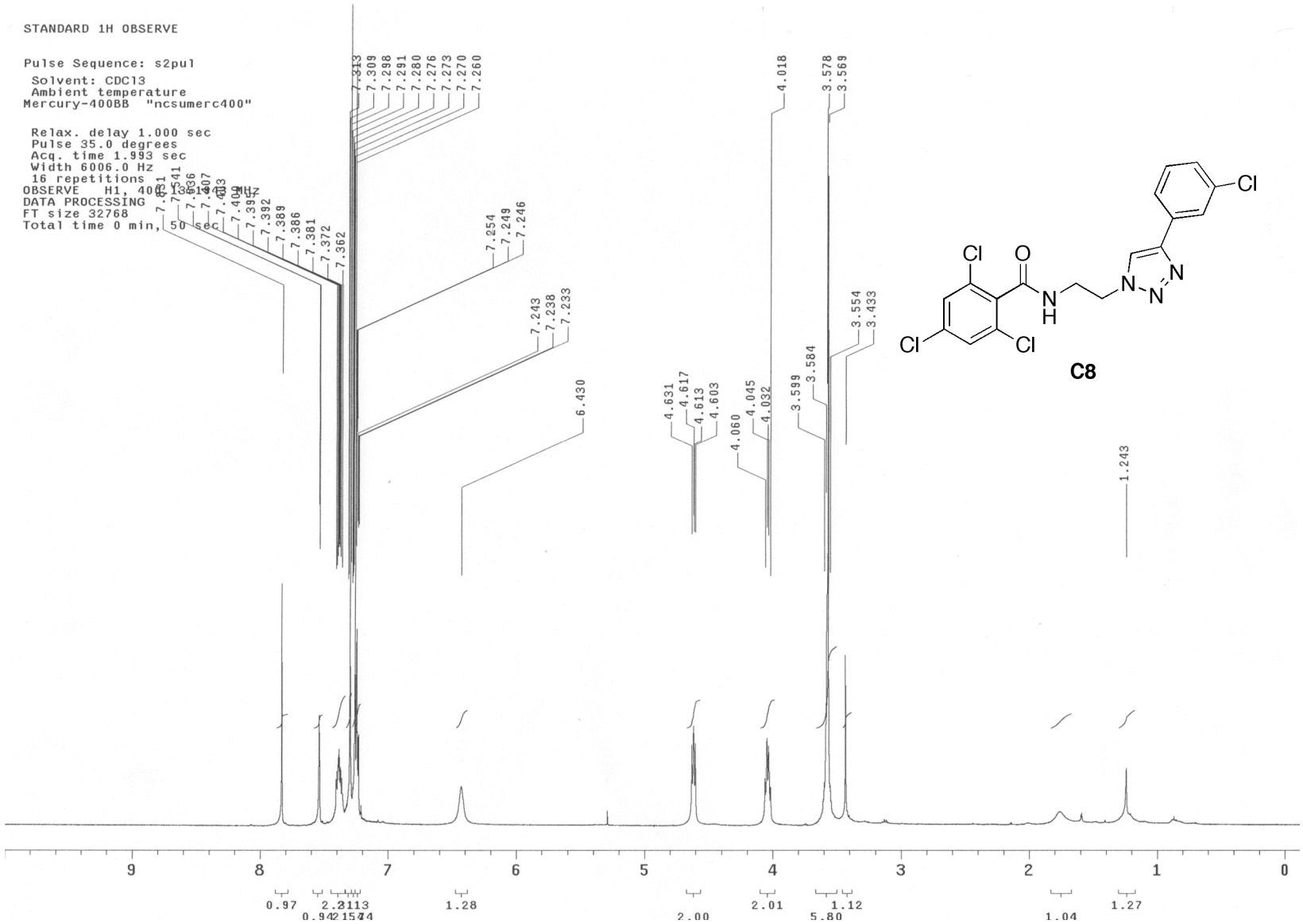
STANDARD 1H OBSERVE
Pulse Sequence: s2pul
Solvent: CDCl3
Ambient temperature
Mercury-400BB "ncsumerc400"
Relax. delay 1.000 sec
Pulse 35.0 degrees
Acq. time 1.993 sec
Width 6006.0 Hz
16 repetitions
OBSERVE H1, 400.1
DATA PROCESSING
FT size 32768
Total time 0 min, 50 sec
7.541
7.536
7.407
7.403
7.392
7.389
7.386
7.381
7.372
7.362
7.313
7.309
7.298
7.291
7.280
7.276
7.273
7.270
7.260
7.254
7.249
7.246
7.243
7.238
7.233
6.430
4.631
4.617
4.613
4.603
4.060
4.045
4.032
4.018
3.599
3.584
3.578
3.569
3.554
3.433
1.243
Cl
Cl
O
N
H
N
N
N
Cl
Cl
C8
9
8
7
6
5
4
3
2
1
0
0.97
2.21
1.28
2.00
2.01
1.12
5.80
1.04
1.27

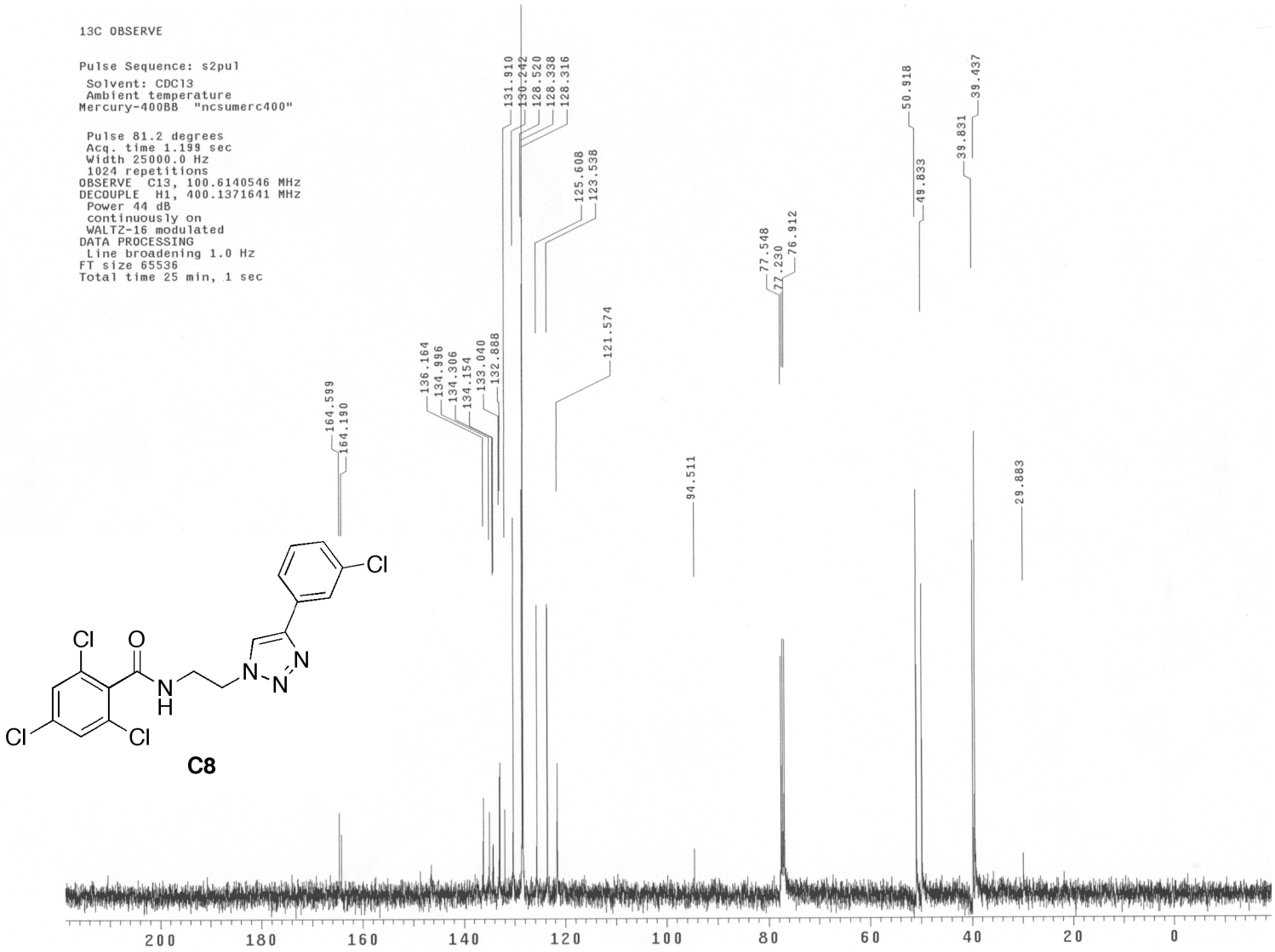
13C OBSERVE
Pulse Sequence: s2pul
Solvent: CDCl3
Ambient temperature
Mercury-400BB "ncsumerc400"
Pulse 81.2 degrees
Acq. time 1.199 sec
Width 25000.0 Hz
1024 repetitions
OBSERVE C13, 100.6140546 MHz
DECOUPLE H1, 400.1371641 MHz
Power 44 dB
continuously on
WALTZ-16 modulated
DATA PROCESSING
Line broadening 1.0 Hz
FT size 65536
Total time 25 min, 1 sec
164.599
164.190
136.164
134.996
134.306
134.154
133.040
132.888
131.910
130.242
128.520
128.338
128.316
125.608
123.538
121.574
94.511
77.548
77.230
76.912
50.918
49.833
39.831
39.437
29.883
200
180
160
140
120
100
80
60
40
20
0

C8

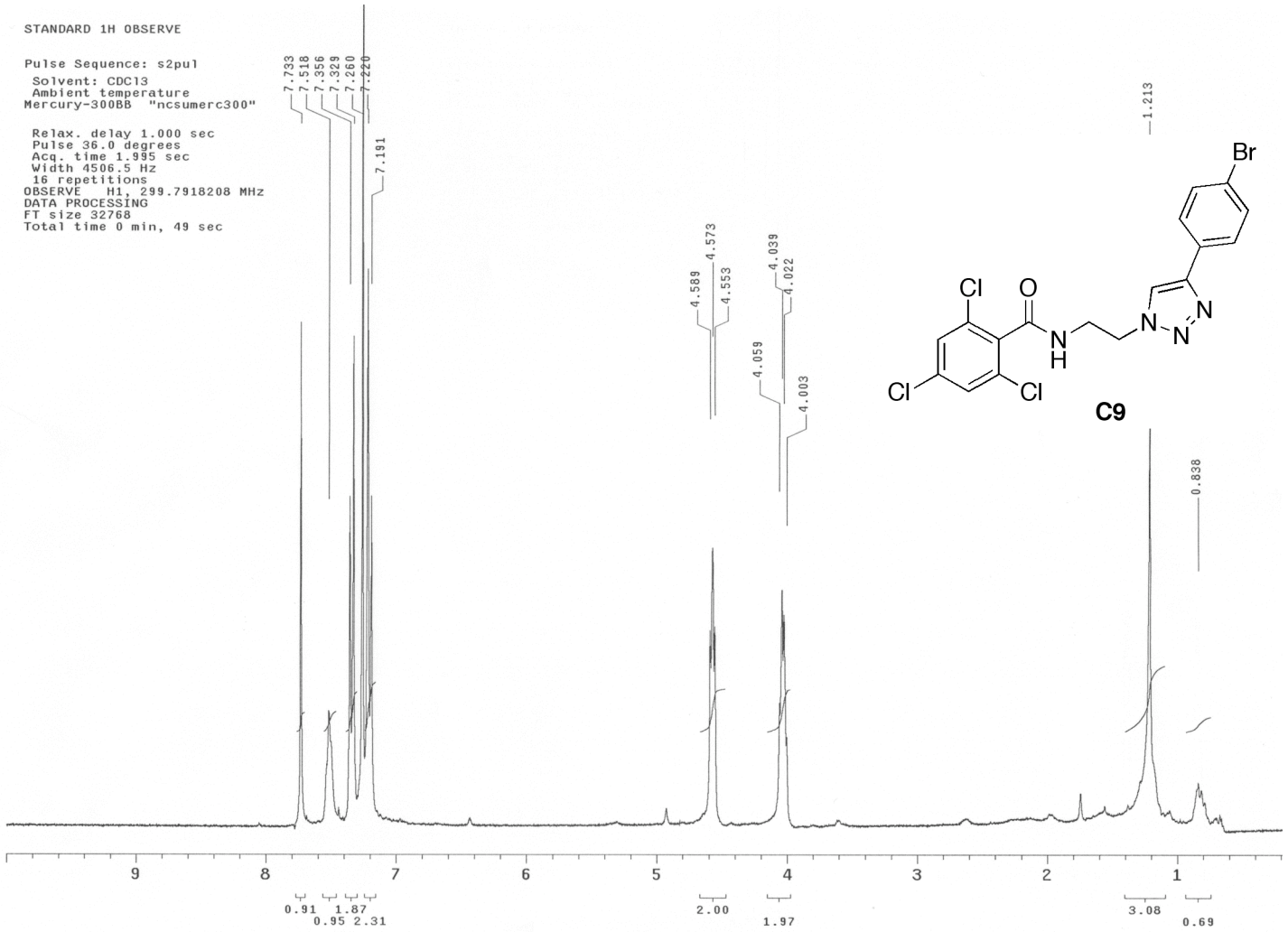
STANDARD 1H OBSERVE
Pulse Sequence: s2pul
Solvent: CDCl3
Ambient temperature
Mercury-300BB "ncsumerc300"
Relax. delay 1.000 sec
Pulse 36.0 degrees
Acq. time 1.995 sec
Width 4506.5 Hz
16 repetitions
OBSERVE H1, 299.7918208 MHz
DATA PROCESSING
FT size 32768
Total time 0 min, 49 sec
7.733
7.518
7.356
7.329
7.260
7.220
7.191
4.589
4.573
4.553
4.059
4.039
4.022
4.003
1.213
0.838
Br
Cl
O
N
H
N
N
N
Cl
Cl
C9
9
8
7
6
5
4
3
2
1
0.91
1.87
0.95
2.31
2.00
1.97
3.08
0.69

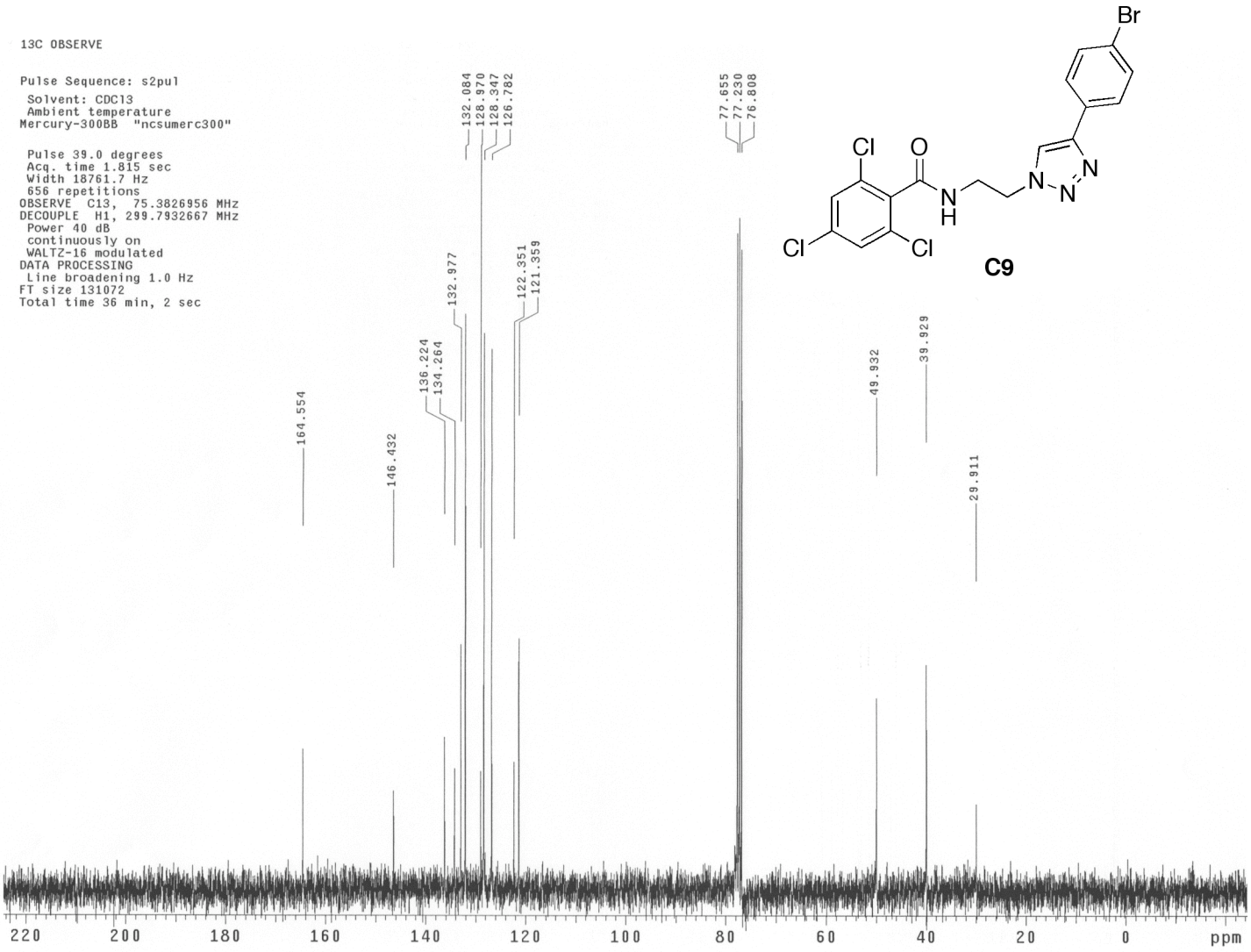
13C OBSERVE
Pulse Sequence: s2pul
Solvent: CDCl3
Ambient temperature
Mercury-300BB "ncsumerc300"
Pulse 39.0 degrees
Acq. time 1.815 sec
Width 18761.7 Hz
656 repetitions
OBSERVE C13, 75.3826956 MHz
DECOUPLE H1, 299.7932667 MHz
Power 40 dB
continuously on
WALTZ-16 modulated
DATA PROCESSING
Line broadening 1.0 Hz
FT size 131072
Total time 36 min, 2 sec
164.554
146.432
136.224
134.264
132.977
132.084
128.970
128.347
126.782
122.351
121.359
77.655
77.230
76.808
49.932
39.929
29.911
220
200
180
160
140
120
100
80
60
40
20
0
ppm
Br
Cl
O
N
H
N
N
N
Cl
Cl
C9

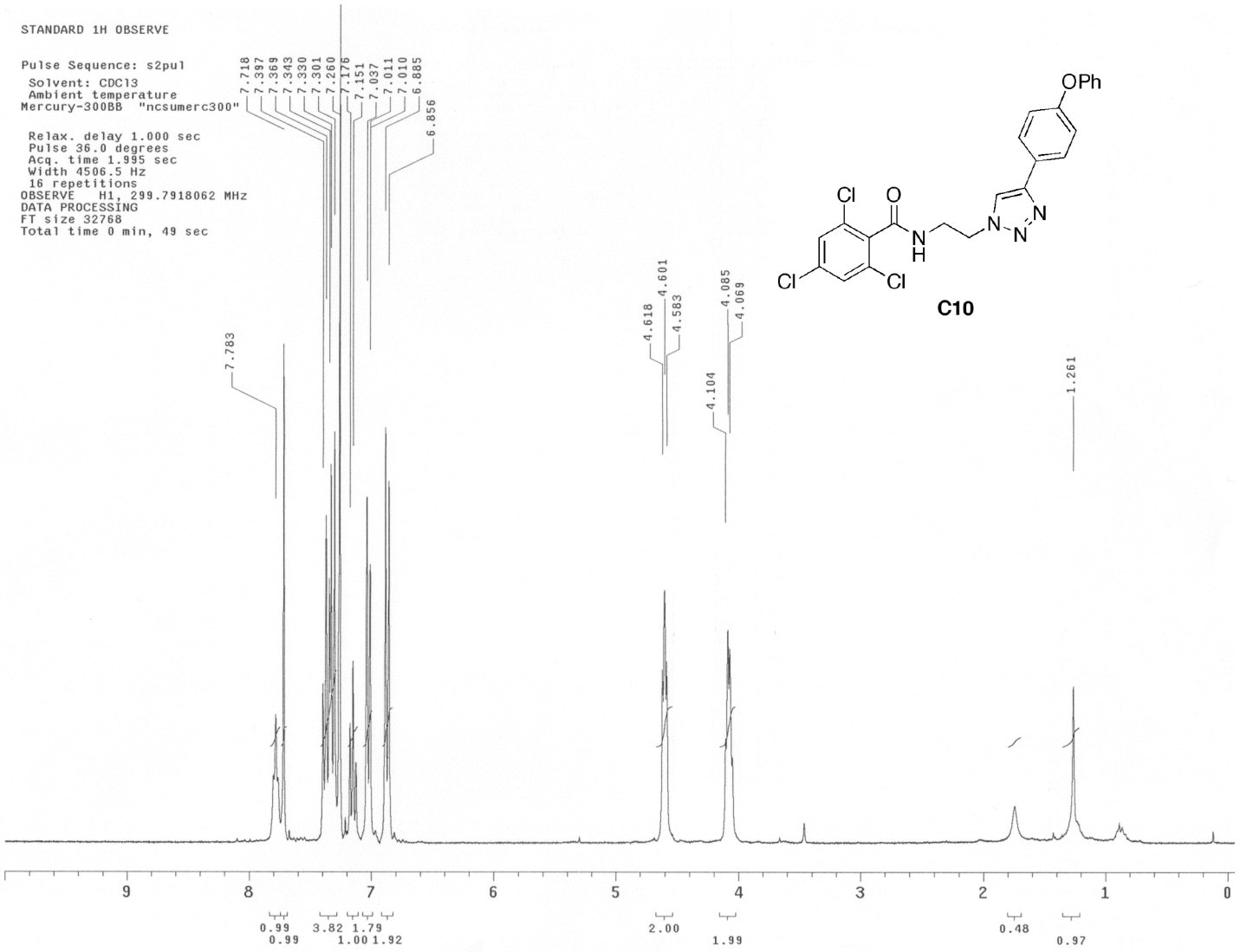
STANDARD 1H OBSERVE
Pulse Sequence: s2pul
Solvent: CDCl3
Ambient temperature
Mercury-300BB "ncsumerc300"
Relax. delay 1.000 sec
Pulse 36.0 degrees
Acq. time 1.995 sec
Width 4506.5 Hz
16 repetitions
OBSERVE H1, 299.7918062 MHz
DATA PROCESSING
FT size 32768
Total time 0 min, 49 sec
7.718
7.397
7.369
7.343
7.330
7.301
7.260
7.176
7.151
7.037
7.011
7.010
6.885
6.856
7.783
4.618
4.601
4.583
4.104
4.085
4.069
1.261
OPh
Cl
O
N
H
N
N
N
Cl
Cl
C10
9
8
7
6
5
4
3
2
1
0
0.99
0.99
3.82
1.00
1.79
1.92
2.00
1.99
0.48
0.97

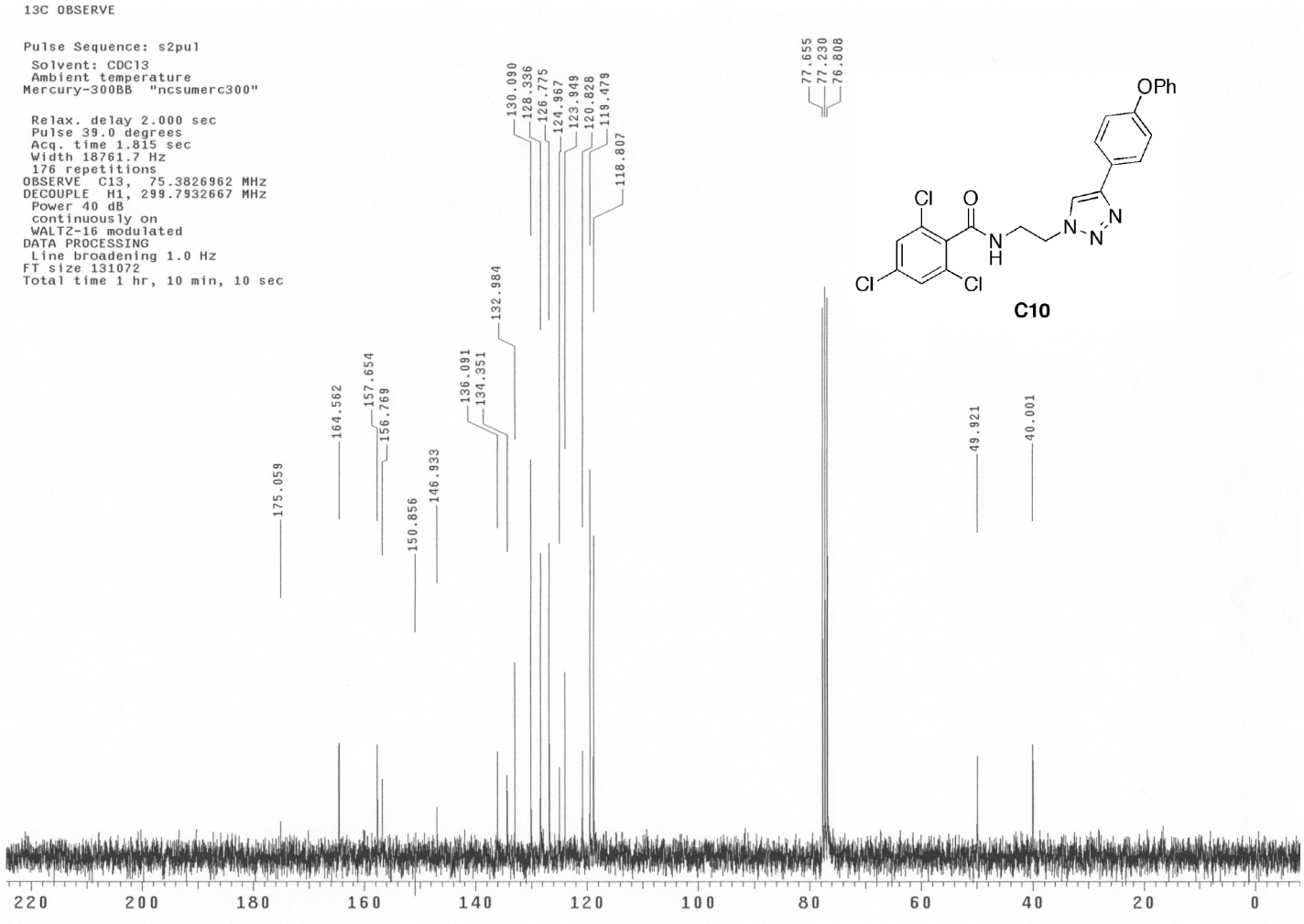
13C OBSERVE
Pulse Sequence: s2pul
Solvent: CDCl3
Ambient temperature
Mercury-300BB "ncsumerc300"
Relax. delay 2.000 sec
Pulse 39.0 degrees
Acq. time 1.815 sec
Width 18761.7 Hz
176 repetitions
OBSERVE C13, 75.3826962 MHz
DECOUPLE H1, 299.7932667 MHz
Power 40 dB
continuously on
WALTZ-16 modulated
DATA PROCESSING
Line broadening 1.0 Hz
FT size 131072
Total time 1 hr, 10 min, 10 sec
175.059
164.562
157.654
156.769
150.856
146.933
136.091
134.351
132.984
130.090
128.336
126.775
124.967
123.949
120.828
119.479
118.807
77.655
77.230
76.808
49.921
40.001
OPh
Cl
O
N
H
N
N
N
Cl
Cl
C10
220
200
180
160
140
120
100
80
60
40
20
0

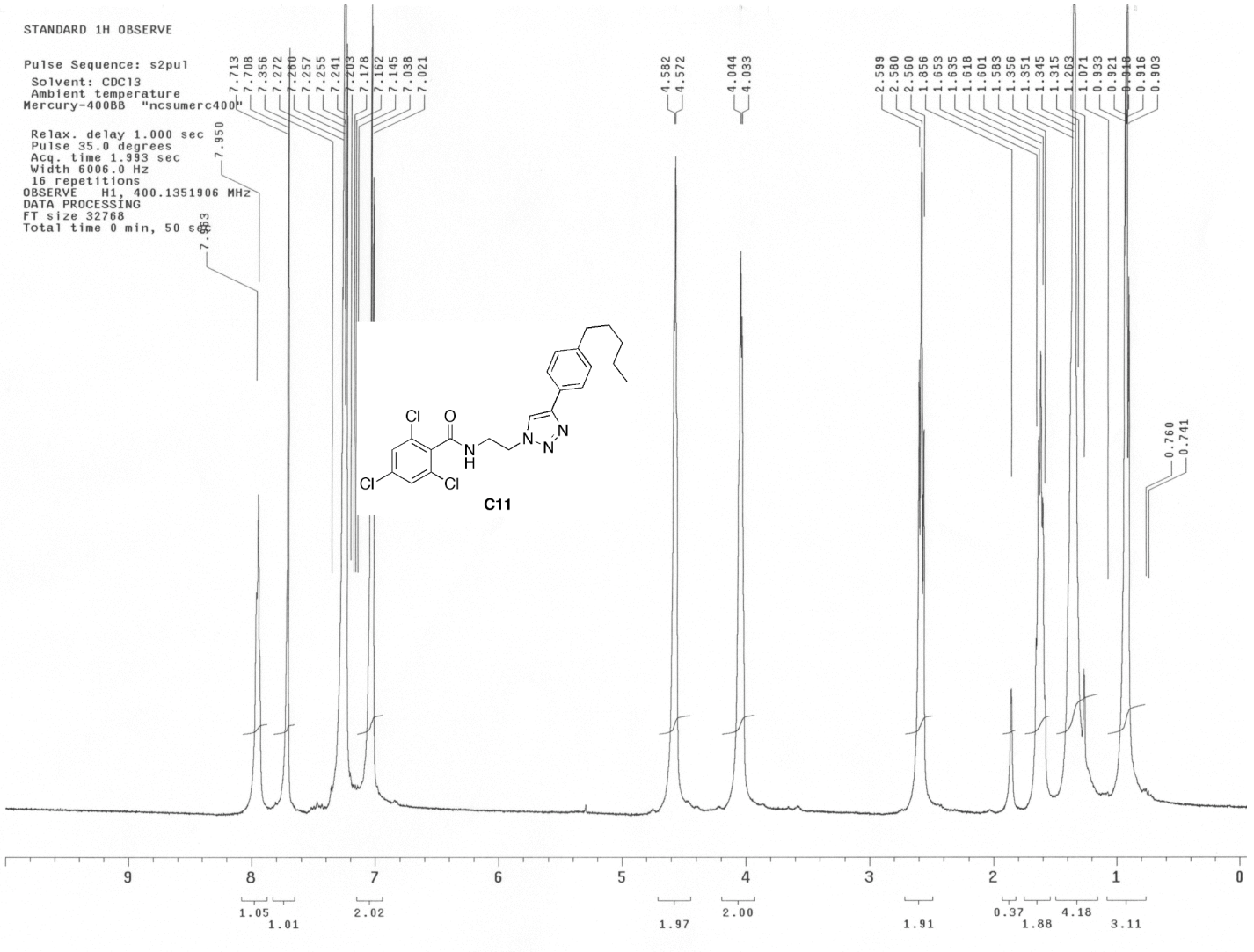
STANDARD 1H OBSERVE
Pulse Sequence: s2pul
Solvent: CDCl3
Ambient temperature
Mercury-400BB "ncsumerc400"
Relax. delay 1.000 sec
Pulse 35.0 degrees
Acq. time 1.993 sec
Width 6006.0 Hz
16 repetitions
OBSERVE H1, 400.1351906 MHz
DATA PROCESSING
FT size 32768
Total time 0 min, 50 sec
7.950
7.933
7.713
7.708
7.356
7.272
7.260
7.257
7.255
7.241
7.203
7.178
7.162
7.145
7.038
7.021
4.582
4.572
4.044
4.033
2.599
2.580
2.560
1.856
1.653
1.635
1.618
1.601
1.583
1.356
1.351
1.345
1.315
1.263
1.071
0.933
0.921
0.916
0.903
0.760
0.741
Cl
O
N
H
N
N
N
Cl
Cl
C11
9
8
7
6
5
4
3
2
1
0
1.05
1.01
2.02
1.97
2.00
1.91
0.37
1.88
4.18
3.11

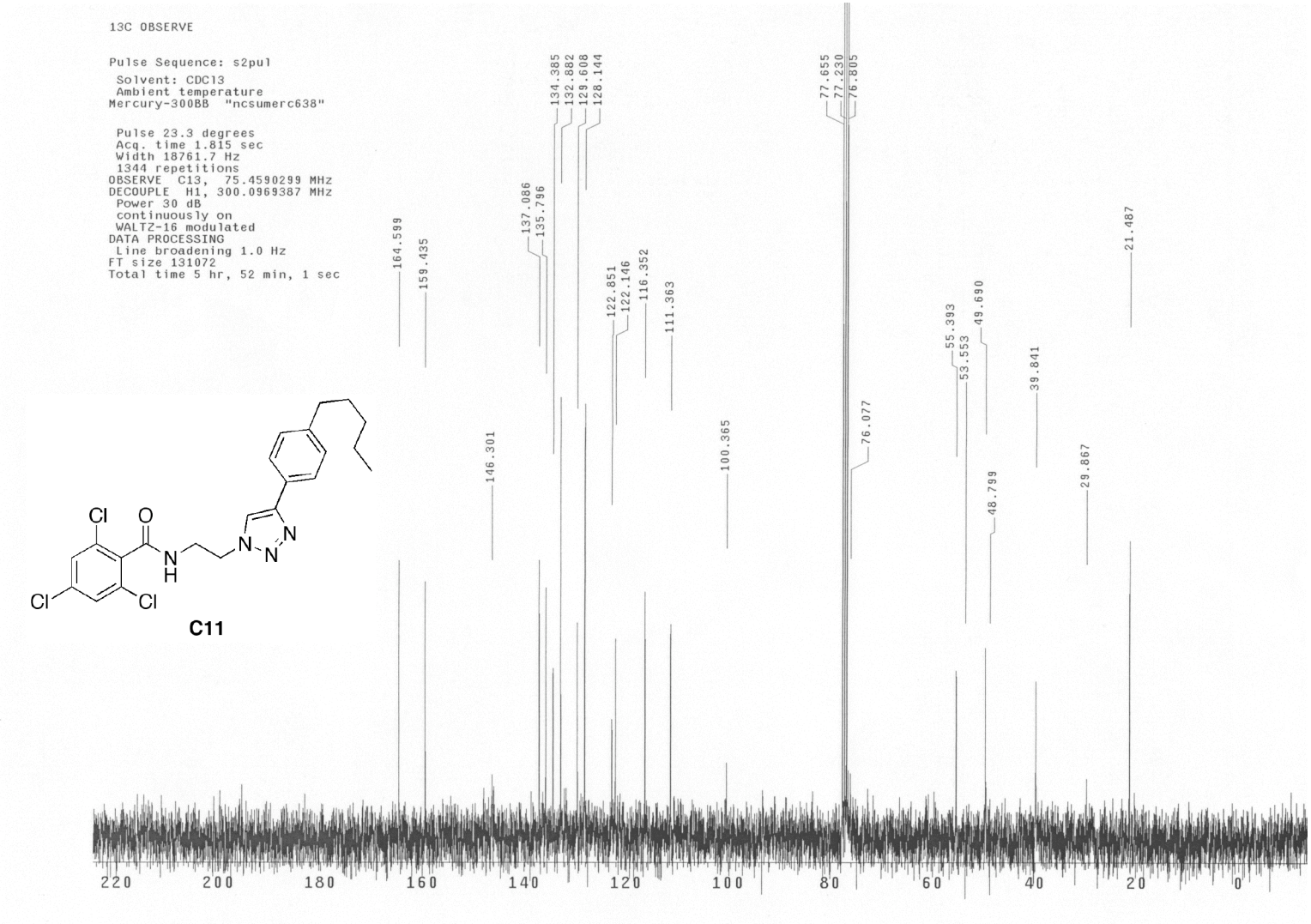
13C OBSERVE
Pulse Sequence: s2pul
Solvent: CDCl3
Ambient temperature
Mercury-300BB "ncsumerc638"
Pulse 23.3 degrees
Acq. time 1.815 sec
Width 18761.7 Hz
1344 repetitions
OBSERVE C13, 75.4590299 MHz
DECOUPLE H1, 300.0969387 MHz
Power 30 dB
continuously on
WALTZ-16 modulated
DATA PROCESSING
Line broadening 1.0 Hz
FT size 131072
Total time 5 hr, 52 min, 1 sec
164.599
159.435
146.301
137.086
135.796
134.385
132.882
129.608
128.144
122.851
122.146
116.352
111.363
100.365
77.655
77.230
76.805
76.077
55.393
53.553
49.690
48.799
39.841
29.867
21.487
Cl
O
N
H
N
N
N
Cl
Cl
C11
220
200
180
160
140
120
100
80
60
40
20
0

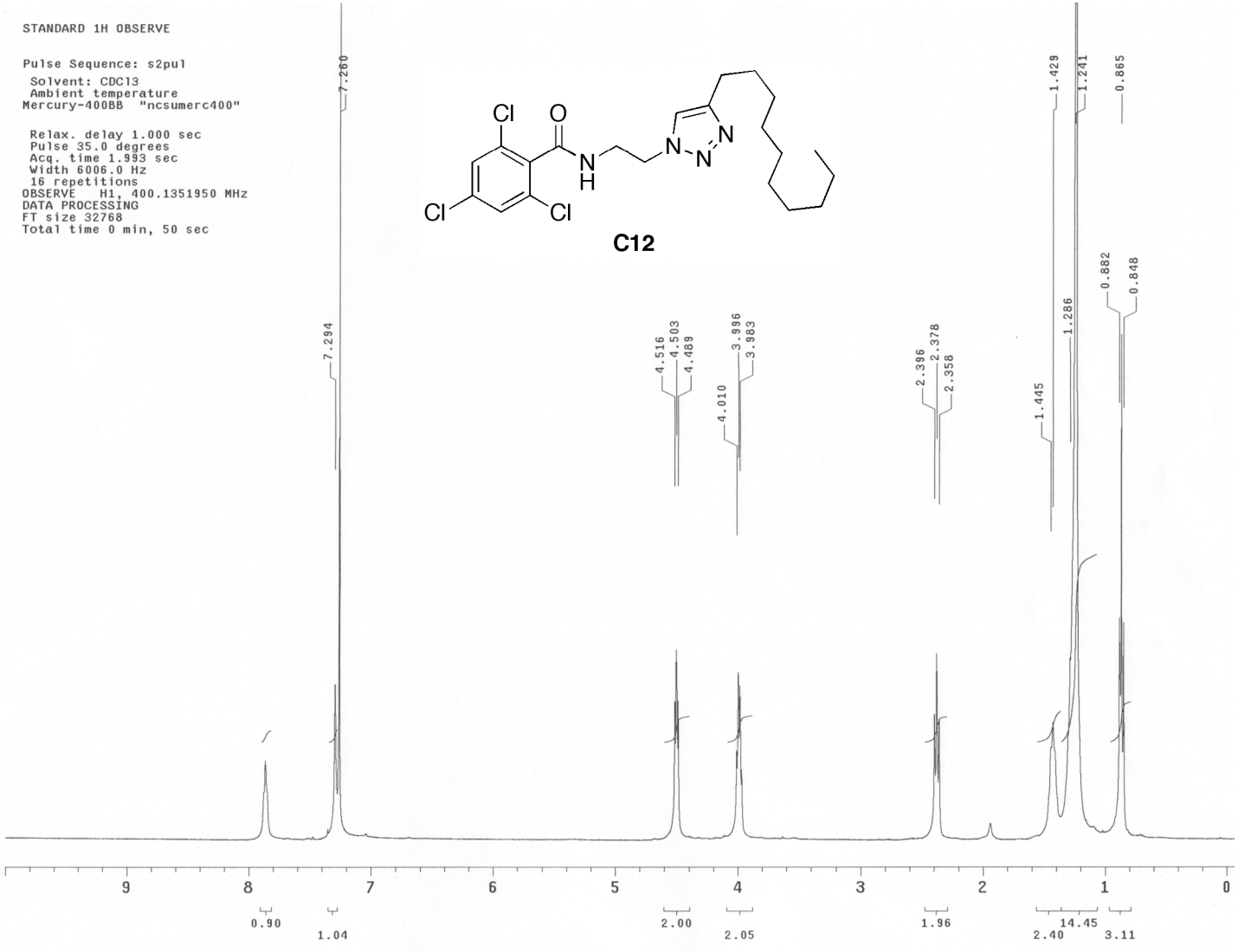
STANDARD 1H OBSERVE
Pulse Sequence: s2pul
Solvent: CDCl3
Ambient temperature
Mercury-400BB "ncsumerc400"
Relax. delay 1.000 sec
Pulse 35.0 degrees
Acq. time 1.993 sec
Width 6006.0 Hz
16 repetitions
OBSERVE H1, 400.1351950 MHz
DATA PROCESSING
FT size 32768
Total time 0 min, 50 sec
Cl
O
N
H
N
N
N
Cl
Cl
C12
7.260
7.294
4.516
4.503
4.489
4.010
3.996
3.983
2.396
2.378
2.358
1.445
1.429
1.286
1.241
0.882
0.865
0.848
9
8
7
6
5
4
3
2
1
0
0.90
1.04
2.00
2.05
1.96
2.40
14.45
3.11

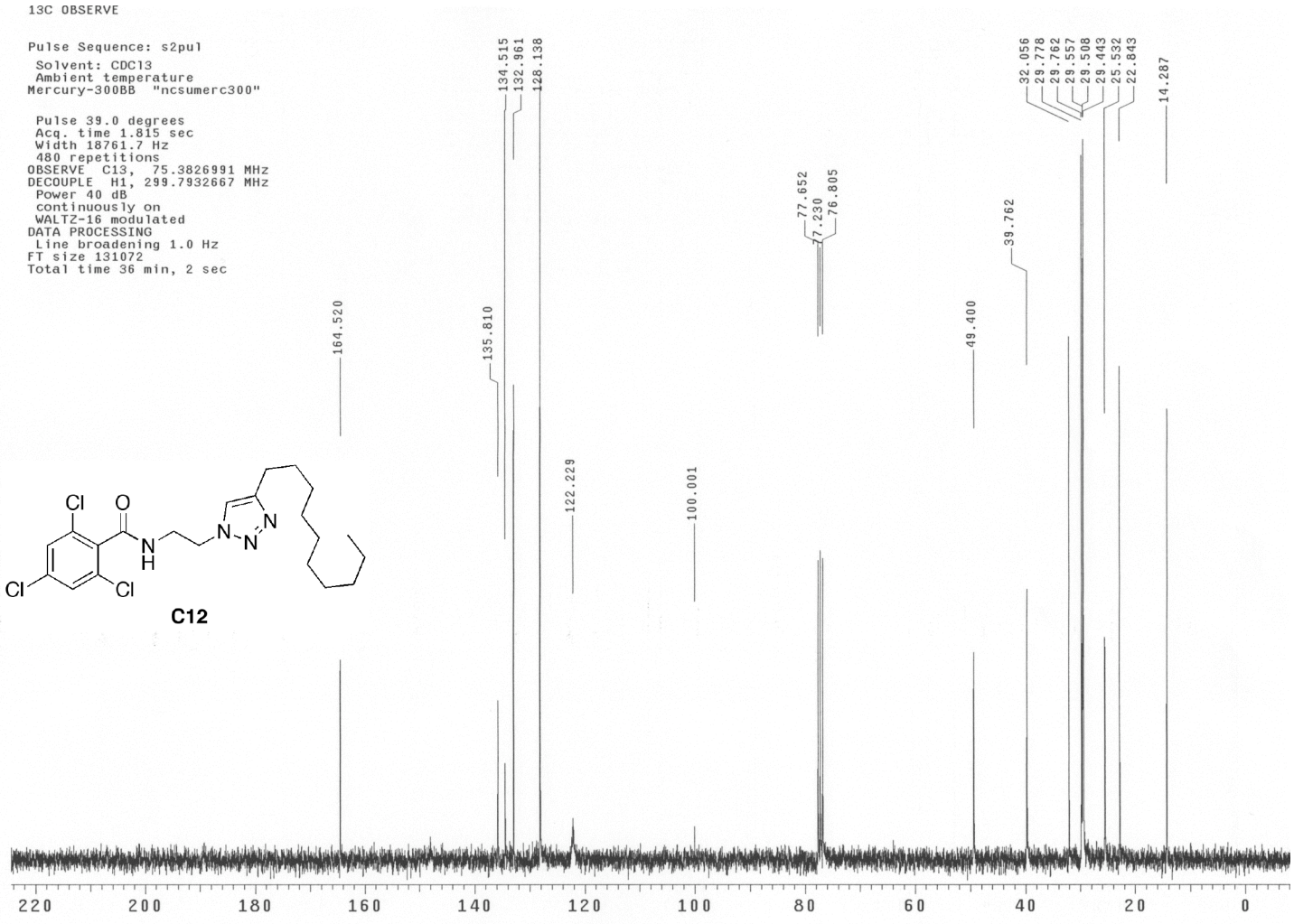
13C OBSERVE
Pulse Sequence: s2pul
Solvent: CDCl3
Ambient temperature
Mercury-300BB "ncsumerc300"
Pulse 39.0 degrees
Acq. time 1.815 sec
Width 18761.7 Hz
480 repetitions
OBSERVE C13, 75.3826991 MHz
DECOUPLE H1, 299.7932667 MHz
Power 40 dB
continuously on
WALTZ-16 modulated
DATA PROCESSING
Line broadening 1.0 Hz
FT size 131072
Total time 36 min, 2 sec
164.520
135.810
134.515
132.961
128.138
122.229
100.001
77.652
77.230
76.805
49.400
39.762
32.056
29.778
29.762
29.557
29.508
29.443
25.532
22.843
14.287
Cl
O
N
H
N
N
N
Cl
Cl
C12
220
200
180
160
140
120
100
80
60
40
20
0

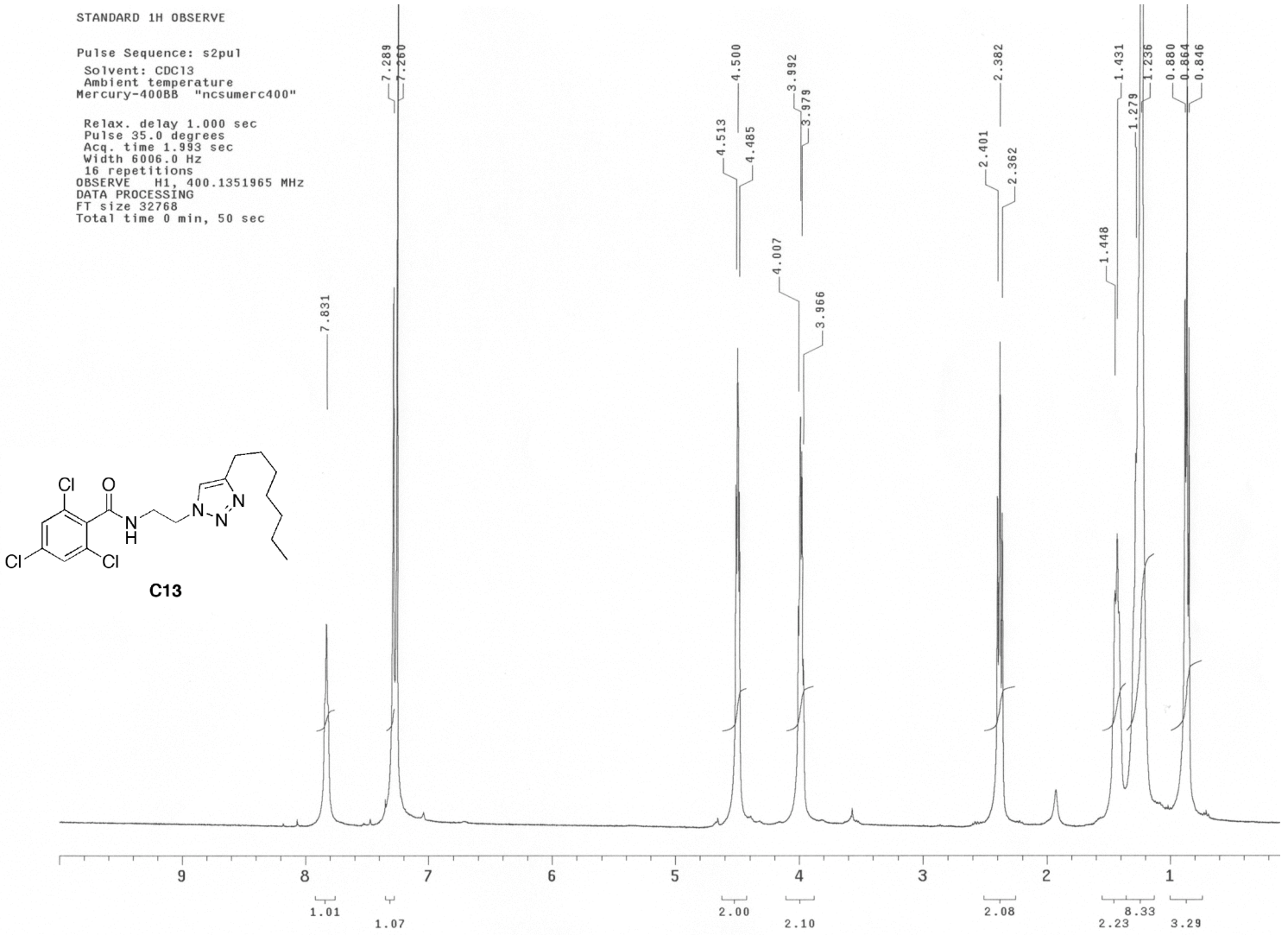
STANDARD 1H OBSERVE
Pulse Sequence: s2pul
Solvent: CDCl3
Ambient temperature
Mercury-400BB "ncsumerc400"
Relax. delay 1.000 sec
Pulse 35.0 degrees
Acq. time 1.993 sec
Width 6006.0 Hz
16 repetitions
OBSERVE H1, 400.1351965 MHz
DATA PROCESSING
FT size 32768
Total time 0 min, 50 sec
7.831
7.289
7.260
4.513
4.500
4.485
4.007
3.992
3.979
3.966
2.401
2.382
2.362
1.448
1.431
1.279
1.236
0.880
0.864
0.846
Cl
O
N
H
N
N
N
Cl
Cl
C13
9
8
7
6
5
4
3
2
1
1.01
1.07
2.00
2.10
2.08
2.23
8.33
3.29

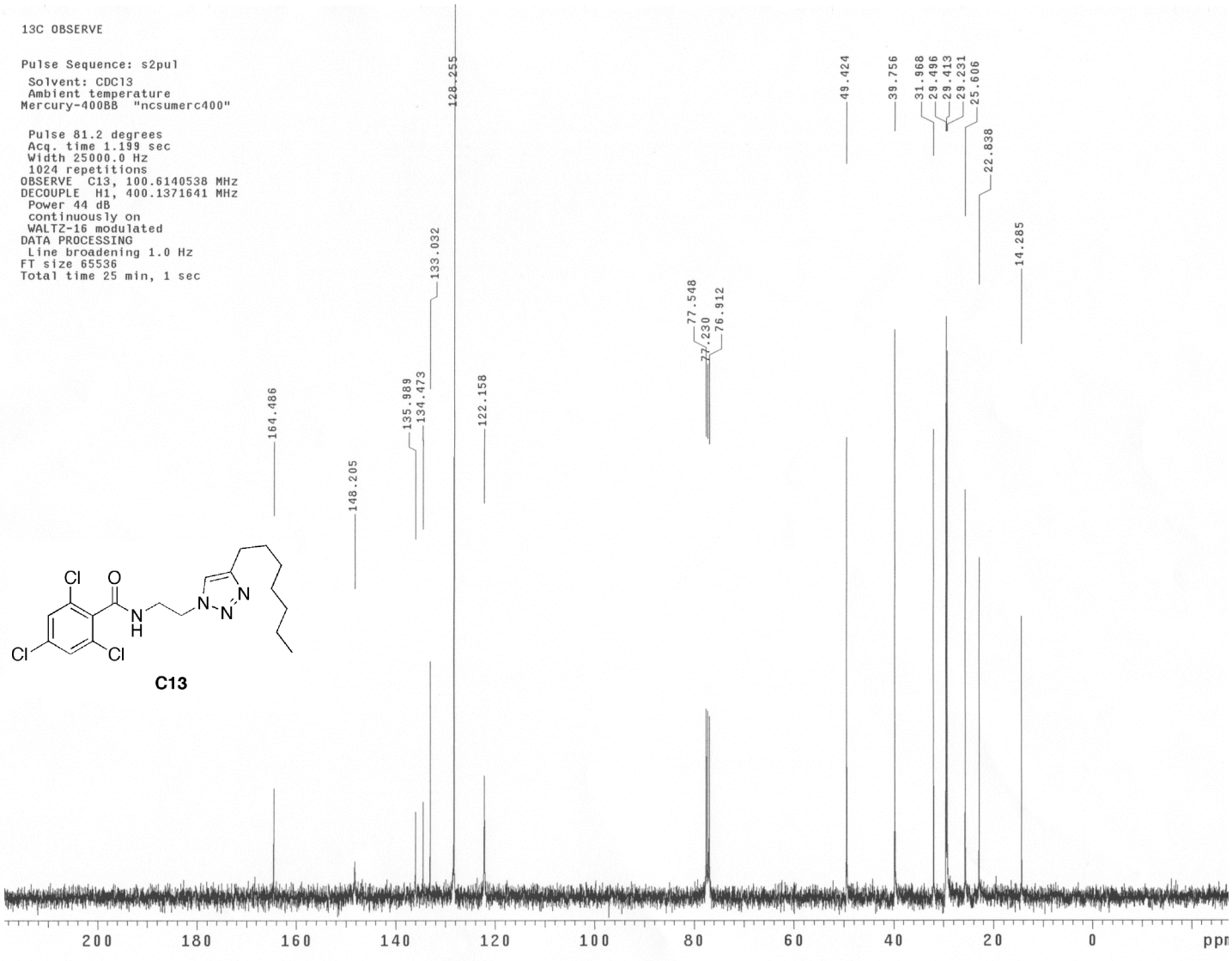
13C OBSERVE
Pulse Sequence: s2pul
Solvent: CDCl3
Ambient temperature
Mercury-400BB "ncsumerc400"
Pulse 81.2 degrees
Acq. time 1.199 sec
Width 25000.0 Hz
1024 repetitions
OBSERVE C13, 100.6140538 MHz
DECOUPLE H1, 400.1371641 MHz
Power 44 dB
continuously on
WALTZ-16 modulated
DATA PROCESSING
Line broadening 1.0 Hz
FT size 65536
Total time 25 min, 1 sec
164.486
148.205
135.989
134.473
133.032
128.255
122.158
77.548
77.230
76.912
49.424
39.756
31.968
29.496
29.413
29.231
25.606
22.838
14.285
Cl
O
N
H
N
N
N
Cl
Cl
C13
200
180
160
140
120
100
80
60
40
20
0
ppm

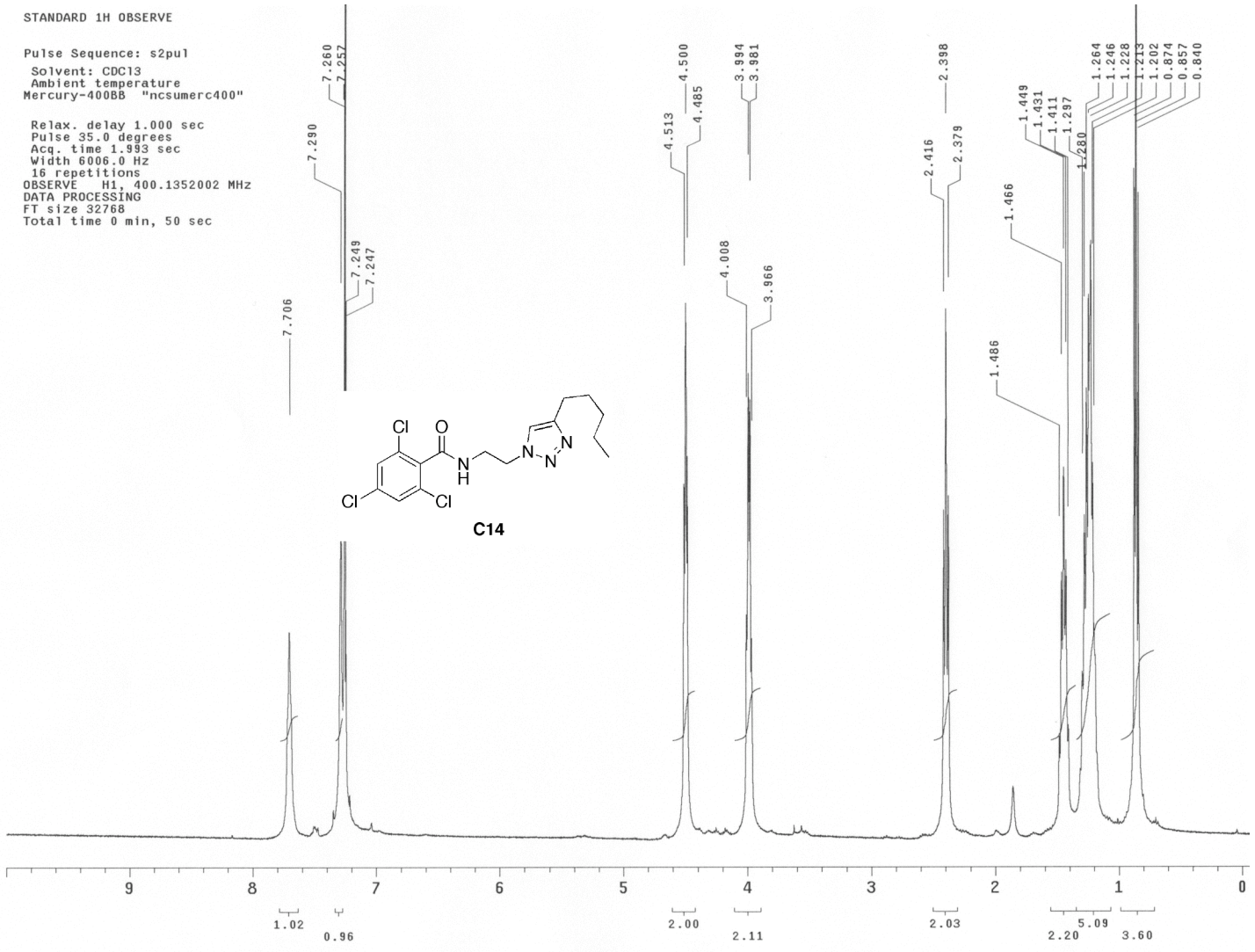
STANDARD 1H OBSERVE
Pulse Sequence: s2pul
Solvent: CDCl3
Ambient temperature
Mercury-400BB "ncsumerc400"
Relax. delay 1.000 sec
Pulse 35.0 degrees
Acq. time 1.993 sec
Width 6006.0 Hz
16 repetitions
OBSERVE H1, 400.1352002 MHz
DATA PROCESSING
FT size 32768
Total time 0 min, 50 sec
7.706
7.290
7.260
7.252
7.249
7.247
4.513
4.500
4.485
4.008
3.994
3.981
3.966
2.416
2.398
2.379
1.486
1.466
1.449
1.431
1.411
1.297
1.280
1.264
1.246
1.228
1.213
1.202
0.874
0.857
0.840
Cl
O
N
H
N
N
N
Cl
Cl
C14
9
8
7
6
5
4
3
2
1
0
1.02
0.96
2.00
2.11
2.03
2.20
5.09
3.60

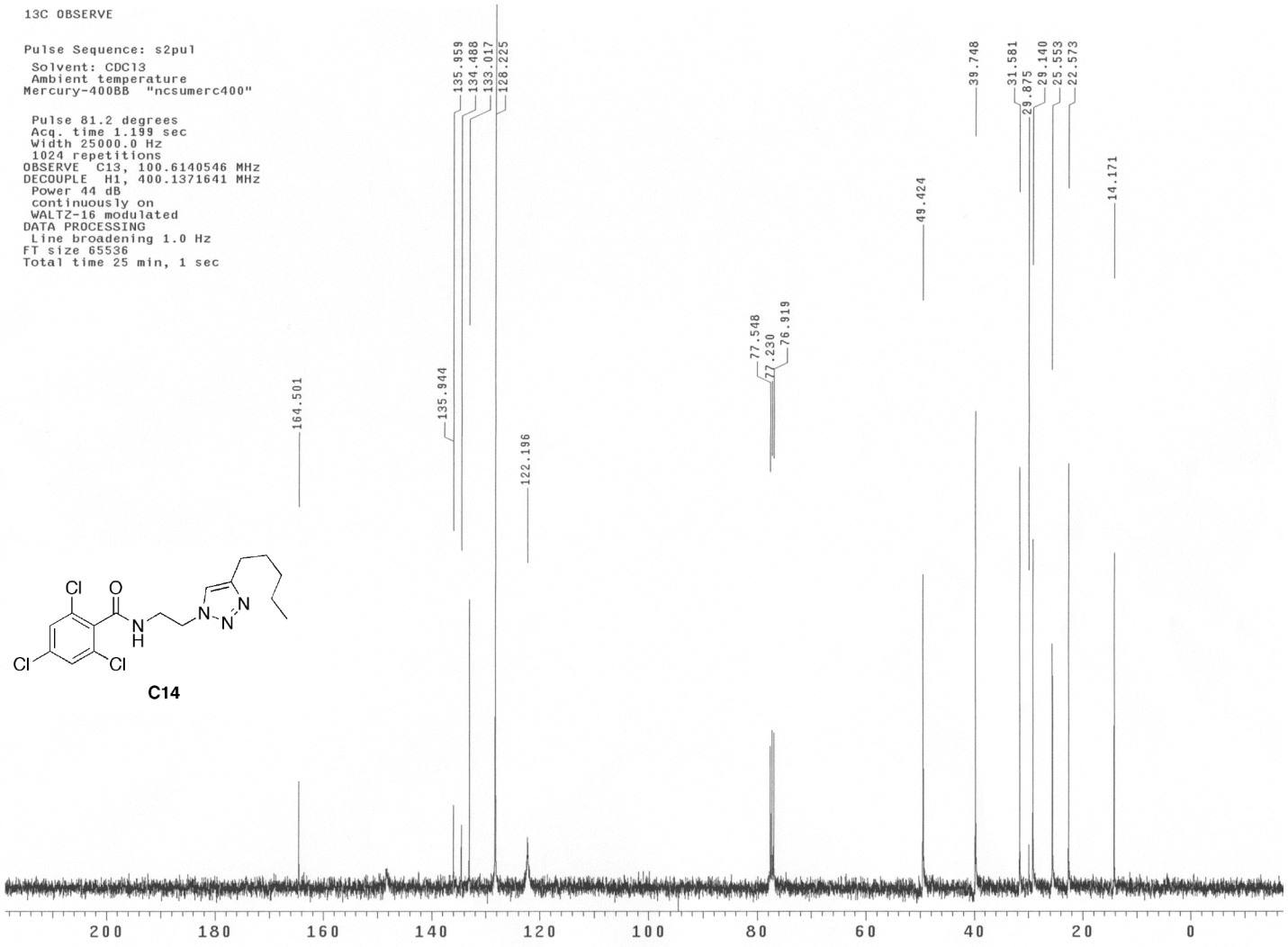
13C OBSERVE
Pulse Sequence: s2pul
Solvent: CDCl3
Ambient temperature
Mercury-400BB "ncsumerc400"
Pulse 81.2 degrees
Acq. time 1.199 sec
Width 25000.0 Hz
1024 repetitions
OBSERVE C13, 100.6140546 MHz
DECOUPLE H1, 400.1371641 MHz
Power 44 dB
continuously on
WALTZ-16 modulated
DATA PROCESSING
Line broadening 1.0 Hz
FT size 65536
Total time 25 min, 1 sec
164.501
135.944
135.959
134.488
133.017
128.225
122.196
77.548
77.230
76.919
49.424
39.748
31.581
29.875
29.140
25.553
22.573
14.171
Cl
O
N
H
N
N
N
Cl
Cl
C14
200
180
160
140
120
100
80
60
40
20
0

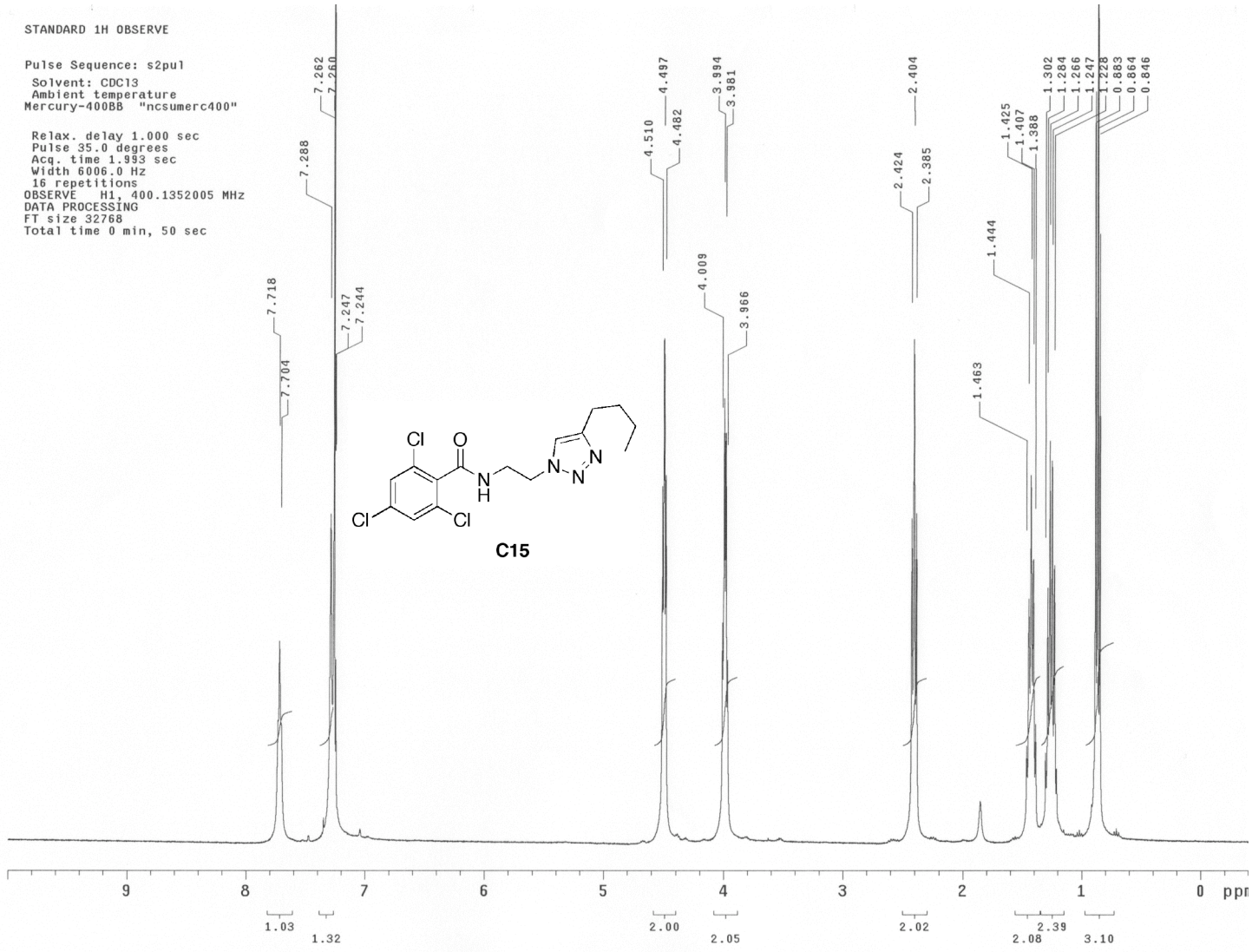
STANDARD 1H OBSERVE
Pulse Sequence: s2pul
Solvent: CDCl3
Ambient temperature
Mercury-400BB "ncsumerc400"
Relax. delay 1.000 sec
Pulse 35.0 degrees
Acq. time 1.993 sec
Width 6006.0 Hz
16 repetitions
OBSERVE H1, 400.1352005 MHz
DATA PROCESSING
FT size 32768
Total time 0 min, 50 sec
7.718
7.704
7.288
7.262
7.260
7.247
7.244
4.510
4.497
4.482
4.009
3.994
3.981
3.966
2.424
2.404
2.385
1.463
1.444
1.425
1.407
1.388
1.302
1.284
1.266
1.247
1.228
0.883
0.864
0.846
Cl
O
N
H
N
N
N
Cl
Cl
C15
9
8
7
6
5
4
3
2
1
0 ppm
1.03
1.32
2.00
2.05
2.02
2.08
2.39
3.10

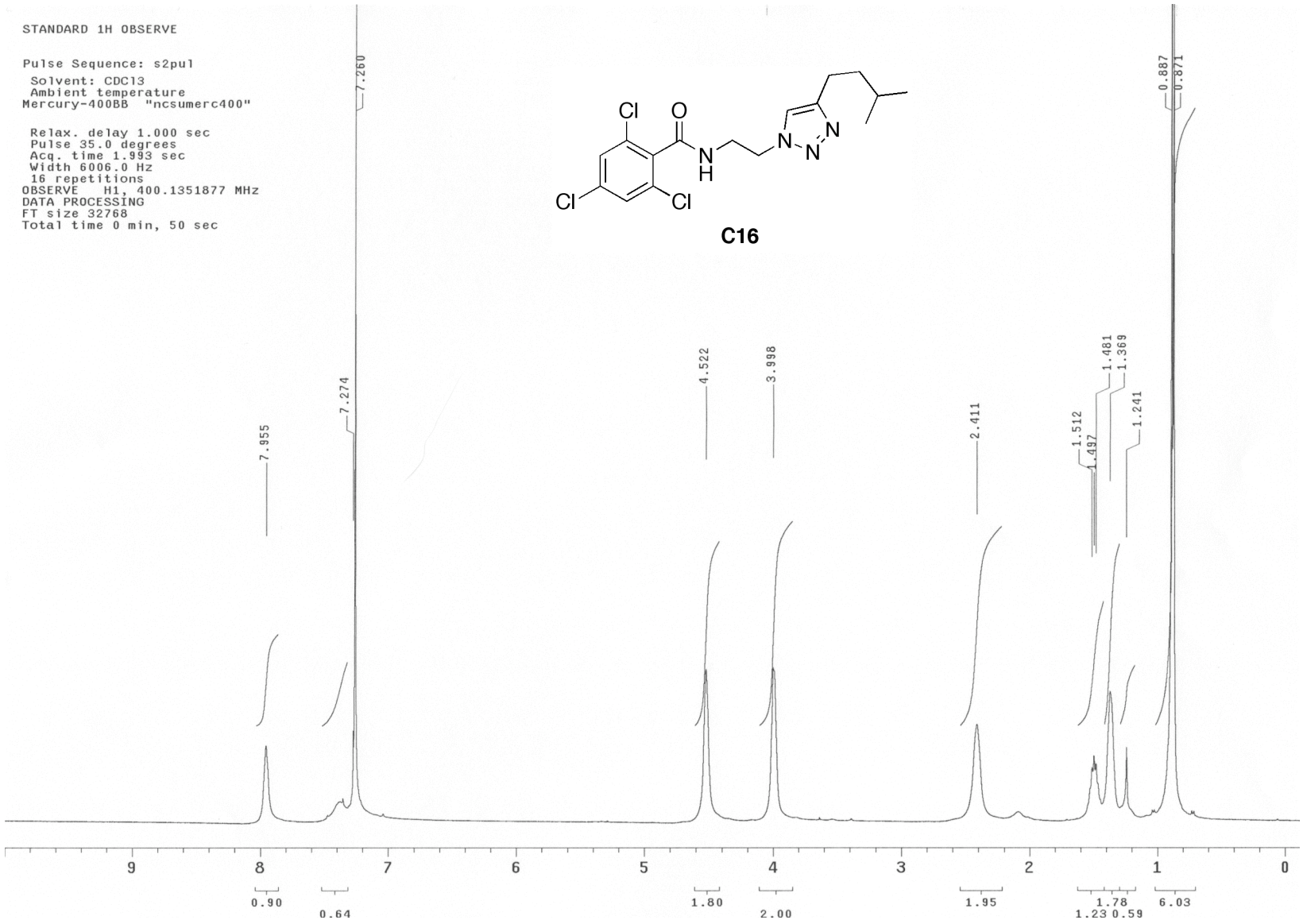
STANDARD 1H OBSERVE
Pulse Sequence: s2pul
Solvent: CDCl3
Ambient temperature
Mercury-400BB "ncsumerc400"
Relax. delay 1.000 sec
Pulse 35.0 degrees
Acq. time 1.993 sec
Width 6006.0 Hz
16 repetitions
OBSERVE H1, 400.1351877 MHz
DATA PROCESSING
FT size 32768
Total time 0 min, 50 sec
Cl
O
N
H
N
N
N
Cl
Cl
C16
7.955
7.274
7.260
4.522
3.998
2.411
1.512
1.497
1.481
1.369
1.241
0.887
0.871
9
8
7
6
5
4
3
2
1
0
0.90
0.64
1.80
2.00
1.95
1.23
0.59
1.78
6.03

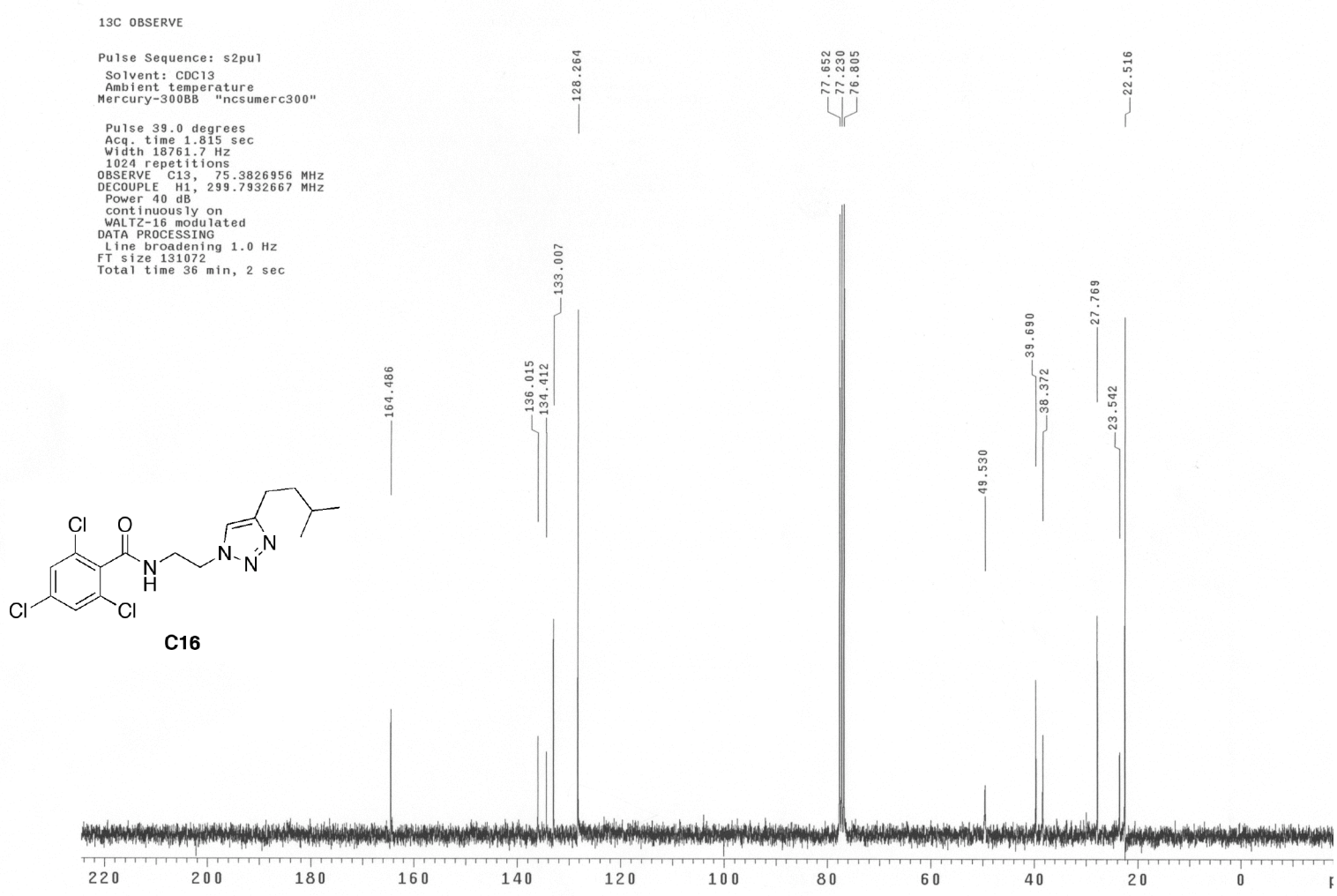
13C OBSERVE
Pulse Sequence: s2pul
Solvent: CDCl3
Ambient temperature
Mercury-300BB "ncsumerc300"
Pulse 39.0 degrees
Acq. time 1.815 sec
Width 18761.7 Hz
1024 repetitions
OBSERVE C13, 75.3826956 MHz
DECOUPLE H1, 299.7932667 MHz
Power 40 dB
continuously on
WALTZ-16 modulated
DATA PROCESSING
Line broadening 1.0 Hz
FT size 131072
Total time 36 min, 2 sec
164.486
136.015
134.412
133.007
128.264
77.652
77.230
76.805
49.530
39.690
38.372
27.769
23.542
22.516
220
200
180
160
140
120
100
80
60
40
20
0

C16

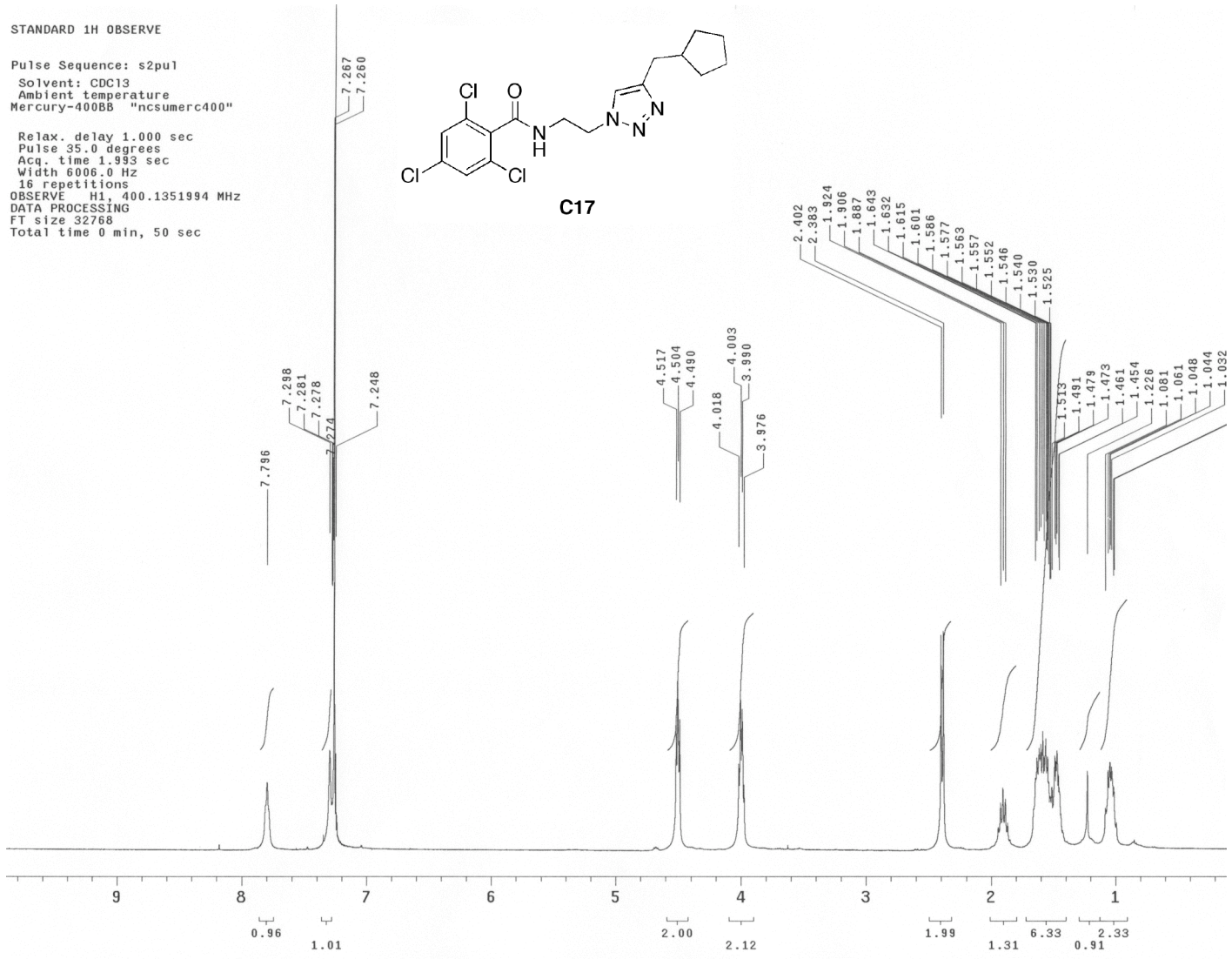
STANDARD 1H OBSERVE
Pulse Sequence: s2pul
Solvent: CDCl3
Ambient temperature
Mercury-400BB "ncsumerc400"
Relax. delay 1.000 sec
Pulse 35.0 degrees
Acq. time 1.993 sec
Width 6006.0 Hz
16 repetitions
OBSERVE H1, 400.1351994 MHz
DATA PROCESSING
FT size 32768
Total time 0 min, 50 sec
C17
7.796
7.298
7.281
7.278
7.274
7.267
7.260
7.248
4.517
4.504
4.490
4.018
4.003
3.990
3.976
2.402
2.383
1.924
1.906
1.887
1.643
1.632
1.615
1.601
1.586
1.577
1.563
1.557
1.552
1.546
1.540
1.530
1.525
1.513
1.491
1.479
1.473
1.461
1.454
1.226
1.081
1.061
1.048
1.044
1.032
0.96
1.01
2.00
2.12
1.99
1.31
6.33
0.91
2.33

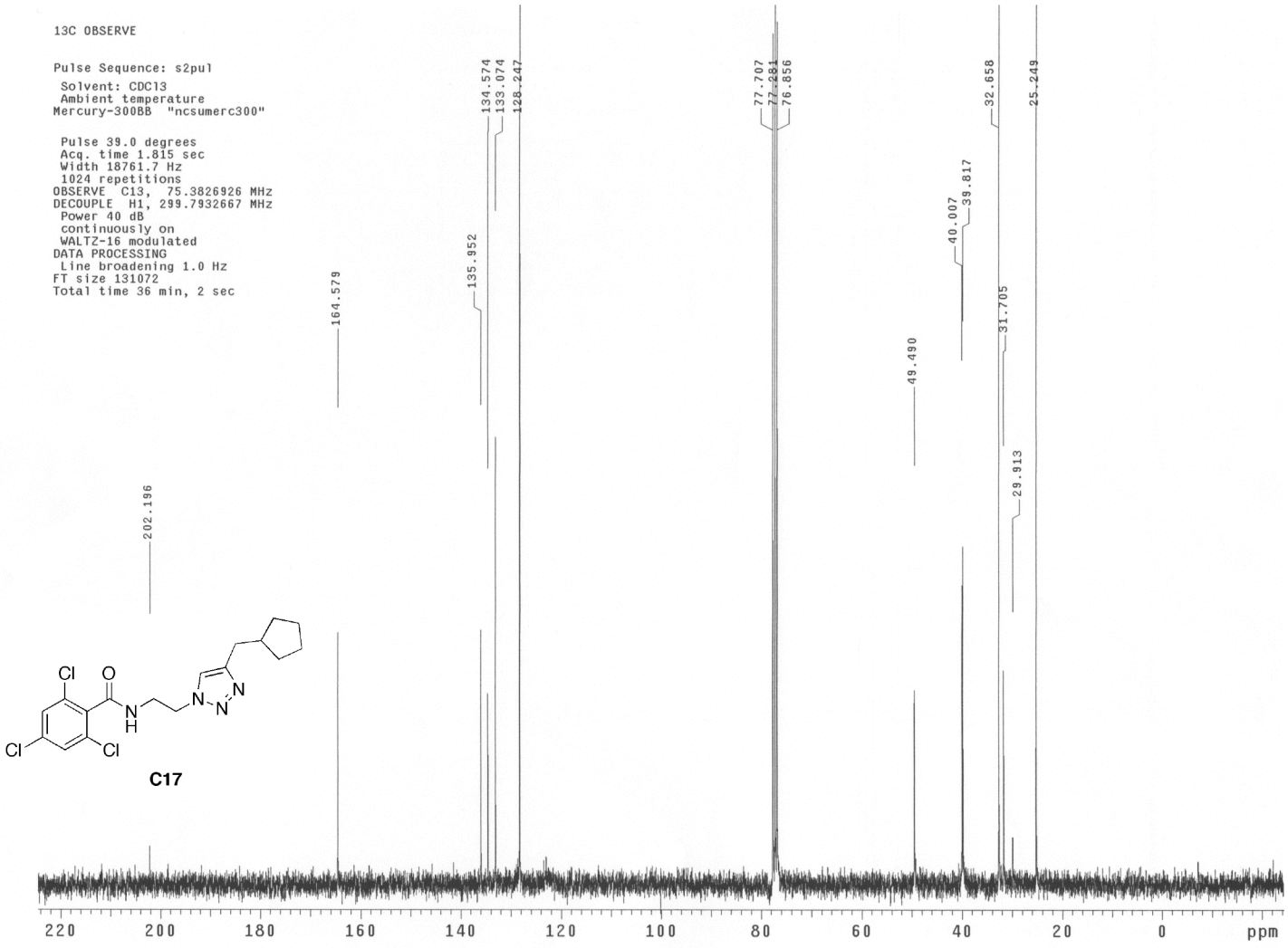
13C OBSERVE
Pulse Sequence: s2pul
Solvent: CDCl3
Ambient temperature
Mercury-300BB "ncsumerc300"
Pulse 39.0 degrees
Acq. time 1.815 sec
Width 18761.7 Hz
1024 repetitions
OBSERVE C13, 75.3826926 MHz
DECOUPLE H1, 299.7932667 MHz
Power 40 dB
continuously on
WALTZ-16 modulated
DATA PROCESSING
Line broadening 1.0 Hz
FT size 131072
Total time 36 min, 2 sec
202.196
164.579
135.952
134.574
133.074
128.247
77.707
77.281
76.856
49.490
40.007
39.817
32.658
31.705
29.913
25.249
220
200
180
160
140
120
100
80
60
40
20
0
ppm
Cl
O
N
H
N
N
N
Cl
Cl
C17

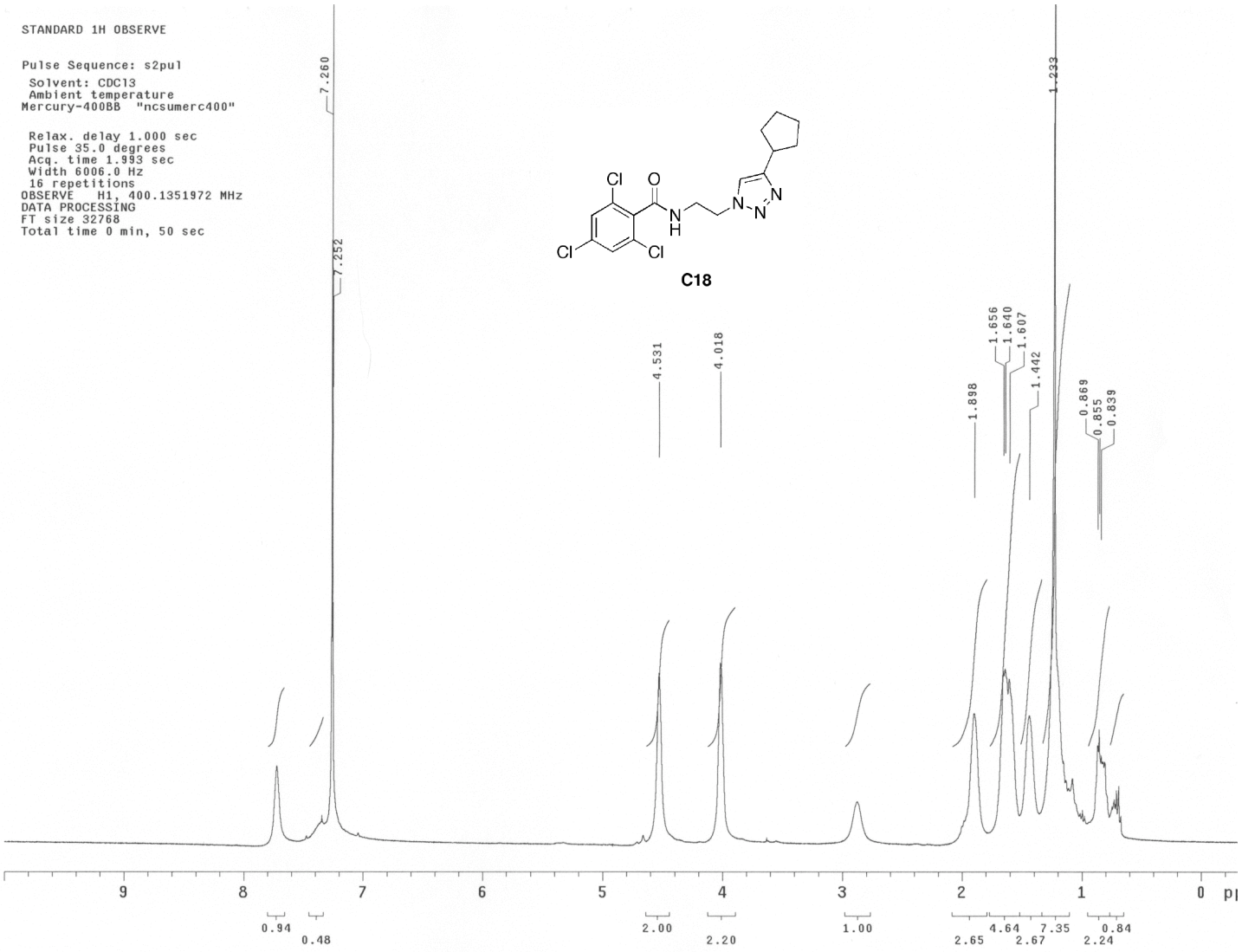
STANDARD 1H OBSERVE
Pulse Sequence: s2pul
Solvent: CDCl3
Ambient temperature
Mercury-400BB "ncsumerc400"
Relax. delay 1.000 sec
Pulse 35.0 degrees
Acq. time 1.993 sec
Width 6006.0 Hz
16 repetitions
OBSERVE H1, 400.1351972 MHz
DATA PROCESSING
FT size 32768
Total time 0 min, 50 sec
C18
7.260
7.252
4.531
4.018
1.898
1.656
1.640
1.607
1.442
1.233
0.869
0.855
0.839
0.94
0.48
2.00
2.20
1.00
2.65
4.64
2.67
7.35
2.24
0.84

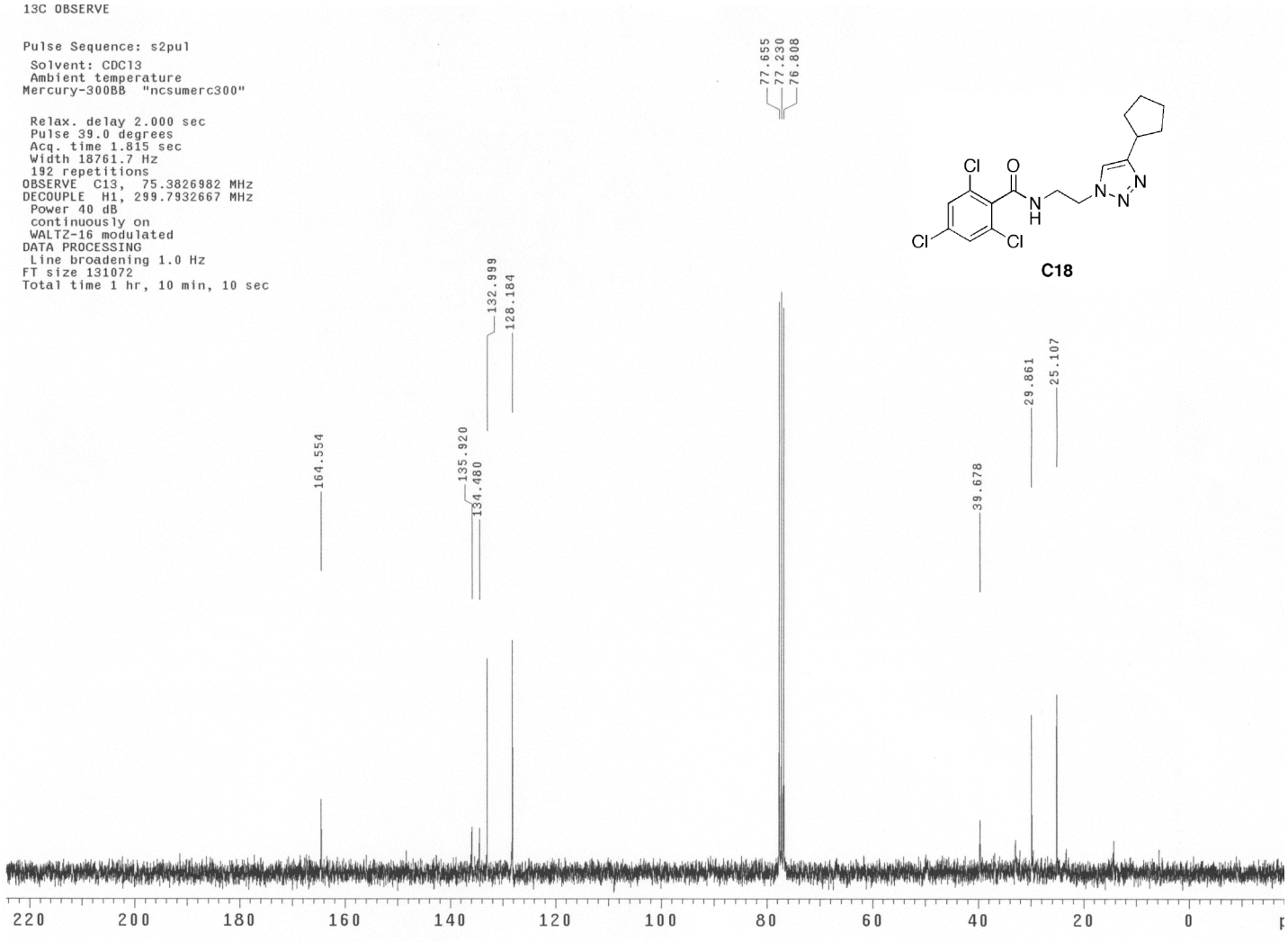
13C OBSERVE
Pulse Sequence: s2pul
Solvent: CDCl3
Ambient temperature
Mercury-300BB "ncsumerc300"
Relax. delay 2.000 sec
Pulse 39.0 degrees
Acq. time 1.815 sec
Width 18761.7 Hz
192 repetitions
OBSERVE C13, 75.3826982 MHz
DECOUPLE H1, 299.7932667 MHz
Power 40 dB
continuously on
WALTZ-16 modulated
DATA PROCESSING
Line broadening 1.0 Hz
FT size 131072
Total time 1 hr, 10 min, 10 sec
77.655
77.230
76.808
132.999
128.184
135.920
134.480
164.554
39.678
29.861
25.107
Cl
O
N
H
N
N
N
Cl
Cl
C18
220
200
180
160
140
120
100
80
60
40
20
0

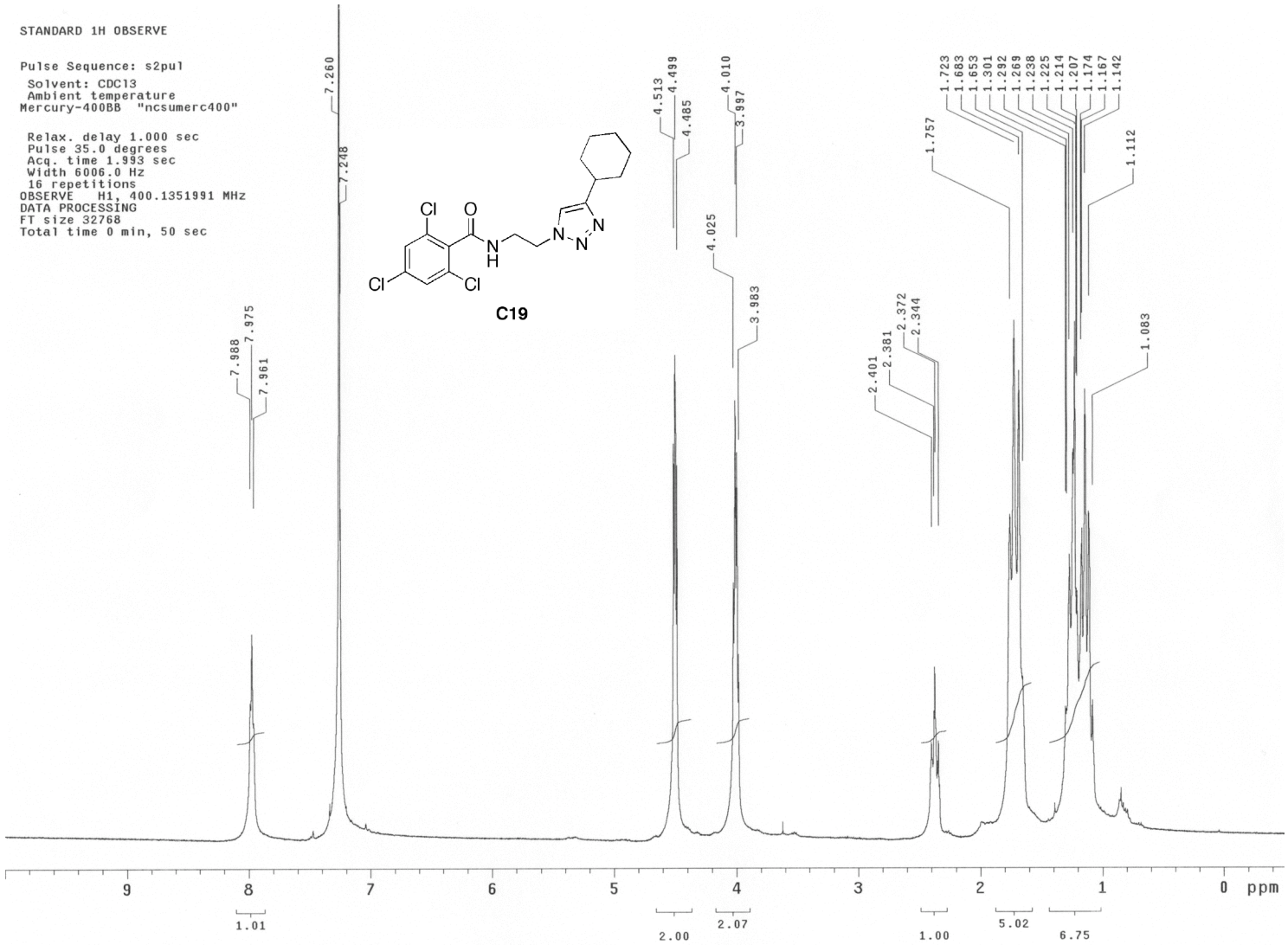
STANDARD 1H OBSERVE
Pulse Sequence: s2pul
Solvent: CDCl3
Ambient temperature
Mercury-400BB "ncsumerc400"
Relax. delay 1.000 sec
Pulse 35.0 degrees
Acq. time 1.993 sec
Width 6006.0 Hz
16 repetitions
OBSERVE H1, 400.1351991 MHz
DATA PROCESSING
FT size 32768
Total time 0 min, 50 sec
C19
7.988
7.975
7.961
7.260
7.248
4.513
4.499
4.485
4.025
4.010
3.997
3.983
2.401
2.381
2.372
2.344
1.757
1.723
1.683
1.653
1.301
1.292
1.269
1.238
1.225
1.214
1.207
1.174
1.167
1.142
1.112
1.083
9
8
7
6
5
4
3
2
1
0 ppm
1.01
2.00
2.07
1.00
5.02
6.75

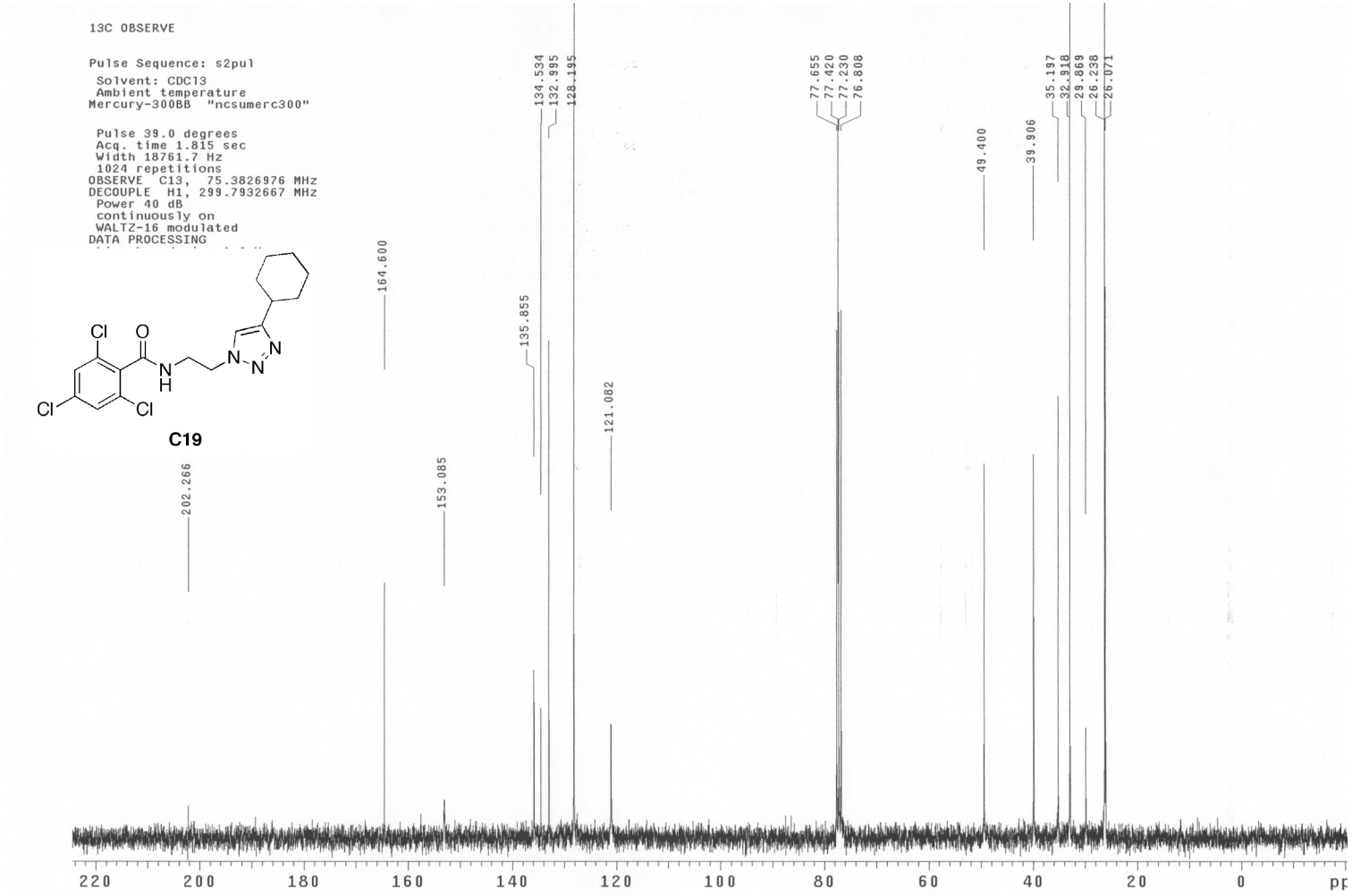
13C OBSERVE
Pulse Sequence: s2pul
Solvent: CDCl3
Ambient temperature
Mercury-300BB "ncsumerc300"
Pulse 39.0 degrees
Acq. time 1.815 sec
Width 18761.7 Hz
1024 repetitions
OBSERVE C13, 75.3826976 MHz
DECOUPLE H1, 299.7932667 MHz
Power 40 dB
continuously on
WALTZ-16 modulated
DATA PROCESSING
C19
202.266
164.600
153.085
135.855
134.534
132.995
128.195
121.082
77.655
77.420
77.230
76.808
49.400
39.906
35.197
32.918
29.869
26.238
26.071
220
200
180
160
140
120
100
80
60
40
20
0
ppm

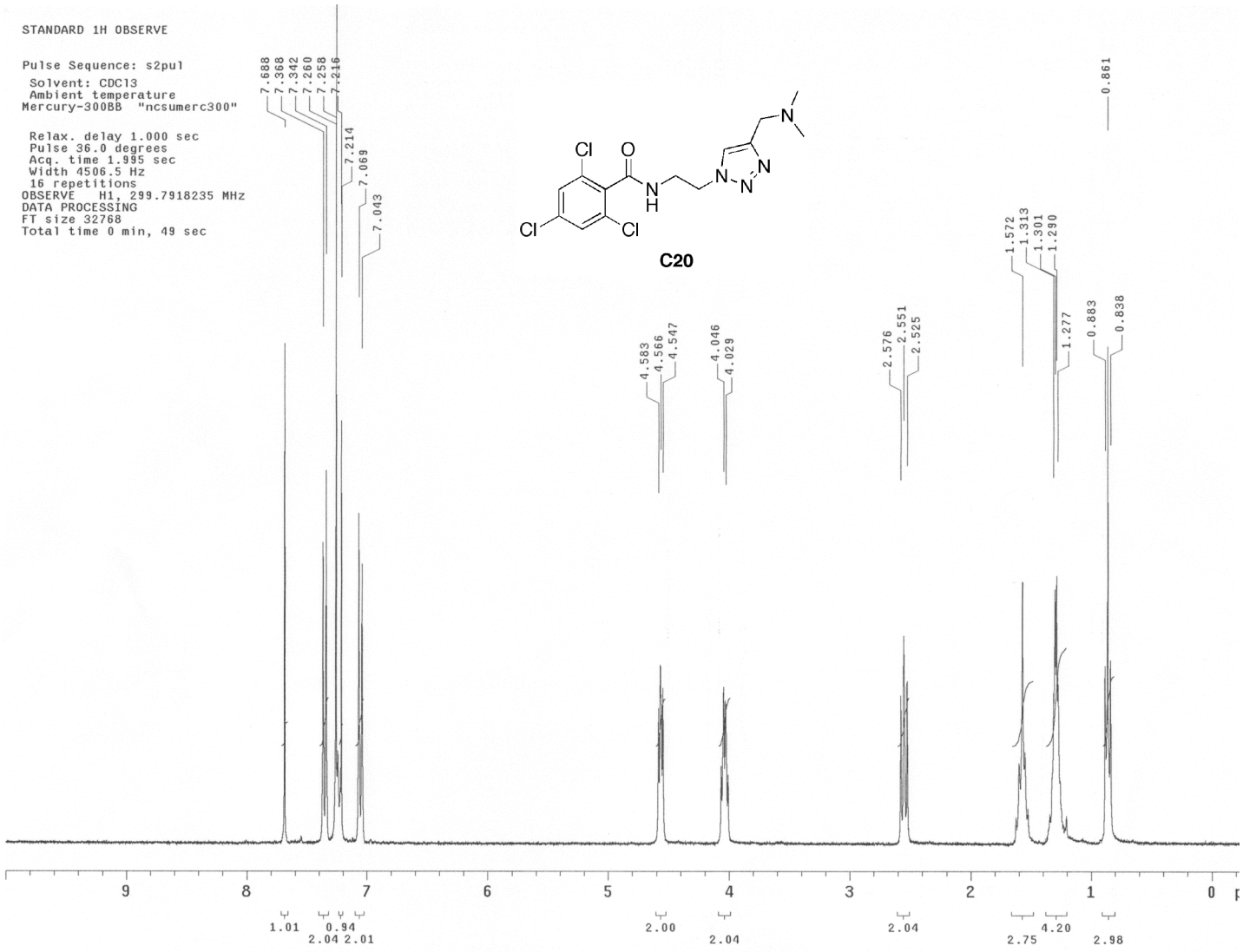
STANDARD 1H OBSERVE
Pulse Sequence: s2pul
Solvent: CDCl3
Ambient temperature
Mercury-300BB "ncsumerc300"
Relax. delay 1.000 sec
Pulse 36.0 degrees
Acq. time 1.995 sec
Width 4506.5 Hz
16 repetitions
OBSERVE H1, 299.7918235 MHz
DATA PROCESSING
FT size 32768
Total time 0 min, 49 sec
7.688
7.368
7.342
7.260
7.258
7.216
7.214
7.069
7.043
4.583
4.566
4.547
4.046
4.029
2.576
2.551
2.525
1.572
1.313
1.301
1.290
1.277
0.883
0.838
0.861
Cl
O
N
H
N
N
N
Cl
Cl
C20
9
8
7
6
5
4
3
2
1
0
1.01
2.04
0.94
2.01
2.00
2.04
2.04
2.75
4.20
2.98

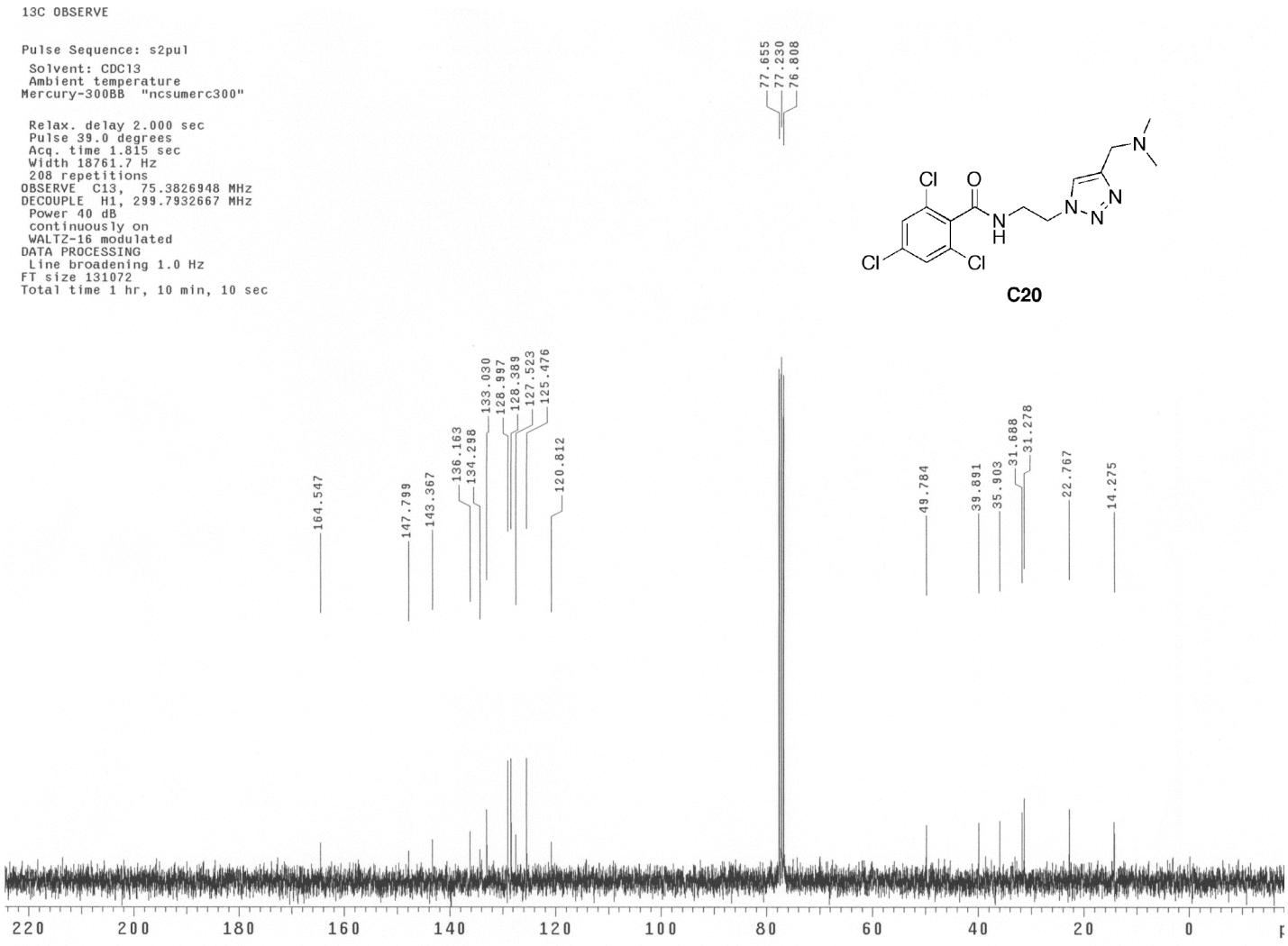
13C OBSERVE
Pulse Sequence: s2pul
Solvent: CDCl3
Ambient temperature
Mercury-300BB "ncsumerc300"
Relax. delay 2.000 sec
Pulse 39.0 degrees
Acq. time 1.815 sec
Width 18761.7 Hz
208 repetitions
OBSERVE C13, 75.3826948 MHz
DECOUPLE H1, 299.7932667 MHz
Power 40 dB
continuously on
WALTZ-16 modulated
DATA PROCESSING
Line broadening 1.0 Hz
FT size 131072
Total time 1 hr, 10 min, 10 sec
77.655
77.230
76.808
Cl
O
N
H
N
N
N
N
Cl
Cl
C20
164.547
147.799
143.367
136.163
134.298
133.030
128.997
128.389
127.523
125.476
120.812
49.784
39.891
35.903
31.688
31.278
22.767
14.275
220
200
180
160
140
120
100
80
60
40
20
0

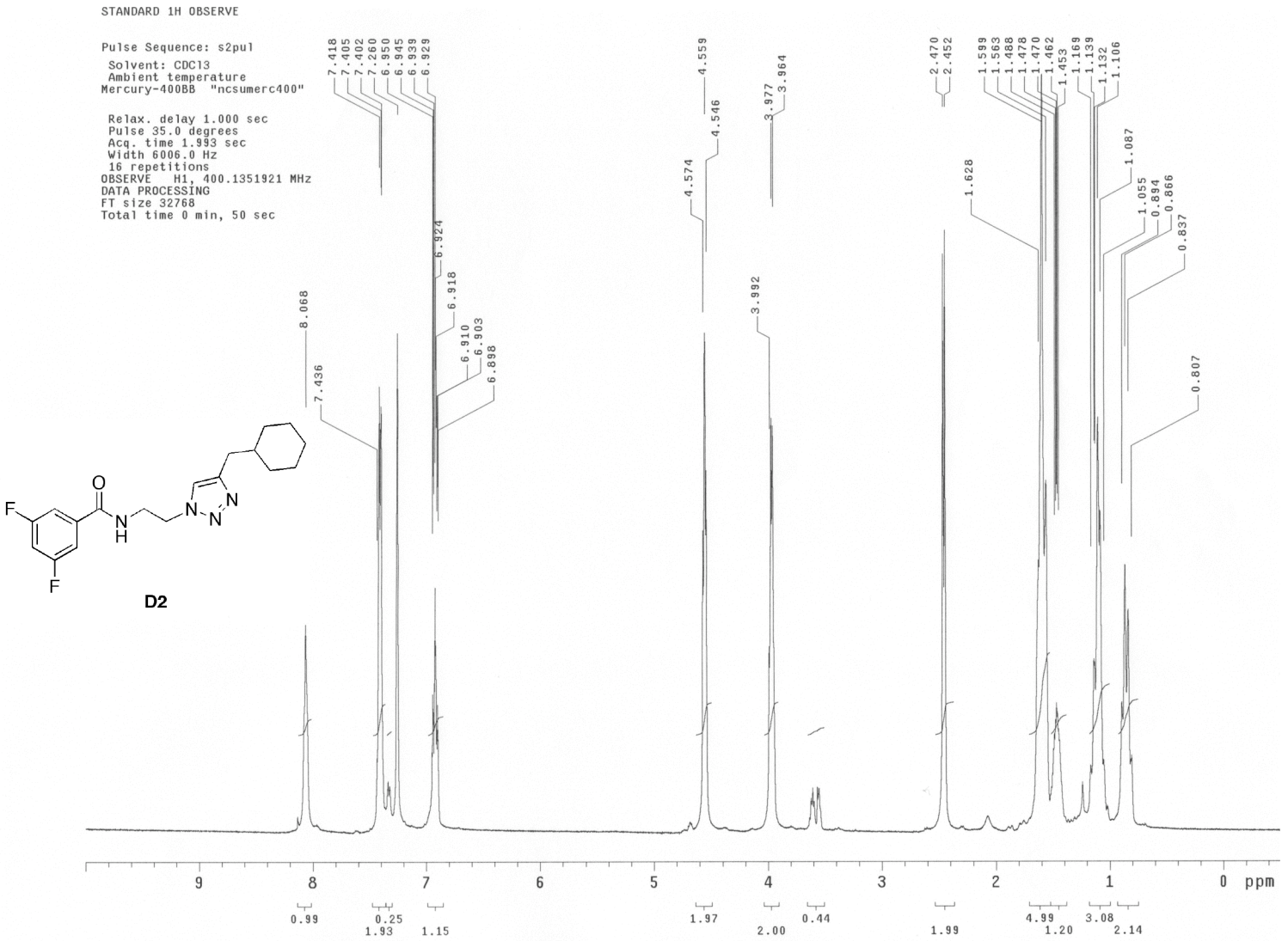
STANDARD 1H OBSERVE
Pulse Sequence: s2pul
Solvent: CDCl3
Ambient temperature
Mercury-400BB "ncsumerc400"
Relax. delay 1.000 sec
Pulse 35.0 degrees
Acq. time 1.993 sec
Width 6006.0 Hz
16 repetitions
OBSERVE H1, 400.1351921 MHz
DATA PROCESSING
FT size 32768
Total time 0 min, 50 sec
7.418
7.405
7.402
7.260
6.950
6.945
6.939
6.929
6.924
6.918
6.910
6.903
6.898
8.068
7.436
4.559
4.546
4.574
3.977
3.964
3.992
2.470
2.452
1.628
1.599
1.563
1.488
1.478
1.470
1.462
1.453
1.169
1.139
1.132
1.106
1.087
1.055
0.894
0.866
0.837
0.807
O
F
N
H
N
N
N
F
D2
9
8
7
6
5
4
3
2
1
0 ppm
0.99
0.25
1.93
1.15
1.97
2.00
0.44
1.99
4.99
1.20
3.08
2.14

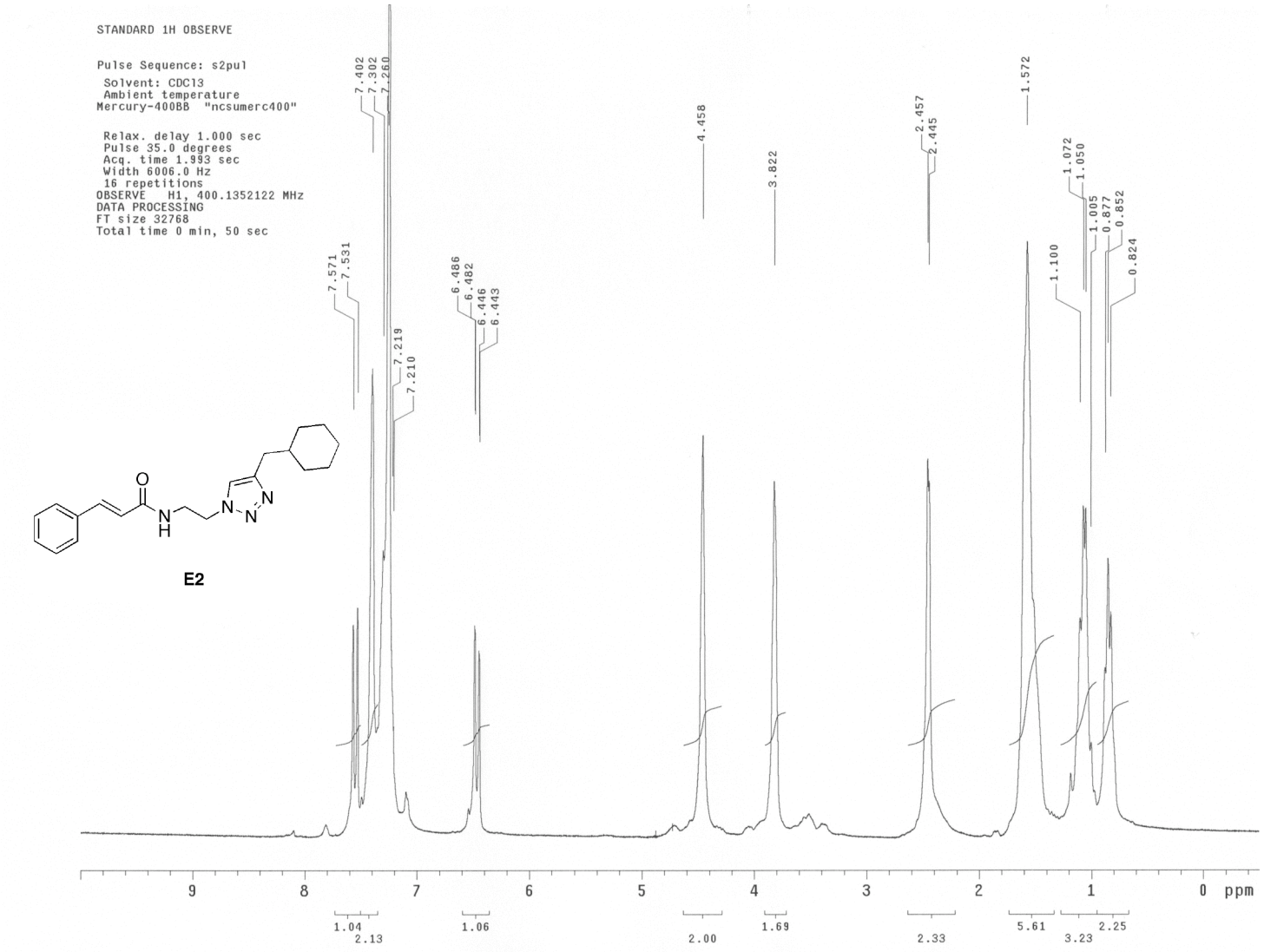
STANDARD 1H OBSERVE
Pulse Sequence: s2pul
Solvent: CDCl3
Ambient temperature
Mercury-400BB "ncsumerc400"
Relax. delay 1.000 sec
Pulse 35.0 degrees
Acq. time 1.993 sec
Width 6006.0 Hz
16 repetitions
OBSERVE H1, 400.1352122 MHz
DATA PROCESSING
FT size 32768
Total time 0 min, 50 sec
7.571
7.531
7.402
7.302
7.260
7.219
7.210
6.486
6.482
6.446
6.443
4.458
3.822
2.457
2.445
1.572
1.100
1.072
1.050
1.005
0.877
0.852
0.824
O
N
H
N
N
N
E2
9
8
7
6
5
4
3
2
1
0
ppm
1.04
2.13
1.06
2.00
1.69
2.33
5.61
3.23
2.25

CHAPTER 4

Substituted 1,4-Triazole Modulation of *Bordetella bronchiseptica* Biofilms

4.1 Bacterial Biofilms

Biofilms are surface attached communities of bacteria encased within a protective polymeric matrix.[1] The elaborate organizational capabilities bacteria possess through the formation of biofilms gained appreciation only a few decades ago;[2] yet it is currently estimated by the NIH that the majority (~80%) of the microbial biomass population exists within a biofilm state. These sessile communities are implicated as the basis for many persistent and chronic infections due to antimicrobial resistance and virulence factors conferred by their protective extracellular matrices.[3, 4] Bacterial biofilm infections commonly develop on inert surfaces such as dead tissue or indwelling medical devices and upon maturation release planktonic bacteria with the same genetic traits to develop robust biofilms once attached to a free surface.[2, 5] Although planktonic bacteria can be managed through conventional host defense mechanisms or antibiotic regimens, once they have colonized a surface and develop into a biofilm, it is extremely difficult to eradicate them. The propensity for biofilm formation and current evidence indicative of emerging antibiotic resistant strains of bacteria make biofilms an especially important target for chemical management.

Bacteria communicate with each other through a chemical signaling process termed quorum sensing (QS).[6] QS regulates gene expression as a function of bacterial population density by releasing chemical signaling molecules called autoinducers in a linear relationship to cellular density. Chemical communication through the release and detection of autoinducers controls a variety of physiological functions including virulence, motility and biofilm formation.[6] Upon attaining sufficient biomass to secrete and detect a threshold level of autoinducers, an alteration in gene expression initiates the coordinated formation of biofilms. The biofilm development cycle is depicted in **Figure 28**.

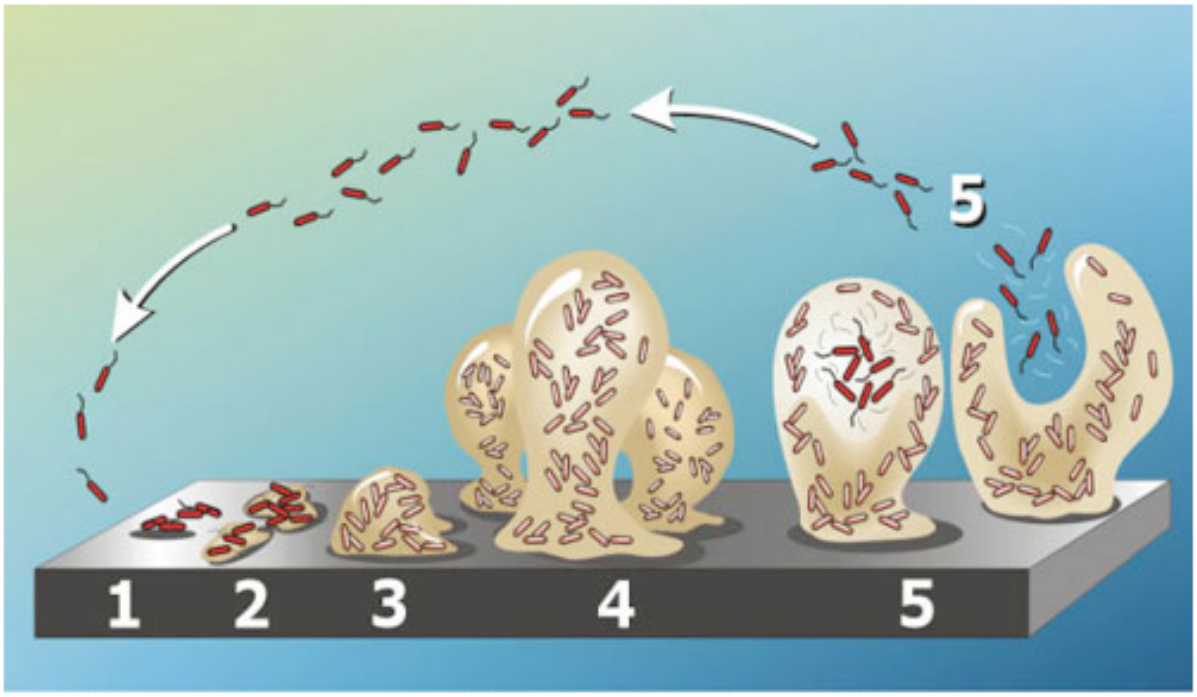

Figure 28. Stages of biofilm maturation. 1) Reversible attachement of bacteria to a surface. 2) Irreversible attachment. 3) Microcolony formation. 4) Mature biofilm. 5) Biofilm dispersion perpetuating the cycle.

4.1.1 Anti-Biofilm Modulating Small Molecules

Although biofilms are ubiquitous in nature, until recently there has been a paucity of small molecules known to modulate their formation. One molecular scaffold known to inhibit the formation of biofilms is based on naturally occurring QS signaling molecules, *N*-acylhomoserine lactones (AHL).[7] Although multiple synthetic libraries based off this scaffold have been synthesized,[8, 9] none of them have been reported to disperse a pre-formed biofilm. Additional naturally occurring scaffolds demonstrated to inhibit biofilms include brominated furanones[10] and ursene triterpenes;[11] however, these small molecules are also unable to disperse an established biofilm. Representatives of these small molecules are illustrated in **Figure 29**.

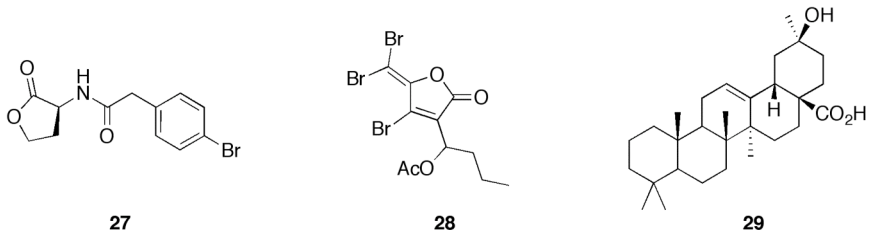

Figure 29. Representative small molecules that inhibit biofilm formation.

Reports of antifouling properties effected by bromopyrrole alkaloids isolated from marine sponges[12] encouraged our laboratory to investigate the possibility of anti-biofilm modulation based on these architectures. A variety of libraries based on bromoageliferin[13-15] and oroidin[16-19] have been synthesized and successfully shown to inhibit and disperse established biofilms for a variety of bacterial pathogens highlighting the utility of the 2-aminoimidazole (2-AI) architectural unit. In addition, a small molecule from a library of 2-aminoimidazole-triazoles (2-AIT) was synthesized by Steven Rogers and shown to inhibit and disperse bacterial biofilms across order, class and phylum.[20]

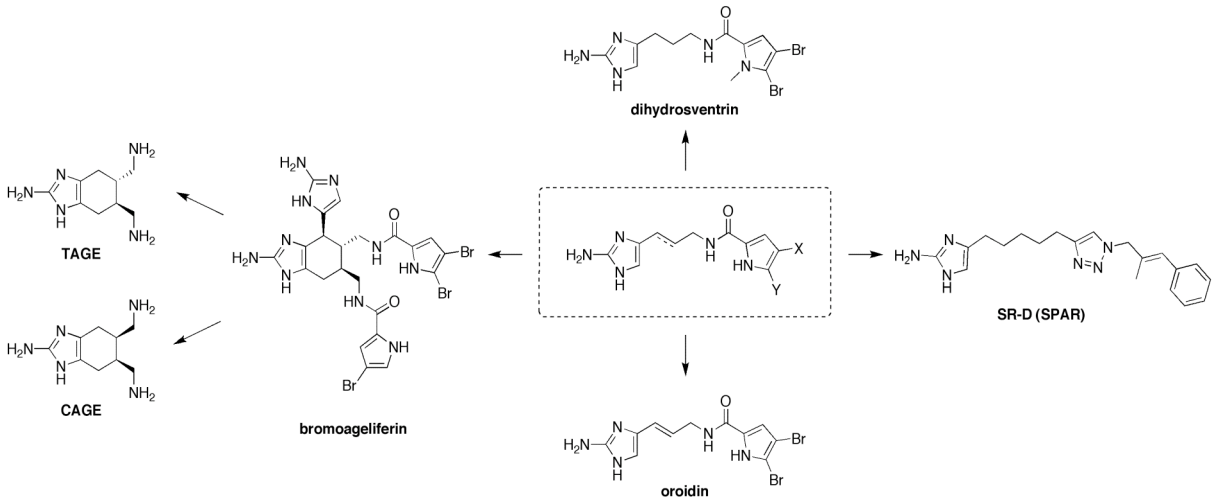

Figure 30. Representative 2-aminoimidazole containing small molecules.

4.2 *Bordetella* Genus

Bordetellae are small, gram-negative bacterial pathogens, which typically colonize the respiratory tracts of mammals.[21] *Bordetella pertussis* is the causative agent for whooping

cough in humans,[22] whereas *Bordetella bronchiseptica* produces a variety of respiratory disease pathologies (e.g. kennel cough, atrophic rhinitis) typically in domestic and farm animals.[23] *B. bronchiseptica* does not express the virulence factor pertussis toxin characteristic of *B. pertussis*; however it does contain the genes to do so,[24] thus emphasizing the intimate evolutionary relationship of these bacterial strains. Although *B. bronchiseptica* does not typically infect humans it has been shown to form biofilms that are highly resistant to a number of antimicrobial agents, including those which are prescribed clinically.[25] Considering the antibiotic resistance of these pathogens, and developing countries where vaccination against them is not prevalent, it is imperative to develop small molecules that can modulate anti-biofilm activity. Given the close relationship between these bacterial strains, *B. bronchiseptica* constitutes a safer alternative for exploring chemical control of biofilm modulation of the *Bordetella* genus in a laboratory setting.

4.3 Library Design

As part of a control screening for a library of 2-AITs, Steven Rogers screened 1,2,3-*H*-triazole for biofilm inhibition against *B. bronchiseptica* (RB50) and discovered that 1,2,3-*H*-triazole has an inhibitory concentration at 50% (IC_{50}) of 100 μM against this bacterial strain. Given these promising inhibition data and the facile synthesis of triazoles through the 1,3-dipolar cycloaddition reaction of terminal azides and alkynes, we sought to investigate the possibility of the triazole subunit as an architectural feature capable of modulating biofilm formation. Toward this end, a library of 1,4-substitued triazoles was synthesized by employing the Huisgen 1,3-dipolar cycloaddition reaction and screened for biofilm modulation against *B. bronchiseptica*.

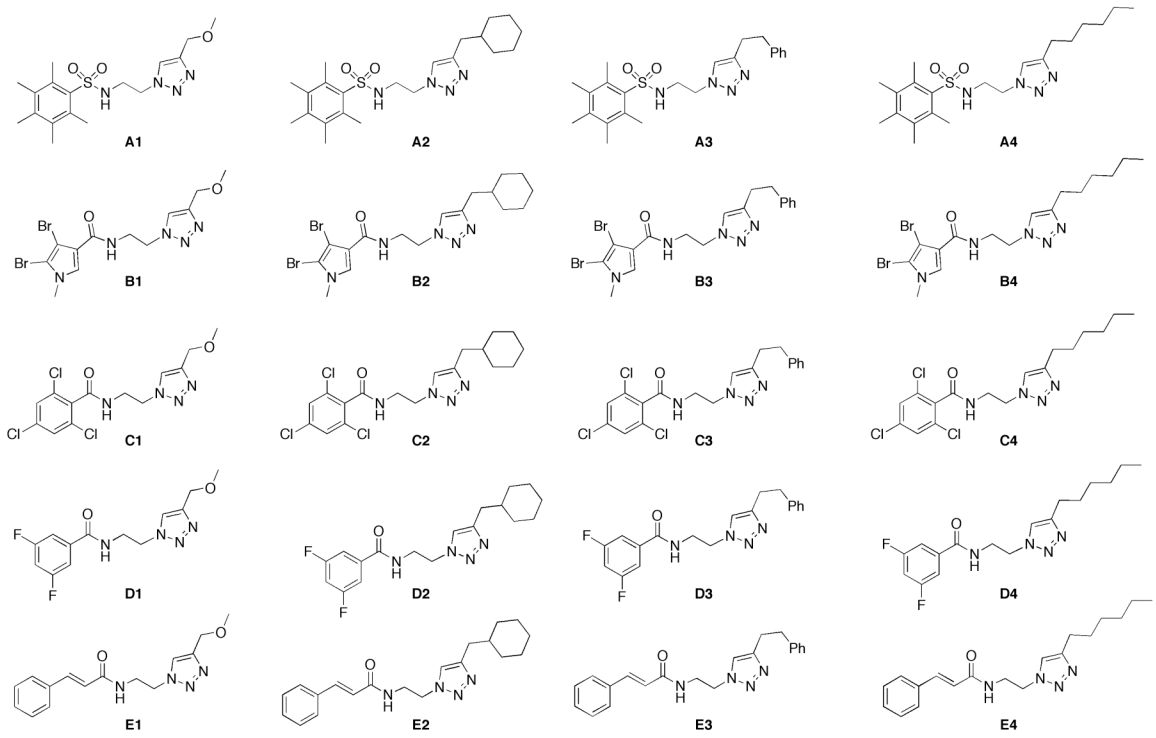

Figure 31. 1,4-Substituted triazole library for biofilm modulation screens.

The synthesis of 1,4-substitued triazoles is delineated in Chapter 3: **Scheme 7** as many of these molecules were originally designed for osteoclast inhibition screening. However, additional 1,4-substituted triazoles (depicted in **Figure 31**) were synthesized and screened for their ability to modulate biofilm formation.

4.4 Biofilm Screening Results

Given the intimate relationship between environmental conditions and the propensity to form biofilms, assays for biofilm formation with the triazole library were first conducted under a variety of nutrient sources to identify compounds that were active regardless of media composition.

4.4.1 Nutrient Broth Mediated RB50 Screens

The pilot screens of our triazole library were performed in Nutrient Broth (NB), given that this nutrient source hosted the 1,2,3-*H*-triazole inhibitory data Rogers achieved previously. Library screening at 100 μM against RB50 revealed the following biofilm modulation activity.

Table 6. RB50 biofilm inhibition results in NB at 100 μM (S.D. = standard deviation).

Compound	% Inhibition	S. D.	Compound	% Inhibition	S. D.
A1	30	26	**A3**	4	55
B1	56	18	**B3**	-88	30
C1	60	32	**C3**	52	33
D1	51	38	**D3**	43	7
E1	8	10	**E3**	48	4
A2	12	28	**A4**	-22	57
B2	-285	45	**B4**	72	1
C2	57	7	**C4**	63	1
D2	36	1	**D4**	30	18
E2	-28	9	**E4**	54	10

The data presented in **Table 6** for the initial RB50 inhibition screen is represented as the percent difference (e.g. percent inhibition of biofilm formation) where positive numbers indicate the percent at which molecules *decreased* the mass of RB50 in comparison to a bacteria only control. Negative numbers indicate molecules that *increased* the formation of RB50 biofilms at the absolute value of the indicated percent. This initial screen revealed molecules capable of inhibiting and promoting biofilm formation. **B2** and **B3** were shown to have a dramatic agonistic effect on RB50. A dose-response assay of **B3** was performed (**Figure 32**), illustrating a noticeable effect of increased biofilm formation with increasing concentrations.

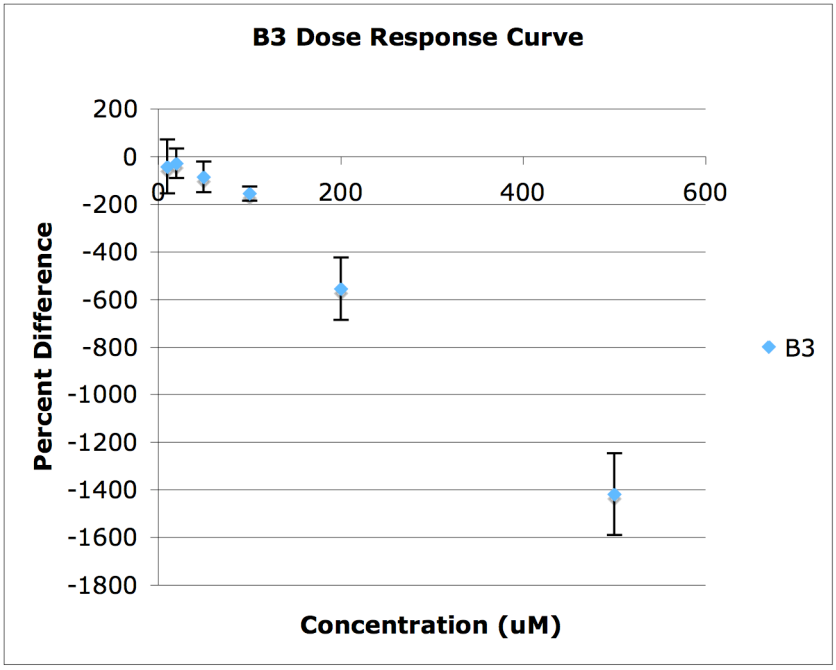

Figure 32. Dose response curve of **B3** against RB50.

Compounds **C1**, **C2**, **C4** and **B4** were also employed in dose-response assays given their promising inhibitory data at 100 µM; however, at this point repeated assays revealed RB50 could no longer produce a biofilm in NB. Interestingly, biofilms were *only* formed when dosed with these small molecules, even at 1 µM concentrations.

4.4.2 Stainer Scholte Mediated RB50 Screens

Once RB50 could no longer establish a biofilm in NB, we attempted to induce biofilm formation using Mueller Hinton Broth (MHB). However, film establishment in this nutrient source was not consistent. Therefore, we employed the recommended media for RB50 biofilm formation, Stainer Scholte Broth (SSB). Additionally, we discovered it was necessary to streak the RB50 cell line onto Bordet-Gengou Agar plates supplemented with 15% defibrinated sheep's blood in order to promote the phenotype for biofilm formation (as opposed to NB Agar as done previously, also explaining the loss in biofilm establishment over time in NB). After we switched to this plating medium and inoculated RB50 in SSB,

very robust biofilms were established. With the successful establishment of biofilms using these conditions, we chose to re-subject our triazole library for biofilm modulation effects. A static inhibition assay was then performed with 100 μM of each library component as had been done previously in NB. The results of this screen are shown below in **Table 7**.

Table 7. RB50 biofilm inhibition results in SSB at 100 μM (S.D. = standard deviation).

Compound	% Inhibition	S. D.	Compound	% Inhibition	S. D.
A1	-11	22	**A3**	6	8
B1	-2	14	**B3**	-7	12
C1	13	1	**C3**	9	13
D1	15	2	**D3**	6	17
E1	8	1	**E3**	-2	17
A2	5	2	**A4**	9	18
B2	-53	3	**B4**	9	12
C2	9	1	**C4**	18	18
D2	-79	16	**D4**	-5	5
E2	7	11	**E4**	2	26

The substitution of nutrients shows a marked effect on the ability of our triazole library to modulate biofilm formation. With the aggressive biofilm establishment conferred by SSB, nearly all of the library members had a negligible effect on biofilm structure. The only library members able to elicit a noticeable response were **B2** and **D2**, both of which increased the biomass of RB50. However, we clearly see partial antagonism at lower concentrations. The earlier screens employing NB also indicated an agonistic role for **B2**. We found these results to be promising, especially given that each of these molecules contained a cyclohexylmethyl pendant group. Dose response assays for each of these triazoles were performed are shown in **Figure 33**.

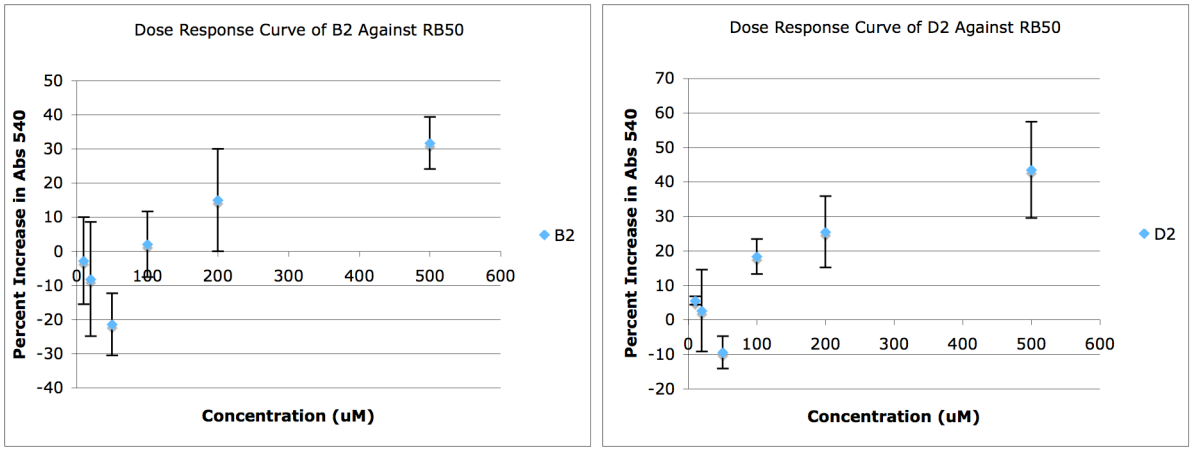

Figure 33. Dose response curves of **B2** and **D2** against RB50.

The dose response assays of **B2** and **D2**; although indicative of increasing absorbances at 540 nm (thus increasing bacterial biomass) at the higher concentrations tested, do not show the same propensity for increased biofilm formation as observed earlier in the full library screen.

4.5 Conclusion

We have synthesized a 1,4-substituted triazole library for the purpose of modulating *B. bronchiseptica* biofilms. This library was screened against the *B. bronchiseptica* wild-type strain RB50 in a variety of nutrient sources in order to identify small molecules capable of inhibiting or promoting biofilm formation. From these screens, we have identified compound **B2** as a compound that will promote biofilm formation regardless of media employed. Therefore, this molecule represents a small molecule probe that can be employed to potentially deconvolute pathways of biofilm formation in *B. bronchiseptica.*

4.6 Experimental

All ^{1}H NMR (400 MHz or 300 MHz) and ^{13}C NMR (400 MHz or 300 MHz) spectra were recorded at 25.0 ºC on a Varian Mercury spectrometer. Chemical shifts (δ) are given in ppm relative to $CDCl_3$; coupling constants (*J*) are in hertz. Abbreviations used are s = singlet, bs = broad singlet, d = doublet, dd = doublet of doublets, t = triplet, dt = doublet of triplets, m =

multiplet, and b = broad. Electrospray Ionization (ESI) exact mass measurements were carried out on an Agilent Technologies 6210 LC-TOF mass spectrometer. The sample matrix used was a H_2O/MeOH (1:3) mixture with 0.1% formic acid. Silica gel (40 μm average particle size) was used for flash column chromatography.

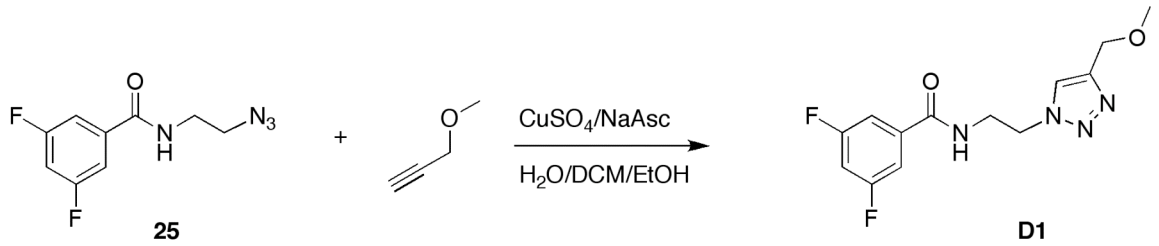

3,5-difluoro-*N*-(2-(4-(methoxymethyl)-1*H*-1,2,3-triazol-1-yl)ethyl)benzamide (D1). DCM (500 μL), EtOH (500 μL) and H_2O (500 μL) were added into a vial. Methylpropargyl ether (3.55 μL, 70.7 μmol) and **25** (17.7 mg, 66.5 μmol) were then added, followed by sodium ascorbate (7.0 mg, 35 μmol) and 1 M $CuSO_4$ (10.0 μL, 10.0 μmol). The reaction was stirred at RT for 16 h, DCM (3 mL) and H_2O (4 mL) were added and the H_2O layer was extracted with DCM (3 x 5 mL). The organic layer was dried over Na_2SO_4, filtered and reduced in vacuo. The product was purified via flash column chromatography using a DCM/MeOH gradient (100:1 to 96:4) mobile phase (R_f ~ 0.3 4% MeOH/DCM). The product was isolated as a sand colored amorphous solid (14 mg, 70%). ^{1}H NMR (400 MHz, $CDCl_3$) δ 7.52 (2H, m), 7.33 (3H, bm), 6.94 (1H, m), 4.60 (2H, t, J = 4.8 Hz), 4.49 (2H, s), 3.99 (2H, d, J = 4.8 Hz), 3.61 (2H, m), 3.36 (3H, s); HRMS (ESI) *m/z*, ($[M + H]^+$, $C_{13}H_{14}F_2N_4O_2$): theoretical 297.1164, observed 297.1167.

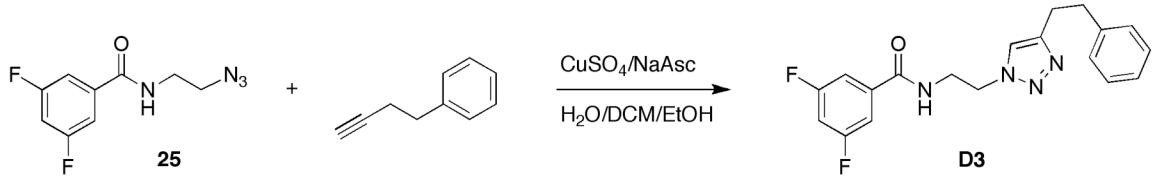

3,5-difluoro-*N*-(2-(4-phenethyl-1*H*-1,2,3-triazol-1-yl)ethyl)benzamide (D3). DCM (500 μL), EtOH (500 μL) and H_2O (500 μL) were added into a vial. 4-phenyl-1-butyne (31.7 μL,

225 µmol) and **25** (49.7 mg, 187 µmol) were then added, followed by sodium ascorbate (17.4 mg, 87.8 µmol) and 1 M $CuSO_4$ (28.0 µL, 28.0 µmol). The reaction was stirred at RT for 16 h, DCM (3 mL) and H_2O (4 mL) were added and the H_2O layer was extracted with DCM (3 x 5 mL). The organic layer was dried over Na_2SO_4, filtered and reduced in vacuo. The product was purified via flash column chromatography using a DCM/MeOH (96:4) mobile phase (R_f ~ 0.4 in 5% MeOH/DCM). The product was isolated as an off white solid (50 mg, 57%). ^{1}H NMR (400 MHz, $CDCl_3$) δ 8.09 (1H, s), 7.47 (2H, m), 7.24 (2H, m), 7.22 (2H, m), 7.10 (2H, m), 6.95 (1H, m), 4.54 (2H, t, *J* = 5.2 Hz), 3.97 (2H, dt, *J* = 5.2 Hz, 5.6 Hz), 2.96 (2H, m), 2.91 (2H, m); HRMS (ESI) *m/z*, ($[M + H]^+$, $C_{19}H_{18}F_2N_4O$): theoretical 357.1528, observed 357.1524.

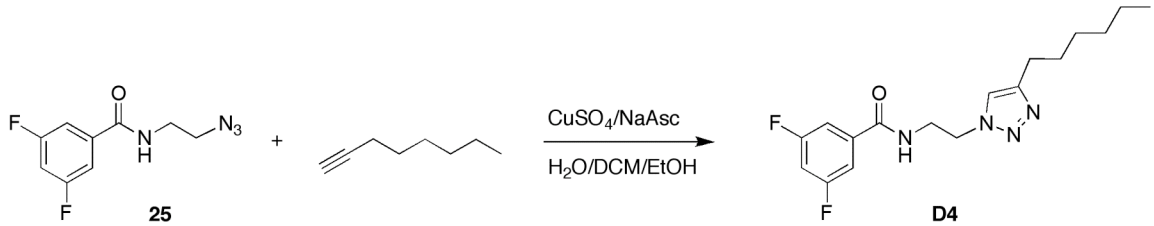

3,5-difluoro-*N*-(2-(4-hexyl-1*H*-1,2,3-triazol-1-yl)ethyl)benzamide (D4). DCM (500 µL), EtOH (500 µL) and H_2O (500 µL) were added into a vial. 1-octyne (14.6 µL, 99.2 µmol) and **25** (26.0 mg, 99.2 µmol) were then added, followed by sodium ascorbate (9.0 mg, 45 µmol) and 1 M $CuSO_4$ (14.9 µL, 14.9 µmol). The reaction was stirred at RT for 28 h, DCM (3 mL) and H_2O (4 mL) were added and the H_2O layer was extracted with DCM (3 x 5 mL). The organic layer was dried over Na_2SO_4, filtered and reduced in vacuo. The product was purified via flash column chromatography using a DCM/MeOH gradient (100:0 to 98:2) mobile phase (R_f ~ 0.4 in 2% MeOH/DCM). The product was isolated as a white solid (29 mg, 88%). ^{1}H NMR (400 MHz, $CDCl_3$) δ 7.96 (1H, d, *J* = 5.2 Hz), 7.43 (2H, m), 6.94 (1H, m), 4.55 (2H, t, *J* = 5.6 Hz), 3.99 (2H, dt, *J* = 5.6 Hz, 5.2 Hz), 2.59 (2H, t, *J* = 8.0 Hz), 1.52 (2H, m), 1.25 (6H, m), 0.86 (3H, m); HRMS (ESI) *m/z*, ($[M + H]^+$, $C_{17}H_{22}F_2N_4O$): theoretical 337.1841, observed 337.1831.

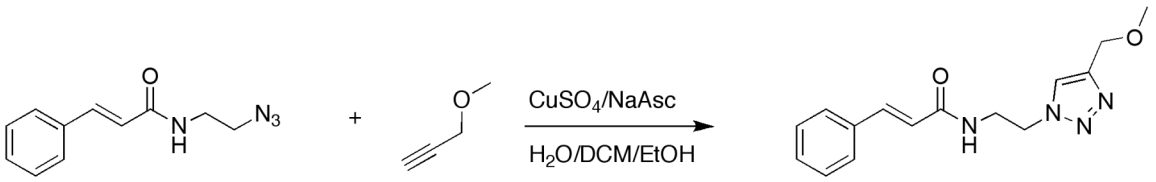

26 **E1**

***N*-(2-(4-(methoxymethyl)-1*H*-1,2,3-triazol-1-yl)ethyl)cinnamamide (E1)**. DCM (500 µL), EtOH (500 µL) and H_2O (500 µL) were added into a vial. Methylpropargyl ether (15.3 µL, 305 µmol) and **26** (60.0 mg, 278 µmol) were then added, followed by sodium ascorbate (27.0 mg, 136 µmol) and 1 M $CuSO_4$ (41.6 µL, 41.6 µmol). The reaction was stirred at RT for 14 h, DCM (6 mL) and H_2O (8 mL) were added and the H_2O layer was extracted with DCM (3 x 6 mL). The organic layer was dried over Na_2SO_4, filtered and reduced in vacuo. The product was purified via flash column chromatography using a DCM/MeOH gradient (100:0 to 98:2) mobile phase (R_f ~ 0.4 in 2% MeOH/DCM). The product was isolated as a white solid (31 mg, 39%). ^{1}H NMR (400 MHz, $CDCl_3$) δ 7.54 (1H, d, J = 15.6 Hz), 7.49 (1H, s), 7.41 (2H, m), 7.27 (2H, m), 6.90 (1H, m), 6.40 (1H, d, J = 15.6 Hz), 4.49 (2H, t, J = 5.6 Hz), 4.46 (2H, s), 3.82 (2H, dt, J = 5.6 Hz, 5.2 Hz), 3.30 (3H, s); HRMS (ESI) *m/z*, ($[M + H]^+$, $C_{15}H_{18}N_4O_2$): theoretical 287.1509, observed 287.1512.

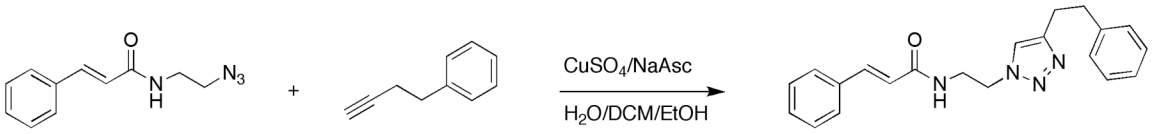

26 **E3**

***N*-(2-(4-phenethyl-1*H*-1,2,3-triazol-1-yl)ethyl)cinnamamide (E3)**. DCM (1 mL), EtOH (1 mL) and H_2O (1 mL) were added into a vial. 4-phenyl-1-butyne (71.5 µL, 506 µmol) and **26** (100.0 mg, 463 µmol) were then added, followed by sodium ascorbate (42.0 mg, 212 µmol) and 1 M $CuSO_4$ (69.4 µL, 69.4 µmol). The reaction was stirred at RT for 18 h, DCM (6 mL) and H_2O (8 mL) were added and the H_2O layer was extracted with DCM (3 x 6 mL). The organic layer was dried over Na_2SO_4, filtered and reduced in vacuo. The product was purified via flash column chromatography using a DCM/MeOH gradient (99:1 to 97:3) mobile phase (R_f ~ 0.1 in 1% MeOH/DCM). The product was isolated as an off white solid

(149 mg, 93%). ^{1}H NMR (400 MHz, $CDCl_3$) δ 7.56 (1H, d, *J* = 15.6 Hz), 7.40 (2H, m), 7.24 – 7.06 (7H, bm), 6.45 (1H, d, *J* = 15.6 Hz), 4.42 (2H, t, *J* = 5.6 Hz), 3.77 (2H, dt, *J* = 5.6 Hz, 5.2 Hz), 2.89 (4H, bm); HRMS (ESI) *m/z*, ($[M + H]^+$, $C_{21}H_{22}N_4O$): theoretical 347.1866, observed 347.1868.

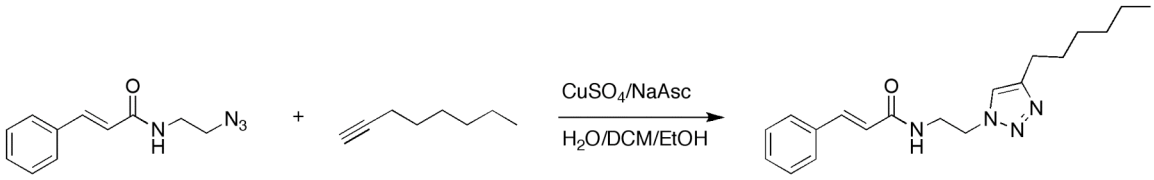

26 **E4**

***N*-(2-(4-hexyl-1*H*-1,2,3-triazol-1-yl)ethyl)cinnamamide (E4)**. DCM (1 mL), EtOH (1 mL) and H_2O (1 mL) were added into a vial. 1-octyne (74.9 µL, 509 µmol) and **26** (100.0 mg, 463 µmol) were then added, followed by sodium ascorbate (43.0 mg, 217 µmol) and 1 M $CuSO_4$ (69.4 µL, 69.4 µmol). The reaction was stirred at RT for 16 h, DCM (6 mL) and H_2O (8 mL) were added and the H_2O layer was extracted with DCM (3 x 6 mL). The organic layer was dried over Na_2SO_4, filtered and reduced in vacuo. The product was purified via flash column chromatography using a DCM/MeOH (97:3) mobile phase (R_f ~ 0.5 in 5% MeOH/DCM). The product was isolated as an off white solid (97 mg, 64%). ^{1}H NMR (400 MHz, $CDCl_3$) δ 7.57 (1H, d, *J* = 15.6 Hz), 7.41 (2H, m), 7.27 (3H, m), 6.52 (1H, d, *J* = 15.6 Hz), 4.74 (2H, s), 3.83 (2H, s), 2.57 (2H, s), 1.55 (2H, s), 1.19 (6H, m), 0.76 (3H, m); HRMS (ESI) *m/z*, ($[M + H]^+$, $C_{19}H_{26}N_4O$): theoretical 327.2179, observed 327.2182.

Biofilm Inhibition Protocol

B. bronchiseptica strain RB50 was received from the Wozniak Laboratory at Wake Forest University. The RB50 cell line was streaked onto either Nutrient Broth Agar plates or Bordet Gengou Agar plates supplemented with 15% definbrinated sheep's blood and incubated for 24 – 48 hours at 37 ºC. Single colonies were inoculated overnight in either Nutrient Broth, Mueller Hinton Broth or Stainer Scholte Broth with shaking at 220 rpm, 37 ºC overnight. The

following morning the cultures were diluted to an OD_{600} = 0.01 in the same media as the overnight culture. 1 mL of bacterial suspensions were aliquotted into 3 mL culture tubes and the library members (100 mM in DMSO) were individually introduced (1 µL/1 mL culture) to the suspensions and vortexed for a final concentration of 100 µM. A multichannel micropipet then dispensed 8 x 100 µL of treated bacterial suspensions into a full row of a 96-well plate. Multiple bacteria and media only controls were also seeded into the remaining wells of the 96-well plate. The 96-well plate was covered in GLAD Press'n Seal® wrap, placed in a sealed chamber supplemented with a damp towel to prevent evaporation. The suspensions were subjected to static incubations at 37 ºC for a period of 24 hours. After incubation the planktonic bacteria was evacuated from the wells and they were copiously washed with water and allowed to air dry. A 0.1% aqueous solution of crystal violet stain (125 µL) was added to each of the wells and allowed to incubate for 30 min. After staining, the wells were copiously washed with water and allowed to dry. Then 200 µL of 95% ethanol was added to each of the wells and allowed to incubate for 5 min to dissolve film-bound crystal violet. 125 µL of the staining solution was then transferred into another 96-well plate and UV-Vis absorbances were measured at 540 nm on a Bio-Tek® ELx808 Absorbance Microplate Reader.

REFERENCES

1. J. W. Costerton, Z. Lewandowski, D. E. Caldwell, D. R. Korber and H. M. Lappin-Scott, *Annu Rev Microbiol*, 1995, **49**, 711-745.

2. R. M. Donlan and J. W. Costerton, *Clin Microbiol Rev*, 2002, **15**, 167-193.

3. J. W. Costerton, P. S. Stewart and E. P. Greenberg, *Science*, 1999, **284**, 1318-1322.

4. S. Furukawa, S. L. Kuchma and G. A. O'Toole, *J Bacteriol*, 2006, **188**, 1211-1217.

5. D. Davies, *Nat Rev Drug Discov*, 2003, **2**, 114-122.

6. M. B. Miller and B. L. Bassler, *Annu Rev Microbiol*, 2001, **55**, 165-199.

7. C. Fuqua and E. P. Greenberg, *Nat Rev Mol Cell Biol*, 2002, **3**, 685-695.

8. G. D. Geske, R. J. Wezeman, A. P. Siegel and H. E. Blackwell, *J Am Chem Soc*, 2005, **127**, 12762-12763.

9. G. D. Geske, J. C. O'Neill, D. M. Miller, M. E. Mattmann and H. E. Blackwell, *J Am Chem Soc*, 2007, **129**, 13613-13625.

10. M. Hentzer, K. Riedel, T. B. Rasmussen, A. Heydorn, J. B. Andersen, M. R. Parsek, S. A. Rice, L. Eberl, S. Molin, N. Hoiby, S. Kjelleberg and M. Givskov, *Microbiology*, 2002, **148**, 87-102.

11. J. F. Hu, E. Garo, M. G. Goering, M. Pasmore, H. D. Yoo, T. Esser, J. Sestrich, P. A. Cremin, G. W. Hough, P. Perrone, Y. S. Lee, N. T. Le, M. O'Neil-Johnson, J. W. Costerton and G. R. Eldridge, *J Nat Prod*, 2006, **69**, 118-120.

12. N. Fusetani, *Nat Prod Rep*, 2004, **21**, 94-104.

13. R. W. Huigens, L. Y. Ma, C. Gambino, P. D. R. Moeller, A. Basso, J. Cavanagh, D. J. Wozniak and C. Melander, *Mol BioSyst*, 2008, **4**, 614-621.

14. R. W. Huigens, J. J. Richards, G. Parise, T. E. Ballard, W. Zeng, R. Deora and C. Melander, *J Am Chem Soc*, 2007, **129**, 6966.

15. R. W. Huigens, S. A. Rogers, A. T. Steinhauer and C. Melander, *Org Biomol Chem*, 2009, **7**, 794-802.

16. J. J. Richards, T. E. Ballard, R. W. Huigens and C. Melander, *Chembiochem*, 2008, **9**, 1267-1279.

17. J. J. Richards, T. E. Ballard and C. Melander, *Org Biomol Chem*, 2008, **6**, 1356-1363.

18. J. J. Richards, C. S. Reed and C. Melander, *Bioorg Med Chem Lett*, 2008, **18**, 4325-4327.

19. J. J. Richards, S. Reyes, S. D. Stowe, A. T. Tucker, T. E. Ballard, L. D. Mathies, J. Cavanagh and C. Melander, *J Med Chem*, 2009, **52**, 4582-4585.

20. S. A. Rogers and C. Melander, *Angew Chem Int Ed Engl*, 2008, **47**, 5229-5231.

21. S. Mattoo and J. D. Cherry, *Clin Microbiol Rev*, 2005, **18**, 326-382.

22. A. A. Weiss, E. L. Hewlett, G. A. Myers and S. Falkow, *J Infect Dis*, 1984, **150**, 219-222.

23. S. H. Yeh, *Expert Rev Vaccines*, 2003, **2**, 113-127.

24. D. A. Diavatopoulos, C. A. Cummings, L. M. Schouls, M. M. Brinig, D. A. Relman and F. R. Mooi, *PLoS Pathog*, 2005, **1**, e45.

25. M. Mishra, G. Parise, K. D. Jackson, D. J. Wozniak and R. Deora, *J Bacteriol*, 2005, **187**, 1474-1484.

APPENDIX

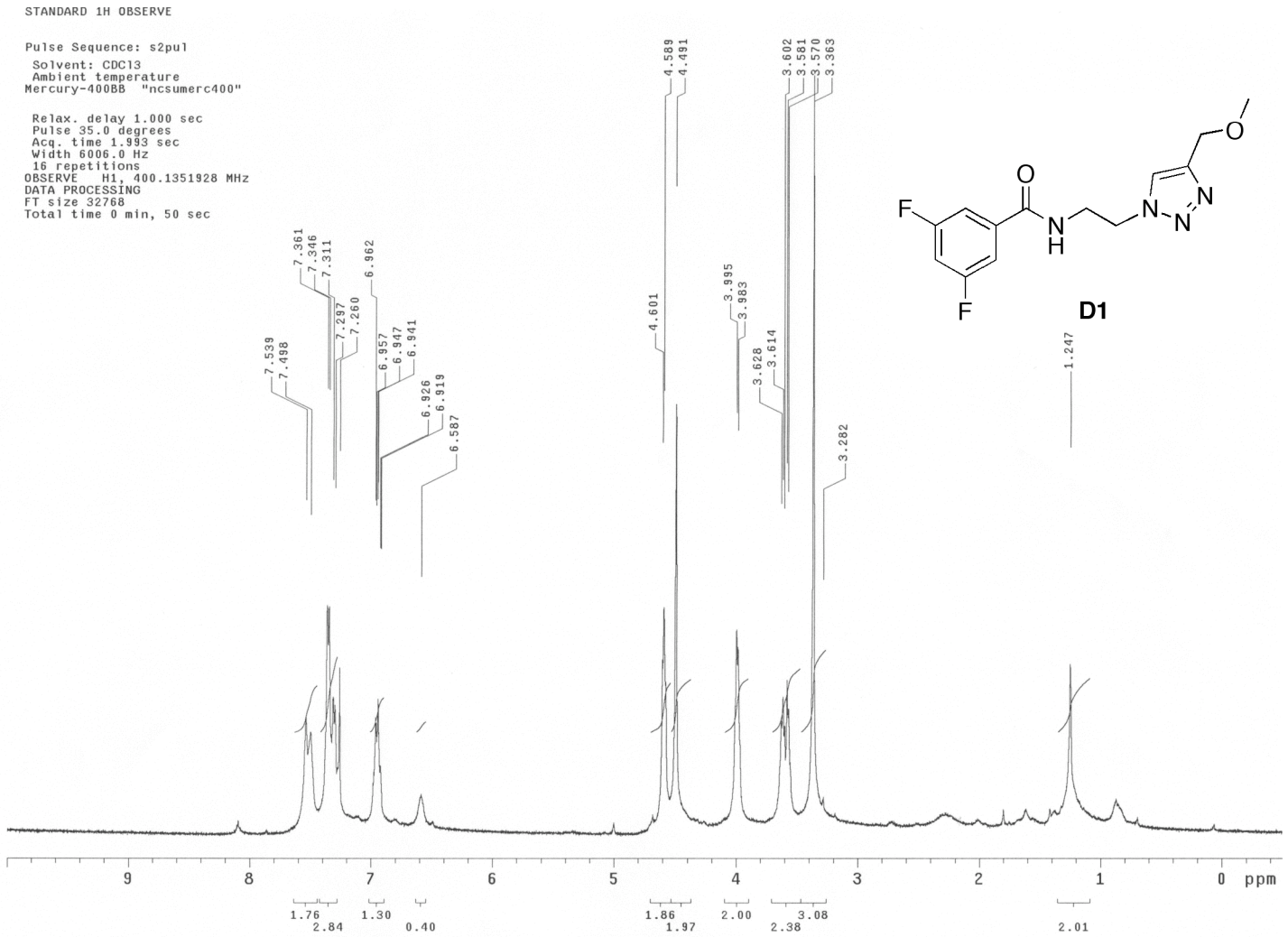
STANDARD 1H OBSERVE
Pulse Sequence: s2pul
Solvent: CDCl3
Ambient temperature
Mercury-400BB "ncsumerc400"
Relax. delay 1.000 sec
Pulse 35.0 degrees
Acq. time 1.993 sec
Width 6006.0 Hz
16 repetitions
OBSERVE H1, 400.1351928 MHz
DATA PROCESSING
FT size 32768
Total time 0 min, 50 sec
7.539
7.498
7.361
7.346
7.311
7.297
7.260
6.962
6.957
6.947
6.941
6.926
6.919
6.587
4.589
4.491
4.601
3.995
3.983
3.628
3.614
3.602
3.581
3.570
3.363
3.282
1.247
F
O
N
H
N
N
N
O
F
D1
9
8
7
6
5
4
3
2
1
0 ppm
1.76
2.84
1.30
0.40
1.86
1.97
2.00
3.08
2.38
2.01

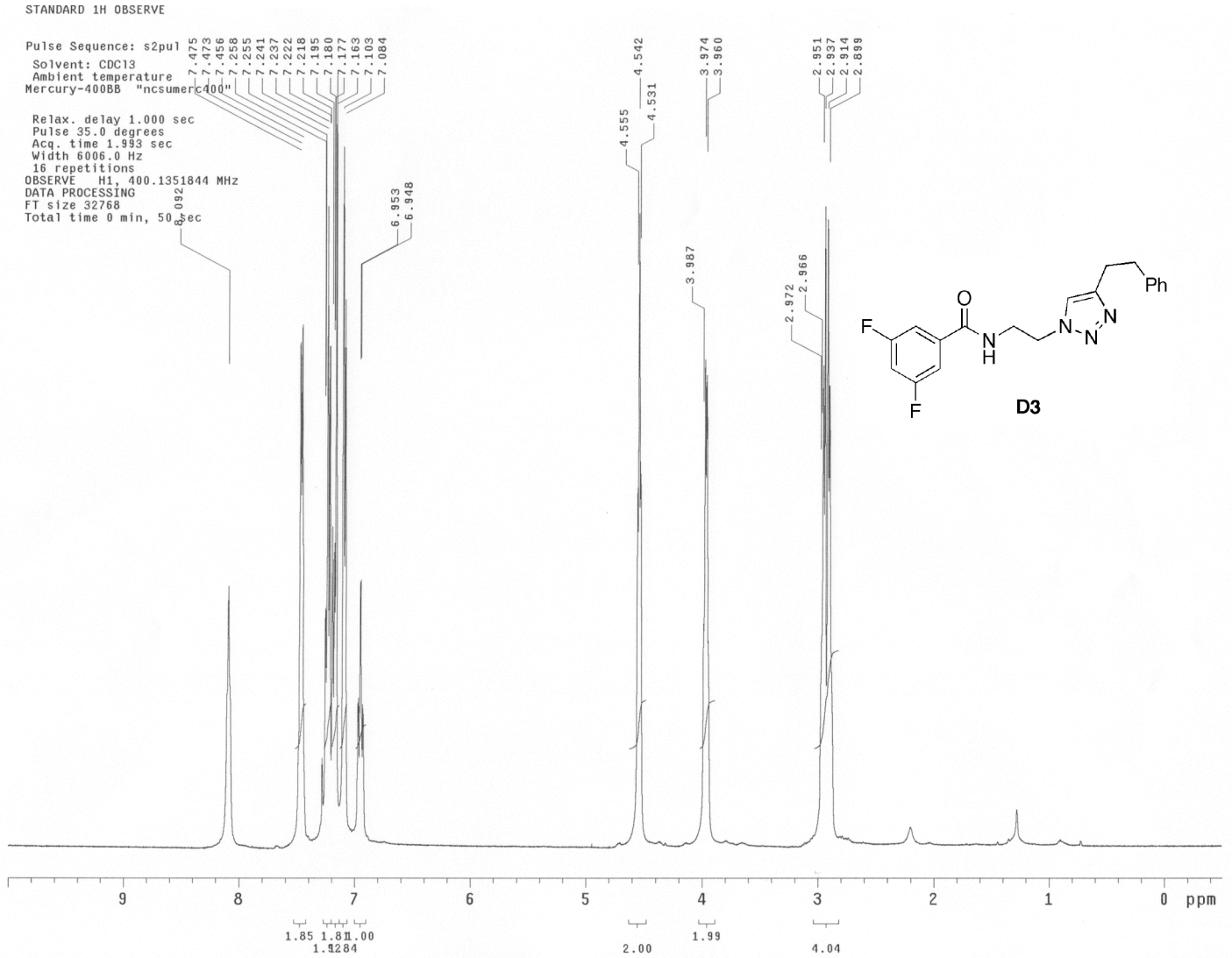
STANDARD 1H OBSERVE
Pulse Sequence: s2pul
Solvent: CDCl3
Ambient temperature
Mercury-400BB "ncsumerc400"
Relax. delay 1.000 sec
Pulse 35.0 degrees
Acq. time 1.993 sec
Width 6006.0 Hz
16 repetitions
OBSERVE H1, 400.1351844 MHz
DATA PROCESSING
FT size 32768
Total time 0 min, 50 sec
8.092
7.475
7.473
7.456
7.258
7.255
7.241
7.237
7.222
7.218
7.195
7.180
7.177
7.163
7.103
7.084
6.953
6.948
4.555
4.542
4.531
3.987
3.974
3.960
2.972
2.966
2.951
2.937
2.914
2.899
F
O
N
H
N
N
N
Ph
F
D3
9
8
7
6
5
4
3
2
1
0 ppm
1.85
1.81
1.00
2.00
1.99
4.04

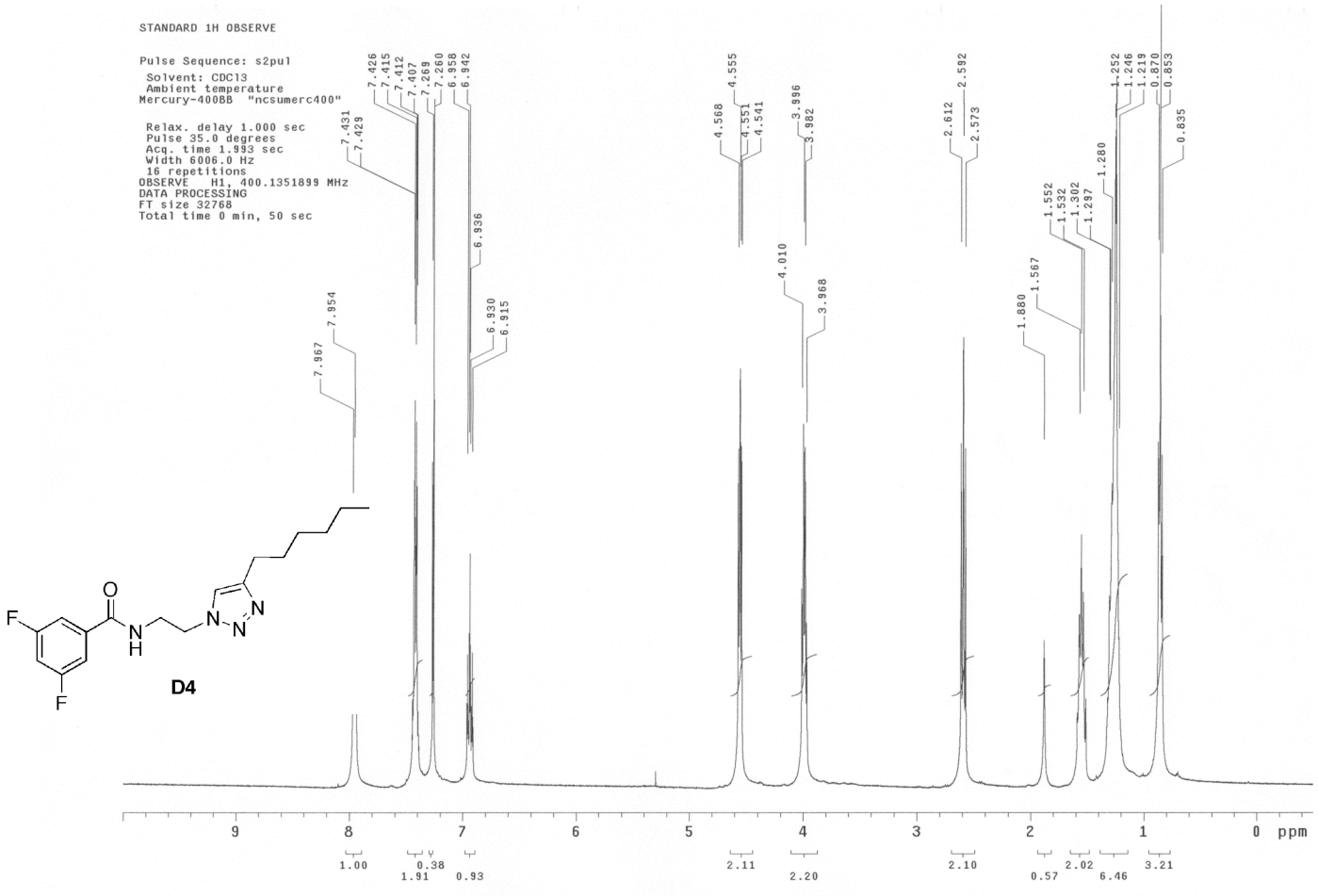
STANDARD 1H OBSERVE
Pulse Sequence: s2pul
Solvent: CDCl3
Ambient temperature
Mercury-400BB "ncsumerc400"
Relax. delay 1.000 sec
Pulse 35.0 degrees
Acq. time 1.993 sec
Width 6006.0 Hz
16 repetitions
OBSERVE H1, 400.1351899 MHz
DATA PROCESSING
FT size 32768
Total time 0 min, 50 sec
7.967
7.854
7.431
7.429
7.426
7.415
7.412
7.407
7.268
7.260
6.958
6.942
6.936
6.930
6.915
4.568
4.555
4.551
4.541
4.010
3.996
3.982
3.968
2.612
2.592
2.573
1.880
1.567
1.552
1.532
1.302
1.297
1.280
1.252
1.246
1.219
0.870
0.853
0.835
F
O
N
H
N
N
N
F
D4
9
8
7
6
5
4
3
2
1
0
ppm
1.00
0.38
1.91
0.93
2.11
2.20
2.10
0.57
2.02
6.46
3.21

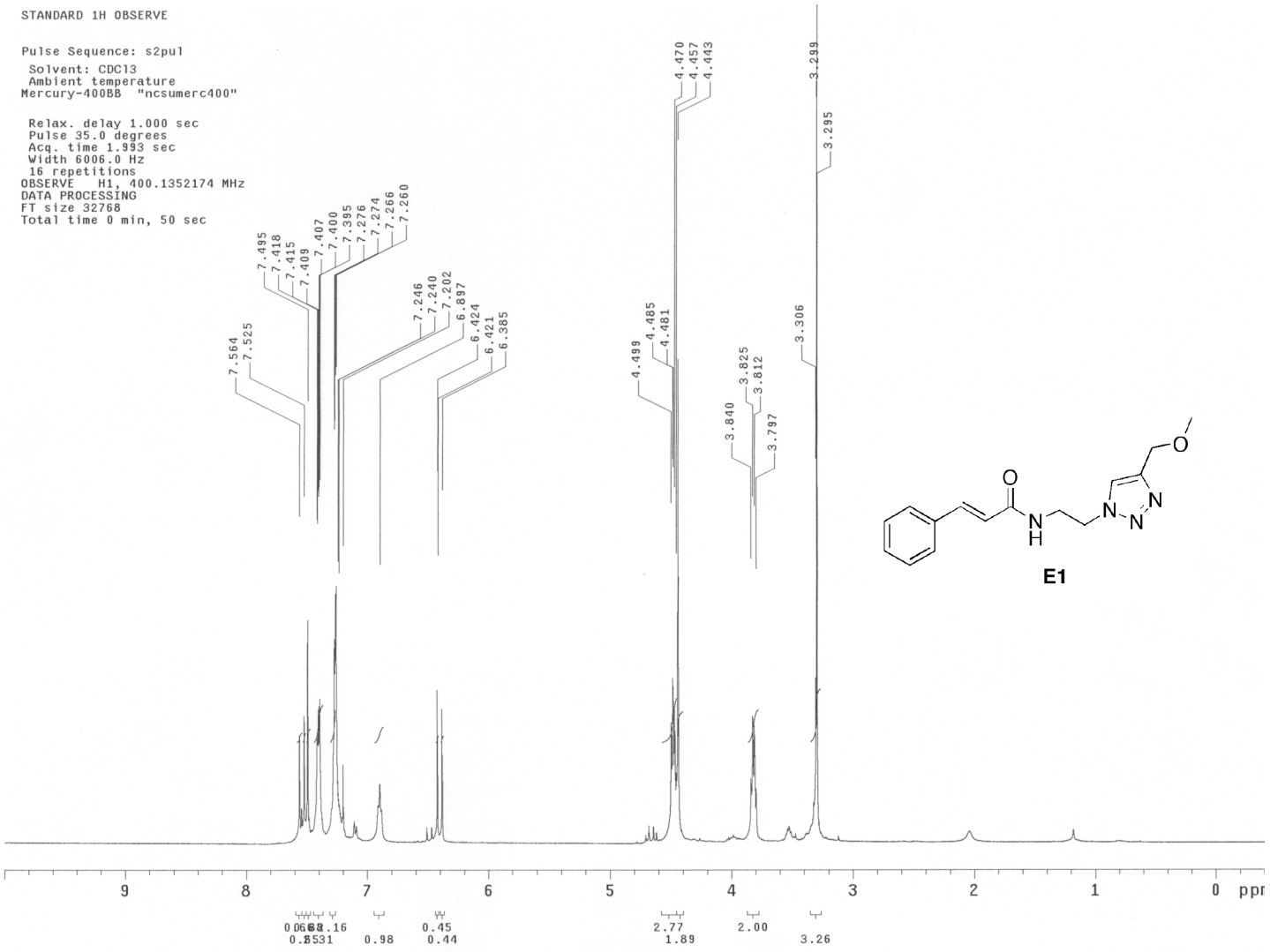
STANDARD 1H OBSERVE
Pulse Sequence: s2pul
Solvent: CDCl3
Ambient temperature
Mercury-400BB "ncsumerc400"
Relax. delay 1.000 sec
Pulse 35.0 degrees
Acq. time 1.993 sec
Width 6006.0 Hz
16 repetitions
OBSERVE H1, 400.1352174 MHz
DATA PROCESSING
FT size 32768
Total time 0 min, 50 sec
7.564
7.525
7.495
7.418
7.415
7.409
7.407
7.400
7.395
7.276
7.274
7.266
7.260
7.246
7.240
7.202
6.897
6.424
6.421
6.385
4.499
4.485
4.481
4.470
4.457
4.443
3.840
3.825
3.812
3.797
3.306
3.299
3.295
O
N
H
N
N
N
O
E1
9
8
7
6
5
4
3
2
1
0
ppm
0.45
0.44
0.98
2.77
1.89
2.00
3.26

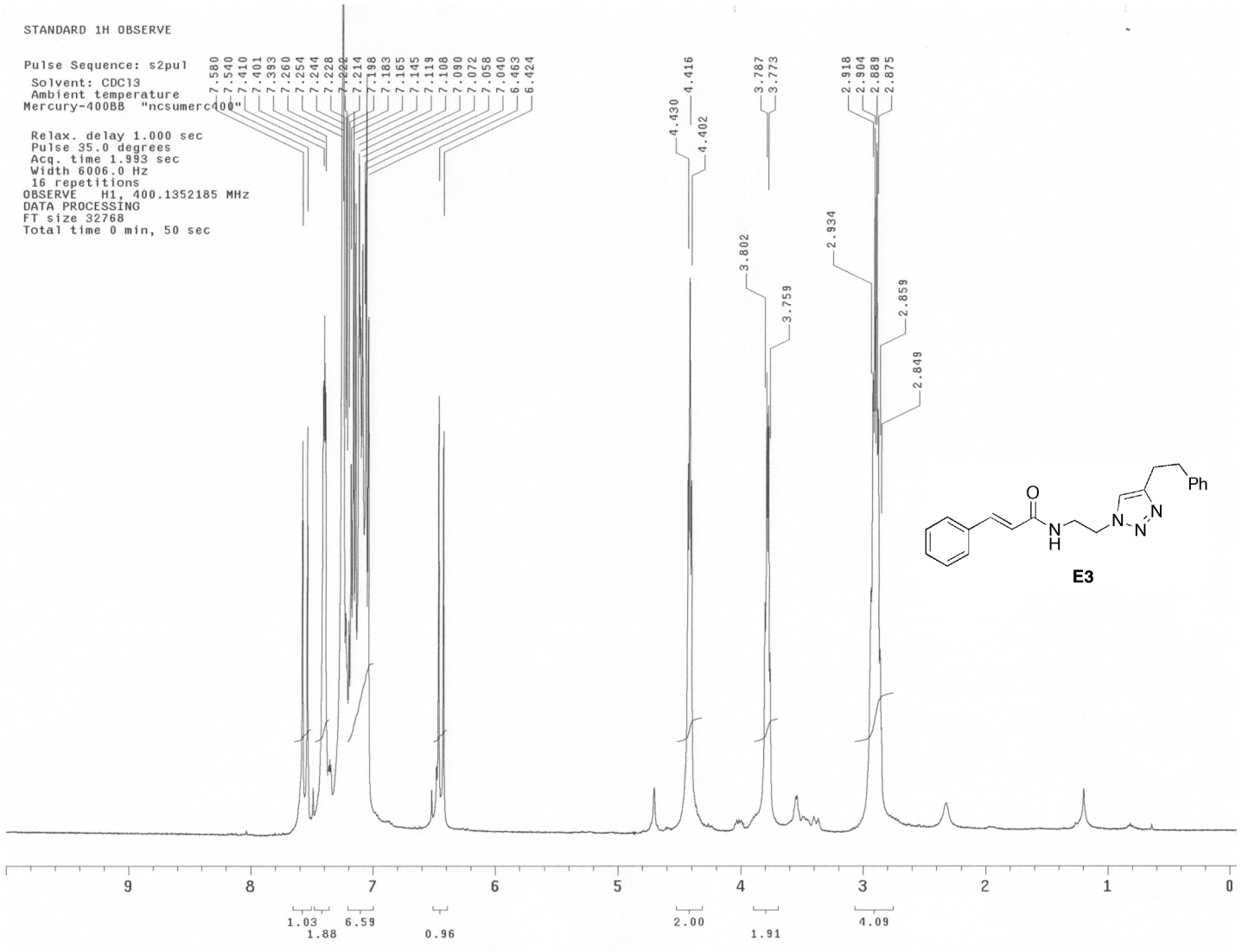
STANDARD 1H OBSERVE
Pulse Sequence: s2pul
Solvent: CDCl3
Ambient temperature
Mercury-400BB "ncsumerc400"
Relax. delay 1.000 sec
Pulse 35.0 degrees
Acq. time 1.993 sec
Width 6006.0 Hz
16 repetitions
OBSERVE H1, 400.1352185 MHz
DATA PROCESSING
FT size 32768
Total time 0 min, 50 sec
7.580
7.540
7.410
7.401
7.393
7.260
7.254
7.244
7.228
7.222
7.214
7.198
7.183
7.165
7.145
7.119
7.108
7.080
7.072
7.058
7.040
6.463
6.424
4.430
4.416
4.402
3.802
3.787
3.773
3.759
2.934
2.918
2.904
2.889
2.875
2.859
2.849
1.03
1.88
6.59
0.96
2.00
1.91
4.09
Ph
O
N
H
N
N
N
E3

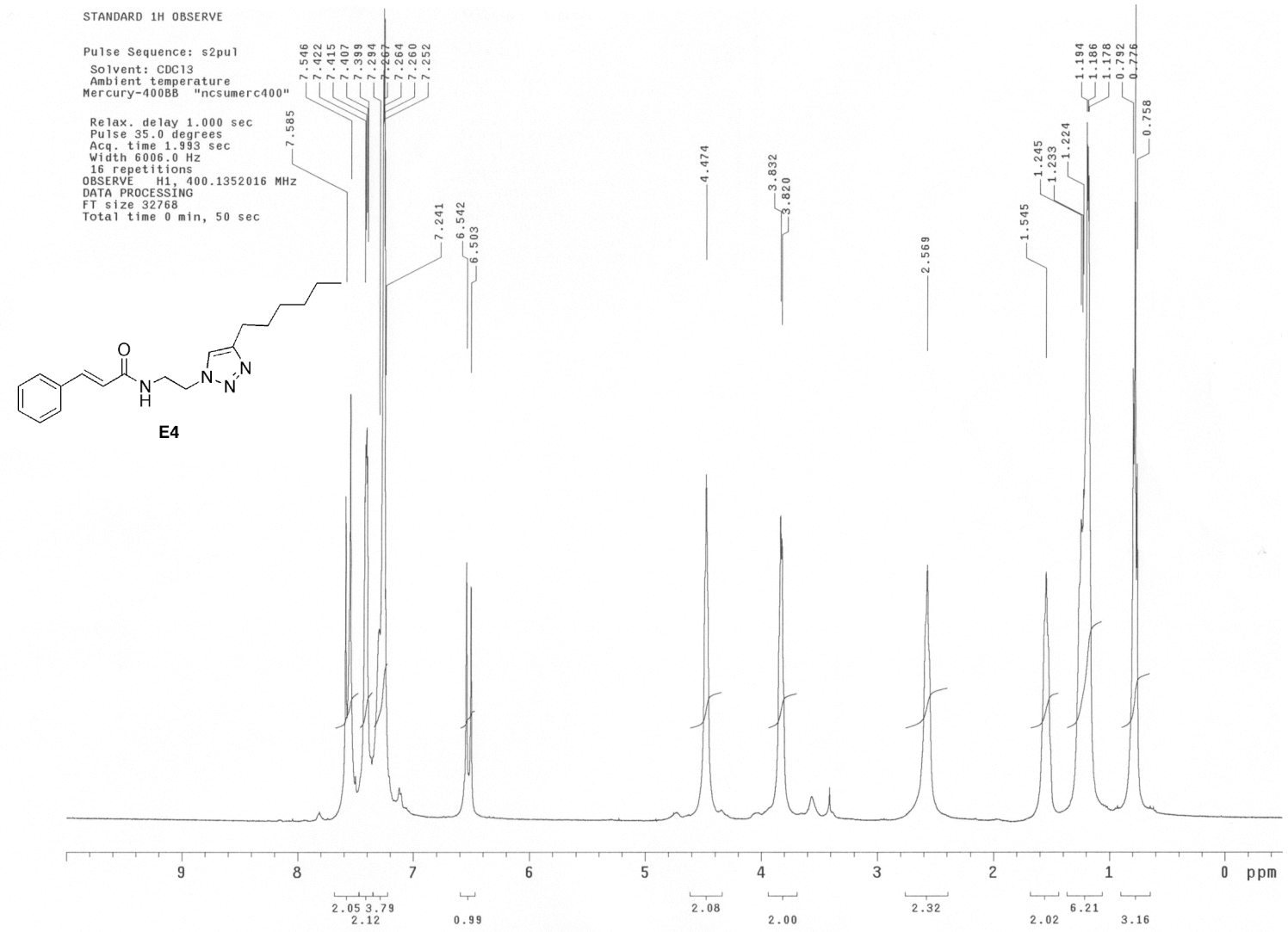
STANDARD 1H OBSERVE
Pulse Sequence: s2pul
Solvent: CDCl3
Ambient temperature
Mercury-400BB "ncsumerc400"
Relax. delay 1.000 sec
Pulse 35.0 degrees
Acq. time 1.993 sec
Width 6006.0 Hz
16 repetitions
OBSERVE H1, 400.1352016 MHz
DATA PROCESSING
FT size 32768
Total time 0 min, 50 sec
7.585
7.546
7.422
7.415
7.407
7.399
7.294
7.267
7.264
7.260
7.252
7.241
6.542
6.503
4.474
3.832
3.820
2.569
1.545
1.245
1.233
1.224
1.194
1.186
1.178
0.792
0.776
0.758
O
N
H
N
N
N
E4
9
8
7
6
5
4
3
2
1
0
ppm
2.05
3.79
2.12
0.99
2.08
2.00
2.32
2.02
6.21
3.16

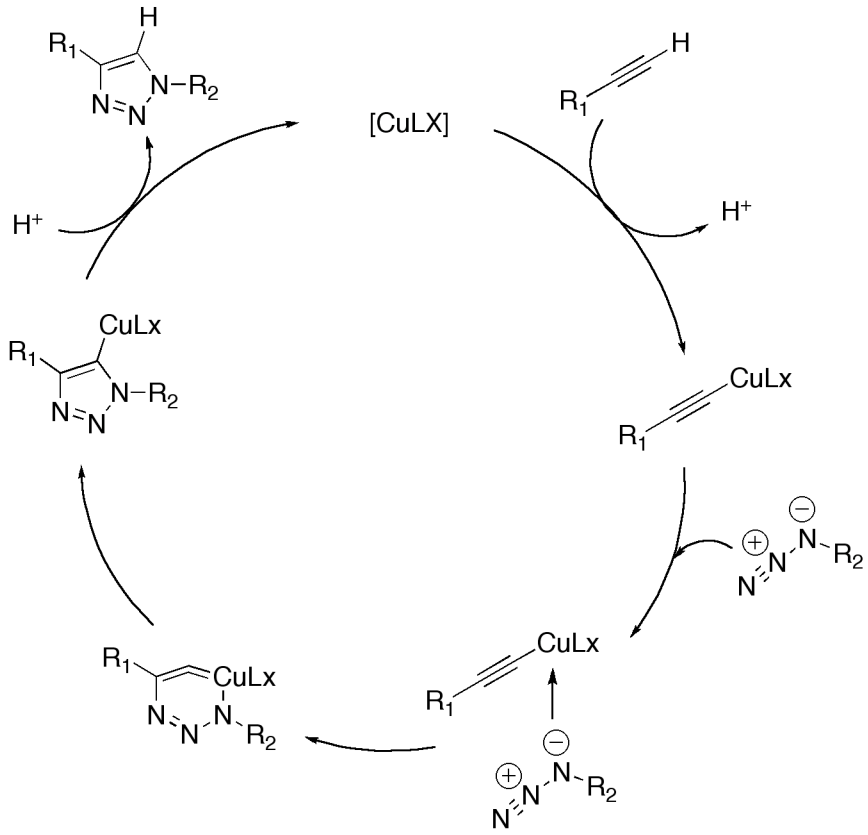

Current proposed mechanism for Cu(I) catalyzed 1,3-dipolar cycloaddition.